論文 / 著書情報
Article / Book Information

題目(和文)	ODE/IM対応におけるWKB周期とTBA方程式
Title(English)	WKB periods and TBA equations in ODE/IM correspondence
著者(和文)	近藤宇泰
Author(English)	Takayasu Kondo
出典(和文)	学位:博士(理学), 学位授与機関:東京工業大学, 報告番号:甲第11688号, 授与年月日:2022年3月26日, 学位の種別:課程博士, 審査員:伊藤 克司,今村 洋介,慈道 大介,笹本 智弘,関澤 一之
Citation(English)	Degree:Doctor (Science), Conferring organization: Tokyo Institute of Technology, Report number:甲第11688号, Conferred date:2022/3/26, Degree Type:Course doctor, Examiner:,,,,
学位種別(和文)	博士論文
Type(English)	Doctoral Thesis

Ph.D thesis

WKB periods and TBA equations in ODE/IM correspondence

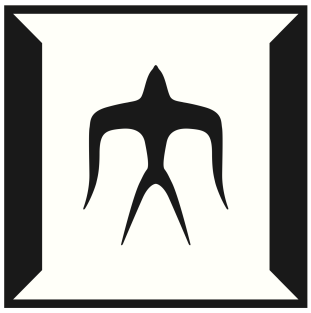

Takayasu Kondo

Depertment of Physics
Tokyo Institute of Technology

February 23, 2022

Abstract

The ODE/IM correspondence provides the relation between the spectral analysis of ordinary differential equations (ODE) and the approach of functional relations of two dimensional integrable models (IM). The Stokes multipliers which appear in the asymptotic analysis of the second order ODE are identified to the Y-functions in IM. The Y-functions are the analytic functions satisfying a system of integral equations describing the models in a thermodynamic setting. These integral equations are useful to compute the free energies of the equilibrium states of integrable models and are called the thermodynamic Bethe ansatz (TBA) equations. By using the asymptotic analysis i.e. the WKB method, we can relate the Stokes multipliers to the WKB periods. The main purpose of this thesis is the generalization of the correspondence between the WKB periods and Y-functions to the higher order ODE with the polynomial potential. The ODE we study can be regarded as the Seiberg-Witten curve of the Argyres-Douglas theory, which is a class of the simplest four dimensional $\mathcal{N} = 2$ superconformal field theory, in the Nekrasov-Shatashvili limit of the Ω-background. The classical parts of the WKB periods compute the central charges of the BPS states of the four dimensional theory. In four dimensional $\mathcal{N} = 2$ theories, there have been studied the wall-crossing phenomenon of the BPS spectrum. The TBA equations also capture the wall-crossing of the four dimensional theory. Continuous deformations of the potential in the ODE induce the analytic continuation of the TBA equations satisfied by the corresponding Y-functions, which we also call the wall-crossing. After establishing the formula which relates the WKB periods to the Y-functions, we study the wall-crossing of the TBA equations for the third order ODE with cubic and quartic potentials in detail. From the detailed analysis of the wall-crossing of TBA equations for the third order ODE, we find the connections between the different types of the TBA equations, which are associated with the dualities of the four dimensional theories.

Acknowledgement

Firstly, I would like to express my gratitude to my supervisor Prof. Katsushi Ito for his patient and attentive guidance throughout the three years of my Ph.D. course.

The author also thanks all the members of the particle physics group at Tokyo Institute of Technology for their guidance and helpful discussion, Prof. Yosuke Imamura, Prof. Yoshiyuki Watabiki, Shoichi Kanno, Yoshishige Kobayashi, Saki Koizumi, Yutaka Yoshida, Kohei Kuroda, Shota Fujiwara, Tatsuya Mori, Keita Imaizumi, Shuichi Murayama, Sumiya Umezu, Mingshuo Zhu, Ibuki Hashimoto, Jingjing Yang, Hibiki Kano and Juri Shima. I also greatly appreciate all of my collaborators, Prof. Katsushi Ito, Hongfei Shu, and Kohei Kuroda. My Ph.D. course is supported by the Tokyo Tech Tsubame Scholarship.

Last but not least, I would like to give thanks to my family for their support in all aspects.

Contents

Chapter 1

Introduction

The ODE/IM correspondence relates the spectral analysis of the ordinary differential equation (ODE) and the approach of the functional relations in the two dimensional quantum integrable models (IM), which was first discovered by Dorey and Tateo in [1]. In this thesis, we will study the ODE/IM correspondence focusing on the relation between the WKB periods, which are defined in the WKB analysis of ODE, and the Y-functions, logarithm of which satisfy the thermodynamic Bethe ansatz (TBA) equations in IM. This chapter explains a brief introduction of the ODE/IM correspondence, its relation to the four dimensional supersymmetric field theory, as well as the motivation and the brief summary of this thesis.

1.1 Backgrounds and motivations

Quantum field theory (QFT) is the fundamental framework of theoretical physics, which has many applications in vast areas: particle physics, nuclear physics, cosmology, statistical mechanics, condensed matter physics, and so on. In some cases of these usages, one of the useful tools could be the perturbative expansion. This method enables us to calculate physical quantities as formal sums with respect to the coupling constant if the system is weakly interacting. However, if the system is strongly coupled, the formal sum breaks down and does not provide us with any meaningful quantities. In such a situation, the non-perturbative effects are important to understand the theory, with which we could compute the exact values regardless of the strength of the interaction.

Both in two dimensional theories and in supersymmetric theories, there have been discovered many models which we can, at least in principle, analyze exactly. In two dimensions, the conformal theory has an infinite number of conserved charges, and one can study it in non-perturbative ways. Among the two dimensional massive theory, there are also models which have an infinite number of conserved charges and can also be studied exactly. These are known as the (quantum) integrable models. On the other hand, in supersymmetric theories, the four dimensions might be particularly fascinating if one thinks of them as toy models of the elementary particles. The four dimensional theories with extended $\mathcal{N} = 2$ supersymmetry have been well studied, and some strongly coupled models have been analyzed non-perturbatively. Interestingly, there have been known non-trivial relations between the four dimensional $\mathcal{N} = 2$ theory and the two dimensional integrable models, which we will mention in the latter section of this chapter.

The perturbative effects and the non-perturbative effects are not mutually independent. Their relations have also been studied and used in physics, which is called resurgence. Although, the resurgence was originally born in a field of mathematics, which is the theory of differential equations. Applying the resurgence to the WKB approximations of ordinary differential equations, one can recover the exact solution. This technique is called the exact WKB analysis. The ODE/IM correspondence, which is the topic of this thesis, relates the exact WKB analysis of ODE to the TBA equations of integrable models. The TBA equations are integral equations that can be used to compute the free energies of the systems in thermodynamic equilibrium. Some kinds of ODE are also related to the four dimensional $\mathcal{N} = 2$ theory. There are 4d theories on a particular background metric, whose strongly coupled low-energy regions are, in some sense, governed by the ODE. The exact WKB analysis is expected to be related to the theory of wall-crossings in 4d models, which deals with particular states which are important in the low-energy regions of supersymmetric theories.

Motivated from the relation between the above three i.e. the exact WKB analysis of ODE, two dimensional integrable models, and the four dimensional $\mathcal{N} = 2$ theory, our big goal is to understand these in a uniform perspective. This would bring the following impacts on each field. In the exact WKB analysis, we could establish the theory for the

ODE with higher order differential terms, which has not been studied well even in the context of mathematics. This might be guided by the relation to the theory of wall-crossings in 4d models since it is well formulated. In integrable models, one could find a new classification of the theories since one ODE is associated with many integrable models in the ODE/IM correspondence. Furthermore, this classification might help us to discover new theories. In 4d theory, we could understand the non-perturbative effects and dynamics in the strongly coupled phases exactly in more detail from the 2d integrable models. This might provide us with hints to understand the non-supersymmetric strongly coupled theory in the real world, like quantum chromodynamics.

In the following sections, let us introduce each topic explained above in detail.

1.2 Integrability

Since Newton solved the Kepler problem in the seventeenth century, there had been discovered many exactly solvable classical models by *ad hoc* methods. About two hundred later, the notion of integrability in classical mechanics was established by Liouville in the nineteenth century for general Hamiltonian systems. The integrability is ensured by the existence of the conserved charges of number not less than the degrees of freedom and provides the possibility to be solvable with the system. The extension of the notion of integrability to the systems with infinite numbers of degrees of freedom was accomplished in the 1960s. It was devised in the application of the so-called inverse scattering method to the Korteweg-de Vries equation which appears in fluid mechanics [2].

In one dimensional quantum many-body systems, the method to obtain the exact solutions was first invented by Bethe, which is called the Bethe ansatz [3]. In two dimensional statistical mechanics, the solvable models have been known since Onsager solved the Ising model in the mid-40s. In 1967, it was shown the exact solution to the six-vertex model by Lieb and Sutherland in [4, 5]. For the study of the eight-vertex model, Baxter applied the method of Bethe ansatz and obtained the exact solution [6]. Also, he showed that the eigenvalues of the transfer matrix of the eight-vertex model were also that of the Hamiltonian of the XXZ spin chain [7, 8]. The critical point of the work was that he

showed that the S-matrices of the integrable models satisfy the Yang-Baxter equations (the star-triangle relation) which indicate integrability i.e. the existence of an infinite number of conserved charges. Many functional relations associated with integrability can be driven from the Yang-Baxter equations. This functional approach was elaborated by Faddeev *et al.* as the quantum version of the inverse scattering method. Their systematic approach connects to the quantum group [9] and furnishes an algebraic reformulation called the algebraic Bethe ansatz. The classification of the algebraic Bethe ansatz can be found in [10–13]. There have also been attempts to apply the Bethe ansatz in the thermodynamic setting by Yang and Yang. They studied the one dimensional Bose gas with repulsive interactions expressed by delta function, and derived an integral equation, which is called the thermodynamic Bethe ansatz (TBA) equations, which were used to compute the free energy of the equilibrium state in the thermodynamic setting of the system [14]. This TBA approach was also adapted to lattice models. In relativistic field theories, it was also used the TBA formalism to compute the ground state energy in a finite volume by Al. B. Zamolodchikov [15]. The integral equations in this formalism, the TBA equations, can be converted into a functional relation called the Y-system [16]. The Y-system is the universal concept among different integrable models, and its classification can be found in [17, 18].

1.3 ODE/IM correspondence

In the asymptotic analysis of the second order differential equations, it was shown by Sibuya that the Stokes multipliers satisfied a system of functional relations which is equivalent to the so-called T-/Y-system in the integrable models. See [19]. For the monomial potential, Dorey and Tateo pointed out the connection to the A_r-type TBA system, which was supported by the spectral analysis of the ODE [1]. Other than T-/Y-system, there was also derived the functional relation of integrable models from the ODE, which is Baxter's TQ-relation [20, 21]. The Q-functions were defined, in the context of ODE, as the spectral determinants of the differential operator, while the T-functions were defined as the Stokes multipliers. This correspondence was also studied for the higher order cases with

the monomial potentials [22–25]. The zeros of the Q-functions were shown to satisfy the Bethe ansatz equations (BAEs) of A_r-type vertex models, which are the algebraic equation satisfied by the spectral parameters in integrable models. This was also tested by the numerical calculations in which the non-linear integral equations[1] (NLIEs) [26–28] were used to compute the Bethe roots since solving the BAEs is a highly non-trivial algebraic problem. For BAEs of other types of classical Lie algebras, the corresponding (pseudo) differential equations were proposed [29]. (Also, see the review [30].) The term pseudo means that the ODE contains the pseudo-differential operator which is a formally defined inverse differential operator. The BAEs were derived from the functional relations of the Wronskians of the solutions, which is called the ψ-system. The pseudo-ODE includes the formal inverse differential operator, so the treatment is often subtle. Furthermore, unlike the Schrödinger equations, the physical origin of the pseudo ODE is not clear. In [31], a clearer reformulation of these pseudo ODE was accomplished by Sun, in which she introduced the matrix-valued differential equations, say linear problems, associated with the Langlands dual of the classical Lie algebras. Motivated by these and massive ODE/IM correspondence [32,33], it was shown that the linear problem is nothing but the modified affine Toda field equations [34,35]. The ψ-system turned out to be a functional relation of solutions to the linear problem. Taking the conformal limit, one can derive the BAEs of any semisimple Lie algebra $\mathfrak{g}$ from the linear problem of $\mathfrak{g}^\vee$-type, where $\mathfrak{g}^\vee$ is the Langlands dual of $\mathfrak{g}$. These developments are correspondences for the ground states eigenvalues, but the ODE/IM for the excited states also have been studied [36]. See also the recent works [37,38].

In [39], we performed a further study of the ODE/IM correspondence, including the establishment of a new method to compute the zeros of Q-functions associated with arbitrary representations as well as the BAEs of folded types which are related to the linear problems based on non-simply affine Lie algebras. The numerical matching between the spectrum of the linear problems and the Bethe roots is another non-trivial test of the correspondence, especially for the exceptional type Lie algebras, which had not been able to study. We will discuss these topics in chapter 3.

[1] NLIEs are often called the DDV equations.

1.4 WKB analysis and wall-crossing phenomena

The WKB approximation played an important role in the discovery of the connection between the Stokes multipliers and T-functions by Dorey and Tateo. The WKB expansion is a kind of formal sum of asymptotic series. Thus, one can consider the Borel resummation of the WKB expansion, which is the method to obtain analytic functions from asymptotic series used in the exact WKB analysis [40, 41]. In the WKB analysis, it is natural to consider the cycle integrals of the differentials on the WKB curve, which are called the WKB periods. Note that the WKB periods are defined as the formal power series of the expansion parameter, which is interpreted as the Plank constant but is complex, and then they can be Borel resumed converting into the analytic function. The Borel resummation can be performed in two steps. First, one defines a formal sum of an auxiliary complex variable from the WKB expanded quantity, which is called the Borel transformation. After that, the Borel resummation is defined from an integral of the Borel transformation with respect to the auxiliary variable along some direction in the complex plane. It is known that the Borel resumed quantity jumps in some directions in the integration. Such directions are called the Borel nonsummable directions. The gaps of the quantity along the Borel nonsummable directions are expressed as the so-called discontinuity formula. In [42], it was shown that the discontinuity formula for the WKB periods leads the TBA equations. The WKB periods were interpreted as the logarithm of Y-functions. This connects the exact WKB analysis to the TBA equations directly, which is the alternative approach for the study of the ODE/IM correspondence.

The authors of [42] also generalized the correspondence for the second order ODE with the polynomial potentials. For such a potential, essentially new phenomena occur, which we call the wall-crossing of the TBA equations. The notion of the wall-crossing or the analytic continuation of the TBA equations was first discussed in [43]. It is caused by the poles of the kernel functions of the TBA equations. In the context of the ODE/IM correspondence, as we deform the polynomial potential continuously, the phases of the WKB periods change, and then we pick up the contributions of the poles. The Borel nonsummable directions are related to the locations of the poles of the kernel functions.

Through the wall-crossing phenomena, one obtains the different Y-systems and TBA equations in each process. The systematic way to obtain the TBA equations in each process was established by Toledo in [44] (See also [45].), which we will introduce in chapter 4. The interesting point in the view of the ODE/IM correspondence is that different integrable models are related to a common ODE through the wall-crossing. In this sense, the ODE uniforms some kinds of integrable models. One of the main purposes of this thesis is the establishment of the correspondence between the WKB periods and the Y-functions and the investigation of the wall-crossing phenomena for the higher-order ODE with polynomial potentials.

1.5 Four dimensional $\mathcal{N} = 2$ theories

Physics in four dimensions may be the most interesting subject for us. The gauge theory in four dimensions is particularly important since it describes the dynamics of fundamental particles. Even though it has been past the decades of years since the gauge theory was started to be studied, there remain many unsolved problems. Among these problems, one of the hardest things is the study of the gauge theory at the strong coupling confined phase since one cannot use the perturbative analysis anymore. Supersymmetry might shed light on the analysis of these strongly coupled physics, which is a symmetry relating bosons with fermions. It has been adopted in different areas of physics because of its controllable features. One of the significant consequences of supersymmetry is the nonrenormalization theorem which restricts the quantum effects of physical quantities. For example, in the four dimensional supersymmetric gauge theories, the perturbative corrections of a kind of quantities become exact at one-loop order. However, it is still hard to analyze the gauge theory in the strongly coupled phase with the least number of supersymmetric charges i.e. $\mathcal{N} = 1$ theory. The extended supersymmetry sometimes enables us to obtain the exact results. In this section, let us discuss the exact analysis of the four dimensional $\mathcal{N} = 2$ theory as well as the relation to the ODE/IM correspondence.

The Seiberg-Witten solution and the Argyres-Douglas theory

The $\mathcal{N} = 2$ supersymmetry imposes a lot of constraints on the gauge theory. As the representation of the $\mathcal{N} = 2$ supersymmetry, there are two types of fundamental fields which are vector multiplet and hyper multiplet. Analogous to the non-supersymmetric case, the UV Lagrangian of $\mathcal{N} = 2$ supersymmetric pure Yang-Mills theories are composed of $\mathcal{N} = 2$ vector multiplet. The $\mathcal{N} = 2$ vector multiplet contains one vector field, two Weyl fermions, and one complex scalar. The classical vacuum of the pure Yang-Mills theory is parameterized by the vacuum expectation values (vevs) of the scalar in the UV Lagrangian. Since the theory is asymptotic freedom, the low energy effective theory is strongly coupled. However, fortunately, the form of the low energy effective Lagrangian is strongly restricted by the extended supersymmetry and expressed by a holomorphic function of the multiplet, which is called the prepotential [46]. The prepotential includes the contributions from the classical part, one-loop part, and the instanton part which is the non-perturbative effect. Resolution to obtain the prepotential including all the instanton part was provided to the $SU(2)$ theory by Seiberg and Witten in 1994 [47, 48], which is an example of the exact results of the strongly coupled gauge theory. They considered the theories with different scalar vevs simultaneously and uncovered the structures of the moduli space of vacua. Here we mean by the moduli space of vacua that the space of the parameters which determine the scalar vevs. A point in the moduli space represents one vacuum. The structure of the moduli space was turned out to be expressed by an elliptic curve called the Seiberg-Witten (SW) curve. The scalar vevs and the prepotential are computed from the cycle integrals of a one-form on the SW curve, which is called the SW periods. Hence, the SW curve and the periods give us whole information of the moduli space of the supersymmetric Yang-Mills theory. The application of this analysis to other gauge groups (without matter) fields can be found in [49–52]. The connection of the $\mathcal{N} = 2$ theories to the classical integrable models was also studied and used to compute these SW curves [53–55].

In the moduli space of vacua in pure $SU(3)$ theory, a special point was discovered, where the SW curve degenerates and strongly coupled interacting superconformal theory

appears, which is called the Argyres-Douglas (AD) theory [56]. At the AD point, mutually non-local monopole and dyon become massless; hence the theory has no Lorentz covariant Lagrangian. Here the locality means the proportionality of the electric-magnetic charges. The AD theory is also known as the simplest theory since its central charge as a conformal theory saturates the unitarity bound. The same theory was obtained from $SU(2)$ theory with matter fields [57]. This is because the conformal theory defines the universality class, and these two theories belong to the same universality class. The AD theories obtained from the degeneration of the SW curves were studied, and the curves were classified in ADE-types [58]. There is also a more general class of AD theory which was obtained from the geometric engineering of type IIB string theory or Hitchin system [59–61]. A remarkable property of the AD theory is its duality. If two theories describe the same Hilbert space, we say these two are dual. Some AD theories are mutually dual at the superconformal point. These can be observed through the study of the wall-crossing phenomena of the TBA equations which correspond to the third order ODE with polynomial potential.

BPS spectra and wall-crossing in four dimensions

The four dimensional $\mathcal{N} = 2$ algebra has the center in the anti-commutation relation of the supercharges [62, 63]. In each representation, the center takes a constant complex value which we call the central charge. The mass of any state preserving the supersymmetry is bounded by the central charge [64, 65]. The state/particle saturating the bound is called the BPS state/particle. The BPS particles are important because they are not affected by quantum corrections and control the low energy behaviors of the supersymmetric theory. If we consider the theory described by the SW curve, the central charge of the BPS particle is given by its electric and magnetic charges as well as the scalar vevs of the components in the vector multiplets of the theory both in electric and magnetic descriptions. The central charges change continuously in the moduli space of vacua. The spectrum of the BPS state suddenly changes if any two central charges have the same arguments in the complex plane. Since the mass of the BPS particle is the absolute value of the central charge, at the point where two central charges align, BPS particles could decay, or new BPS

particles could emerge. This phenomenon is also called wall-crossing. The wall-crossing phenomena are conjectured to be governed and classified by the Kontsevich-Soibelman wall-crossing formula (KSWCF) [66]. Using the KSWCF and the relations to the Hitchin system, it was proposed the systematic way to obtain the BPS spectrum of a certain class of $\mathcal{N} = 2$ theories in [67, 68]. In these papers, It was also discovered that a quantity associated with BPS charges, which is called the spectral coordinate, satisfies TBA-like integral equations. The interesting point is that since the spectral coordinates enjoy the wall-crossing phenomena, the TBA-like equations also wall-cross. The wall-crossing of the TBA equations in the context of the ODE/IM correspondence is related to that in the four dimensional $\mathcal{N} = 2$ theory. However, there is no convincing explanation of this relation. This is one of the motivations of our study.

Nekrasov-Shatashvili limit of the Ω-background

The prepotential in the weak coupling region is also computed by directly path integrating around all the instanton configurations. For $SU(N)$ theory, it was carried out using the localization method by Nekrasov *et al.* [69, 70]. In the calculation, they used the dimensional reduction of a six dimensional theory on the so-called Ω-background. Then, the resulting partition function, which is called the Nekrasov partition function, includes two deformation parameters. The prepotential is obtained from the Nekrasov partition function by taking the logarithm in the limit where the deformation parameters are taken to zero. It is also possible to consider the limit where one of the parameters remains finite, where the prepotential in the limit is defined from the Nekrasov partition function. This limit is called the Nekrasov-Shatashvili (NS) limit [71]. The SW curve, which reproduces the prepotential in the NS limit, becomes the quantized one which is no longer the Riemann surface but the ordinary differential equation [72, 73]. The SW periods also become the quantized ones, say the quantum SW periods. The SW curve and the quantum SW periods are, in the ODE language, identified with the WKB curve and the WKB period, respectively.

If we consider the (A_1, A_N)-type AD theory in the NS limit, the quantum curve is nothing but the one studied in [42], which is the second order ODE with the polynomial

potential of degree $N+1$. We interpret the remaining deformation parameter of the Ω-background as the expansion parameter of the WKB analysis in the ODE. The quantization of the SW curves of other types of AD theories was studied in [74–76]. The leading part of the WKB period is found to be the SW period. Furthermore, the coefficients of the potential in the ODE correspond to the parameters of the moduli space of vacua in 4d theory. Then, the wall-crossing condition of the TBA equations, derived in the context of the ODE/IM correspondence, is exactly the same as that of the four-dimensional theory, i.e., the condition of the alignment of any two SW periods.

As we mentioned, one can consider the TBA-like equations for the spectral coordinate of a four dimensional $\mathcal{N}=2$ theory. In [77], it was pointed out that there are TBA-like equations whose conformal limit reproduces the solutions to the quantum SW curve of the (A_1, A_2)-type AD theory. Inspired by this, it was studied for the (A_2, A_2) case [78, 79]. The ODE/IM correspondence may provide some insight into these non-trivial phenomena since the TBA equations for the quantum curve of AD theory also gives the solutions to the ODE and enjoy the same wall-crossing phenomena. This is another motivation for this thesis.

4d/2d correspondence and the ODE/IM correspondence

There is also a non-trivial connection of the ODE/IM correspondence to the four and two dimensional field theories. In [80], it was conjectured that any four dimensional $\mathcal{N}=2$ superconformal theory has a special sector whose Hilbert space is isomorphic to that of a certain two dimensional CFT. This is called the 4d/2d correspondence. For AD theories, see [81–83]. There is also a conjecture of the generalization of this relation [84]. In these studies, the important quantity was the trace of the operator which is also used to construct the KSWCF. In this sense, the wall-crossing phenomena are considered to play an important role in the 4d/2d correspondence.

The relation to the ODE/IM correspondence was observed in [74] that the central charges computed from the TBA equations, which corresponds to the quantum curve of the (A_r, A_1)-type AD theory, become the same as that of the two dimensional CFT in [84]. As discussed in [59, 81, 84], the 4d/2d correspondence is related to the wall-

crossing phenomena of four dimensional theory. Hence we consider that the relation to the ODE/IM would shed light on some aspects of this non-trivial relation. This is also one of the motivations to study the ODE/IM correspondence.

1.6 The brief summary of this thesis

The ODE/IM correspondence for the polynomial potential relates one ODE with several integrable models, which can be studied from the wall-crossing phenomena of the TBA equations. The exact WKB analysis played an important role in the understanding of this correspondence for the second order ODE. For the higher ODE, however, the exact WKB analysis has not yet been studied well. On the other hand, there are relations between 4d $\mathcal{N} = 2$ theories and 2d integrable models, including conformal theories. This relation is considered to be deeply connected with the wall-crossing phenomena of 4d theory. The connection of the 4d $\mathcal{N} = 2$ theory to the ODE can be understood from the SW analysis in the NS limit of the Ω-background. In contrast, the wall-crossing of the TBA equations and that in the 4d theory have not been well understood. We believe that after uncovering these relations above, one could understand the (exact) WKB analysis, the structure of the BPS spectrum of 4d $\mathcal{N} = 2$ theories, the relations between 2d integrable models in a unified perspective. As mentioned in the first section, this is the ultimate goal of our study.

In this thesis, we will study the ODE/IM correspondence for higher order ODE with the polynomial potential, which is also considered as the quantum SW curve of the AD theory. This is the higher order generalization of the correspondence for the second order ODE with polynomial potential, studied in [42]. In our study, we will apply the WKB analysis to the ODE and establish the relation between the WKB periods and the Y-functions. The TBA equations satisfied by the Y-functions enjoy the wall-crossing phenomenon as we deform the potential continuously, which is more complicated than that for the second order case. As discussed in the previous section, the classical parts of the WKB periods for this ODE provide the mass of the BPS particles of the corresponding AD theory. The Y-functions are related to the spectral coordinates. We will also discuss

the relation to the wall crossing of the AD theory.

Generalizing the arguments in [74] and [42], we will first discuss the identification of the cross ratios of the Stokes multipliers with the Y-functions through the ODE/IM correspondence for the higher ODE with the general polynomial potential based on our work [85]. From the asymptotic analysis, the cross ratios of the Stokes multipliers will be turned out to be the WKB periods. The asymptotic behaviors of the WKB periods can be discussed by using the Stokes graphs and the abelianization trees, which are the techniques used in [78] and [79]. We will also show the evidence of the correspondence between the WKB periods and the Y-functions in several aspects, which includes the numerical comparisons in the formal expansion, analytic relations, and the relation of the discontinuity structure of the WKB periods to the pole structures of the kernel functions of the TBA. The last one may provide some hints to the exact WKB analysis for higher order ODE.

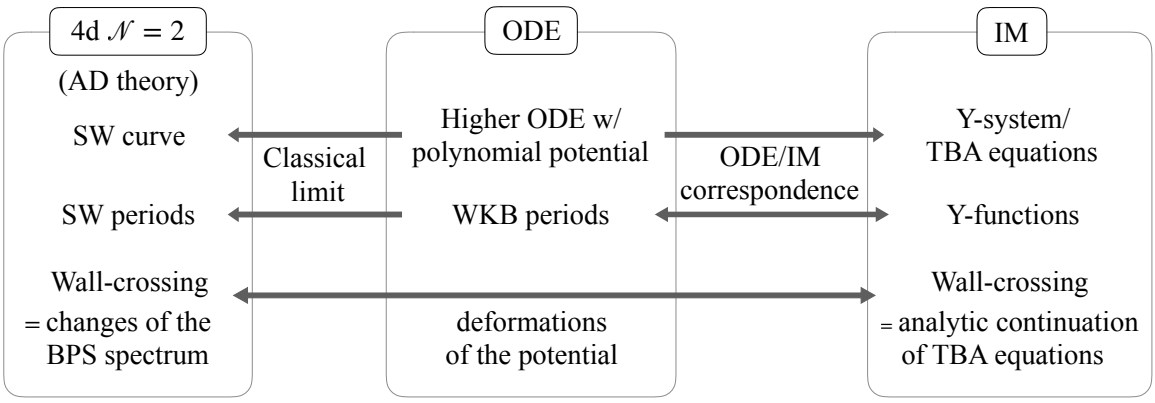

Figure 1.6.1: The relations of the ODE, integrable models, and the 4d $\mathcal{N}=2$ theory.

Once we have established the correspondence, we will study the wall-crossing phenomena. Concretely, we will investigate the wall-crossing of the TBA equations for the third order, which we studied in [86]. Unlike the second order case, there has no known systematic method of wall-crossing. Thus, we compute the TBA equations in each process step-by-step algebraically. We will also check that the wall-crossing condition becomes the same as that of the four dimensional one. The remarkably interesting results are

obtained at the point in the moduli space, where the potential becomes the monomial one. This point is the AD point in the four-dimensional language, where the theory becomes superconformal. The TBA equations will reduce to the simplified ones, and then we will observe that different types of TBA equations are connected associated with the dualities of the AD theories. The relations of the ODE, integrable models, and the four dimensional $\mathcal{N} = 2$ theory are summarized in figure 1.6.1.

1.7 Outline

This thesis is based on our works [39], [85], and [86]. We will introduce the ODE/IM correspondence and discuss the non-trivial test of the correspondence for the modified affine Toda field equations associated with any affine Lie algebras based on [39]. After some reviews of former works and relation to the four dimensional theory, we will discuss the higher order generalization of the correspondence and the wall-crossings of TBA equations based on [85, 86]. This thesis is organized as follows.

Chapter 2 We introduce the notion of integrability in two dimensions. We will see that the functional relations characteristic to the integrable models are also derived through the analysis of the six-vertex models. The integral equations, i.e. the NLIEs and the TBA equations, are also derived from the BAEs and Y-system, respectively.

Chapter 3 We discuss the ODE/IM correspondence for modified affine Toda field equations. The method to calculate the zeros of the Q-functions is also introduced, which is applicable to the linear problem for any representations of affine Lie algebras.

Chapter 4 This chapter is devoted to the review of the ODE/IM correspondence of the second order ODE with the polynomial potential. The relation of the WKB periods and the Y-functions, as well as the wall-crossing of the TBA equations, will be discussed in detail.

Chapter 5 The four dimensional $\mathcal{N} = 2$ theory and the relations to the ODE/IM correspondence will be argued. The AD theory, its quantum SW curve, and the wall-crossing of the four dimensional theory will be introduced in this chapter. These arguments are the background and one of the motivations of our study of higher order ODE.

Chapter 6 We will generalize the ODE/IM correspondence to the higher order ODE with the polynomial potential. Through the analysis by using the abelianization tree and the Stoked graphs, we identify the WKB periods with the Y-functions. We will also test the identification in several ways, including the numerical computation, PNP relations, and the discontinuity structure.

Chapter 7 The wall-crossing phenomena of TBA equations will be investigated for the third order ODE in great detail. We especially focus on the cubic and the quartic potentials. In each process of wall-crossings, we compute the TBA equations and extend the relation between the WKB periods and Y-functions. At the point in the moduli space of (A_2, A_2) and (A_2, A_3), where the potential becomes the monomial one, we will observe the TBA equations reduce to the D_4-type and E_6-type, respectively. This is the consequence related to the duality of the AD theories.

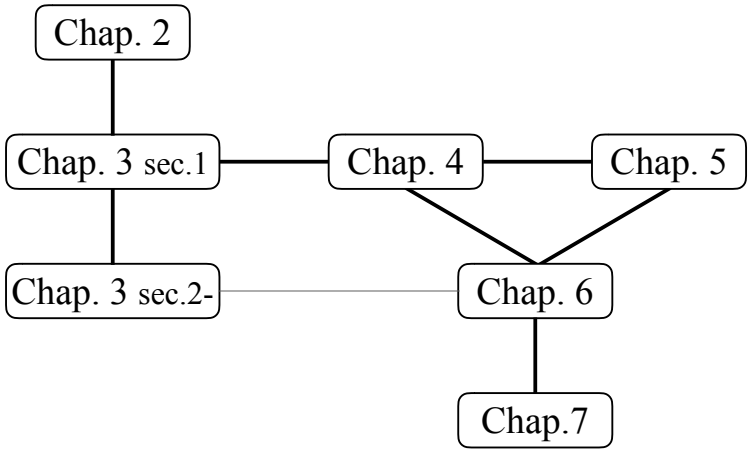

Figure 1.7.1: The connections of the topics in chapter from 2 to 7.

The connections of the topics in each chapter are shown in figure 1.7.1. Chapter 3 is

based on both the former works and our work in [39]. Chapter 6 and 7 are based on our works in [85, 86]. Lastly, we should note that other chapters are the review part and are based on many former papers and reviews.

Chapter 2

Integrability in two dimensions

In this chapter, we briefly review the property of the two dimensional integrable systems. We first review the integrability following [87], and then, as a simple example of the quantum integrable model in two dimensions, we consider the six vertex model and introduce the functional relations based on the review paper [30]. We also introduce the integral equations, the TBA equations, which are useful to compute the free energy of the system or the effective central charge of the underlying conformal theory.

2.1 Classical and quantum integrability

In classical mechanics, the model which has sufficiently many conserved charges are said to be integrable. The most famous example of the classical integrable system may be the Kepler problem which is also solvable. However, integrability does not guarantee solvability in general. The notion of integrability of classical models with finite degrees of freedom is based on the Liouville theorem. The theorem claims that in the Hamilton system of $2d$-dimensional phase space, if there exist more than d conserved charges F_k $(k = 1, 2, \ldots, d)$ which are involutive:

$$\{F_k, F_l\} = 0, \qquad k, l = 1, 2, \ldots, d, \tag{2.1.1}$$

the system is integrable. Here the symbol $\{\cdot, \cdot\}$ implies the Poisson braket. The Hamiltonian itself is included in the conserved charges or constructed by the charges. In the formulation of the classical integrable models, it is often used the Lax formalism, in which

the equation of motion in Hamiltonian formalism is recast by two matrices L and M called the Lax pair into

$$\frac{\mathrm{d}L}{\mathrm{d}t} = [M, L]. \tag{2.1.2}$$

Here the right hand side is the commutator of the pair. The conserved charges are obtained by

$$F_k = \operatorname{tr} L^k, \tag{2.1.3}$$

where one can easily show the conservation by differentiating and using the Lax equation (2.1.2). Suppose the Lax pair is the element of a matrix algebra $\mathfrak{g}$. To the charges be involution, there exists a so-called classical R-matrix $r_{12} \in \otimes^2\mathfrak{g}$ such that

$$\{L_1, L_2\} = [r_{12}, L_1] - [r_{21}, L_2]. \tag{2.1.4}$$

Here L_1 and L_2 are defined by $L_1 = L \otimes 1$ and $L_2 = 1 \otimes L$, respectively. The classical R-matrix satisfy $r_{12} = -r_{21}$ and the classical Yang-Baxter equation:

$$[r_{12}, r_{13}] + [r_{12}, r_{23}] + [r_{13}, r_{23}] = 0, \tag{2.1.5}$$

which follows from the Jacobi identity on the tensor product $\otimes^3\mathfrak{g}$. Here r_{23} and r_{13} are defined in a same way as r_{12}.

There are also the classical integrable field theories, for example, the Korteweg de Vries (KdV) equation in fluid mechanics. In classical field theories, we have an infinite number of degrees of freedom. Instead of the Liouville theorem which does not provide a sufficient definition of integrability in this case, we define the integrable field theory by the Lax formalism. In the following, let us restrict ourselves to the two dimensional theory, where the coordinate of the space is x while that of time is t. We call the field theory whose Euler-Lagrange equation can be reformulated by the Lax pair (L, M) as

$$\frac{\partial L}{\partial t} - \frac{\partial M}{\partial x} = [M, L]. \tag{2.1.6}$$

To construct the conserved charges, we introduce the monodromy matrix $\mathcal{T}$ by

$$\mathcal{T}(\nu) \coloneqq P \exp\left[\int_{x_i}^{x_f} L(x, t, \nu)\right], \tag{2.1.7}$$

where P denotes the path-ordered product, and we also introduced an auxiliary parameter ν called the spectral parameter. If we move x_i and x_f to the endpoints of the space and impose the periodic boundary condition, the integral is performed over a cycle. The differential of the monodromy matrix by t becomes

$$\partial_t \mathcal{T} = [M(0,t,\nu), \mathcal{T}]. \tag{2.1.8}$$

This implies that the trace of the monodromy matrix, which we denote $T \coloneqq \operatorname{tr} \mathcal{T}$ and call the transfer matrix, conserves. Thus, the coefficients of the expansion of the transfer matrix in the spectral parameter are also conserved:

$$\partial_t F_k = 0, \qquad T(\nu) =: \sum_k F_k \nu^k. \tag{2.1.9}$$

The infinite tower $\{F_k\}_k$ is nothing but the conserved charges. As in the case of the integrable model with finite degrees of freedom, we assume the Poisson structure of the matrix of the Lax pair. Suppose there exist the classical R-matrix which satisfies

$$\{L_1(x,t,\nu), L_2(y,t,\nu')\} = [r_{12}(\nu-\nu'), L_1(x,t,\nu) + L_2(y,t,\nu')]\delta(x-y), \tag{2.1.10}$$

$$r_{12}(\nu-\nu') = -r_{21}(\nu'-\nu). \tag{2.1.11}$$

The Poisson structure in which the derivative terms of the delta function are absent is called the ultralocal. For general cases, there are also non-ultralocal Poisson structures which we do not discuss here. The equation (2.1.10) leads the Sklyanin exchange relation:

$$\{\mathcal{T}_1(\nu), \mathcal{T}_2(\nu')\} = [r_{12}(\nu-\nu'), \mathcal{T}_1(\nu)\mathcal{T}_2(\nu')], \tag{2.1.12}$$

where $\mathcal{T}_i$ $(i = 1, 2)$ is defined in the same sense as the definition of L_i. Taking the trace over the space on $\mathfrak{g} \otimes \mathfrak{g}$, the transfer matrix is turned out to satisfy

$$\{T(\nu), T(\nu')\} = 0. \tag{2.1.13}$$

This guarantees the involution property of the conserved charges: $\{F_k, F_l\} = 0$. Again, from the Jacobi identity, one obtains the classical Yang-Baxter equation of form

$$[r_{12}(\nu_1,\nu_2), r_{13}(\nu_1,\nu_3)] + [r_{12}(\nu_1,\nu_2), r_{23}(\nu_2,\nu_3)] + [r_{13}(\nu_1,\nu_3), r_{23}(\nu_2,\nu_3)] = 0. \tag{2.1.14}$$

The classical R-matrix, in this case, satisfies $r_{ij}(\nu_i, \nu_j) = r_{ij}(\nu_i - \nu_j)$, but one can also consider the case this does not hold.

The classical R-matrices for simple Lie algebras are reformulated and classified, for example, see [88]. Once the classical integrable structures are obtained, one can perform the quantization which leads to the possible quantum groups as well as integrable structures of quantum integrable models. The quantization of the integrability structure leads to the (quantum) Yang-Baxter equation

$$R_{12}R_{13}R_{23} = R_{23}R_{13}R_{12}, \tag{2.1.15}$$

where R_{ij} plays the role of the R-matrix in corresponding quantum integrable models and is related to the classical R-matrix by $R_{ij} \sim 1 \otimes 1 + i\hbar r_{ij} + \cdots$. The canonical quantization scheme, i.e. we replace as $\{\cdot, \cdot\} \to -i\hbar[\cdot, \cdot]$, leads the commutation property of the transfer matrices at different spectral parameters:

$$[\mathbb{T}(\nu), \mathbb{T}(\nu')] = 0. \tag{2.1.16}$$

Here we denote the quantum transfer matrix as $\mathbb{T}$. The Sklyanin exchange relation under the quantization procedure becomes the so-called RTT relation:

$$R(\nu - \nu')\hat{\mathcal{T}}_2(\nu')\hat{\mathcal{T}}_1(\nu) = \hat{\mathcal{T}}_1(\nu)\hat{\mathcal{T}}_2(\nu')R(\nu - \nu'), \tag{2.1.17}$$

where the quantum transfer matrix is related to the classical one by $\hat{\mathcal{T}}(\nu) = \mathcal{T}(\nu) + \mathcal{O}(\hbar)$. These structures are also derived from the analysis of the integrable lattice models. In such a context, the monodromy matrix and the transfer matrix are naturally introduced as in the usual approach of the study. In the next section, we will see the derivation of the integrable structure of the six-vertex model as well as many functional relations which are essential to discuss the ODE/IM correspondence in the next chapter. We will also discuss the algebraic way to obtain the eigenvalues of the transfer matrix, which leads to the Bethe ansatz equations.

2.2 An example of IM: the six-vertex model

Let us consider the six-vertex model [4,5] as the simplest example of the integrable models, which is suitable to explain the properties of integrability. Arguments in this section are

followed from the review [30]. To define the model, consider the $N \times N$ lattice with periodic boundary conditions. To avoid the unimportant problem in the analysis below, we set $N/2$ to be even. Each vertex of the lattice is linked to both horizontal and vertical neighbors. We assign one of the two spin states on each link, which is depicted by the arrows in fig. 2.2.1. Also we impose a rule to the assignation: only the configuration, in which the flux of the arrows through the vertices are preserved, is permitted. For each

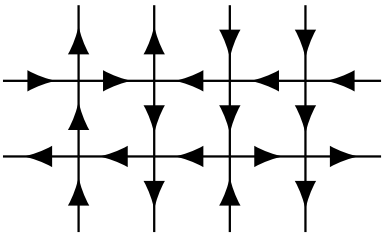

Figure 2.2.1: six vertex model

vertex, one can introduce the Boltzmann weight L which is determined from the spin states of the links connecting to the vertex. If we further impose the invariance of the Boltzmann weight under the simultaneous reversal of the directions of the arrows, there can be three types of weights:

$$\begin{aligned} L\left[\rightarrow \begin{smallmatrix}\uparrow\\ \uparrow\end{smallmatrix} \rightarrow\right] &= L\left[\leftarrow \begin{smallmatrix}\downarrow\\ \downarrow\end{smallmatrix} \leftarrow\right] = a, \\ L\left[\rightarrow \begin{smallmatrix}\downarrow\\ \downarrow\end{smallmatrix} \rightarrow\right] &= L\left[\leftarrow \begin{smallmatrix}\uparrow\\ \uparrow\end{smallmatrix} \leftarrow\right] = b, \\ L\left[\rightarrow \begin{smallmatrix}\uparrow\\ \downarrow\end{smallmatrix} \leftarrow\right] &= L\left[\leftarrow \begin{smallmatrix}\downarrow\\ \uparrow\end{smallmatrix} \rightarrow\right] = c. \end{aligned} \tag{2.2.1}$$

Normalizing the overall factor, we parameterize a, b and c as[1]

$$a(\nu,\eta) = \sin(\eta + i\nu), \qquad b(\nu,\eta) = \sin(\eta - i\nu), \qquad c(\nu,\eta) = \sin(2\eta), \tag{2.2.2}$$

where ν is called the spectral parameter while η is anisotropy.[2] For the later convenience, we set η/π irrational. We consider the models for different spectral parameters νs simultaneously. As the usual technique of the statistical mechanics, one can introduce the

[1] One can find other two parameterization regimes in [100].

[2] For the relation to the XXZ spin chain, see [7].

transfer matrix $\mathbb{T}$:

$$\mathbb{T}^{\vec{\alpha}'}_{\vec{\alpha}}(\nu) \coloneqq \sum_{\{\beta\}} \prod_{i=1}^{N} L\begin{bmatrix} \beta_i & \alpha'_i \\ \alpha_i & \beta_{i+1} \end{bmatrix}(\nu), \qquad \beta_{N+1} = \beta_1, \tag{2.2.3}$$

where $\vec{\alpha} = (\alpha_1, \alpha_2, \ldots, \alpha_N)$, $\vec{\alpha}' = (\alpha'_1, \alpha'_2, \ldots, \alpha'_N)$, and the sum over $\{\beta\}$ represent the summation of all the sets of the horizontal configurations. With the boundary condition set to be periodic, the partition function Z is calculated by

$$Z = \mathrm{Tr}\left[\mathbb{T}^N\right]. \tag{2.2.4}$$

Then the calculation of the partition function Z reduces to the diagonalization of the transfer matrix $\mathbb{T}$.

Bethe ansatz equations and Baxter's TQ-relation

To solve the eigenvalue problem, we introduce the monodromy matrix $\mathcal{T}$:

$$\mathcal{T}^{\vec{\alpha}'}_{\vec{\alpha}}(\nu)_{ab} \coloneqq \sum_{\{\beta\}} L\begin{bmatrix} a & \alpha'_1 \\ \alpha_1 & \beta_2 \end{bmatrix}(\nu) \prod_{i=2}^{N-1} L\begin{bmatrix} \beta_i & \alpha'_i \\ \alpha_i & \beta_{i+1} \end{bmatrix}(\nu) L\begin{bmatrix} \beta_{N-1} & \alpha'_N \\ \alpha_N & b \end{bmatrix}(\nu). \tag{2.2.5}$$

Of course, if we take the trace over a, b, the transfer matrix is recovered. The monodromy matrix has four components which we denote A, B, C, and D:

$$\mathcal{T}(\nu)_{ab} = \begin{pmatrix} \mathcal{T}(\nu)_{\rightarrow\rightarrow} & \mathcal{T}(\nu)_{\rightarrow\leftarrow} \\ \mathcal{T}(\nu)_{\leftarrow\rightarrow} & \mathcal{T}(\nu)_{\leftarrow\leftarrow} \end{pmatrix} =: \begin{pmatrix} A(\nu) & B(\nu) \\ C(\nu) & D(\nu) \end{pmatrix}. \tag{2.2.6}$$

The key property of the Boltzmann weight is that if we define R-matrix whose component $R^{cd}_{ab}(\nu)$ is defined by

$$R^{cd}_{ab}(\nu) \coloneqq L\begin{bmatrix} a & b \\ d & c \end{bmatrix}(\nu - i\eta), \tag{2.2.7}$$

where the R-matrix and the Boltzmann weight satisfy the so-called RLL relation:

$$R^{c'c}_{aa'}(\nu - \nu') L\begin{bmatrix} c & \delta \\ \alpha & b \end{bmatrix}(\nu) L\begin{bmatrix} c' & \alpha' \\ \delta & b' \end{bmatrix}(\nu') = L\begin{bmatrix} a & \delta \\ \alpha & c \end{bmatrix}(\nu') L\begin{bmatrix} a' & \alpha' \\ \delta & c' \end{bmatrix}(\nu) R^{b'b}_{cc'}(\nu - \nu'). \tag{2.2.8}$$

(2.2.8) is also represented in figure 2.2.2. Here the Boltzmann weight and the component of the R-matrix are denoted by the diagram shown in figure 2.2.3. The non-zero components

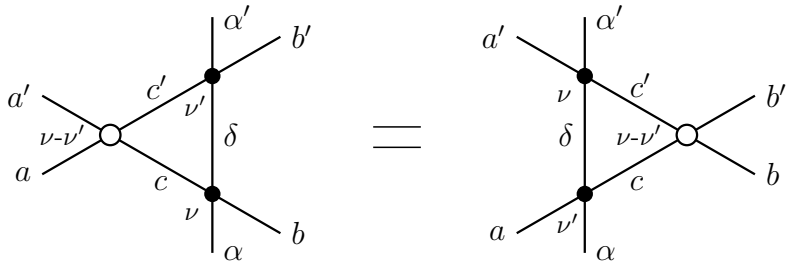

Figure 2.2.2: The RLL relation (2.2.8) in diagrammatic form.

(a) (b)

Figure 2.2.3: (a) The Boltzmann weight $L\begin{bmatrix}\beta & \alpha' \\ \alpha & \beta'\end{bmatrix}(\nu)$ and (b) the R-matrix $R^{cd}_{ab}(\nu)$.

of the R-matrix are

$$\begin{aligned} R^{\rightarrow\rightarrow}_{\rightarrow\rightarrow}(\nu) &= R^{\leftarrow\leftarrow}_{\leftarrow\leftarrow}(\nu) = a(\nu - i\eta, \eta) = \sin(2\eta + i\nu), \\ R^{\leftarrow\rightarrow}_{\leftarrow\rightarrow}(\nu) &= R^{\rightarrow\leftarrow}_{\rightarrow\leftarrow}(\nu) = b(\nu - i\eta, \eta) = -\sin(i\nu), \\ R^{\rightarrow\leftarrow}_{\leftarrow\rightarrow}(\nu) &= R^{\leftarrow\rightarrow}_{\rightarrow\leftarrow}(\nu) = c(\nu - i\eta, \eta) = \sin(2\eta). \end{aligned} \tag{2.2.9}$$

Once the relation (2.2.8) for the Boltzmann weight is obtained, it is not hard to generalize the relation to that for the product of the weights i.e. the monodromy matrix:

$$R^{c'c}_{aa'}(\nu - \nu')\mathcal{T}^{\vec{\delta}}_{\vec{\alpha}}(\nu')_{cb}\mathcal{T}^{\vec{\alpha}'}_{\vec{\delta}}(\nu)_{c'b'} = \mathcal{T}^{\vec{\delta}}_{\vec{\alpha}}(\nu)_{ac}\mathcal{T}^{\vec{\alpha}'}_{\vec{\delta}}(\nu')_{a'c'}R^{b'b}_{cc'}(\nu - \nu'). \tag{2.2.10}$$

This is the RTT relation, from which we can obtain an important and characteristic property of integrable models. Multiply both sides of (2.2.10) by $R^{d'd}_{b'b}(\nu' - \nu)$, taking the sum over b and b', and taking the trace on a, d as well as a', d' with using the identity

$$R^{ef}_{ab}(\nu)R^{cd}_{ef}(-\nu) = \sin(2\eta + i\nu)\sin(2\eta - i\nu)\delta^c_a\delta^d_b, \tag{2.2.11}$$

one obtains the commutativity property of the transfer matrices:

$$[\mathbb{T}(\nu), \mathbb{T}(\nu')] = 0. \tag{2.2.12}$$

(2.2.12) indicates that we can diagonalize the transfer matrices evaluated at different values of the spectral parameters simultaneously. That is the reason we did not fix the spectral parameter ν. (2.2.10) shows other relations for the components of the monodromy matrix:

$$[B(\nu), B(\nu')] = 0, \tag{2.2.13}$$

$$A(\nu)B(\nu') = g(\nu' - \nu)B(\nu')A(\nu) - h(\nu' - \nu)B(\nu)A(\nu'), \tag{2.2.14}$$

$$D(\nu)B(\nu') = g(\nu - \nu')B(\nu')D(\nu) - h(\nu - \nu')B(\nu)D(\nu'), \tag{2.2.15}$$

where $g(\nu)$ and $h(\nu)$ are given by

$$g(\nu) \coloneqq \frac{R^{\leftarrow\leftarrow}_{\leftarrow\leftarrow}(\nu)}{R^{\rightarrow\leftarrow}_{\rightarrow\leftarrow}(\nu)} = \frac{a(\nu - i\eta, \eta)}{b(\nu - i\eta, \eta)}, \qquad h(\nu) \coloneqq \frac{R^{\leftarrow\rightarrow}_{\rightarrow\leftarrow}(\nu)}{R^{\rightarrow\leftarrow}_{\rightarrow\leftarrow}(\nu)} = \frac{c(\eta)}{b(\nu - i\eta, \eta)}. \tag{2.2.16}$$

The problem of the diagonalization of the transfer matrix can be rephrased by taking the so-called Bethe ansatz. Regarding $\vec{\alpha}$ and $\vec{\alpha}'$ as the labels of states in a one dimensional spin chain, the component of the monodromy matrix $\mathcal{T}^{\vec{\alpha}'}_{\vec{\alpha}}$ is considered as the operator acting on the 2^N dimensional vector space, which changes the state $|\vec{\alpha}'\rangle$ to another state $|\vec{\alpha}\rangle$. In this interpretation, $A(\nu)$ and $D(\nu)$ preserve the number which is the number of the up spins minus that of down spins, while $B(\nu)$ and $C(\nu)$ play the role of the creation and the annihilation operators. Defining the highest weight state $|\Omega\rangle \coloneqq \otimes^N |\uparrow\rangle$ where

$$A(\nu)|\Omega\rangle = a^N(\nu, \eta)|\Omega\rangle, \qquad D(\nu)|\Omega\rangle = b^N(\nu, \eta)|\Omega\rangle, \qquad C(\nu)|\Omega\rangle = 0, \tag{2.2.17}$$

one might expect the state $|\Psi\rangle$ defined by

$$|\Psi(\nu_1, \nu_2, \ldots, \nu_n)\rangle = \prod_{i=1}^{n} B(\nu_i)|\Omega\rangle \tag{2.2.18}$$

also becomes the eigenstate of the transfer matrix $\mathbb{T}$ with some conditions for the spectral parameters $\nu_1, \ldots, \nu_n$. Note that the commutativity (2.2.13) ensures that we don't have to take care of the ordering of $B(\nu_i)$. Acting $A(\nu)$ and $D(\nu)$ on $|\Psi\rangle$ respectively and using the exchange relations (2.2.14) and (2.2.15), we obtain

$$A(\nu)|\Psi\rangle = \Lambda^+|\Psi\rangle + \sum_{k=1}^{n} \Lambda^+_k |\Psi_k\rangle, \qquad D(\nu)|\Psi\rangle = \Lambda^-|\Psi\rangle + \sum_{k=1}^{n} \Lambda^-_k |\Psi_k\rangle, \tag{2.2.19}$$

where $\Lambda^{\pm}, \Lambda_k^{\pm}$ and $|\Psi_k\rangle$ are given by

$$\Lambda^+ \coloneqq a^N(\nu,\eta)\prod_{i=1}^{n} g(\nu_i-\nu), \qquad \Lambda_k^+ \coloneqq -a^N(\nu_k,\eta)h(\nu_k-\nu)\prod_{i=1,i\neq k}^{n} g(\nu_i-\nu_k), \tag{2.2.20}$$

$$\Lambda^- \coloneqq b^N(\nu,\eta)\prod_{i=1}^{n} g(\nu-\nu_i), \qquad \Lambda_k^- \coloneqq -b^N(\nu_k,\eta)h(\nu-\nu_k)\prod_{i=1,i\neq k}^{n} g(\nu_k-\nu_i), \tag{2.2.21}$$

$$|\Psi_k\rangle \coloneqq B(\nu)\prod_{i=1,i\neq k} B(\nu_i)|\Psi\rangle. \tag{2.2.22}$$

The state $|\Psi\rangle$ becomes the eigenvector of the transfer matrix $\mathbb{T}(\nu) = A(\nu) + D(\nu)$ if and only if $\Lambda_k^+ + \Lambda_k^- = 0$ $(k = 1, 2, \ldots, n)$ which is written in the following form:

$$(-1)^n \prod_{i=1}^{n} \frac{\sinh(2i\eta - \nu_k + \nu_i)}{\sinh(2i\eta - \nu_i + \nu_k)} = -\frac{a^N(\nu_k,\eta)}{b^N(\nu_k,\eta)}, \qquad k = 1, 2, \ldots, n. \tag{2.2.23}$$

(2.2.23) is the Bethe ansatz equation (BAE) for roots $\{\nu_1, \ldots, \nu_n\}$. The corresponding eigenvalue $t(\nu)$ is

$$t(\nu) = \Lambda^+ + \Lambda^- = a^N(\nu,\eta)\prod_{i=1}^{n} g(\nu_i-\nu) + b^N(\nu,\eta)\prod_{i=1}^{n} g(\nu-\nu_i). \tag{2.2.24}$$

Introducing the function $q(\nu)$ by

$$q(\nu) \coloneqq \prod_{i=1}^{n} \sinh(\nu-\nu_i), \tag{2.2.25}$$

(2.2.24) is also written as

$$t(\nu)q(\nu) = a^N(\nu,\eta)q(\nu+2i\eta) + b^N(\nu,\eta)q(\nu-2i\eta). \tag{2.2.26}$$

This is called the TQ-relation. Associated to the eigenfunction $q(\nu)$, a matrix $\mathbb{Q}(\nu)$ exists, which we call the Q-operator.

One can adapt this analysis to the model with a twisted boundary condition in which the BAE (2.2.23) is modified:

$$(-1)^n \prod_{i=1}^{n} \frac{\sinh(2i\eta - \nu_k + \nu_i)}{\sinh(2i\eta - \nu_i + \nu_k)} = -e^{-2i\phi}\frac{a^N(\nu_k,\eta)}{b^N(\nu_k,\eta)}, \qquad k = 1, 2, \ldots, n, \tag{2.2.27}$$

where ϕ is the twist parameter. With the twist, the operator $\mathbb{T}(\nu,\phi)$ enjoys

$$\mathbb{T}(\nu,\phi) = U\mathbb{T}(\nu,-\phi)U, \qquad U \coloneqq \overset{N}{\otimes}\sigma_x, \tag{2.2.28}$$

where σ_x represents the Pauli matrix. Let us discuss the ground state which is the Bethe state with $n = N/2$. Note that there are many solutions to the BAE, which differ by the periodicity, however, these configurations provide a unique ground state. The ground state eigenvalue $t_0(\nu,\phi)$ is an even function with respect to the twist parameter ϕ since t_0 is continuous at $\phi = 0$ and the ground state is singlet under the transformation (2.2.28), which obeys from the Perron-Frobenius theorem. Then the TQ-relation for the ground state eigenvalues with the twisted boundary condition becomes

$$t_0(\nu,|\phi|)q_0(\nu,\pm\phi) = a^N(\nu,\eta)\widetilde{q}_0(\nu+2i\eta,\pm\phi) + b^N(\nu,\eta)\widetilde{q}_0(\nu-2i\eta,\pm\phi), \tag{2.2.29}$$

where $\widetilde{q}_0(\nu,\phi) \coloneqq e^{-\frac{\nu\phi}{2\eta}}q_0(\nu,\phi)$ and $q_0(\nu,\phi)$ is the ground state eigenvalue of $\mathbb{Q}$ operator. We assume that q_0 is entire and $i\pi$-periodic as it was in the untwisted case (2.2.25).

The fusion hierarchy

The TQ-relation leads to other functional relations which are characteristic and useful in the study of the integrable models. In this subsection, we derive the so-called fusion hierarchy [89–93]. Let us introduce a function $\mathcal{W}$ defined by

$$\mathcal{W}(\nu) \coloneqq \frac{1}{\sinh^N\nu}[\widetilde{q}_0(\nu+i\eta,-\phi)\widetilde{q}_0(\nu-i\eta,\phi) - \widetilde{q}_0(\nu+i\eta,\phi)\widetilde{q}_0(\nu-i\eta,-\phi)], \tag{2.2.30}$$

which we call the quantum Wronskian. Multiplying both sides of the TQ-relation (2.2.29) by $\widetilde{q}_0(\nu,\mp\phi)a^{-N}(\nu,\eta)b^{-N}(\nu,\eta)$ and subtracting the terms, one obtains

$$\mathcal{W}(\nu+i\eta) = \mathcal{W}(\nu-i\eta), \tag{2.2.31}$$

where we used that N is even. From the periodicity of q_0 and (2.2.31), the quantum Wronskian $\mathcal{W}$ is $2i\eta$-periodic as well as $2i\pi$-periodic. Then, $\mathcal{W}$ becomes constant since we have set η/π irrational. The constant term is dependent on the twist parameter as [89]:

$$\mathcal{W} = 2i\sin\phi. \tag{2.2.32}$$

Again, Multiplying the TQ-relation by $\widetilde{q}_0(\nu - 2i\eta, \mp\phi)$ and subtracting, the ground state eigenvalue t_0 is written as

$$t_0(\nu, |\phi|) = \frac{1}{-\mathcal{W}}[\widetilde{q}_0(\nu + 2i\eta, -\phi)\widetilde{q}_0(\nu - 2i\eta, \phi) - \widetilde{q}_0(\nu + 2i\eta, \phi)\widetilde{q}_0(\nu - 2i\eta, -\phi)]. \quad (2.2.33)$$

Introducing the generalized quantum Wronskian

$$\mathcal{W}_q[k, -k](\nu) \coloneqq \det(\vec{q}_k, \vec{q}_{-k}), \quad (2.2.34)$$

where a two dimensional vector $\vec{q}_k$ is defined by

$$\vec{q}_k \coloneqq \frac{1}{\sqrt{-\mathcal{W}}}\big(e^{-ik\phi}q_0(\nu - ik\tilde{\eta}, \phi), e^{ik\phi}q_0(\nu - ik\tilde{\eta}, -\phi)\big)^T, \qquad \tilde{\eta} = \frac{\pi}{2} - \eta, \quad (2.2.35)$$

one finds $t_0 = \mathcal{W}_q[2, -2]$. The generalized quantum Wronskians $\mathcal{W}_q[k, -k]$ $(k = 0, 1, \dots)$ satisfy functional relations. Defining

$$t^{(m/2)}(\nu) \coloneqq \mathcal{W}_q[k + 1, -k - 1](\nu), \quad (2.2.36)$$

the Plücker type relation for the 2×2 matrix:

$$\det\left[\vec{a}, \vec{b}\right] \det\left[\vec{c}, \vec{d}\right] = \det\left[\vec{a}, \vec{d}\right] \det\left[\vec{c}, \vec{b}\right] + \det\left[\vec{a}, \vec{c}\right] \det\left[\vec{b}, \vec{d}\right], \quad (2.2.37)$$

where $\vec{a}, \vec{b}, \vec{c}$ and $\vec{d}$ are 2-vectors, leads to a set of functional relations called the fusion hierarchy:

$$\begin{aligned} &t^{(m)}(\nu - i\tilde{\eta})t^{(m)}(\nu + i\tilde{\eta}) \\ &\quad = t^{(0)}(\nu - i(2m + 1)\tilde{\eta})t^{(0)}(\nu + i(2m + 1)\tilde{\eta}) + t^{(m-1/2)}(\nu)t^{(m+1/2)}(\nu), \\ &t^{(1/2)}(\nu)t^{(m)}(\nu - i(2m + 1)\tilde{\eta}) \\ &\quad = t^{(0)}(\nu - i\tilde{\eta})t^{(m+1/2)}(\nu - i2m\tilde{\eta}) + t^{(0)}(\nu + i\tilde{\eta})t^{(m-1/2)}(\nu - i(2m + 2)\tilde{\eta}), \end{aligned} \quad (2.2.38)$$

where m takes the value of half-integer $\frac{1}{2}, 1, \frac{3}{2}, \dots$. If we consider the case where η/π is rational or the twist parameter ϕ is zero, one needs to more arguments in the derivation of (2.2.38), see [94–96], which we do not discuss here. An important consequence of the rational case is that the fusion hierarchy is truncated to a set of the finite number of functional equations. For the case where

$$\tilde{\eta} = \phi = \frac{\pi}{2M + 2}, \qquad M = \frac{1}{2}, 1, \frac{3}{2}, \dots, \quad (2.2.39)$$

the periodicity of the ground state eigenvalue q_0 and leads

$$t^M(\nu) = t^{(0)}(\nu), \qquad t^{(M+1/2)}(\nu) = 0, \tag{2.2.40}$$

$$t^{(m)}(\nu) = t^{(M-m)}(\nu), \qquad m = 0, \frac{1}{2}, 1, \ldots, \frac{M}{2}. \tag{2.2.41}$$

Also, for the generic value of the twist parameter ϕ, this truncation occurs [89].

Conformal limit

In the study of statistical mechanics, one of the main subjects of study is the phase transition. At the critical point where the transition occurs, the length of interaction diverges, and then it is believed that the system becomes conformal. From the point of view of the lattice model, we can study the model at the critical point by taking the continuum limit $N \to \infty$. For the 2-dimensional models, the system at the critical point would have the infinite-dimensional Virasoro symmetry and be characterized by the (effective) Virasoro central charge c_{eff}. The effective central charge of the six-vertex model in the limit is [97–99]

$$c_{\text{eff}} = 1 - \frac{6\phi^2}{\pi(\pi - 2\eta)} = 1 - 24\left(\frac{p}{\beta}\right)^2, \qquad \beta^2 = 1 - \frac{2\eta}{\pi}, \quad p = \frac{\phi}{2\pi}. \tag{2.2.42}$$

In the continuum limit, only the ground state is in our interest. The ground state is the state $|\Psi(\nu_1, \nu_2, \ldots, \nu_n)\rangle$ where $n = N/2$ and the distinct roots ν_i $(i = 1, 2, \ldots, n)$, satisfying the BAE in the limit, are real numbers [14, 100]. Since the roots behave as $\nu \sim -\frac{2\eta}{\pi} \log N$ at $N \to \infty$ [101], we set the alternative roots E_i as

$$E_i = N^{\frac{4\eta}{\pi}} e^{2\nu_i}, \qquad i = 1, 2, \ldots, \tag{2.2.43}$$

so that E_i remains finite in this limit. Then, the BAE (2.2.27) becomes

$$\prod_{k=1}^{\infty} e^{2i\phi} \frac{E_k - \omega^2 E_i}{E_k - \omega^{-2} E_i} = -1, \qquad i = 1, 2, \ldots, \tag{2.2.44}$$

where we defined $\omega = -e^{-2i\eta}$. Taking the continuum limit to the ground state eigenvalues t_0 and q_0, TQ-relation (2.2.29) results in

$$t_0(E) q_0(E) = e^{i\phi} q_0(\omega^2 E) + e^{-i\phi} q_0(\omega^{-2} E). \tag{2.2.45}$$

We can also take the limit of the fusion hierarchy (2.2.38):

$$\begin{aligned} t^{(m)}(\omega^{-1}E)t^{(m)}(\omega E) &= 1 + t^{(m-1/2)}(E)t^{(m+1/2)}(E), \\ t^{(1/2)}(E)t^{(m)}(\omega^{2m+1}E) &= t^{(m+1/2)}(\omega^{2m}E) + t^{(m-1/2)}(\omega^{2m+2}E). \end{aligned} \tag{2.2.46}$$

If we set $\eta/M = \phi = \frac{\pi}{2M+2}$ with $2M \in \mathbb{Z}_{>0}$, these relations would be truncated. Introducing the T-functions by

$$T_m(E) \coloneqq t^{(m/2)}(E), \qquad m = 1, 2, \ldots, r, \tag{2.2.47}$$

where $r = 2M - 1$, the fusion hierarchy (2.2.46) is uniformly written as

$$T_a(\omega^{-1}E)T_a(\omega E) = 1 + \prod_{b=1}^{r} [T_b(E)]^{G_{ab}}, \qquad a = 1, 2, \ldots, r. \tag{2.2.48}$$

Here we defined G_{ab} as the incidence matrix of A_r-type Lie algebra. We call (2.2.48) the T-system. One can write the T-system as another functional relation called Y-system [16]:

$$Y_a(\omega E)Y_a(\omega^{-1}E) = \prod_{b=1}^{r} (1 + Y_b(E))^{G_{ab}}, \qquad a = 1, 2, \ldots, r, \tag{2.2.49}$$

where we defined the Y-function by

$$Y_a(E) \coloneqq \prod_{b=1}^{r} [T_b(E)]^{G_{ab}}. \tag{2.2.50}$$

It may be more convenient to write (2.2.49) by introducing a canonical variable $\theta \coloneqq \frac{M+1}{hM} \log E$ where $h = r + 1$ is the Coxeter number of A_r:

$$Y_a(\theta + i\frac{\pi}{h})Y_a(\theta - i\frac{\pi}{h}) = \prod_{b=1}^{r} (1 + Y_b(\theta))^{G_{ab}}, \qquad a = 1, 2, \ldots, r. \tag{2.2.51}$$

The BAEs for other lattice models

In this section, we have seen that there are functional relations which is characteristic to the integrable models from the analysis of the six-vertex models. We also saw that the ground state energy of the six-vertex model is controlled by the algebraic equations of the spectral parameters, which is the Bethe ansatz equation. The lattice models in two

dimensions have been classified for any semi-simple Lie algebras $\mathfrak{g}$. The BAEs for the models in the conformal limit are given by [10–13]

$$\prod_{b=1}^{\operatorname{rank}\mathfrak{g}} \Omega^{-C_{ab}\gamma_b/2}\frac{Q^{(b)}(\Omega^{-C_{ab}/2}E_i^{(a)},\vec{\gamma})}{Q^{(b)}(\Omega^{C_{ab}/2}E_i^{(a)},\vec{\gamma})} = -1, \qquad i=1,2,\dots, \quad a=1,\dots,\operatorname{rank}\mathfrak{g}. \tag{2.2.52}$$

Here $Q^{(a)}(E,\vec{\gamma})$ is the Q-function, the ground state eigenvalue of the Q-operator, which has zeros at $E_i^{(b)}$ $(i=1,2,\dots)$:

$$Q^{(a)}(E,\vec{\gamma}) = Q^{(a)}(0,\vec{\gamma})\prod_{i=1}^{\infty}\left(1-\frac{E}{E_i^{(a)}}\right). \tag{2.2.53}$$

$\vec{\gamma} = (\gamma_1,\dots,\gamma_{\operatorname{rank}\mathfrak{g}})$ is the twist parameter, C_{ab} is the Cartan matrix[3] of $\mathfrak{g}$, and $\Omega = \exp\left(\frac{2\pi i}{h^\vee\mu}\right)$ with the dual Coxeter number $h^\vee$ and anisotropy μ. The six-vertex model corresponds to $\mathfrak{g}=A_1$ case. If we choose $\mathfrak{g}=A_1$, $\gamma_1 = -\frac{\eta}{\pi}\phi$, and $\mu = \frac{\pi}{4\eta}$, we recover the BAE of the six-vertex model in the conformal limit (2.2.44).

2.3 NLIE for simply-laced Lie algebras

In the previous subsection, we introduced the BAEs for any semi-simple Lie algebras $\mathfrak{g}$. The spectrum of the theory in the thermodynamic limit is calculated by solving the BAEs, which is hard in algebraic methods. There is an alternative way to solve it, in which we convert the BAE into a system of non-linear integral equations (NLIE). In the following, we see the NLIE for the simply-laced Lie algebras [26–28], for which the Bethe roots E_i are real and positive. Let us introduce a function $\mathfrak{a}^{(a)}(E)$ defined by

$$\mathfrak{a}^{(a)}(E) \coloneqq \prod_{b=1}^{\operatorname{rank}\mathfrak{g}} \Omega^{-C_{ab}\gamma_b/2}\frac{Q^{(b)}(\Omega^{-C_{ab}/2}E,\vec{\gamma})}{Q^{(b)}(\Omega^{C_{ab}/2}E,\vec{\gamma})}, \qquad a=1,\dots,\mathfrak{g}. \tag{2.3.1}$$

Clearly, the BAE (2.2.52) is equivalent to $\mathfrak{a}^{(a)}(E_i^{(a)})+1=0$ for $i\in\mathbb{N}$ and $a=1,\dots,\mathfrak{g}$. Taking the logarithm of the counting function, one obtains

$$\log\mathfrak{a}^{(a)}(E) = -\frac{\pi i}{h\mu}\sum_b C_{ab}\gamma_b + \sum_b\sum_{k=1}^{\infty} f_{ab}\left(\frac{E}{E_k^{(b)}}\right), \tag{2.3.2}$$

[3]For the notation of Lie algebras, see appendix A.

where $f_{ab}(E)$ is defined by

$$f_{ab}(E) \coloneqq \log\left(\frac{1-\Omega^{-C_{ab}/2}E}{1-\Omega^{C_{ab}/2}E}\right). \tag{2.3.3}$$

Since the logarithmic derivative $\partial_E \log\bigl(1+\mathfrak{a}^{(a)}(E)\bigr)$ has simple poles at $E_k^{(a)}$, the sum of k in (2.3.2) can be replaced by an integral:

$$\log \mathfrak{a}^{(a)}(E) = -\frac{\pi i}{h\mu}\sum_b C_{ab}\gamma_b + \sum_b \int_{\mathcal{C}} \frac{\mathrm{d}E'}{2\pi i} f_{ab}\left(\frac{E}{E'}\right)\partial_{E'}\log\bigl(1+\mathfrak{a}^{(b)}(E')\bigr), \tag{2.3.4}$$

where the contour $\mathcal{C}$ runs from ∞ to the origin above the real axis and return to ∞ below the real axis. It is convenient to regard $\mathfrak{a}^{(a)}(E)$ as a function of $\theta = \mu \log E$ rather than E. Integrating by parts, (2.3.4) becomes

$$\begin{aligned}\log \mathfrak{a}^{(a)}(\theta) = -\frac{\pi i}{h\mu}\sum_b C_{ab}\gamma_b &- \sum_b \int_{\mathcal{C}_1} \mathrm{d}\theta' \partial_{\theta'} R_{ab}(\theta-\theta')\log\bigl(1+\mathfrak{a}^{(b)}(\theta')\bigr) \\ &+ \sum_b \int_{\mathcal{C}_2} \mathrm{d}\theta' \partial_{\theta'} R_{ab}(\theta-\theta')\log\bigl(1+\mathfrak{a}^{(b)}(\theta')\bigr),\end{aligned} \tag{2.3.5}$$

where we defined $R_{ab}(\theta)$ by

$$R_{ab}(\theta) = \frac{i}{2\pi}\partial_\theta f_{ab}(e^{\frac{\theta}{\mu}}), \tag{2.3.6}$$

and the contour $\mathcal{C}_1$ runs from $-\infty$ to ∞ above the real axis while the contour $\mathcal{C}_2$ runs from ∞ to $-\infty$ below the real axis. The Bethe roots and the integration contours on the θ-plane are illustrated in figure 2.3.1.

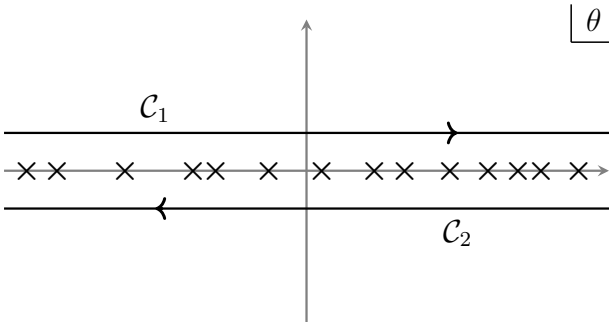

Figure 2.3.1: The Bethe roots (cross points) and the contours $\mathcal{C}_1$ and $\mathcal{C}_2$ on the θ-plane.

Using the property $\mathfrak{a}^{(a)}(\theta)^* = \mathfrak{a}(\theta^*)^{-1}$, which obeys from the BAE, and applying the Fourier transformation, (2.3.5) leads

$$\begin{aligned}&\sum_b (\delta_{ab} - \mathcal{F}[R_{ab}](k))\mathcal{F}\big[\log \mathfrak{a}^{(b)}\big](k)\\ &\qquad = -\frac{2\pi^2 i}{h\mu}\sum_b C_{ab}\gamma_b\delta(k) - 2i\sum_b \mathcal{F}[R_{ab}](k)\,\mathrm{Im}\,\mathcal{F}\big[\log\big(1+\mathfrak{a}^{(b)}\big)\big](k),\end{aligned} \tag{2.3.7}$$

where the (inverse) Fourier transformation is

$$\mathcal{F}[g](k) \coloneqq \int_{-\infty}^{\infty} \mathrm{d}x e^{-ikx}\, g(x), \qquad \mathcal{F}^{-1}[\widetilde{g}](x) \coloneqq \frac{1}{2\pi}\int_{-\infty}^{\infty} \mathrm{d}k e^{ikx}\, g(x). \tag{2.3.8}$$

Multiplying both sides by the inverse matrix $(\mathbf{I} - \mathcal{F}[R](k))^{-1}$ and taking the inverse Fourier transformation, one obtains

$$\begin{aligned}\log\mathfrak{a}^{(a)}(\theta) &= -\frac{\pi i}{h\mu}\sum_{b,c}\mathcal{F}^{-1}\big[(\mathbf{I}-\mathcal{F}[R])^{-1}_{ab}\big](0)C_{bc}\gamma_c - ib_0 M_a e^{\theta}\\ &\quad - 2i\sum_b \int_{-\infty-i0}^{\infty-i0}\mathrm{d}\theta'\mathcal{F}^{-1}\big[(\mathbf{I}-\mathcal{F}[R])^{-1}\mathcal{F}[R]\big]_{ab}(\theta-\theta')\,\mathrm{Im}\log\big(1+\mathfrak{a}^{(b)}(\theta')\big),\end{aligned} \tag{2.3.9}$$

where the second term in the right hand side is real constant and arises from the zero modes, which is determined from the asymptotic behavior of $\log\mathfrak{a}^{(a)}$ with M_a satisfying

$$2M_a\cos\frac{\pi}{h} = \sum_{b=1}^{\mathrm{rank}\,\mathfrak{g}} G_{ab}M_a, \tag{2.3.10}$$

where G_{ab} is the incidence matrix of $\mathfrak{g}$. The vector $(M_1, M_2, \ldots, M_{\mathrm{rank}\,\mathfrak{g}})$ is called the Perron-Frobenius eigenvector. Normalizing $M_1 = 1$, each component of the Perron-Frobenius eigenvector takes the value as in Table 2.3.1. Simplifying the equation (2.3.9), we obtain the NLIE:

$$\begin{aligned}\ln\mathfrak{a}^{(a)}(\theta) = i\pi\hat{\alpha}_a - ib_0M_ae^{\theta} &+ \sum_{b=1}^{\mathrm{rank}\,\mathfrak{g}}\int_{\mathcal{C}_1}\mathrm{d}\theta'\,\varphi_{ab}(\theta-\theta')\ln\big(1+\mathfrak{a}^{(b)}(\theta')\big)\\ &- \sum_{b=1}^{\mathrm{rank}\,\mathfrak{g}}\int_{\mathcal{C}_2}\mathrm{d}\theta'\,\varphi_{ab}(\theta-\theta')\ln\left(1+\frac{1}{\mathfrak{a}^{(b)}(\theta')}\right),\end{aligned} \tag{2.3.11}$$

where the kernel function $\phi_{ab}(\theta)$ is defined by

$$\varphi_{ab}(\theta) = \int_{-\infty}^{\infty}\frac{\mathrm{d}k}{2\pi}e^{ik\theta}\left(\delta_{ab} - \frac{\sinh(\mu\pi k)}{\sinh((h\mu-1)\pi k/h)\cosh(\pi k/h)}C^{-1}_{ab}(k)\right). \tag{2.3.12}$$

$\mathfrak{g}$	M_a
A_r $(h=r+1)$	$M_a=\dfrac{\sin(a\pi/h)}{\sin(\pi/h)},\quad (a=1,\dots,r)$
D_r $(h=2r-2)$	$M_a=\dfrac{\sin(a\pi/h)}{\sin(\pi/h)},\quad (a=1,\dots,r-2),\qquad M_{r-1}=M_r=\dfrac{1}{2\sin(\pi/h)}$
E_6 $(h=12)$	$M_1=M_5=1,\quad M_2=M_4=\dfrac{\sin(2\pi/h)}{\sin(\pi/h)},\quad M_3=\dfrac{\sin(3\pi/h)}{\sin(\pi/h)},\qquad M_6=\dfrac{\sin(3\pi/h)}{\sin(2\pi/h)}$
E_7 $(h=18)$	$M_1=1,\quad M_2=\dfrac{\sin(2\pi/h)}{\sin(\pi/h)},\quad M_3=\dfrac{\sin(3\pi/h)}{\sin(\pi/h)},\quad M_4=\dfrac{\sin(4\pi/h)}{\sin(\pi/h)}$ $M_5=\dfrac{\sin(5\pi/h)}{\sin(\pi/h)}-\dfrac{\sin(4\pi/h)}{\sin(2\pi/h)},\quad M_6=\dfrac{\sin(6\pi/h)}{\sin(\pi/h)}-\dfrac{\sin(4\pi/h)}{\sin(\pi/h)},\quad M_7=\dfrac{\sin(4\pi/h)}{\sin(2\pi/h)}$
E_8 $(h=30)$	$M_1=1,\quad M_2=\dfrac{\sin(2\pi/h)}{\sin(\pi/h)},\quad M_3=\dfrac{\sin(3\pi/h)}{\sin(\pi/h)},\quad M_4=\dfrac{\sin(4\pi/h)}{\sin(\pi/h)},\qquad M_5=\dfrac{\sin(5\pi/h)}{\sin(\pi/h)},$ $M_6=\dfrac{\sin(6\pi/h)}{\sin(\pi/h)}-\dfrac{\sin(5\pi/h)}{\sin(2\pi/h)},\quad M_7=\dfrac{\sin(7\pi/h)}{\sin(\pi/h)}-\dfrac{\sin(5\pi/h)}{\sin(\pi/h)},\quad M_8=\dfrac{\sin(5\pi/h)}{\sin(2\pi/h)}$

Table 2.3.1: The Perron-Frobenius vectors for simply-laced Lie algebras

$C_{ab}(k)$ is the deformed Cartan matrix:

$$C_{ab}(k) \coloneqq \begin{cases} 2, & a=b, \\ \dfrac{C_{ab}}{\cosh(\pi k/h)}, & a\neq b, \end{cases} \tag{2.3.13}$$

and the constant $\hat{\alpha}_a$ is defined from γ_a by

$$\hat{\alpha}_a \coloneqq (1-h\mu)^{-1}\,\gamma_a. \tag{2.3.14}$$

The effective central charge of the conformal theory characterized by the BAE (2.2.52) of simply-laced Lie algebra is computed from the counting function as [22, 27, 28]

$$c_{\text{eff}} = 2\times\frac{3}{\pi^2}\sum_{a}^{\text{rank }\mathfrak{g}} ib_0 M_a\left[\int_{\mathcal{C}_1} \mathrm{d}\theta\, e^{\theta}\log\bigl(1+\mathfrak{a}^{(a)}(\theta)\bigr) - \int_{\mathcal{C}_2}\mathrm{d}\theta\, e^{\theta}\log\left(1+\frac{1}{\mathfrak{a}^{(a)}(\theta)}\right)\right]. \tag{2.3.15}$$

The factor 2 comes from the kink and anti-kink configuration of the counting function. Evaluating the counting function at the $\theta\to-\infty$ limit:

$$i\ln\mathfrak{a}^{(a)}(-\infty) = \left(\frac{1}{h\mu}-1\right)\pi\sum_{b=1}^{\text{rank }\mathfrak{g}} C_{ab}\hat{\alpha}_b, \tag{2.3.16}$$

we find

$$c_{\text{eff}} = \text{rank }\mathfrak{g} - \frac{3(h\mu-1)}{h\mu}\sum_{a,b=1}^{\text{rank }\mathfrak{g}}\hat{\alpha}_a C_{ab}\hat{\alpha}_b. \tag{2.3.17}$$

2.4 Thermodynamic Bethe ansatz equations

The free energies of the equilibrium states of integrable models in thermodynamic settings, whose spectrum obeys the Bethe ansatz, are computed from a system of integral equations called the Thermodynamic Bethe ansatz (TBA) equations [15]. The TBA equations are converted to a functional relation which is the Y-system. In this section, we introduce the TBA equations from the T-/Y-systems. Another derivation for the TBA equations is shown in appendix B, in which the physical meanings of quantities in the TBA may be clear.

The G-type TBA equations

As we saw in section 2.2, the G-type Y-system where G is the simply-laced Lie algebra is [16]

$$Y_a^{[+1]}(\theta)Y_a^{[-1]}(\theta) = \prod_{b=1}^{r} (1 + Y_b(\theta))^{G_{ab}}, \tag{2.4.1}$$

where we have introduced the notation $Y^{[\pm k]}$ by

$$Y^{[\pm k]}(\theta) \coloneqq Y(\theta \pm i\frac{\pi k}{h}). \tag{2.4.2}$$

Here G_{ab} is the incidence matrix, r is the rank, and h is the Coxeter number of G. The TBA equation is a system of integral equations with respect to the logarithm of the Y-functions. Then we introduce $\epsilon(\theta)$ by

$$\epsilon_a(\theta) \coloneqq \log Y_a(\theta), \tag{2.4.3}$$

which is called the pseudoenergy. Taking the logarithm of the Y-system (2.4.1), one obtains

$$\epsilon_a^{[+1]}(\theta) + \epsilon_a^{[-1]}(\theta) - \sum_{b=1}^{r} G_{ab}\epsilon_b(\theta) = \sum_{b=1}^{r} L_b(\theta), \tag{2.4.4}$$

where we defined $L_a(\theta)$ by

$$L_a(\theta) \coloneqq \log\left(1 + Y_a^{-1}(\theta)\right). \tag{2.4.5}$$

As we saw for the $G = A_r$ case, the Y-function is the product of the T-function. Then, the asymptotic behavior of the pseudo-energy is assumed to be[4]

$$\epsilon_a(\theta) = m_a e^{\theta}, \qquad \theta \to \infty. \tag{2.4.6}$$

We call m_a the mass. Evaluating the equation (2.4.4) at the large θ, since the right hand side vanishes, one finds that m_a satisfies the equation (2.3.10) and is then proportional to the Perron-Frobenius eigenvector. Taking the Fourier transform of (2.4.4), one obtains

$$\sum_{b=1}^{r} \left(2\delta_{ab} \cosh\left(\frac{\pi k}{h}\right) - G_{ab} \right) \widetilde{f}_b(k) = \sum_{b=1}^{r} G_{ab} \widetilde{L}_b(k), \tag{2.4.7}$$

where $f_a(\theta) \coloneqq \log Y_a(\theta) - m_a e^{\theta}$, and $\widetilde{f}$ and $\widetilde{L}_a$ are defined according to (2.3.8). Solving (2.4.7) with respect to $\widetilde{f}_a$ and applying the inverse Fourier transform, one obtains the TBA equation of G-type:

$$\epsilon_a(\theta) = m_a e^{\theta} - \frac{1}{2\pi} \sum_{b=1}^{r} (K_{ab} \star L_b)(\theta), \qquad a = 1, 2, \ldots, r, \tag{2.4.8}$$

where we denote the convolution of functions by

$$(g \star h)(\theta) \coloneqq \int_{-\infty}^{\infty} g(\theta - \theta') h(\theta') \mathrm{d}\theta, \tag{2.4.9}$$

and the kernel function K_{ab} is defined by

$$K_{ab}(\theta) \coloneqq - \int_{-\infty}^{\infty} \left[\sum_{c=1}^{r} \left(2\delta_{ac} \cosh\left(\frac{\pi k}{h}\right) - G_{ac} \right)^{-1} G_{cb} \right] e^{ik\theta} \, \mathrm{d}k \, . \tag{2.4.10}$$

The kernel function is also represented by the S-matrix S_{ab} of integrable models [30]:

$$K_{ab}(\theta) = -i \frac{\mathrm{d}}{\mathrm{d}\theta} \log S_{ab}(\theta). \tag{2.4.11}$$

The S-matrix for the simply-laced Lie algebra G is studied in [102]. For $G = A_r$, the S-matrix is

$$S_{ab}(\theta) = \prod_{\substack{x = |a-b|+1 \\ \text{step2}}}^{a+b-1} \{x\}, \qquad a, b = 1, 2, \ldots, r, \tag{2.4.12}$$

[4]We are considering only the kink contribution. Together with the anti-kink contribution, the deriving term is proportional to $\cosh\theta$.

where $\{x\}$ is defined by

$$\{x\} \coloneqq (x-1)(x+1), \qquad (x) \coloneqq \frac{\sinh\left(\frac{\theta}{2}+i\frac{\pi x}{2h}\right)}{\sinh\left(\frac{\theta}{2}-i\frac{\pi x}{2h}\right)}. \tag{2.4.13}$$

Together with the symmetry $m_a = m_{h-a}$ $(a = 1, 2, \ldots, r)$ and the explicit form of the kernel function, we obtain the $\mathbb{Z}_2$ symmetry of the Y-functions:

$$Y_a = Y_{h-a}, \qquad a = 1, 2, \ldots, r. \tag{2.4.14}$$

For $G = D_r$, we need to distinguish the r even and r odd cases. For the even r, the S-matrix becomes

$$\begin{aligned}
S_{a,b} &= \prod_{\substack{x=|a-b|+1 \\ \text{step2}}}^{a+b-1} \{x\}\{h-x\}, \qquad a, b = 1, 2, \ldots, r-2, \\
S_{a,r-1} = S_{a,r} &= \prod_{\substack{x=0 \\ \text{step2}}}^{2a-2} \{r-a+x\}, \qquad a = 1, 2, \ldots, r-2, \\
S_{r-1,r-1} = S_{r,r} &= \prod_{\substack{x=1 \\ \text{step4}}}^{h-1} \{x\}, \qquad S_{r-1,r} = \prod_{\substack{x=3 \\ \text{step4}}}^{h-3} \{x\},
\end{aligned} \tag{2.4.15}$$

where $h = 2r-2$ is the Coxeter number of D_r and $\{x\}$ is defined in (2.4.13). For the odd r, the differences of the S-matrix for the even r case are

$$S_{r-1,r-1} = S_{r,r} = \prod_{\substack{x=1 \\ \text{step4}}}^{h-3} \{x\}, \qquad S_{r-1,r} = \prod_{\substack{x=3 \\ \text{step4}}}^{h-1} \{x\}. \tag{2.4.16}$$

For E-type S-matrix, we do not have the uniform formula. Here we only write down that for E_6:

$$\begin{aligned}
&S_{11} = \{1\}\{7\}, \quad S_{21} = \{4\}\{6\}\{10\}, \qquad S_{22} = \{1\}\{3\}\{5\}\{7\}^2\{9\}, \\
&S_{31} = 3\ 5, \qquad S_{32} = 2\ 4^2\ 6, \qquad S_{33} = 1\ 3^2\ 5^2, \\
&S_{41} = \{2\}\{6\}\{8\}, \quad S_{42} = \{3\}\{5\}^2\{7\}\{9\}\{11\}, \quad S_{43} = 2\ 4^2\ 6, \\
&S_{44} = \{1\}\{3\}\{5\}\{7\}^2\{9\}, \\
&S_{51} = \{5\}\{11\}, \quad S_{52} = \{2\}\{6\}\{8\}, \quad S_{53} = 3\ 5, \quad S_{54} = \{4\}\{6\}\{10\}, \\
&S_{55} = \{1\}\{7\}, \\
&S_{61} = 4, \quad S_{62} = 3\ 5, \quad S_{63} = 2\ 4\ 6, \quad S_{64} = 3\ 5, \quad S_{65} = 4, \quad S_{66} = 1\ 5,
\end{aligned} \tag{2.4.17}$$

where we defined $x \coloneqq \{x\}\{12-x\}$.

The (A_r, A_N)-type TBA equations

The generalization of the Y-system and TBA equations can be found in [17, 18]. The (G, G')-type Y-system [17], where G and G' are the simply-laced Lie algebra, is

$$Y_{a,i}(\theta + i\frac{\pi}{h})Y_{a,i}(\theta - i\frac{\pi}{h}) = \frac{\prod_{b=1}^{r}(1+Y_{b,i}(\theta))^{G_{ab}}}{\prod_{j}^{r'}\left(1+Y_{a,j}^{-1}(\theta)\right)^{G'_{ij}}}, \tag{2.4.18}$$

where G_{ab} (G'_{ij}) is the incidence matrix, r (r') is the rank, and h is the Coxeter number of G (G').[5] In this thesis, we especially focus on the case $G = A_r$ and $G' = A_N$. The (A_r, A_N)-type Y-system becomes

$$Y_{a,i}^{[+1]}(\theta)Y_{a,i}^{[-1]}(\theta) = \frac{\prod_{b=1}^{r}(1+Y_{b,i}(\theta))^{G_{ab}}}{\left(1+Y_{a,i-1}^{-1}(\theta)\right)\left(1+Y_{a,i+1}^{-1}(\theta)\right)}. \tag{2.4.19}$$

Note that this system follows from the (A_r, A_N)-type T-system:

$$T_{a,i}^{[+1]}T_{a,i}^{[-1]} = T_{a,i+1}T_{a,i-1} + T_{a+1,i}T_{a-1,i}, \tag{2.4.20}$$

with the relations between the T-functions and the Y-functions:

$$Y_{a,i} = \frac{T_{a-1,i}T_{a+1,i}}{T_{a,i+1}T_{a,i-1}}. \tag{2.4.21}$$

In a similar way for the G-type TBA equation, we can derive (A_r, A_N)-type TBA equations. Defining the pseudoenergy by $\epsilon_{a,i} \coloneqq \log Y_{a,i}$, $f_{a,i} \coloneqq \epsilon_{a,i} - m_{a,i}$ where $\epsilon_{a,i} \sim m_{a,i}e^{\theta}$ ($\theta \to \infty$), and $L_{a,i} = \log\left(1+Y_{a,i}^{-1}\right)$, one obtains

$$f_{a,i}^{[+1]} + f_{a,i}^{[-1]} - \sum_{b=1}^{r} G_{ab}f_{b,i} = \sum_{b=1}^{r} G_{ab}L_{b,i} - L_{a,i+1} - L_{a,i-1}. \tag{2.4.22}$$

Here we used the fact that the vector $(m_{1,i}, m_{2,i}, \ldots, m_{r,i})$ $(i = 1, 2, \ldots, N)$ is proportional to the Perron-Frobenius eigenvector. Solving this in terms of $f_{a,i}$, the (A_r, A_N)-type TBA equations are obtained as:

$$\epsilon_{a,i}(\theta) = m_{a,i}e^{\theta} - \frac{1}{2\pi}\sum_{b=1}^{r}(K_{ab} \star L_{b,i})(\theta) + \frac{1}{2\pi}\sum_{b=1}^{r}(K'_{ab} \star (L_{b,i-1} + L_{b,i+1}))(\theta), \tag{2.4.23}$$

[5] Our notation is different from [17]. The (G, G')-type Y-system in our notation is (G', G)-type in [17].

where K_{ab} is the same as the one defined in (2.4.10), while K'_{ab} is given by

$$K'_{ab} \coloneqq -\mathcal{F}^{-1}\left[\left(2\delta_{ab}\cosh\left(\frac{\pi k}{h}\right) - G_{ab}\right)^{-1}\right]. \tag{2.4.24}$$

One can compute the effective central charges of the conformal theory by the formula:

$$c_{\text{eff}} \coloneqq \frac{6}{\pi^2}\sum_{a=1}^{r}\sum_{k=1}^{N}\int_{-\infty}^{\infty} m_{a,k}L_{a,k}(\theta)e^{\theta}\,\mathrm{d}\theta\,. \tag{2.4.25}$$

This can be evaluated by the UV limit of the Y-function $\log Y(-\infty)$ which takes the constant value [93, 103]:

$$c_{\text{eff}} = \frac{rN(N+1)}{r+N+2}. \tag{2.4.26}$$

Summary

In this chapter, we reviewed the properties of the integrable models. The two dimensional (quantum) integrable model is ensured its integrability by the Yang-Baxter equation. We also derived the functional relations which are characteristic of the integrable models. As an example of the two dimensional integrable lattice model, we reviewed the analysis of the six-vertex model. The spectrum of the model was governed by the Bethe ansatz equations. In the conformal limit, the roots of the BAEs are obtained by the non-linear integral equations (NLIEs). In the thermodynamic setting, we converted the Y-system into a system of integral equations, the thermodynamic Bethe ansatz (TBA) equations. From the TBA equation, one can compute the effective central charge which is the leading term of the free energy of the equilibrium state.

Chapter 3

ODE/IM correspondence and numerical tests for affine Lie algabras

The functional relations which we found in the integrable model in the previous section also emerge in the context of the ordinary differential equation (ODE). This implies the non-trivial connection between the theory of the ordinary differential equation and 2-dimensional integrable models, which we call the ODE/IM correspondence. In this chapter, we will first discuss the ODE/IM correspondence for the Schrödinger equation with monomial potential as well as the angular momentum term. Then, we will introduce the generalization of the correspondence for any semi-simple Lie algebras following [34, 35, 39]. We will also discuss the method to compute the zeros of the Q-functions from the ODE, which is useful to test the correspondence numerically.

3.1 The ODE/IM for the Schrödinger equation

It was first uncovered that there exists the ODE/IM correspondence for the Schrödinger equation with monomial potential [1]. The corresponding integrable model was the six-vertex model which we reviewed in section 2.2. Soon after that, the generalization to the potential with the angular momentum was discussed in [20, 21]. The ODE considered there has the form:

$$\left[-\frac{\mathrm{d}^2}{\mathrm{d}x^2} + x^{2M} + \frac{l(l+1)}{x^2}\right]\psi(x, E, l) = E\psi(x, E, l). \tag{3.1.1}$$

Here we denote the angular momentum as l and the eigenenergy as E, and we suppose the real value l satisfies $l > -\frac{1}{2}$, and the variables x and E could take the complex values. The physically natural solution $y(x, E, l)$ to this problem has the asymptotic behaviors $y \to 0$ as $x \to \infty$. The WKB approximation leads that such a solution, on the real axis, $y(x, E, l)$ behaves as

$$y(x, E, l) \sim \frac{x^{-\frac{M}{2}}}{\sqrt{2i}} \exp\left[-\frac{1}{M+1}x^{M+1}\right], \qquad |x| \to \infty. \tag{3.1.2}$$

(3.1.2) implies that the solution y decays not only along the real axis but also in the complex domain:

$$\left\{x \in \mathbb{C}; \arg x < \frac{\pi}{2M+2}\right\}. \tag{3.1.3}$$

Since the order of the differential equation is second, there is another solution that exponentially grows in the domain. We call the exponentially growing solution the dominant solution, while we call the exponentially decaying solution y the subdominant solution. Note that the subdominant solution is unique up to the constant multiplier. The solution y is subdominant in the domain but no longer subdominant in other regions. To find the subdominant solutions in other regions, we use the invariance of the differential equation with respect to the simultaneous rescaling of the coordinate x and the energy E:

$$x \to \omega^{-1}x, \qquad E \to \omega^2 E, \qquad \omega \coloneqq e^{\frac{2\pi i}{2M+2}}, \tag{3.1.4}$$

which is called the Symanzik (Sibuya) rotation [19, 104]. Then, the Symanzik rotated solution $y(\omega^{-1}x, \omega^{-2}E, l)$ also solves the differential equation (3.1.1). Let us introduce the k-rotated solution $y_k(x, E, l)$ for $k \in \mathbb{Z}$ by

$$y_k(x, E) \coloneqq \omega^{\frac{k}{2}} y(\omega^{-k}x, \omega^{2k}E, l), \qquad k \in \mathbb{Z}, \tag{3.1.5}$$

which is subdominant in the domain $\mathcal{S}_k$:

$$\mathcal{S}_k \coloneqq \left\{x \in \mathbb{C}; \left|\arg x - \frac{2\pi i k}{2M+2}\right| < \frac{\pi i}{2M+2}\right\}, \qquad k \in \mathbb{Z}. \tag{3.1.6}$$

We call the domain $\mathcal{S}_k$ the Stokes sector. Figure 3.1.1 illustrates the Stokes sectors. For any k, the set of the linearly independent solutions $\{y_k, y_{k+1}\}$ forms the basis of the

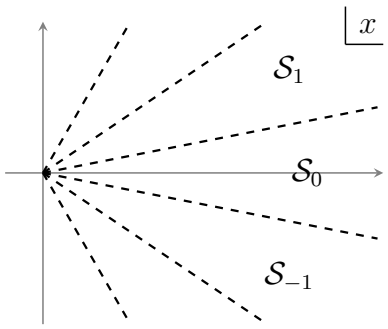

Figure 3.1.1: The Stokes sectors.

solution to the differential equation (3.1.1). Consider $k = 0$ case, and expand the solution y_{-1} by the basis:

$$y_{-1}(x, E, l) = C(E, l)y_0(x, E, l) + \widetilde{C}(E, l)y_1(x, E, l), \tag{3.1.7}$$

where the coefficients $C(E, l)$ and $\widetilde{C}(E, l)$ are the Stokes multipliers. It is easy to find the Stokes multipliers are given by

$$C(E, l) = \frac{W_{-1,1}}{W_{0,1}}, \qquad \widetilde{C}(E, l) = -\frac{W_{-1,0}}{W_{0,1}}. \tag{3.1.8}$$

Here W_{k_1,k_2} are defined by the Wronskian $W[\cdot, \cdot]$:

$$W_{k_1,k_2} \coloneqq W[y_{k_1}, y_{k_2}] = y_{k_1}\partial_x y_{k_2} - \partial_x y_{k_1} y_{k_2}. \tag{3.1.9}$$

Using the property

$$W[y_{k_1+1}, y_{k_2+1}](E, l) = W[y_{k_1}, y_{k_2}](\omega^{-2}E, l), \tag{3.1.10}$$

and $W_{0,1} = 1$, which is led from the linear independence of the basis and the normalization, we reach

$$C(E, l)y_0(x, E, l) = y_{-1}(x, E, l) + y_1(x, E, l). \tag{3.1.11}$$

where $C(E, l) = W_{-1,1}$. The above arguments are all about the solution of which we set the asymptotic behaviors at $|x| \to \infty$. To see the correspondence to the six-vertex model, we also have to consider the solutions whose asymptotic behaviors near the origin are

defined. Let $\chi^{\pm}(x, E, l)$ be the solutions that behave near the origin as

$$\begin{aligned} \chi^{+}(x, E, l) &\sim x^{l+1} + \cdots, \\ \chi^{-}(x, E, l) &\sim x^{-l} + \cdots, \end{aligned} \qquad x \to 0. \tag{3.1.12}$$

χ^{+} and χ^{-} are linearly independent. Analogous to (3.1.5), we introduce the Symanzik rotation of $\chi^{\pm}$:

$$\chi_k^{\pm}(x, E, l) \coloneqq \chi^{\pm}(\omega^{-k}x, \omega^{2k}E, l), \tag{3.1.13}$$

which, from the consideration of the behavior near the origin, is found to be proportional to the original one:

$$\chi_k^{\pm}(x, E, l) = \omega^{\mp(l+1/2)k}\chi^{\pm}(x, E, l). \tag{3.1.14}$$

Combining with a similar relation to (3.1.10): $W[y_k, \chi_k^{\pm}](E, l) = W[y_0, \chi^{\pm}](\omega^{2k}E, l)$, one obtains

$$W[y_k, \chi^{\pm}](E, l) = \omega^{\mp(l+1/2)k}W[y_0, \chi^{\pm}](\omega^{2k}E, l). \tag{3.1.15}$$

Taking the Wronskian with $\chi^{\pm}$ on both sides of (3.1.11), we finally reach

$$C(E, l)D_{\mp}(E, l) = \omega^{\pm(l+1/2)}D_{\mp}(\omega^2 E, l) + \omega^{\mp(l+1/2)}D_{\mp}(\omega^{-2}E, l), \tag{3.1.16}$$

where we defined $D_{\pm}(E, l)$ by

$$D_{\pm}(E, l) \coloneqq W[y_0, \chi^{\mp}]. \tag{3.1.17}$$

The equation (3.1.16) for $D_{-}(E, l)$ is nothing but the TQ-relation in the continuum limit (2.2.26) under the identification $t_0 \leftrightarrow C$ and $q_0 \leftrightarrow D_{-}$, and the parameter setting:

$$\eta = \frac{M\pi}{2M+2}, \qquad \phi = \frac{(2l+1)\pi}{2M+2}. \tag{3.1.18}$$

We also find that the roots of the Bethe ansatz equation are interpreted as the eigenvalues in the spectral problem of the ODE.

One can also see the mapping of the functional relation onto the context of the ODE/IM correspondence. As we have seen, the ground state eigenvalue t_0 was mapped to the Stokes multiplier. Then it is natural to assume that the fusion hierarchy and the

T-system are obtained by considering the other Stokes multipliers. Let us define the Stokes multipliers $C_k^{(n)}$ and $\widetilde{C}_k^{(n)}$ by

$$y_{k-1} = C_k^{(n)} y_{k+n-1} + \widetilde{C}_k^{(n)} y_{k+n}. \tag{3.1.19}$$

Using the Wronskian, they are also written as

$$C_k^{(n)} = W_{k-1,k+n}, \qquad \widetilde{C}_k^{(n)} = -W_{k-1,k+n-1}. \tag{3.1.20}$$

We can also put together the multipliers to form the 2×2 monodromy matrix $\mathbf{C}_k^{(n)}$:

$$(y_{k-1}, y_k) = (y_{k+n-1}, y_{k+n})^t \mathbf{C}_k^{(n)}, \qquad \mathbf{C}_k^{(n)} = \begin{pmatrix} C_k^{(n)} & \widetilde{C}_k^{(n)} \\ C_{k+1}^{(n-1)} & \widetilde{C}_{k+1}^{(n-1)} \end{pmatrix}. \tag{3.1.21}$$

The Wronskian property (3.1.10) leads

$$\mathbf{C}_k^{(n)}(E, l) = \mathbf{C}_0^{(n)}(\omega^{2k} E, l). \tag{3.1.22}$$

Since the linear transformation from the basis $(y_{k+n_1+n_2-1}, y_{k+n_1+n_2})$ to (y_{k-1}, y_k) is equivalent to the successive transformation from the basis $(y_{k+n_1+n_2-1}, y_{k+n_1+n_2})$ to (y_{k+n_1-1}, y_{k+n_1}) followed by the transform from (y_{k+n_1-1}, y_{k+n_1}) to (y_{k-1}, y_k), one finds the identity of the monodromy matrix:

$$\mathbf{C}_k^{(n_1)} \mathbf{C}_{k+n_1}^{(n_2)} = \mathbf{C}_k^{(n_1+n_2)}. \tag{3.1.23}$$

Evaluating this at $n_1 = 1$ and $n_2 = n - 1$ as well as $n_1 = n_2 = n$, we obtain

$$\begin{aligned} &C^{(n)}(\omega^{-1}E) C^{(n)}(\omega E) = 1 + C^{(n+1)}(E) C^{(n-1)}(E), \\ &C^{(1)}(E) C^{(n)}(\omega^{n+1} E) = C^{(n+1)}(\omega^n E) + C^{(n-1)}(\omega^{n+2} E), \end{aligned} \tag{3.1.24}$$

where we defined $C^{(n)}(E) \coloneqq C^{(n)}(\omega^{-n+1}E)$. (3.1.24) is exactly the same relation of the fusion hierarchy (2.2.46) with the identification $t^{(n/2)} \leftrightarrow C^n$.

If the order of the potential M is rational and the angular momentum term $l(l+1)/x^2$ is absent, the solutions become single-valued. Then from the asymptotic behavior, one can show that $y_k = -y_{k+2M+2}$. This means that the fusion hierarchy is truncated since we have $C^{(2M)} = 1$ and $C^{(2M+1)} = 0$. The fusion relation of the Stokes multipliers (3.1.24) is uniformly written as

$$C^{(a)}(\omega E) C^{(a)}(\omega^{-1} E) = 1 + \prod_{b=1}^{2M-1} \left(C^{(b)}(E) \right)^{G_{ab}}, \qquad a = 1, 2, \ldots, 2M-1, \tag{3.1.25}$$

where G_{ab} is the incident matrix of A_{2M-1}. This is the T-system we saw in (2.2.48). The T-function mapped onto the context of the differential equation is

$$T_a(E) = W[y_{-1}, y_a]\,(\omega^{-a+1}E), \qquad a = 1, 2, \ldots, 2M-1. \tag{3.1.26}$$

To summarise the ODE/IM correspondence between the Schrödinger equation and the six-vertex model, we show the dictionary of the mappings in table (3.1.1).

Schrödinger equation	six-vertex model
Eigenvalue energy E	Spectral parameter E_i (root of BAE)
The order of the potential M	Anisotropy η
Angular momentum l	Twist parameter ϕ
The coefficients in the expansion of WKB solution y by the basis near the origin $\chi^{\pm}$	Ground state eigenvalue q_0 (Q-function)
Stokes multiplier $C^{(n)}$	Ground state eigenvalue t_0 and $t^{n/2}$ T-function T_n (truncated case)

Table 3.1.1: The dictionary of the correspondence between the Schrödinger equation and the six-vertex model.

3.2 Generalization to affine Lie algebras

Since the first discovery of the correspondence between the ordinary differential equation and 2-dimensional integrable model [1], which we saw in section 3.1, many other examples of the correspondence were found. For the Schrödinger equation with other potentials, see [25, 105–107] for example. There is also another direction of study, in which the correspondence was extended to not only the ground state energy but also the excited states [36, 38]. In this section, we introduce the generalization to any semi-simple Lie algebras.

3.2.1 The pseudo-differential equations

The correspondence for the Schrödinger type ODE was generalized to the ODE with higher order differential terms, which corresponds to A_r-type integrable models [22–24]. Then the correspondence has been extended to classical Lie algebras [29], in which the

pseudo-differential equation was introduced. The pseudo-differential equations are the higher order differential equations. To write down them, it is convenient to introduce the n-th order differential operator:

$$D_n(\mathbf{g}) \coloneqq \prod_{k=1}^{n} D(g_{n-i} - (n-i)), \qquad D(g) \coloneqq \frac{\mathrm{d}}{\mathrm{d}x} - \frac{g}{x}, \tag{3.2.1}$$

where $\mathbf{g} = \{g_{n-1}, g_{n-2}, \ldots, g_0\}$ is an ordered set of parameters that correspond to the angular momentum in the Schrödinger equation. The A_r-type (pseudo) ODE is written as

$$\big[(-1)^{r+1} D_{r+1}(\mathbf{g}) - P_K(x, E; M)\big]\psi(x, E; \mathbf{g}) = 0, \tag{3.2.2}$$

where the potential term is $P_K(x, E; M) = (x^{h^\vee M/K} - E)^K$ and $\mathbf{g}$ satisfies $\sum_{i=0}^{r} g_i = \frac{r(r+1)}{2}$. This equation is actually not the pseudo ODE, but ODE for other types of classical Lie algebras contains the pseudo-differential operator $(\mathrm{d}/\mathrm{d}x)^{-1}$ which is defined by the formal action on the monomial:

$$\left(\frac{\mathrm{d}}{\mathrm{d}x}\right)^{-1} x^n = \frac{x^{n+1}}{n+1}. \tag{3.2.3}$$

The pseudo-ODEs of B_r, C_r and D_r type Lie algebras are as follows

$$B_r: \qquad \left[D_r(\mathbf{g}^\dagger) D_r(\mathbf{g}) + \sqrt{P_K}\frac{\mathrm{d}}{\mathrm{d}x}\sqrt{P_K}\right]\psi(x, E; \mathbf{g}) = 0, \tag{3.2.4}$$

$$C_r: \qquad \left[D_r(\mathbf{g}^\dagger)\frac{\mathrm{d}}{\mathrm{d}x} D_r(\mathbf{g}) - \sqrt{P_K}\left(\frac{\mathrm{d}}{\mathrm{d}x}\right)^{-1}\sqrt{P_K}\right]\psi(x, E; \mathbf{g}) = 0, \tag{3.2.5}$$

$$D_r: \qquad \left[D_r(\mathbf{g}^\dagger)\left(\frac{\mathrm{d}}{\mathrm{d}x}\right)^{-1} D_r(\mathbf{g}) - \sqrt{P_K}\frac{\mathrm{d}}{\mathrm{d}x}\sqrt{P_K}\right]\psi(x, E; \mathbf{g}) = 0. \tag{3.2.6}$$

Here we omitted the arguments of the potential P_K. The authors of [29] showed that the BAEs for the $\mathfrak{g}$-type vertex models in the conformal limit could be derived from the identities of the Wronskians, which are called the ψ-system, of the solutions to the $\mathfrak{g}$-type pseudo-ODEs. Let us demonstrate this for the A_r case. Denote the subdominant solution along the real axis as ψ and its Symanzik rotation as ψ_k which is defined by

$$\psi_k(x, E) \coloneqq \psi(\omega^{-k}x, \Omega^{-k}E), \qquad \omega = \Omega^{\frac{K}{h^\vee}} = \exp\left(i\frac{2\pi}{h^\vee(M+1)}\right). \tag{3.2.7}$$

Here $h^\vee$ is the dual Coxeter number of A_r. The ψ-system for A_r is

$$\psi^{(a-1)}\psi^{(a+1)} = W[\psi^{(a)}, \psi^{(a)}], \qquad \psi^{(0)} = \psi^{(r+1)} = 1, \tag{3.2.8}$$

where $\psi^{(a)}$ $(a = 1, 2, \ldots, r)$ is defined by

$$\psi^{(a)} \coloneqq W^{(a)}[\psi_{\frac{a-1}{2}}, \psi_{\frac{a-3}{2}}, \ldots, \psi_{\frac{1-a}{2}}]. \tag{3.2.9}$$

The Wronskian $W^{(a)}[f_1, f_2, \ldots, f_a] \coloneqq \det\left[\vec{f}, \partial_x\vec{f}, \ldots, \partial_x^{a-1}\vec{f}\right]$ $(\vec{f} = {}^t(f_1, f_2, \ldots, f_a))$ is the generalization of the Wronskian of two solutions. We also define the Symanzik rotation of $\psi^{(a)}$ by the same definition for the subdominant solution (3.2.7). The ψ-system (3.2.8) is proved from the Jacobi identity for the sub-determinants [29]. The BAEs are the algebraic equations for the zeros of the Q-functions which are defined from the coefficients in the expansions of the functions $\psi^{(a)}$ by the basis around the origin. Letting the basis χ_i $(i = 0, 1, \ldots, r)$ whose asymptotic behavior around the origin is

$$\chi_i(x, E; \mathbf{g}) \sim x^{g_i} + \cdots, \tag{3.2.10}$$

where the ordering of g_i satisfies $g_i < g_j$ $(i < j)$, we expand the subdominant solution ψ by the basis as

$$\psi(x, E; \mathbf{g}) = \sum_{i=0}^{r} Q_{[i]}(E; \mathbf{g})\chi(x, E; \mathbf{g}). \tag{3.2.11}$$

The function $\psi_k^{(a)}$ can be expanded as

$$\begin{aligned}\psi_k^{(a)} =& \omega^{-k\sum_{i=0}^{a-1} g_i} Q_k^{(a)}(E, \mathbf{g}) W^{(a)}[\chi_0, ..., \chi_{a-1}] \\ &+ \omega^{-k\sum_{i=0}^{a-2} g_i + kg_a} \overline{Q}_k^{(a)}(E, \mathbf{g}) W^{(a)}[\chi_0, ..., \chi_{a-2}, \chi_a] + \cdots.\end{aligned} \tag{3.2.12}$$

Note that the expansion coefficients $Q_k^{(a)}$ and $\overline{Q}_k^{(a)}$ can be expressed by $Q_{[i]}$. Substituting this expansion to the ψ-system, one obtains

$$Q^{(a+1)}Q^{(a-1)} = \omega^{\frac{1}{2}(g_a - g_{a-1})} Q^{(a)}_{-\frac{1}{2}} \overline{Q}^{(a)}_{\frac{1}{2}} - \omega^{-\frac{1}{2}(g_a - g_{a-1})} Q^{(a)}_{\frac{1}{2}} \overline{Q}^{(a)}_{-\frac{1}{2}}. \tag{3.2.13}$$

Evaluating this at the zeros of $Q^{(a)}_{\pm\frac{1}{2}}$ i.e. $E = \Omega^{\pm\frac{1}{2}} E^{(a)}$, this relation leads the A_r-type BAEs:

$$\prod_{b=1}^{r} \Omega^{-C_{ab}\gamma_b/2} \frac{Q^{(b)}(\Omega^{1/2} E_i^{(a)}, \vec{\gamma})}{Q^{(b)}(\Omega^{-1/2} E_i^{(a)}, \vec{\gamma})} = -1, \qquad i = 1, 2, \ldots, \quad a = 1, \ldots, r. \tag{3.2.14}$$

Here we identified the twist parameters γ_b as

$$\gamma_b = \frac{2K}{Mh^\vee}\left(\sum_{i=0}^{b-1} g_i - a\frac{n-1}{2}\right). \tag{3.2.15}$$

The BAEs for B_r, C_r and D_r can be derived from the ψ-system similarly.

The unclear point so far is the physical origin of these pseudo ODEs. The answer to this question is that these are the equations for the highest weight component of the solution to the modified affine Toda equations in the conformal limit [31, 34, 35]. This is a system of differential equations of order one, so we do not need to use the pseudo-differential operator. Furthermore, the ODE/IM correspondence was extended for the BAE of any semi-simple Lie algebras.

3.2.2 The modified affine Toda equation and its conformal limit

In this subsection, we introduce the modified affine Toda equation. Consider the two dimensional Euclidean space (x^0, x^1) and r-component scalar field ϕ. For a rank r Lie algebra $\mathfrak{g}$, the affine Toda field equation is derived from the Lagrangian

$$\mathcal{L} = \frac{1}{2}\partial^\mu\phi\partial_\mu\phi - \left(\frac{m}{\beta}\right)^2\sum_{i=0}^{r} n_i[\exp(\beta\alpha_i\cdot\phi) - 1]. \tag{3.2.16}$$

Here α_i is the simple roots, α_0 is the lowest root, and n_i is the label for $\mathfrak{g}$. For the detailed notation of the Lie algebra, see appendix A. The affine Toda field theory is the generalization of the Liouville theory. The physical meaning of the β is the coupling parameter, and m is the mass of the scalar field, but we do not discuss the dynamics of the affine Toda field theory. The affine Toda field equation is also written in the Lax formalism. We Define the curvature F by

$$F = \partial\overline{A} - \overline{\partial}A + [A, \overline{A}], \tag{3.2.17}$$

where

$$A = \frac{\beta}{2}\partial\phi\cdot H - me^{\lambda}\sum_{i=0}^{r}\sqrt{n_i^\vee}E_{\alpha_i}\exp\left(\frac{\beta}{2}\alpha_i\cdot\phi\right), \tag{3.2.18}$$

$$\overline{A} = -\frac{\beta}{2}\partial\phi\cdot H - me^{-\lambda}\sum_{i=0}^{r}\sqrt{n_i^\vee}E_{-\alpha_i}\exp\left(\frac{\beta}{2}\alpha_i\cdot\phi\right). \tag{3.2.19}$$

Here λ is the spectral parameter, H^i is the Cartan generator and E_{α_i} is the generator for the simple root α_i, and $n_i^\vee$ is the co-label of $\mathfrak{g}$. The affine Toda field equation is written as the zero curvature condition: $F = 0$ or $[\partial + A]\Psi = [\overline{\partial} + \overline{A}]\Psi = 0$. Introducing the complex coordinate $(z, \overline{z}) = (x^0 + ix^1, x^0 - ix^1)$ and performing the conformal transformation

$$z \to z' = f(z), \qquad \phi \to \phi' = \phi - \frac{\rho^\vee}{\beta} \log\bigl(\partial f \overline{\partial f}\bigr), \tag{3.2.20}$$

one obtains the modified affine Toda field equation. In the Lax formalism, in which the equation is expressed by the zero curvature condition, the connections A and $\overline{A}$ become

$$A' = \frac{\beta}{2}\partial\phi \cdot H - me^{\lambda}\left(\sum_{i=1}^{r} \sqrt{n_i^\vee} E_{\alpha_i} e^{\frac{\beta}{2}\alpha_i \cdot \phi} + (-1)^h (\partial f)^h E_{\alpha_0} e^{\frac{\beta}{2}\alpha_0 \cdot \phi}\right), \tag{3.2.21}$$

$$\overline{A'} = -\frac{\beta}{2}\partial\phi \cdot H - me^{-\lambda}\left(\sum_{i=0}^{r} \sqrt{n_i^\vee} E_{-\alpha_i} e^{\frac{\beta}{2}\alpha_i \cdot \phi} + (-1)^h (\overline{\partial f})^h E_{-\alpha_0} e^{\frac{\beta}{2}\alpha_0 \cdot \phi}\right). \tag{3.2.22}$$

For the discussion of the conformal limit, it is convenient to use the gauge transformed connections $A'' = UA'U + U\mathrm{d}U^{-1}$ and $\overline{A''} = U\overline{A'}U + U\mathrm{d}U^{-1}$. Choosing $U = e^{-\frac{\beta}{2}\phi \cdot H}$, the explicit forms are

$$A'' = \beta\partial\phi \cdot H + me^{\lambda}\left[\sum_{i=1}^{r} \sqrt{n_i^\vee} E_{\alpha_i} + (\partial f)^h \sqrt{n_o^\vee} E_{\alpha_0}\right], \tag{3.2.23}$$

$$\overline{A''} = me^{-\lambda}\left[\sum_{i=1}^{r} \sqrt{n_i^\vee} e^{\beta\alpha_i \cdot \phi} E_{-\alpha_i} + (\overline{\partial f})^h \sqrt{n_0^\vee} e^{\beta\alpha_0 \cdot \phi} E_{\alpha_0}\right]. \tag{3.2.24}$$

Defining $(\partial f)^h = z^{hM} - s^{hM}$, $(\overline{\partial f})^h = \overline{z}^{hM} - s^{hM}$, and

$$x \coloneqq z(me^{\lambda})^{\frac{1}{M+1}}, \quad \widetilde{x} \coloneqq \overline{z}(me^{-\lambda})^{\frac{1}{M+1}}, \tag{3.2.25}$$

$$E \coloneqq s^{hM}(me^{\lambda})^{\frac{hM}{M+1}}, \quad \widetilde{E} \coloneqq s^{hM}(me^{-\lambda})^{\frac{hM}{M+1}}, \tag{3.2.26}$$

we take the conformal limit: first taking the limit $\overline{z} \to 0, \lambda \to \infty$, and then take $z \to 0$ with keeping x and E finite. The resulting equation is derived from the holomorphic one $[\partial + A'']\Psi = 0$ and becomes

$$\mathcal{L}_{\hat{\mathfrak{g}}}(x, E, l; \zeta)\ \Psi(x, E, l) = \left[\frac{\mathrm{d}}{\mathrm{d}x} + A_{\hat{\mathfrak{g}}}\right]\Psi(x, E, l) = 0, \tag{3.2.27}$$

where the $\hat{\mathfrak{g}}$-valued matrix $A_{\hat{\mathfrak{g}}}$ is defined by

$$A_{\hat{\mathfrak{g}}} \coloneqq -\frac{1}{x}\sum_{a=1}^{r} l_a(\alpha_a^\vee \cdot H) + \sum_{a=1}^{r}\sqrt{n_a^\vee}E_{\alpha_a} + \sqrt{n_0^\vee}p(x,E)\,\zeta E_{\alpha_0}. \tag{3.2.28}$$

The parameter ζ takes the value $+1$ or -1 depending on the representation V, and $l = (l_1, l_2, \ldots, l_r)$ are the monodromy parameters given by

$$l_a \coloneqq -\omega_a \cdot g, \qquad a = 1, 2, \ldots, r, \tag{3.2.29}$$

where r-dimensional vector g satisfies the condition:

$$1 + \alpha_a \cdot g > 0, \qquad a = 0, \ldots, r. \tag{3.2.30}$$

This condition follows from the logarithmic behavior of the solutions of the modified affine Toda field equation [34, 35]. The potential term $p(x, E)$ becomes the monomial one:

$$p(x, E) \coloneqq x^{hM} - E. \tag{3.2.31}$$

(3.2.27) is the equation we will consider in the ODE/IM correspondence which we will discuss in the next subsection.

Before closing this subsection, we argue the relation to the pseudo-ODE. As an example, let us consider the linear problem for the first fundamental $V^{(1)}$ representation of $A_r^{(1)}$. Let $\mathbf{e}_i$ $(i = 1, 2, \ldots, \dim V^{(1)})$ be the weight vector which satisfies

$$H^a \mathbf{e}_j = (h_j)^a \mathbf{e}_j, \qquad a = 1, 2, \ldots, r. \tag{3.2.32}$$

Denoting the matrix representation of A_r in $V^{(1)}$ as $\rho^{(1)}$, the generators are given by

$$\rho^{(1)}(E_{\alpha_0}) = e_{r+1,1}, \quad \rho^{(1)}(E_{\alpha_a}) = e_{a,a+1}, \quad a = 1, \ldots, r, \tag{3.2.33}$$

where $e_{a,b}$ denotes the matrix whose (i, j) element is $\delta_{ia}\delta_{bj}$. Then the linear problem for $\Psi = \sum_{a=1}^{r+1}\psi_i \mathbf{e}_i$ in the representation $V^{(1)}$ leads

$$\left[\begin{pmatrix} \frac{\mathrm{d}}{\mathrm{d}x} - \frac{l_1}{x} & & & \\ & \frac{\mathrm{d}}{\mathrm{d}x} - \frac{l_2}{x} & & \\ & & \ddots & \\ & & & \frac{\mathrm{d}}{\mathrm{d}x} - \frac{l_{r+1}}{x} \end{pmatrix} + \begin{pmatrix} 0 & 1 & & \\ & \ddots & \ddots & \\ & & 0 & 1 \\ p(x,E) & & & 0 \end{pmatrix}\right]\begin{pmatrix} \psi_1 \\ \psi_2 \\ \vdots \\ \psi_{r+1} \end{pmatrix} = 0, \tag{3.2.34}$$

where the monodromy parameters satisfy the condition:

$$\sum_{a=1}^{r+1} l_a = 0. \tag{3.2.35}$$

Rearranging the linear problem, one obtains the differential equation for the component ψ_1:

$$\left[(-1)^{r+1} D(l_{r+1}) D(l_r) \dots D(l_1) - p(x,E)\right] \psi_1(x,E) = 0, \tag{3.2.36}$$

where $D(l)$ is given by

$$D(l) \coloneqq \frac{\mathrm{d}}{\mathrm{d}x} - \frac{l}{x}. \tag{3.2.37}$$

(3.2.36) is the pseudo-differential equation of A_r-type (3.2.2). Especially for $r = 1$, we recover the Schrödinger equation which we dealt with in section 3.1, in which the monodromy parameter l_1 is the angular momentum. Similarly, for the first fundamental representation of classical Lie algebra, this linear system (3.2.27) reduces to the pseudo-ODEs (3.2.4), (3.2.5), and (3.2.6) by considering the equation for the component corresponding to the highest weight vector $\mathbf{e}_1$.

3.2.3 ODE/IM correspondence

Now, let us discuss the ODE/IM correspondence for the linear problem (3.2.27). As we consider in the Schrödinger case, the Symanzik rotation of the linear problem is also defined by the rotation:

$$x \to \omega^{-k} x, \qquad E \to \Omega^{-k} E, \qquad \omega \coloneqq e^{\frac{2\pi i}{h(M+1)}}, \qquad \Omega \coloneqq e^{\frac{2\pi i M}{M+1}}. \tag{3.2.38}$$

Under this rotation, the linear differential operator $\mathcal{L}_{\hat{\mathfrak{g}}}$ transforms as

$$\omega^{-k} \mathcal{L}_{\hat{\mathfrak{g}}}(\omega^{-k} x, \Omega^{-k} E, l; \zeta) = \omega^{-k\rho^\vee \cdot H} \mathcal{L}_{\hat{\mathfrak{g}}}(x, E, l; \zeta e^{-2\pi i k}) \omega^{k\rho^\vee \cdot H}. \tag{3.2.39}$$

Defining the k-Symanzik rotation of the subdominant solution along the real axis: $\Psi_{[k]}(x,E,l)$ by

$$\Psi_{[k]}(x,E,l) \coloneqq \omega^{k\rho^\vee \cdot H} \Psi(\omega^{-k} x, \Omega^{-k} E, l), \tag{3.2.40}$$

the linear problem becomes invariant under the rotation (3.2.38) except for the replacement $E_{\alpha_0} \to e^{-2\pi ik} E_{\alpha_0}$:

$$\mathcal{L}_{\hat{\mathfrak{g}}}(x, E, l; \zeta e^{-2\pi ik}) \Psi_{[k]}(x, E, l) = 0. \tag{3.2.41}$$

If k is an integer, we recover the original linear problem. Associated with the rotated solution $\Psi_{[k]}$, let us define the representation $V_{[k]}$ in which the generator E_{α_0} acts on V as $e^{-2\pi ik} E_{\alpha_0}$. Then $\Psi_{[k]}$ becomes the solution of the linear problem in the representation $V_{[k]}$.

The asymptotic behavior of the subdominant solutions is similar to that of the Schrödinger case. To apply the WKB approximation to the solution of the linear problem, consider the gauge transformation:

$$\mathcal{L}_{\hat{\mathfrak{g}}} \to \mathcal{L}'_{\hat{\mathfrak{g}}} = U(x) \mathcal{L}_{\hat{\mathfrak{g}}} U^{-1}(x), \qquad \Psi(x) \to \Psi'(x) = U(x) \Psi(x), \tag{3.2.42}$$

where

$$U(x) = \exp\Big(\log \left(p(x, E)\right)^{\frac{1}{h}} \rho^\vee \cdot H \Big). \tag{3.2.43}$$

Here $\rho^\vee$ represents the co-Wyle vector and h is the Coxeter number. Under this transformation, the linear differential operator transforms as

$$\mathcal{L}'_{\hat{\mathfrak{g}}} = \frac{\mathrm{d}}{\mathrm{d}x} - \frac{1}{x} \sum_{a=1}^{r} l_a \, \alpha_a \cdot H - \frac{1}{h} \frac{d \log p(x, E)}{dx} \rho^\vee \cdot H + p(x, E)^{1/h} \Lambda_+, \tag{3.2.44}$$

where the constant matrix Λ_+ is given by

$$\Lambda_+ = \sum_{a=1}^{r} \sqrt{n_a^\vee} \; E_{\alpha_a} + \sqrt{n_0^\vee} \; \zeta E_{\alpha_0}. \tag{3.2.45}$$

In the asymptotic region $x \to \infty$, the second and the third term of $\mathcal{L}'_{\hat{\mathfrak{g}}}$ can be ignored since their orders are $\mathcal{O}(x^{-1})$. Then, the asymptotic behavior of the WKB solution Ψ' is

$$\Psi'(x, E) \sim \sum_{i=1}^{\dim V} C_i \exp\left(-\nu_i \int^x \left(p(x', E)\right)^{1/h} dx' \right) \boldsymbol{\nu}_i, \tag{3.2.46}$$

where C_i is constant and $\boldsymbol{\nu}_i$ is the eigenvector of Λ_+ with the eigenvalue ν_i for $i = 1, 2, \ldots, \dim V$. Let us denote the subdominant solution along the real axis by $\Psi(x, E, l)$.

From the WKB approximation (3.2.46) and the inverse gauge transformation, one finds

$$\begin{aligned}\Psi(x,E,l) &\sim C\exp\left(-\nu\int^{x}(p(x',E))^{1/h}dx'\right)\exp\left(-\frac{1}{h}\log p(x,E)\ \rho^{\vee}\cdot H\right)\boldsymbol{\nu}\\ &\sim Cx^{-M\rho^{\vee}\cdot H}\exp\left(-\frac{\nu}{M+1}\ x^{M+1}\right)\boldsymbol{\nu}, \qquad x\to\infty,\end{aligned} \tag{3.2.47}$$

where ν is the largest eigenvalue among ν_i $(i=1,2,\ldots,\dim V)$ and $\boldsymbol{\nu}$ is the associated eigenvector. One can define the Symanzik rotation of solution $\Psi_{[k]}(x,E,l)$ $(k\in\mathbf{Z})$, which is subdominant in the Stokes sector $\mathcal{S}_k$:

$$\mathcal{S}_k=\left\{c\in\mathbb{C};|\arg x-\arg\omega|<\frac{1}{2}\arg\omega\right\}. \tag{3.2.48}$$

The Q-function was, in the Schrödinger case, defined as the Wronskian of the subdominant solution and the basis χ^{+} which bahaves near origin as (3.1.12). In the analogy to this argument, we consider the basis of the solution near the origin, which we denote $\mathcal{X}_i(x,E,l)$ $(i=1,2,\ldots,\dim V)$. We set the asymptotic behavior of the basis as

$$\mathcal{X}_i(x,E,l)=x^{-h_i\cdot g}\mathbf{e}_i+\cdots, \qquad x\to 0. \tag{3.2.49}$$

From this asymptotics, the Symanzik rotation of the basis $\mathcal{X}_i$ becomes

$$\mathcal{X}_{i[k]}(x,E,l)=\omega^{kh_i\cdot(\rho^{\vee}+g)}\mathcal{X}_i(x,E,l). \tag{3.2.50}$$

The subdominant solution Ψ is expanded by this basis as

$$\Psi(x,E,l)=\sum_{i=1}^{\dim V}\mathcal{Q}_i(E,l)\ \mathcal{X}_i(x,E,l), \tag{3.2.51}$$

where we defined the expansion coefficients as $\mathcal{Q}_i$. To identify the coefficients $\mathcal{Q}_i(E,l)$ with the Q-functions of the integrable model characterized by the BAEs (2.2.52), we focus on coefficient $\mathcal{Q}_1(E,l)$ and define the Q-function by

$$Q(E,l)\coloneqq\mathcal{Q}_1(E,l). \tag{3.2.52}$$

As we will see, the zeros of the Q-function, i.e. E satisfying $Q(E,l)=0$, are the roots of the BAEs. This equation corresponds to the spectral problem with the special boundary

condition for the solution: the solution Ψ decays fastest along the positive real axis and does not depend on the basis $\mathcal{X}_1$ near the origin. For the Schrödinger case, this corresponds to the physical condition where the wave function does not diverge both at the origin and infinity.

Let us consider the linear problem (3.2.27) for the fundamental representations $V^{(a)}$ $(a = 1, \ldots, r)$ with the highest weight ω_a. We denote the subdominant solution as $\Psi^{(a)}$ and the basis around the origin as $\mathcal{X}_i^{(a)}$. We also denote the Q-function $Q(E, l)$ as $Q^{(a)}(E, l)$. For the fundamental representations $V^{(a)}$ of semi-simple Lie algebra, we have the inclusion map

$$\iota : V^{(a)} \wedge V^{(a)} \to \bigotimes_{b=1}^{r} (V^{(b)})^{G_{ab}}, \tag{3.2.53}$$

where G_{ab} is the incident matrix. Associated with this relation, the subdominant solutions $\Psi^{(a)}$ satisfy a type of relations which is called the ψ-system [31, 35, 108]. For the classical Lie algebra, this ψ-system is the same one for the pseudo-ODE. The ψ-system for affine Lie algebra $\hat{\mathfrak{g}}$ takes the form:

$$\iota\left(\Psi^{(a)}_{[-1/2]} \wedge \Psi^{(a)}_{[1/2]}\right) = \bigotimes_{b=1}^{r} \left(\Psi^{(b)}\right)^{G_{ab}}. \tag{3.2.54}$$

Substituting the expansion (3.2.51) into the ψ-system (3.2.54) and comparing the coefficient of the highest weight state, one finds the relations:

$$\omega^{-\frac{1}{2}\left(\lambda_1^{(a)}-\lambda_2^{(a)}\right)} \mathcal{Q}^{(a)}_{1[-1/2]} \mathcal{Q}^{(a)}_{2[1/2]} - \omega^{\frac{1}{2}\left(\lambda_1^{(a)}-\lambda_2^{(a)}\right)} \mathcal{Q}^{(a)}_{1[1/2]} \mathcal{Q}^{(a)}_{2[-1/2]} = \prod_{b=1}^{r} \left[\mathcal{Q}_1^{(b)}\right]^{G_{ab}}. \tag{3.2.55}$$

where $\lambda^{(a)}$ is defined by

$$\lambda_i^{(a)} = \rho^\vee \cdot (\omega_a - h_i^{(a)}) - h_i^{(a)} \cdot g, \qquad a = 1, 2, \ldots, r. \tag{3.2.56}$$

For affine Lie algebra $\mathfrak{g}^\vee$ which is the Langlands dual of semi-simple Lie algebra $\mathfrak{g}$, evaluating the 1/2- and $-1/2$-Symanzik rotations of (3.2.55) at the zeros $E_i^{(a)}$ $(i = 0, 1, \ldots)$ of the Q-functions $Q^{(a)}$ and taking the ratio of them, we arrive at the Bethe ansatz equations of $\mathfrak{g}$-type:

$$\prod_{b=1}^{r} \Omega^{C_{ab}\gamma_b/2} \left.\frac{Q^{(b)}_{[C_{ab}/2]}}{Q^{(b)}_{[-C_{ab}/2]}}\right|_{E_i^{(a)}} = -1, \qquad i = 0, 1, \ldots, \tag{3.2.57}$$

which we saw in section 2.3. Here the twist parameter is defined by

$$\gamma_a := \frac{2}{h^\vee M}(l_a - \omega_a \cdot \rho^\vee), \qquad a = 1, 2, \ldots, r. \tag{3.2.58}$$

For the simply-laced Lie algebras $\mathfrak{g}$, the Langlands dual is the original one of untwisted affine-types $\mathfrak{g}^{(1)}$. On the other hand, the Langlands dual of non-simply-laced Lie algebra becomes the twisted one. If we consider the linear problem for untwisted affine non-simply-laced algebras, the resulting BAEs are the folded ones of simply-laced types associated with the folding of the simply-laced Lie algebras. Here we summarize the BAEs for folded types:

$\hat{\mathfrak{g}} = B_r^{(1)}$ case ($D_{r+1}/\mathbf{Z}_2$-type BAEs):

$$\begin{aligned}
&\prod_{b=1}^{r} \Omega^{C_{ab}\gamma_b/2} \left.\frac{Q^{(b)}_{[C_{ab}/2]}}{Q^{(b)}_{[-C_{ab}/2]}}\right|_{E_i^{(a)}} = -1, \qquad \text{for} \qquad a = 1, \ldots, r-2, r, \\
&\Omega^{-\frac{1}{2}\gamma_{r-2}+\gamma_{r-1}-\gamma_r} \left.\frac{Q^{(r-2)}_{[-1/2]} Q^{(r-1)}_{[1]} \left[Q^{(r)}_{[-1/2]}\right]^2}{Q^{(r-2)}_{[1/2]} Q^{(r-1)}_{[-1]} \left[Q^{(r)}_{[1/2]}\right]^2}\right|_{E_i^{(r-1)}} = -1.
\end{aligned} \tag{3.2.59}$$

$\hat{\mathfrak{g}} = C_r^{(1)}$ case ($A_{2r-1}/\mathbf{Z}_2$-type BAEs):

$$\begin{aligned}
&\prod_{b=1}^{r} \Omega^{C_{ab}\gamma_b/2} \left.\frac{Q^{(b)}_{[C_{ab}/2]}}{Q^{(b)}_{[-C_{ab}/2]}}\right|_{E_i^{(a)}} = -1, \qquad \text{for} \qquad a = 1, \ldots, r-1, \\
&\Omega^{\gamma_r-\gamma_{r-1}} \left.\frac{\left[Q^{(r-1)}_{[-1/2]}\right]^2 Q^{(r)}_{[1]}}{\left[Q^{(r-1)}_{[1/2]}\right]^2 Q^{(r)}_{[-1]}}\right|_{E_i^{(r)}} = -1.
\end{aligned} \tag{3.2.60}$$

$\hat{\mathfrak{g}} = F_4^{(1)}$ case ($E_6/\mathbf{Z}_2$-type BAEs):

$$\begin{aligned}
&\prod_{b=1}^{4} \Omega^{C_{ab}\gamma_b/2} \left.\frac{Q^{(b)}_{[C_{ab}/2]}}{Q^{(b)}_{[-C_{ab}/2]}}\right|_{E_i^{(a)}} = -1, \qquad \text{for} \qquad a = 1, 2, 4, \\
&\Omega^{-\gamma_2+\gamma_3-\frac{1}{2}\gamma_4} \left.\frac{\left[Q^{(2)}_{[-1/2]}\right]^2 Q^{(3)}_{[1]} Q^{(4)}_{[-1/2]}}{\left[Q^{(2)}_{[1/2]}\right]^2 Q^{(3)}_{[-1]} Q^{(4)}_{[1/2]}}\right|_{E_i^{(3)}} = -1.
\end{aligned} \tag{3.2.61}$$

$\hat{\mathfrak{g}} = G_2^{(1)}$ case ($D_4/\mathbf{Z}_3$-type BAEs):

$$\Omega^{\gamma_1-\frac{1}{2}\gamma_2}\left.\frac{Q^{(1)}_{[1]}Q^{(2)}_{[-1/2]}}{Q^{(1)}_{[-1]}Q^{(2)}_{[1/2]}}\right|_{E_i^{(1)}} = -1, \qquad \Omega^{-\frac{3}{2}\gamma_1+\gamma_2}\left.\frac{\left[Q^{(1)}_{[-1/2]}\right]^3 Q^{(2)}_{[1]}}{\left[Q^{(1)}_{[1/2]}\right]^3 Q^{(2)}_{[-1]}}\right|_{E_i^{(2)}} = -1. \quad (3.2.62)$$

Here C_{ab} is the Cartan matrix of the corresponding Lie algebra $\mathfrak{g}$.

3.3 Study for searching the zeros of Q-functions

We saw, in section 3.2, that the ODE/IM correspondence was generalized to the relation between the linear problem associated to affine Lie algebra $\mathfrak{g}^\vee$ and the Bethe ansatz equation of $\mathfrak{g}$-type, in which the Bethe roots are mapped to the eigenvalues of the spectral problem of the linear system with the certain boundary condition. These eigenvalues are zeros of the Q-function defined in (3.2.52). Then, we expect that if we calculate the roots of the BAEs as well as the zeros of the Q-function from the linear problem, these two agree. And this could be the non-trivial test of the ODE/IM correspondence. In the integrable model side, the BAEs can be converted into the Non-linear integral equation which we introduced in 2.3, so that we can compute the roots numerically. Then in this section, we discuss the method to obtain the zeros of the Q-function from the linear problem.

Instead of only considering the zeros of the Q-function, we deal with the expansion coefficients $\mathcal{Q}_i$ in (3.2.51), which is given by

$$\mathcal{Q}_i = \frac{\det[\mathcal{X}_1, \mathcal{X}_2, \ldots, \mathcal{X}_{i-1}, \Psi, \mathcal{X}_{i+1}, \ldots, \mathcal{X}_{n-1}, \mathcal{X}_n]}{\det[\mathcal{X}_1, \mathcal{X}_2, \ldots, \mathcal{X}_n]}, \quad (3.3.1)$$

where $\mathcal{X}_i$ is the basis which behaves near origin as in (3.2.49), Ψ is the subdominant solution along the real axis, and n is the dimension of the representation on which the linear problem is defined. Since $\mathcal{X}_i$ $(i = 1, 2, \ldots, n)$ form the basis of the linear problem, the denominator of (3.3.1) is x-independent:

$$\partial_x \det[\mathcal{X}_1, \mathcal{X}_2, \ldots, \mathcal{X}_n] = 0. \quad (3.3.2)$$

Hence one can ignore the constant denominator for the study of the zeros of $\mathcal{Q}_i$. In the numerical calculation, we express the basis and the subdominant solution by the formal series expansion of x. For large x, the formal series expression of the basis diverges, while for small x, that of the subdominant solution diverges. Using (3.3.1), one obtain the x-dependent determinant. Evaluating this at the appropriate x_{fix} where both expressions converge, one can estimate the E-dependence of $\mathcal{Q}_i$. This method works well for the linear problem in the representation with small dimensions, and the agreements to the Bethe roots can be confirmed. However, for the large dimensional representation, one would fail to estimate because of the size of the determinant. This occurs to the linear problem of higher rank Lie algebras. In [29], this was resolved for the first fundamental representation of the classical Lie algebras by introducing the adjoint ODE. Let us explain the A_r case in which the form of the linear problem is in (3.2.34); hence the components of the solution satisfy $\psi_{i+1} = \partial_x \psi_i$ for $i = 1, 2, \ldots, r$. As a result, the Q-function $Q^{(1)}$ is written by the Wronskian:

$$Q^{(1)} = \mathcal{Q}_1^{(1)} = W[\psi_1, \chi_{2,1}, \chi_{3,1}, \ldots, \chi_{r+1,1}], \tag{3.3.3}$$

where the Wronskian of n functions f_i $(i = 1, 2, \ldots, n)$ is given by

$$W[f_1, f_2, \ldots, f_n] = \det \begin{pmatrix} f_1 & f_2 & \cdots & f_n \\ \partial_x f_1 & \partial_x f_2 & \cdots & \partial_x f_n \\ \vdots & \vdots & \ddots & \vdots \\ \partial_x^{n-1} f_1 & \partial_x^{n-1} f_2 & \cdots & \partial_x^{n-1} f_n \end{pmatrix}, \tag{3.3.4}$$

and ψ_1 and $\chi_{i,1}$ $(i = 1, 2, \ldots, r+1)$ are the highest components of the subdominant solution and the basis, respectively. The co-factor expansion of the Wronskian reads

$$Q^{(1)} = (-1)^{r+2} \partial_x^r \psi_1 W[\chi_{2,1}, \chi_{3,1}, \ldots, \chi_{r+1,1}] + \cdots . \tag{3.3.5}$$

Here in (3.3.5), we only show the leading contribution of the expansion at sufficiently large x, which follows from the asymptotic behavior of the subdominant solution ψ_1. Therefore it is enough to calculate the co-factor $W[\chi_{2,1}, \chi_{3,1}, \ldots, \chi_{r+1,1}]$ and evaluate it at sufficiently large x for the leading order estimation of the Q-function. Short calculation shows the co-factor becomes the solution of the A_r-type adjoint ODE [29]:

$$[D(l_1)D(l_2)\ldots D(l_{r+1}) - p(x, E)]\widetilde{\psi} = 0, \tag{3.3.6}$$

where $D(l)$ is defined in (3.2.37). Note that though (3.3.6) only differs from the A_r-type ODE (3.2.36) by the sign of the potential, for other types of algebras, the adjoint ODE has more differences from the pseudo ODE. In conclusion, solving the adjoint ODE (3.3.6) with the boundary condition $\widetilde{\psi} \sim x^{l_{r+1}}$, one obtains the co-factor which contributes the most to the Q-function, so one could estimate the Q-function by evaluating the solution $\widetilde{\psi}$ at the large x:

$$Q^{(1)}(E) = \widetilde{\psi}(x_{\text{fixed}}, E), \qquad x_{\text{fixed}} \gg 1. \tag{3.3.7}$$

This method is efficient to the first fundamental representation of classical algebras. However, it is hard to apply this to other representations or exceptional Lie algebras since the adjoint ODE will be complicated and difficult to derive.

In [39], we established the method to calculate the zeros of the Q-functions for any representation of semi-simple Lie algebras, in which we introduced the dual linear problem which is the matrix version of the adjoint ODE. Let V any representation of semi-simple Lie algebra $\mathfrak{g}$ and $\langle\cdot,\cdot\rangle$ the $\mathfrak{g}$-invariant inner product $\langle\cdot,\cdot\rangle : V^* \times V \to \mathbb{C}$ where V^* is the dual space of V. From the inner product, the $\mathfrak{g}$-action on the dual space is defined by

$$\langle X^*\psi^*, \chi\rangle = \langle \psi^*, X\chi\rangle, \quad \chi \in V, \quad \psi^* \in V^*, \quad X \in \mathfrak{g}. \tag{3.3.8}$$

If we define the $\mathfrak{g}$-invariant quadratic-form by ${}^t\psi J\chi$ $(\psi, \chi \in V)$, where J is an invertible symmetric matrix, one finds the dual representation becomes $-J^{-1t}XJ$. Identifying the dual space V^* with V, we map $\psi^* \in V^*$ to the vector $\overline{\psi} \in V$. The matrix J exchanges the basis, which corresponds to an automorphism of the Lie algebra. The dual linear problem is defined as the linear problem (3.2.27) in the dual representation:

$$\mathcal{L}^{\text{dual}}_{\mathfrak{g}}\ \bar{\Psi}(x,E,l) = \left[\frac{\mathrm{d}}{\mathrm{d}x} + \bar{A}_{\mathfrak{g}}\right]\bar{\Psi}(x,E,l) = 0, \qquad \bar{A}_{\mathfrak{g}} = -J^{-1}\ {}^tA_{\mathfrak{g}}J. \tag{3.3.9}$$

Note that considering the ODE of the lowest weight component $\overline{\psi}_n$ for the first fundamental representation of $A_r^{(1)}$ and $D_r^{(1)}$, one can recover the adjoint ODE. Since we defined the inner product to be the $\mathfrak{g}$-invariant, the inner product of the solutions to the original and the dual ODE are independent of x:

$$\begin{aligned} \partial_x\langle\Psi^*,\Psi\rangle &= \langle\partial_x\Psi^*,\Psi\rangle + \langle\Psi^*,\partial_x\Psi\rangle \\ &= -\langle A^*_{\mathfrak{g}}\Psi^*,\Psi\rangle - \langle\Psi^*, A_{\mathfrak{g}}\Psi\rangle = 0. \end{aligned} \tag{3.3.10}$$

We define the subdominant solution and the basis, which we refer the dual basis, in the same way as the original linear problem and denote $\overline{\Psi}$ and $\overline{\mathcal{X}}_i$ $(i = 1, 2, \ldots, \dim\, V)$, respectively. We define the asymptotic behavior of the dual basis near the origin by

$$\overline{\mathcal{X}}_i(x, E, l) = x^{h_i \cdot g} J^{-1} \mathbf{e}_i + \cdots, \qquad x \to 0, \tag{3.3.11}$$

so that the basis and the dual basis satisfy the orthonormal condition:

$$\langle \mathcal{X}_i^*, \mathcal{X}_j \rangle = {}^t\bar{\mathcal{X}}_i J \mathcal{X}_j = \delta_{ij}. \tag{3.3.12}$$

Then we arrive at the simple expression of the expansion coefficients $\mathcal{Q}_i$ in (3.3.1):

$$\mathcal{Q}_i(E, l) = \langle \mathcal{X}_i^*, \Psi \rangle, \tag{3.3.13}$$

where Ψ is the subdominant solution to the original linear problem. The zeros of $\mathcal{Q}_i$ are evaluated in a similar way which we discussed in the argument of the adjoint ODE. Let n be the dimension of the representation V and expand the subdominant solution and the basis by the weight vector: $\Psi = \sum_{j=1}^n \psi_j \boldsymbol{e}_j$, $\mathcal{X}_i = \sum_{j=1}^n \chi_{i,j} \boldsymbol{e}_j$. The coefficient is expanded as

$$\mathcal{Q}_i(E, l) = \langle \mathcal{X}_i^*, \Psi \rangle = \sum_{j=1}^n \bar{\chi}_{i,j}\ \psi_j. \tag{3.3.14}$$

As discussed before, we need to find the dominant contribution in this summation at large but finite x. We have already derived the asymptotic behavior of the subdominant solution Ψ in (3.2.47). Then it is easy to find such a term is the component of the lowest weight vector. Therefore the E-dependence of the coefficient $\mathcal{Q}_i$ is evaluated by

$$\mathcal{Q}_i(E, l)\ \sim\ \bar{\chi}_{i,n}(x_{\text{fixed}}, E, l)\ \psi_n(x_{\text{fixed}}) \qquad \text{for } x_{\text{fixed}} \gg 1, \tag{3.3.15}$$

so that zeros of $\mathcal{Q}_i$ are calculated by equating the solution[1] and zero: $\bar{\chi}_{i,n}(x_{\text{fixed}}, E, l) = 0$. Considering the dual linear problem for all the fundamental representations of rank r affine Lie algebra $\hat{\mathfrak{g}}$, one could obtain all Q-functions $Q^{(a)}$ $(a = 1, 2, \ldots, r)$. Although, this is not still efficient in the practical calculation because of the large dimension of the linear problem for higher rank affine Lie algebras.

[1]The algorithm to calculate the power series of the solution to the (dual) linear problem near the origin is described in appendix C.

To calculate all the Q-functions efficiently, we focus on a relation between Q-functions. Let us start with the $A_r^{(1)}$ case. Same as the argument of the ψ-system, remind the relation between the fundamental representations, which is an isomorphism between the a-th fundamental representation and the anti-symmetric tensor product of the first fundamental representation: $V^{(a)} \simeq \wedge^a V^{(1)}$. Associated with this relation, the solution to the linear problem for the a-th and the first fundamental representations are related by

$$\Psi^{(a)} = \bigwedge_{b=1}^{a} \Psi^{(1)}_{\left[b-\frac{a+1}{2}\right]}, \qquad a = 1, 2, \ldots, r. \tag{3.3.16}$$

Here we applied the Symanzik rotation to the solution $\Psi^{(1)}$ so that the right hand side of this equation satisfies the linear problem for a-th fundamental representation. Substituting the expansion in terms of the basis (3.2.51) into (3.3.16), one obtains the relation between the coefficient $\mathcal{Q}_i^{(1)}$ and the Q-function $Q^{(a)}$:

$$Q^{(a)}(E,l) = \sum_{j_0,\ldots,j_{a-1}=1}^{a} \epsilon_{j_0\cdots j_{a-1}} \prod_{k=0}^{a-1} \omega^{-k\lambda^{(1)}_{j_k}/hM} \mathcal{Q}^{(1)}_{j_k\left[\frac{a-1}{2}-k\right]}(E,l), \qquad a = 1, \ldots, r, \tag{3.3.17}$$

where $\epsilon_{j_0\cdots j_{a-1}}$ is the totally anti-symmetric tensor normalized as $\epsilon_{01\cdots a-1} = 1$, $\lambda^{(a)}$ is defined in (3.2.56), h is the Coxeter number:$h = r+1$, and we used the identification between the basis $\mathcal{X}_1^{(a)}$ and $\mathcal{X}_1^{(1)} \wedge \mathcal{X}_2^{(1)} \wedge \cdots \wedge \mathcal{X}_a^{(1)}$. Then we can calculate the a-th Q-function from the linear problem for the first fundamental representation. A similar relation holds for the representation $V^{(r)}$:

$$Q^{(a)} = \sum_{j_0,\ldots,j_{r-a}=1}^{r+1-a} \epsilon_{j_0\cdots j_{r-a}} \prod_{k=0}^{r-a} \Omega^{-k\lambda^{(r)}_{j_k}/hM} \mathcal{Q}^{(r)}_{j_k\left[\frac{r-a}{2}-k\right]}(E), \quad a = 2, \ldots, r. \tag{3.3.18}$$

In the same way, one can find the relation for any affine Lie algebras. As a few examples, we summarize the relation for the $D_r^{(1)}$ and $E_6^{(1)}$ cases. The Dynkin diagram of D_r algebra has partially the same form as the A-type one, which implies the relation: $V^{(a)} = \wedge^a V^{(1)}$ $(a = 1, \ldots, r-2)$. Then we obtain

$$Q^{(a)}(E) = \sum_{j_0,\ldots,j_{a-1}=1}^{a} \epsilon_{j_0\cdots j_{a-1}} \prod_{k=0}^{a-1} \Omega^{-k\lambda^{(1)}_{j_k}/hM} \mathcal{Q}^{(1)}_{j_k\left[\frac{r-a}{2}-k\right]}(E), \quad a = 2, \ldots, r-2. \tag{3.3.19}$$

Here h is the Coxeter number of D_r: $h = 2r-2$ The Similar argument for E_6 leads to the relation: $V^{(2)} = \wedge^2 V^{(1)}$, $V^{(4)} = \wedge^2 V^{(5)}$ and $\wedge^2 V^{(6)} = V^{(3)} \oplus V^{(6)}$, which can be converted to

$$\begin{aligned} Q^{(2)}(E) &= \sum_{j_0,j_1=1}^{2} \epsilon_{j_0 j_1} \Omega^{-\lambda_{j_1}^{(1)}/12M} \mathcal{Q}^{(1)}_{j_0\left[\frac{1}{2}\right]}(E) \mathcal{Q}^{(1)}_{j_1\left[-\frac{1}{2}\right]}(E), \\ Q^{(4)}(E) &= \sum_{j_0,j_2=1}^{2} \epsilon_{j_0 j_1} \Omega^{-\lambda_{j_1}^{(5)}/12M} \mathcal{Q}^{(5)}_{j_0\left[\frac{1}{2}\right]}(E) \mathcal{Q}^{(5)}_{j_1\left[-\frac{1}{2}\right]}(E), \\ Q^{(3)}(E) &= \sum_{j_0,j_2=1}^{2} \epsilon_{j_0 j_1} \Omega^{-\lambda_{j_1}^{(6)}/12M} \mathcal{Q}^{(6)}_{j_0\left[\frac{1}{2}\right]}(E) \mathcal{Q}^{(6)}_{j_1\left[-\frac{1}{2}\right]}(E). \end{aligned} \tag{3.3.20}$$

For other types of untwisted affine algebras, see appendix C of [39].

From the above arguments, we can calculate the zeros of the Q-functions for any fundamental representation of affine Lie algebras, which can be compared to the Bethe roots. To this end, there is one thing left: the determination of the constant v in the non-linear integral equation (2.3.11). One can set b_0 from the asymptotic behavior of the Bethe root at $|E| \to \infty$. Note that the subdominant solution has the asymptotic behavior

$$\Psi(x,E) \sim \exp\left(\nu \int_x^\infty \left(p(x',E)^{1/h} - x'^M\right) dx' - \nu \frac{x^{M+1}}{M+1}\right) e^{-1/h \log p(x,E) \rho^\vee \cdot H} \boldsymbol{\nu}, \tag{3.3.21}$$

where $\boldsymbol{\nu}$ is the eigenvector of Λ_+ defined in (3.2.45) with eigenvalue ν whose real part is the largest among other eigenvalues of Λ_+. Consider the simply-laced affine Lie algebra $\hat{\mathfrak{g}}$ of rank r. For the fundamental representation $V^{(a)}$, we denote the eigenvalue as $\nu^{(a)}$. It can be proven that the vector $(\nu^{(1)}, \nu^{(2)}, \ldots, \nu^{(r)})$ satisfies

$$2\nu^{(a)} \cos\frac{\pi}{h} = \sum_{b=1}^{r} (G_{ab}) \nu^{(b)}, \qquad a = 1, 2, \ldots, r, \tag{3.3.22}$$

which is the same as the relation (2.3.10), so it is proportional to the Perron-Frobenius vector. $\nu^{(1)}$ is calculated from the matrix $\Lambda_+^{(1)}$, which we summarize in table 3.3.1 One is able to analytically continue the WKB solution Ψ to the region where $x < x_*$ around the turning point $x_* = E^{1/hM}$:

$$\begin{aligned} \Psi^{(a)} \sim \exp&\left(\nu^{(a)} \cos\frac{\pi}{h} \int_x^{x_0} |p(x)|^{1/h} \,\mathrm{d}x - \frac{1}{h} \log|p(x)| \rho^\vee \cdot H\right) \\ &\times \cos\left(\nu^{(a)} \sin\frac{\pi}{h} \int_x^{x_0} |p(x)|^{1/h} \,\mathrm{d}x - \frac{\pi}{h} \rho^\vee \cdot H\right) \boldsymbol{\nu}^{(a)}. \end{aligned} \tag{3.3.23}$$

$\mathfrak{g}$	A_r	D_r	E_6	E_7	E_8
$\nu^{(1)}$	1	$\sqrt{2}$	$\sqrt{2\sqrt{6}\cos\left(\frac{\pi}{12}\right)}$	$2\sqrt{2}\cos\left(\frac{\pi}{18}\right)$	$\sqrt{512\sqrt{3}\sin\left(\frac{\pi}{30}\right)\sin\left(\frac{\pi}{5}\right)\cos^2\left(\frac{2\pi}{15}\right)\cos^4\left(\frac{\pi}{5}\right)}$

Table 3.3.1: The first component of the Perron-Frobenius vector $\nu^{(1)}$ for simply-laced Lie algebras.

Here we denote the (co-)Wyle vector as ρ ($\rho^\vee$). If we impose the boundary condition $\Psi = 0$ at $x = 0$, from the dominant term, which is the first component $h_1^{(}a) = \omega_a$ where ω_a is the fundamental weight, one obtains the quantization condition:

$$\nu^{(a)} \sin\frac{\pi}{h}\int_0^{x_0} |p(x)|^{1/h}\,\mathrm{d}x = \frac{\pi}{2}\left(\frac{2}{h}\rho^\vee\cdot\omega_a + 2n + 1\right), \qquad n = 0, 1, 2, \ldots. \tag{3.3.24}$$

Changing the integration variable $x = E^{1/hM}t$, the integral in the left hand side of (3.3.24) is evaluated as

$$\int_0^{x_0} |p(x)|^{1/h}\,\mathrm{d}x = E^{\frac{M+1}{hM}}\int_0^1 (1-t^{hM})^{1/h}\mathrm{d}t = E^{\frac{M+1}{hM}}\frac{\sin\left(\pi\frac{M+1}{hM}\right)}{\sin(h\pi)}\kappa(hM,h), \tag{3.3.25}$$

where $\kappa(a,b)$ is given by

$$\kappa(a,b) \coloneqq \int_0^\infty \left((x^a+1)^{1/b} - x^{a/b}\right)dx = \frac{\Gamma(1+1/a)\Gamma(1+1/b)\sin\frac{\pi}{b}}{\Gamma(1+1/a+1/b)\sin\left(\frac{\pi}{a}+\frac{\pi}{b}\right)}. \tag{3.3.26}$$

Then, one finds the WKB approximation of the energy:

$$\left(E_n^{(a)}\right)^{\frac{M+1}{hM}} \sim \frac{\pi(\omega_a\cdot\rho + 2n + 1)}{\nu^{(a)}\sin\left(\pi(M+1)/hM\right)\kappa(hM,h)}, \qquad n = 0, 1, \ldots, \tag{3.3.27}$$

which is valid for large n. On the other hand, at the large E limit, the driving term $b_0 M_a e^\theta$ becomes dominant so that the Bethe roots are approximately evaluated as

$$E_n^{(a)} \sim \left(\frac{\pi}{b_0 M_a}(\omega_a\cdot\rho + 2n + 1)\right)^{1/\mu}, \qquad n = 0, 1, \ldots, \tag{3.3.28}$$

Comparing the equations (3.3.27) and (3.3.28), one finds the identification $\mu = \frac{M+1}{hM}$ and

$$b_0 = 2\sin(\pi\mu)\kappa(hM,h)\nu^{(1)}. \tag{3.3.29}$$

Together with the relation

$$\hat{\alpha}_a \coloneqq (1-h\mu)^{-1}\,\gamma_a, \qquad a = 1, 2, \ldots, r, \tag{3.3.30}$$

one can compute the Bethe roots from the NLIE. In table 3.3.2, we show both the zeros of the Q-functions, which were not able to compute from the adjoint ODE method, and the Bethe roots which is calculated from NLIE for the $\hat{\mathfrak{g}} = E_6^{(1)}$ case.

	zeros of Q-functions					
i	$E_i^{(1)}$	$E_i^{(2)}$	$E_i^{(3)}$	$E_i^{(4)}$	$E_i^{(5)}$	$E_i^{(6)}$
0	26.16492	19.04286	16.95324	19.98072	29.04567	21.54848
1	76.14709	37.06396	28.48668	38.50821	80.49209	52.00437
2	146.8766	64.52501	44.61201	66.15524	152.5322	93.90413
3	236.0037	95.98720	63.83908	97.97408	242.8648	145.7213
	Bethe roots					
i	$E_i^{(1)}$	$E_i^{(2)}$	$E_i^{(3)}$	$E_i^{(4)}$	$E_i^{(5)}$	$E_i^{(6)}$
0	26.16452	19.04232	16.95299	19.98020	29.04519	21.54807
1	76.14715	37.06297	28.48688	38.50782	80.49126	52.00351
2	146.8773	64.52390	44.61186	66.15433	152.5313	93.90137
3	236.0021	95.98496	63.83727	97.97372	242.8597	145.7216

Table 3.3.2: Spectra of $E_6^{(1)}$-type linear problem with the quadratic potential $p(x) = x^2 - E$ and the monodromy parameter $l = (5/12, 1/3, 0, -1/3, -5/12, 1/10)$. We set the reference point $x_{\text{fixed}} = 58$ for $V^{(1)}, V^{(5)}$ as well as $x_{\text{fixed}} = 46$ for $V^{(6)}$.

The Q-functions $Q^{(1)}, Q^{(5)}$ and $Q^{(6)}$ are computed by using the dual linear problem for the fundamental representations $V^{(1)}, V^{(5)}$ and $V^{(6)}$, respectively, while $Q^{(2)}, Q^{(4)}$ and $Q^{(3)}$ are evaluated from (3.3.20). One can confirm the agreements of these two in about 5-digits, which is a non-trivial test of the ODE/IM correspondence.

Summary

In this section, we first introduced the ODE/IM correspondence for the second order ODE with the monomial potential as the simplex example. The correspondence was generalized for the linear problem, the conformal limit of the modified affine Toda field equation. From the radial spectral problem, we defined the Q-functions from the linear problem. The BAEs were derived from the ψ-system which is the functional relation between the solutions and is associated with the relation in the representation theory of the Lie algebras. The zeros of the Q-functions were computed from the solutions to the dual linear problems. From the numerical computations of them and the Bethe roots from the NLIEs, we tested the ODE/IM correspondence numerically.

Chapter 4

TBA equations and its wall-crossing for the Schrödinder equation

In this chapter, we discuss the ODE/IM correspondence for the Schrödinger equation with polynomial potential [42]. One can derive the T-/Y-system of the integrable model from the Schrödinger equation, and then maps of the T-functions and Y-functions onto the context of the ODE are obtained. The logarithm of the Y-functions satisfy the TBA equations which we introduced in section 2.4. If we vary the parameters in the polynomial potential of the Schrödinger equation, the form of the TBA equations changes. This phenomenon is called the wall-crossing of the TBA equations [42, 44, 45]. Since different TBA equations may describe different integrable models, the ODE/IM correspondence for the polynomial potential is not the one-to-one correspondence. It is not easy to identify each corresponding model from the form of the TBA equations. However, at least, we can discuss the wall-crossing of the TBA equations in a systematic way which may provide some hints to the deeper understanding of the correspondence. The arguments in chapter 6 and 7 are basically the higher order generalization of that in this chapter.

4.1 T-/Y-Syetem from the Schrödinger equation

Let us begin with the ODE/IM correspondence for the Schrödinger equation with any polynomial potential, which is the generalization of the monomial case in section 3.1. We also introduce the parameter ϵ which plays the role of the plank constant but is set

complex. Setting the order of the potential $N+1$ ($N \in \mathbb{N}$), the ODE is given by

$$\left[-\epsilon^2 \frac{\mathrm{d}^2}{\mathrm{d}x^2} + p(x, u_i)\right]\psi(x, u_i; \epsilon) = 0, \qquad p(x, u_i) \coloneqq \sum_{i=0}^{N+1} u_i x^{N+1-i}. \tag{4.1.1}$$

Here the parameters u_i ($i = 0, 1, \ldots, N+1$) of the potential are complex. In relation to the connection to the Y-system and the Argyres-Douglas theory [56–58,60], which we will discuss the latter one in the next chapter, we call the ODE (4.1.1) the (A_1, A_N)-type ODE. Suppose $\psi(x, u_i; \epsilon)$ is the solution of (4.1.1), since it is invariant under the k-Symanzik rotation

$$x \to \omega^{-k} x, \quad u_j \to \omega^{-jk} u_j, \qquad j = 0, 1, \ldots, N+1, \tag{4.1.2}$$

where $\omega = e^{\frac{2\pi i}{N+3}}$, then the Symanzik rotation of the solution $\psi_k(x, \{u_i\}; \epsilon)$:

$$\psi_k(x, u_i; \epsilon) \coloneqq \omega^{\frac{k}{2}} \psi(\omega^{-k} x, \omega^{-ik} u_i; \epsilon) \tag{4.1.3}$$

solves the ODE (4.1.1) for $k \in \mathbb{Z}$. Note that ψ_k is also expressed by the solution ψ as $\psi_k(x, u_i; \epsilon) = \omega^{\frac{k}{2}} \psi(x, u_i; e^{\pi i k} \epsilon)$. Let ϕ be the subdominant solution along the real axis whose asymptotic behavior is

$$\phi(x, u_i; \epsilon) \sim \frac{\epsilon^{\frac{1}{2}} u_0^{-\frac{1}{4}}}{\sqrt{2i}} x^{-\frac{N+1}{4}} \exp\left(-\frac{1}{\epsilon} \frac{2u_0^{\frac{1}{2}}}{N+3} x^{\frac{N+3}{2}}\right), \quad |x| \to \infty, \tag{4.1.4}$$

Define ϕ_k from (4.1.3). ϕ_k becomes the subdominant solution in the Stokes sector $\mathcal{S}_k$:

$$\mathcal{S}_k = \left\{ x \in \mathbb{C}; \left| \arg x - \frac{2\pi k}{N+3} \right| < \frac{\pi}{N+3} \right\}. \tag{4.1.5}$$

As we saw in section 3.1, the T-function is the Stokes multiplier which is the Wronskian of the subdominant solutions. The set of the solutions $\{\phi_k, \phi_{k+1}\}$ forms the basis of the solution. Then, we define the T-function by

$$T_k(u_i; \epsilon) \coloneqq W[\phi_0, \phi_{k+1}]^{[-k-1]}. \tag{4.1.6}$$

Here we defined

$$g^{[k]}(u_i; \epsilon) \coloneqq g(u_i; e^{\frac{\pi i k}{2}} \epsilon). \tag{4.1.7}$$

Since the ODE (4.1.1) does not have the pole at the origin, solutions ϕ_k and ϕ_{k+N+3}, which are both subdominant in sector $\mathcal{S}_k$, have the relation: $\phi_k \propto \phi_{k+N+3}$. Then the T-function has the boundary conditions:

$$T_{-1} = T_{N+2} = 0, \qquad T_1 = T_{N+1} = 1. \tag{4.1.8}$$

Using the Plücker type relation of the Wronskians:

$$\begin{aligned} W[f_{k_1}, f_{k_2}]^{[+2]} W[f_{k_1}, f_{k_2}] &= W[f_{k_1+1}, f_{k_2+1}] W[f_{k_1}, f_{k_2}] \\ &= 1 + W[f_{k_1+1}, f_{k_2}] W[f_{k_1}, f_{k_2+1}], \end{aligned} \tag{4.1.9}$$

where we used the property: $W[f_{k_1}, f_{k_2}]^{[+2l]} = W[f_{k_1+l}, f_{k_2+l}]$, one can show that the T-functions satisfy the T-system:

$$T_k^{[+1]} T_k^{[-1]} = 1 + T_{k+1} T_{k-1}, \qquad a = 1, 2, \ldots, N+1. \tag{4.1.10}$$

The Y-function is defined as the product of the T-function:

$$Y_k^{-1} \coloneqq T_{k-1} T_{k+1}, \qquad k = 0, 1, \ldots, N+1, \tag{4.1.11}$$

which satisfy the (A_1, A_N)-type Y-system

$$Y_k^{[+1]} Y_k^{[-1]} = \left(1 + Y_{k-1}^{-1}\right)^{-1} \left(1 + Y_{k+1}^{-1}\right)^{-1}, \tag{4.1.12}$$

with the boundary condition: $Y_0^{-1} = Y_{N+1}^{-1} = 0$. For the convenience of discussing the relation between the Y-function and the WKB periods in the next section, we explicitly write down the Y-function by the Wronskian:

$$\begin{aligned} Y_{2j}(\{u_i\}; \epsilon) &= \frac{W[\phi_{-j-1}, \phi_{-j}] W[\phi_j, \phi_{j+1}]}{W[\phi_{-j}, \phi_j] W[\phi_{-j-1}, \phi_{j+1}]}(\{u_i\}; \epsilon), \\ Y_{2j+1}(\{u_i\}; \epsilon) &= \frac{W[\phi_{-j-2}, \phi_{-j-1}] W[\phi_j, \phi_{j+1}]}{W[\phi_{-j-1}, \phi_j] W[\phi_{-j-2}, \phi_{j+1}]}(\{u_i\}; e^{\frac{\pi i}{2}} \epsilon). \end{aligned} \tag{4.1.13}$$

Here all the Wronskians in the numerator are equal to one, and the right hand side of the second equation of (4.1.13) is the cross-ratio of the Wronskian evaluated at the shifted ϵ, which follows from the definitions (4.1.6) and (4.1.11).

4.2 WKB periods and Y-functions

In this section, we apply the WKB analysis to the ODE (4.1.1). Without losing the generality, one can set $u_0 = 1$. We define the WKB ansatz of the solution which has the form

$$\psi(x) = \exp\left(\pm\frac{1}{\epsilon}\int^x P(x')dx'\right), \quad P(x) = \sum_{n=0}^{\infty}\epsilon^n p_n(x), \tag{4.2.1}$$

where $P(x)$ satisfy the Riccati equation:

$$P^2(x) \pm \epsilon\partial_x P(x) - p(x) = 0. \tag{4.2.2}$$

Decomposing the expansion into the even part $P_{\text{even}}(x)$ and the odd part $P_{\text{odd}}(x)$:

$$P(x) = P_{\text{even}}(x) + P_{\text{odd}}(x), \tag{4.2.3}$$

where

$$P_{\text{even}}(x) \coloneqq \sum_{m=0}\epsilon^{2m}p_{2m}(x), \qquad P_{\text{odd}}(x) \coloneqq \sum_{m=0}\epsilon^{2m+1}p_{2m+1}(x), \tag{4.2.4}$$

it is straightforward to show that the odd part can be written by the even part:

$$P_{\text{odd}}(x) = \mp\frac{\epsilon}{2}\partial_x \log P_{\text{even}}(x). \tag{4.2.5}$$

Substituting the ϵ-expansion of $P(x)$ into the Riccati equation (4.2.2), one can obtain the relations between p_n:

$$p(x) - \sum_{n,m=0}^{\infty} p_n p_m \epsilon^{n+m} \pm \epsilon\sum_{n=0}^{\infty}\partial_x p_n \epsilon^n = 0. \tag{4.2.6}$$

p_n is calculated from this equation recursively. Here we show the first several terms up to the total derivative terms

$$p_0 = \pm p(x), \tag{4.2.7}$$

$$p_2 = \frac{1}{16}\frac{\partial^2 p_0}{p_0^2}, \tag{4.2.8}$$

$$p_4 = -\frac{5}{226}\frac{(\partial_x p_0)^2}{p_0^5} + \frac{3}{1024}\frac{\partial^4 p_0}{p_0}, \tag{4.2.9}$$

$$p_6 = \frac{371}{16384}\frac{(\partial_x p_0)^2}{p_0^8} + \frac{1}{2048}\frac{(\partial_x^3 p_0)^2}{p_0^7} - \frac{105}{16384}\frac{\partial_x^2 p_0 \partial_x^4 p_0}{p_0^7} + \frac{5}{32768}\frac{\partial_x^6 p_0}{p_0^6}. \tag{4.2.10}$$

To proceed with the WKB analysis, let us introduce the WKB curve Σ:

$$\Sigma : \ y^2 = p(x), \tag{4.2.11}$$

which define the hyper-elliptic curve of genus $g = \lfloor \frac{N+1}{2} \rfloor$ [109]. The Riemann surface Σ is represented by the two sheets of the complex plane with $N+1$ branch points x_k $(k = 0, 1, \ldots, N)$. We suppose these branch points are all distinct, and set the branch cuts such that all of them start from a branch point and end to one of the other branch points for the odd N case, while one of them extends to infinity for the even N case. For the 1-cycle γ on the WKB curve Σ, we define the WKB period Π_γ which is given by

$$\Pi_\gamma \coloneqq \oint_\gamma P(x')\mathrm{d}x. \tag{4.2.12}$$

Expanding $P(x)$ in terms of ϵ, the WKB periods are written in the form:

$$\Pi_\gamma = \sum_{n=0}^{\infty} \epsilon^n \Pi_\gamma^{(n)}, \qquad \Pi_\gamma^{(n)} \coloneqq \oint_\gamma p_n(x')\mathrm{d}x, \tag{4.2.13}$$

where all the odd terms vanish since the integrand of $\Pi_\gamma^{(n)}$ for odd n is the total derivative. We call the leading term $\Pi_\gamma^{(0)}$ the classical period while $\Pi_\gamma^{(n)}$ for $n \neq 0$ is called the quantum correction. Although one can calculate the quantum corrections directly from the definition (4.2.13), there is a useful trick that enables us to compute them more easily. Recall that on the Riemann surface, we can take the basis of the meromorphic basis:

$$\omega_i = \frac{x^{i-1}}{y}\mathrm{d}x, \qquad i = 1, 2, \ldots, N, \tag{4.2.14}$$

where the first $\lfloor \frac{N+1}{2} \rfloor$ differentials are holomorphic. Defining the meromorphic differential $\lambda \coloneqq y\mathrm{d}x$ which we call the Seiberg-Witten (SW) differential due to the connection to the SW theory [47, 48], these bases are expressed by

$$\omega_i = 2\frac{\partial}{\partial u_{N+2-i}}\lambda. \tag{4.2.15}$$

Since the integrands of the quantum corrections of the WKB period are written by the linear combination of the meromorphic basis $\{\omega_1, \omega_2, \ldots, \omega_N\}$ up to the total derivatives:

$$p_n = 2\sum_{i=1}^{N} B_{ni}\omega_i + \mathrm{d}(*) = 2\sum_{i=1}^{N} B_{ni}\partial_{u_{N+2-i}}\lambda + \mathrm{d}(*), \tag{4.2.16}$$

where d(∗) represents the total derivative term, one finds that they can be calculated from the classical period:

$$\Pi_\gamma^{(n)} = 2\sum_{i=1}^{N} B_{ni}\partial_{u_{N+2-i}}\Pi_\gamma^{(0)}. \tag{4.2.17}$$

Here the differential operator $\mathcal{O}_i^{(n)}$ which is defined by

$$\mathcal{O}_i^{(n)} \coloneqq 2\sum_{i=1}^{N} B_{ni}\partial_{u_{N+2-i}}, \tag{4.2.18}$$

is called the Picard-Fuchs operator. Therefore we can compute the formal ϵ-series of the WKB period from the classical period

$$\Pi_\gamma^{(0)} = \oint_\gamma p_0 \mathrm{d}x \tag{4.2.19}$$

and the Picard-Fuchs operators $\mathcal{O}_i^{(n)}$ $(i = 1, 2, \dots, N,\ n = 2, 4, \dots)$.

Now we relate the Y-functions (4.1.13) to the WKB periods. The subdominant solution ϕ_k is evaluated by the WKB approximation as

$$\phi_k(x, \{u_i\}; \epsilon) = (-1)^{\frac{k}{2}} c(\epsilon) \exp\left(\frac{\delta_k}{\epsilon}\int_{q_k}^{x} P(x')\mathrm{d}x\right), \tag{4.2.20}$$

where q_k is the initial point of the integration, $c(\epsilon) = \frac{1}{\sqrt{2i}}\epsilon^{\frac{N+1}{2(N+3)}}$ and $\delta_k = \pm(-1)^k$ is the sign factor which depends on the sheet the end point x of the integral lives: for the sheet on which $y = p(x)$, the plus sign is chosen, while for the sheet where $y = -p(x)$, we choose the minus sign. Then, one finds that the Wronskian $W[\phi_{k_1}, \phi_{k_2}]$ is evaluated by the WKB analysis as

$$W[\phi_{k_1}, \phi_{k_2}] = i(-1)^{\frac{k_1+k_2}{2}}\delta_{k_1}\exp\left[\frac{\delta_k}{\epsilon}\int_{q_{k_1}}^{q_{k_2}} P_{\mathrm{even}}(x')\mathrm{d}x + \frac{1}{2}\sum_{i=1,2}\log P_{\mathrm{even}}(q_{k_i})\right]. \tag{4.2.21}$$

Here we chose the sign factor as $\delta_{k_1} = -\delta_{k_2}$ so that the Wronskian does not have the explicit dependence of x. To define the 1-cycle on the WKB curve, let us suppose the distribution of the branch points. We set the all the branch points are aligned on the real axis and label them such that $x_{k-1} \geq x_k$ $(k = 1, 2, \dots, N)$. The branch cuts stars from x_{2k} and end on x_{2k+1} for $k = 0, 1, \dots$, while for even N, one of them starts from x_N and

extends to $-\infty$. Define cycle γ_{2j+1} $(j = 0, 1, \dots)$ which encircles the branch points x_{2j} and x_{2j+1} anticlockwise on the sheet where $y = p(x)$, and cycle γ_{2j} $(j = 1, \dots)$ which encircles the branch points x_{2j-1} and x_{2j} anticlockwise intersecting the cycles γ_{2j-1} and γ_{2j+1} in the region $\{x \in \mathbb{C}; \operatorname{Im} x > 0\}$. The cycles are shown in figure 4.2.1. For these

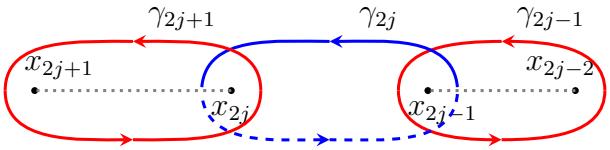

Figure 4.2.1: The cycle γ_{2j-1}, γ_{2j} and γ_{2j+1}. The solid lines are on the sheet where $y = p(x)$ while the dashed line is on the sheet where $y = -p(x)$. The dotted lines represent the branch cuts.

cycles, one can consider the WKB periods and find that they correspond to the logarithm of the Y-functions:

$$\log Y_{2j}(\{u_i\}, \epsilon) = \frac{1}{\epsilon}\Pi_{\gamma_{2j}}(\{u_i\}, \epsilon), \qquad \log Y_{2j+1}(\{u_i\}, \epsilon) = \frac{1}{i\epsilon}\Pi_{\gamma_{2j+1}}(\{u_i\}, i\epsilon), \tag{4.2.22}$$

where, by the equality, we mean that the l.h.s. and the r.h.s. are equal in terms of the formal ϵ-expansions. Note that the Y-functions are analytic functions of u_i while we defined the WKB periods as the formal expansions of ϵ. This relation can be understood by substituting (4.2.21) into the logarithm of (4.1.13) and linking the integration paths together:

$$\begin{aligned}\log Y_{2j}(\{u_i\}; \epsilon) &\propto \frac{1}{\epsilon}\left(\int_{q_{-j-1}}^{q_{-j}} - \int_{q_j}^{q_{-j}} + \int_{q_j}^{q_{j+1}} - \int_{q_{-j-1}}^{q_{j+1}}\right) P_{\text{even}}(x'; \epsilon)\mathrm{d}x' \qquad (4.2.23)\\ &= \frac{1}{\epsilon}\oint_{\gamma_{2j}} P_{\text{even}}(x'; \epsilon)\mathrm{d}x',\\ \log Y_{2j+1}(\{u_i\}; \epsilon) &\propto \frac{1}{i\epsilon}\left(\int_{q_{-j-2}}^{q_{-j-1}} - \int_{q_j}^{q_{-j-1}} + \int_{q_j}^{q_{j+1}} - \int_{q_{-j-2}}^{q_{j+1}}\right) P_{\text{even}}(x'; i\epsilon)\mathrm{d}x' \qquad (4.2.24)\\ &= \frac{1}{i\epsilon}\oint_{\gamma_{2j+1}} P_{\text{even}}(x'; i\epsilon)\mathrm{d}x'.\end{aligned}$$

In figure 4.2.2, we draw the integration paths for Y_{2j} and Y_{2j+1}. From the relation (4.2.22), we can calculate the masses m_k $(k = 1, 2, \dots, N)$ i.e. the leading term of the logarithm

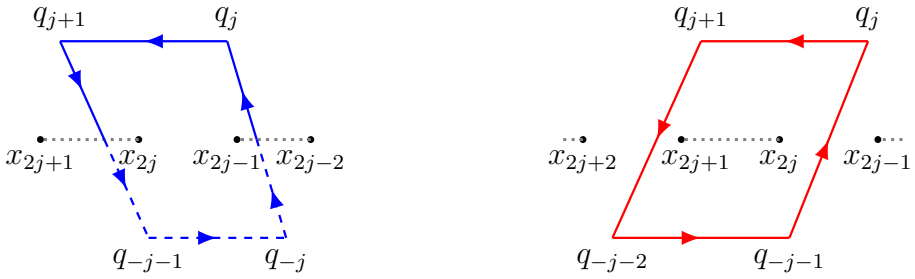

Figure 4.2.2: The integration paths for Y_{2j} (a) and Y_{2j+1} (b).

of the Y-functions:

$$\log Y_k(\{u_i\};\epsilon) \sim i^{\frac{(-1)^k-1}{2}} \frac{1}{\epsilon} \oint_{\gamma_k} p_0(x')\mathrm{d}x \coloneqq \frac{m_k}{\epsilon}, \qquad k = 1, 2, \ldots, N. \tag{4.2.25}$$

If the potential is negative in the interval $[x_{k+1}, x_k] \coloneqq \{x \in \mathbb{R}; x_{k+1} \leq x \leq x_k\}$, we call it the classically allowed region, and if the neighbor interval $[x_k, x_{k-1}]$ where the potential is positive, we call it the classically forbidden region. Then all the masses are real or pure imaginary. In the next section, we consider the more general situation in which the branch points are not aligned in the real axis, and then the phases of the masses changes.

4.3 Wall-crossing phenomenon of TBA equations

In this section, we consider the (A_1, A_N)-type TBA equations which can be obtained from the (A_1, A_N)-type Y-system (2.4.19). We adopt the canonical variable $\theta \coloneqq -\log \epsilon$ for the TBA equations, and suppose that all mass terms are real and positive. The TBA equations lead

$$\log \overline{Y}_k(\theta) = |m_k| e^{\theta} - \frac{1}{2\pi} K_{k,k-1} \star \overline{L}_{k-1} - \frac{1}{2\pi} K_{k,k+1} \star \overline{L}_{k+1}, \qquad k = 1, 2, \ldots, N, \tag{4.3.1}$$

where $\log \overline{Y}_k(\theta) \coloneqq \log Y_k(\theta - i\phi_k)$, $\overline{L}_k(\theta) \coloneqq L_k(\theta - i\phi_k)$, and the kernel function is given by

$$K_{k_1,k_2}(\theta) \coloneqq \frac{1}{2\cosh(\theta - i(\phi_{k_1} - \phi_{k_2}))}. \tag{4.3.2}$$

For $k = 1$ and N, we defined $\overline{L}_0 = \overline{L}_{N+1} = 0$. Since we have set all the mass terms real and positive, $\phi_k = 0$ for $k = 1, 2, \ldots, N$, and the TBA equations (4.3.1) are valid.

However, there is a situation in which the TBA equation is no longer valid. When we vary the parameters u_i in the potential, the phases become non-zero. The kernel function has the poles at $\theta = \frac{\pi i}{2}(2n+1) + i(\phi_{k_1} - \phi_{k_2})$ $(n \in \mathbb{Z})$. Then we have to pick up the residues of the kernel so that the form of the TBA equations change if the absolute values of the differences of the phases are greater than $\frac{\pi}{2}$. Let us consider the case where $\frac{\pi}{2} < \phi_{l+1} - \phi_l < \frac{3\pi}{2}$ and $|\phi_{m+1} - \phi_m| < \frac{\pi}{2}$ $(m \neq l)$, and focus on the convolution term

$$K_{k,k+1} \star \overline{L}_{k+1}(\theta) = \int_{\mathbb{R}} \mathrm{d}\theta' \frac{\overline{L}_{k+1}(\theta')}{2\cosh(\theta - i(\phi_k - \phi_{k+1}) - \theta')}. \tag{4.3.3}$$

If $|\phi_{k+1} - \phi_k| < \frac{\pi}{2}$, there is no contribution from poles, but for $\frac{\pi}{2} < \phi_{k+1} - \phi_k < \frac{3\pi}{2}$, we have to pick up the pole at $\theta' = -\frac{\pi i}{2} + \theta + i(\phi_{k+1} - \phi_k)$ for the analytical continuation, whose residue is $2\pi\overline{L}_{k+1}(\theta + i(\phi_{k+1} - \phi_k) - \frac{\pi i}{2}) = 2\pi L_{k+1}(\theta - i\phi_k - \frac{\pi i}{2})$. Figure 4.3.1 represents the poles of the kernels and the contribution of the residue for $k = m$ and $k = l$. A similar

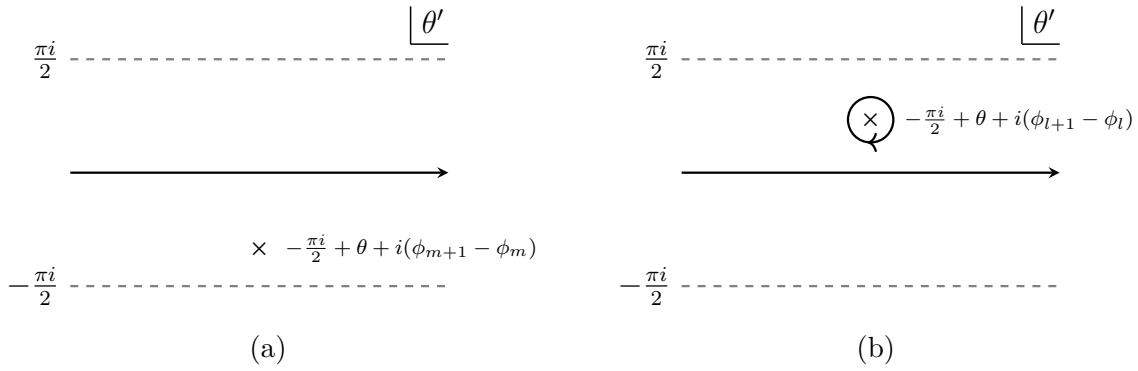

Figure 4.3.1: The pole of the kernel of $K_{m,m+1}$ (a), and that of $K_{l,l+1}$ (b). The arrows represent the integration paths. In (b), there is the contribution from the pole at $\theta' = -\frac{\pi i}{2} + \theta + i(\phi_{l+1} - \phi_l)$.

argument holds for the term $K_{k,k-1} \star \overline{L}_{k-1}$, in which pole at $\frac{\pi i}{2} + \theta - i(\phi_k - \phi_{k-1})$ contributes when $\frac{\pi}{2} < \phi_{k+1} - \phi_k < \frac{3\pi}{2}$. The residue at the pole is $2\pi\overline{L}_{k-1}(\theta - i(\phi_k - \phi_{k-1}) + \frac{\pi i}{2}) = 2\pi L_{k-1}(\theta - i\phi_k + \frac{\pi i}{2})$. As a result, the TBA equations (4.3.1) are analytically continued

to the form:

$$\begin{aligned}
\log \overline{Y}_k(\theta) &= |m_k| e^{\theta} - \frac{1}{2\pi} \sum_{j=k-1,k+1} K_{k,j} \star \overline{L}_j, \qquad k \neq l, l+1, \\
\log \overline{Y}_l(\theta) &= |m_l| e^{\theta} - \frac{1}{2\pi} \sum_{j=l-1,l+1} K_{l,j} \star \overline{L}_j - L_{k+1}\Big(\theta - i\phi_l - \frac{\pi i}{2}\Big), \\
\log \overline{Y}_{l+1}(\theta) &= |m_{l+1}| e^{\theta} - \frac{1}{2\pi} \sum_{j=l,l+2} K_{l+1,j} \star \overline{L}_j - L_k\Big(\theta - i\phi_{l+1} + \frac{\pi i}{2}\Big).
\end{aligned} \tag{4.3.4}$$

This system would not close unless we consider the additional equations for $\log Y_l(\theta - i\phi_{l+1} + \frac{\pi i}{2})$ and $\log Y_{l+1}(\theta - i\phi_l - \frac{\pi i}{2})$. Therefore the resulting TBA system will be formed by $N+2$ equations.

There is another way to obtain the closed TBA system, in which we define the new Y-functions by

$$\begin{gathered}
Y_l^{\mathrm{n}}(\theta) \coloneqq Y_l(\theta)\Big(1 + Y_{l+1}^{-1}(\theta - \frac{\pi i}{2})\Big), \quad Y_{l+1}^{\mathrm{n}}(\theta) \coloneqq Y_{l+1}(\theta)\Big(1 + Y_l^{-1}(\theta + \frac{\pi i}{2})\Big), \\
Y_{\mathrm{ad}}^{\mathrm{n}}(\theta) \coloneqq 1 + Y_l(\theta) + Y_{l+1}(\theta - \frac{\pi i}{2}), \qquad Y_k^{\mathrm{n}} \coloneqq Y_k, \quad k \neq l, l+1.
\end{gathered} \tag{4.3.5}$$

Here we defined Y_l^{n} and Y_{l+1}^{n} so that the contributions from the poles in (4.3.4) are absorbed in the new Y-functions. The additional Y-function $Y_{\mathrm{ad}}^{\mathrm{n}}$ is defined so that, together with Y_l^{n} and Y_{l+1}^{n}, it satisfies

$$\big(1 + Y_l^{-1}(\theta)\big) = \Big(1 + \frac{1}{Y_l^{\mathrm{n}}(\theta)}\Big)\Big(1 + \frac{1}{Y_{\mathrm{ad}}^{\mathrm{n}}(\theta)}\Big), \tag{4.3.6}$$

$$\big(1 + Y_{l+1}^{-1}(\theta)\big) = \Big(1 + \frac{1}{Y_{l+1}^{\mathrm{n}}(\theta))}\Big)\Big(1 + \frac{1}{Y_{\mathrm{ad}}^{\mathrm{n}}(\theta + \frac{\pi i}{2})}\Big), \tag{4.3.7}$$

$$Y_l^{\mathrm{n}}(\theta) Y_{l+1}^{\mathrm{n}}(\theta - \frac{\pi i}{2}) = Y_{\mathrm{ad}}^{\mathrm{n}}(\theta)\Big(1 + \frac{1}{Y_{\mathrm{ad}}^{\mathrm{n}}(\theta)}\Big). \tag{4.3.8}$$

The asymptotic behaviors for the new Y-functions Y_k^{n} $(k = 1, 2, \ldots, N)$ at $\theta \to \infty$ are the same as the original ones: $\log Y_k^{\mathrm{n}} \sim m_k e^{\theta}$, while from (4.3.8), that of the additional Y-functions $Y_{\mathrm{ad}}^{\mathrm{n}}$ is $\log Y_{\mathrm{ad}}^{\mathrm{n}} \sim m_{\mathrm{ad}} e^{\theta}$ where

$$m_{\mathrm{ad}} = |m_{\mathrm{ad}}| e^{i\phi_{\mathrm{ad}}} \coloneqq m_l + e^{-\frac{\pi i}{2}} m_{l+1}, \tag{4.3.9}$$

which is expressed by the classical WKB period as

$$m_{\mathrm{ad}} = i^{\frac{(-1)^l-1}{2}}\Pi^{(0)}_{\gamma_l} + i^{\frac{(-1)^{l+1}-1}{2}}e^{-\frac{\pi i}{2}}\Pi^{(0)}_{\gamma_{l+1}} = i^{\frac{(-1)^l-1}{2}}\Pi^{(0)}_{\gamma_l+\gamma_{l+1}}. \tag{4.3.10}$$

The introduction of the additional Y-function $Y^{\mathrm{n}}_{\mathrm{ad}}$ corresponds to the emergence of the new cycle $\gamma_l+\gamma_{l+1}$ on the WKB curve, which is depicted in figure 4.3.2. Using the relations

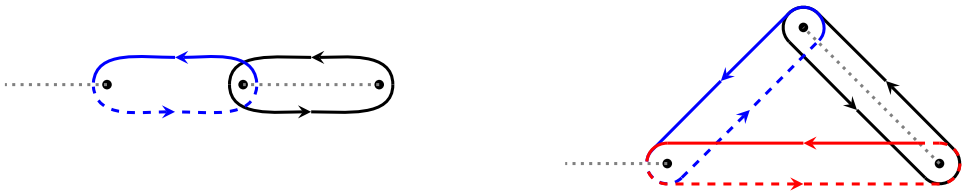

(a) (b)

Figure 4.3.2: The black and blue lines represent 1-cycles γ_l and γ_{l+1}, respectively, in both (a) and (b), while the red line represents the cycle $\gamma_l+\gamma_{l+1}$ in (b) for $l=2j+1$ ($j\in\mathbb{N}$).

(4.3.6) and (4.3.7), and shifting the variable θ so that the integration path is on the real axis without crossing the poles, one finds the TBA equations for the new Y-functions become

$$\begin{aligned}
\log \overline{Y}^{\mathrm{n}}_k &= |m_k|e^{\theta} - \frac{1}{2\pi}\sum_{j=k-1,k+1} K_{k,j}\star \overline{L}^{\mathrm{n}}_j, \qquad k\neq l,l+1,l+2,\\
\log \overline{Y}^{\mathrm{n}}_l &= |m_l|e^{\theta} - \frac{1}{2\pi}\sum_{j=l-1,l+1} K_{l,j}\star \overline{L}^{\mathrm{n}}_j - \frac{1}{2\pi}K^{+}_{l,\mathrm{ad}}\star \overline{L}^{\mathrm{n}}_{\mathrm{ad}},\\
\log \overline{Y}^{\mathrm{n}}_{l+1} &= |m_{l+1}|e^{\theta} - \frac{1}{2\pi}\sum_{j=l,l+2} K_{l+1,j}\star \overline{L}^{\mathrm{n}}_j - \frac{1}{2\pi}K_{l+1,\mathrm{ad}}\star \overline{L}^{\mathrm{n}}_{\mathrm{ad}},\\
\log \overline{Y}^{\mathrm{n}}_{l+2} &= |m_{l+2}|e^{\theta} - \frac{1}{2\pi}\sum_{j=l+1,l+3} K_{l+2,j}\star \overline{L}^{\mathrm{n}}_j - \frac{1}{2\pi}K^{+}_{l+2,\mathrm{ad}}\star \overline{L}^{\mathrm{n}}_{\mathrm{ad}}.
\end{aligned} \tag{4.3.11}$$

Here we defined $\overline{L}^{\mathrm{n}}_{\mathrm{ad}}(\theta) \coloneqq L^{\mathrm{n}}_{\mathrm{ad}}(\theta - i\phi_{\mathrm{ad}}) = \log(1+(Y^{\mathrm{n}}_{\mathrm{ad}}(\theta-i\phi_{\mathrm{ad}}))^{-1})$ and the shifted kernel $K^{\pm}(\theta) \coloneqq K(\theta\pm\frac{\pi}{2})$. The additional equation for $\log Y^{\mathrm{n}}_{\mathrm{ad}}$ is obtained by summing the new TBA equation for Y^{n}_l evaluated at $\theta - i\phi_{l+1} + \frac{\pi i}{2}$ and that for Y^{n}_{l+1} evaluated at $\theta - i\phi_l$:

$$\log \overline{Y}^{\mathrm{n}}_{\mathrm{ad}} = |m_{\mathrm{ad}}|e^{\theta} - \frac{1}{2\pi}\sum_{j=l-1,l+1} K_{\mathrm{ad},j}\overline{L}^{\mathrm{n}}_j - \frac{1}{2\pi}\sum_{j=l,l+2} K^{-}_{\mathrm{ad},j}\overline{L}^{\mathrm{n}}_j. \tag{4.3.12}$$

Together with (4.3.11), these $N+1$ integral equations form the TBA system for the new Y-functions (4.3.5).

The phenomenon explained in this section is called the wall-crossing of the TBA equations [43]. As we will discuss in chapter 5, the classical WKB periods are interpreted as the central charges of the BPS particles in 4-dimensional $\mathcal{N}=2$ theories. Furthermore, the condition in which wall-crossing of the TBA equations occurs is the same as the wall-crossing condition in the context of 4d $\mathcal{N}=2$ theories [67, 68], which is that any two of the classical periods associated with 1-cycles γ and γ' align: $\mathrm{Im}\left(\Pi^{(0)}_{\gamma}/\Pi^{(0)}_{\gamma'}\right)=0$. The emergence of the additional Y-function or cycle implies the creation of the new BPS particle, which is governed by the Kontsevich-Soibelmen wall-crossing formula [66].

4.4 Diagrammatic procedure of wall-crossing

The procedure of the wall-crossing of the TBA equations can be applied to more general settings. Starting with the case that all the mass terms are real or pure imaginary, one has to add a new equation for the additional Y-function to the TBA system by each wall-crossing process. As we have seen in the previous section, the additional Y-function is associated with the new cycle on the WKB curve. Let us Consider the configuration space of the coefficients of the polynomial potential i.e. the space of u_i. This space is expressed by a disjoint union of domains in which the form of the TBA equations is unique. We call each domain the chamber.[1] There are two special chambers in which the numbers of the TBA equations are minimum or maximum, respectively. Such chambers are called the minimal or maximal chambers. For the N-th polynomial potential, the number of the equations of the TBA in the minimal chamber is N while it is $N(N+1)/2$ in the maximal chamber. So, there are, at least, $N(N-1)/2$ wall-crossings when we continuously deform the potential from the minimal to the maximal chamber. Between the minimal and the maximal chambers, there are $N(N-1)/2-1$ intermediate chambers in which the TBA system is composed of n ($N<n<N(N+1)/2$) equations. To obtain the TBA

[1] We regard the all regions in which the TBA are common as a same chamber. Thus, the chamber itself can be a disjoint union of several domains.

equations in the maximal chamber from that of the minimal chamber, one has to apply the wall-crossing procedure $N(N-1)/2$ times, which is hard to carry on by the algebraic computation for the large N. In [44], it was introduced that the diagrammatic method to obtain the TBA equations in any chamber, which is much easier than the algebraic way. In this section, we explain this diagrammatic way of the wall-crossing following the notation in [45] and derive the (A_1, A_N)-type TBA system in the maximal chamber.

Let us denote the cycle which encircles the branch points x_i and x_j as $\gamma_{(i,j)}$, and the classical period and the Y-function associated with this cycle as $\Pi^{(0)}_{(i,j)}$ and $Y_{(i,j)}$, respectively. In the minimal chamber, the phase of the classical period $\varphi_a \coloneqq \arg \Pi^{(0)}_a$ $(a = (a-1, a))$ is 0 or $\pi/2$, depending on whether the cycle γ_a is on the classically allowed or forbidden region. One can write the leading terms of the Y-functions by using the classical periods instead of the masses, which leads the TBA equations in the minimal chamber in the period representation:

$$\log \widetilde{Y}_a(\theta) = \left|\Pi^{(0)}_a\right| e^{\theta} + \frac{1}{2\pi i} \sum_{b \in s^{(0)}_N} \widetilde{K}_{a,b} \star \widetilde{L}_b(\theta), \qquad a \in s^{(0)}_N, \tag{4.4.1}$$

where we defined $\widetilde{Y}_a(\theta) \coloneqq Y_a(\theta - i\varphi_a)$, $\widetilde{L}_a(\theta) \coloneqq L_a(\theta - i\varphi_a)$, the set $s^{(0)}_N \coloneqq \{(i-1, i); i = 1, 2, \ldots, N\}$, and the kernel function $\widetilde{K}_{a,b}$ by

$$\widetilde{K}_{a,b} = \frac{I_{ab}}{\sinh(\theta + i(\varphi_a - \varphi_b))}. \tag{4.4.2}$$

Here each entry of the anti-symmetric matrix I_{ab}, which we call the intersection matrix, is determined from the intersection number of the cycles γ_a and γ_b: $I_{(a-1,a),(b-1,b)} = (-1)^{a-1}\delta_{a,b-1}$, otherwise $I_{ab} = 0$. The poles of the kernel are shifted to $\theta + i(\varphi_a - \varphi_b) = 0$. The advantage of the period representation is that even after the wall-crossings, we do not need to introduce the shifted kernels which we used in the previous section. Let us consider the wall-crossing where $\varphi_{(l+1,l+2)} - \varphi_{(l,l+1)}$ crosses the zero. Performing similar calculations in the previous section, one finds the TBA equations after the wall crossing

become

$$\begin{aligned}\log \widetilde{Y}^{\mathrm{n}}_a(\theta) &= \left|\Pi^{(0)}_a\right| e^{\theta} + \frac{1}{2\pi i}\sum_{b\in s_N^{(1)}} \widetilde{K}_{a,b} \star \widetilde{L}^{\mathrm{n}}_a(\theta), \qquad a \in s_N^{(0)}, \\ \log \widetilde{Y}^{\mathrm{n}}_{(l,l+2)}(\theta) &= \left|\Pi^{(0)}_{(l,l+2)}\right| e^{\theta} + \frac{1}{2\pi i}\sum_{b\in s'_l} \widetilde{K}_{(l,l+2),b} \star \widetilde{L}^{\mathrm{n}}_b(\theta),\end{aligned} \tag{4.4.3}$$

where $s'_l \coloneqq \{(l+k, l+k+1); k = -1, 0, 1, 2\}$, $s_N^{(1)} \coloneqq s_N^{(0)} \cup (l, l+2)$, and the new non-zero entries of the intersection matrix is $I_{(l,l+2),(l+k,l+k+1)} = -I_{(l+k,l+k+1),(l,l+2)} = 1$ $(k = -1, 0, 1, 2)$. Then, the TBA equation (4.4.3) is uniformly written as

$$\log \widetilde{Y}^{\mathrm{n}}_a(\theta) = \left|\Pi^{(0)}_a\right| e^{\theta} + \frac{1}{2\pi i}\sum_{b\in s_N^{(1)}} \widetilde{K}_{a,b} \star \widetilde{L}^{\mathrm{n}}_a(\theta), \qquad a \in s_N^{(1)}, \tag{4.4.4}$$

which is the same as (4.4.1) with the change of the set $s_N^{(0)} \to s_N^{(1)}$ and the intersection matrix I_{ab}. If we define $S_N \coloneqq \{(i,j); i \neq j, i < j\}$ and replace $s_N^{(0)}$ and $s_N^{(1)}$ to S_N in (4.4.1) and (4.4.3), respectively, only the difference between the TBA equations before and after the wall-crossing is the intersection matrix. Therefore the wall-crossing phenomena of the TBA equations are encoded in the intersection matrix. The diagrammatic method of wall-crossing provides the intersection matrix in each chamber.

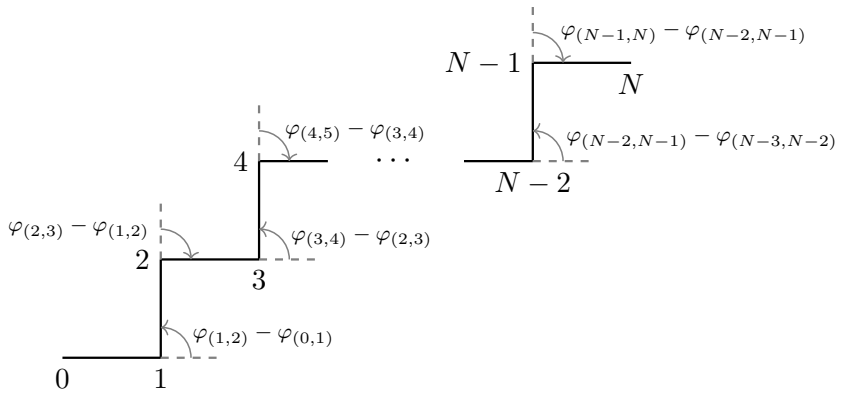

Figure 4.4.1: The diagram representing the TBA equations in the minimal chamber.

First, we define the diagram which represents the TBA equations in the minimal chamber, in which the Y-function associated with the cycle (i,j) corresponds to the vector $(\mathrm{Re}\,\Pi^{(0)}_{(i,j)}, \mathrm{Im}\,\Pi^{(0)}_{(i,j)})$. We also set the endpoint of vector $(\mathrm{Re}\,\Pi^{(0)}_{(i-1,i)}, \mathrm{Im}\,\Pi^{(0)}_{(i-1,i)})$ as the

starting point of vector $(\mathrm{Re}\,\Pi^{(0)}_{(i,i+1)}, \mathrm{Im}\,\Pi^{(0)}_{(i,i+1)})$. Since $\varphi_a = 0, \frac{\pi}{2}$ in the minimal chamber, this construction provides a kind of stair diagram depicted in figure 4.4.1. The difference of the phase $\varphi_a - \varphi_b$ is encoded into the relative angle of the vectors $(\mathrm{Re}\,\Pi^{(0)}_a, \mathrm{Im}\,\Pi^{(0)}_a)$ and $(\mathrm{Re}\,\Pi^{(0)}_b, \mathrm{Im}\,\Pi^{(0)}_b)$. We label the starting and the endpoints of the vector by i ($i = 0, 1, \ldots, N$) associated with the labels of branch points, and call them the vertex i. We also call the line connecting the vertex i and j the edge (i, j). For the purpose of follow the changes of the intersection matrix in each chamber, only the relative angles of the vectors are relevant, and then we do not have to care about the length of the vector. The intersection matrix is real off from the diagram by the rule:

- Rule 1: $I_{ab} = \pm 1$ for the edges a and b which has the common vertex. The sign is the same as that of the relative angle of the vectors of the classical periods associated with the cycles γ_a and γ_b.

One finds this rule recovers the TBA equations (4.4.1). Next, consider the wall crossing where $\varphi_{(l+1,l+2)} - \varphi_{(l,l+1)}$ crosses the zero. After this wall-crossing, we have to add the edge $(l, l+2)$ to the diagram associated with the additional Y-function $Y^{\mathrm{n}}_{(l,l+2)}$, which is illustrated in figure 4.4.2. From rule 1, one finds that the diagram provides the correct

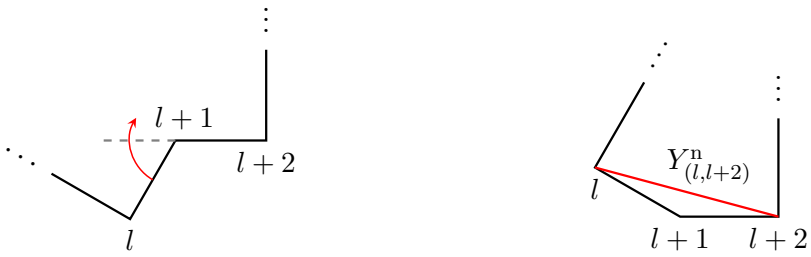

(a) (b)

Figure 4.4.2: The diagram representing the TBA equations (a) before / (b) after the wall-crossing at the wall where $\varphi_{(l+1,l+2)} - \varphi_{(l,l+1)}$ crosses zero.

intersection matrix. Let us rephrase this process in the following rule:

- Rule 2: When the relative angle $\varphi_{(i,j)} - \varphi_{(j,k)}$ crosses zero, add the new edge (i, k) to the diagram.

Successively applying this rule, one obtains the graph which contains the edges intersecting with other ones. This would happen for the $N \geq 3$ case. By the strait forward calculation of wall-crossings, one can see that in addition to the rule 1 and 2, we have to add one more rule:

- Rule 3: $I_{ab} = \pm 2$ for the edges a and b which intersect each other.

Again, the sign is determined from that of the relative angle. These three rules provide the whole procedure to obtain the TBA equations in any chamber. One has to draw first the stair diagram which corresponds to the TBA in the minimal chamber, and then morph it according to the rule 2 until one reaches the desired chamber. The intersection matrix can be read off from the diagram through the rule 1 and 3.

Using the above rules, let us consider the TBA equations in the maximal chamber. The diagram in the maximal chamber is the complete graph with $N+1$ vertices. Then the intersection matrix is $N(N+1)/2$ dimensional. As an example, figure 4.4.3 shows the diagram for the $N = 4$ case. The intersection matrix is then

$$I = \begin{pmatrix} 0 & 0 & -1 & 0 & -1 & -1 & 0 & -1 & -1 & -1 \\ 1 & 0 & 1 & 0 & 1 & 1 & 1 & 2 & 1 & 2 \\ 0 & -1 & 0 & -1 & -1 & -1 & -1 & -1 & -2 & -2 \\ 0 & 0 & 1 & 0 & 0 & 1 & 1 & 1 & 1 & 1 \\ 1 & -1 & 1 & 0 & 0 & 0 & 1 & 1 & 0 & 1 \\ 1 & -1 & 1 & -1 & 0 & 0 & 0 & 1 & -1 & 0 \\ 0 & -1 & 1 & -1 & -1 & 0 & 0 & 0 & -1 & -1 \\ 1 & -2 & 1 & -1 & -1 & -1 & 0 & 0 & -2 & -1 \\ 1 & -1 & 2 & -1 & 0 & 1 & 1 & 2 & 0 & 1 \\ 1 & -2 & 2 & -1 & -1 & 0 & 1 & 1 & -1 & 0 \end{pmatrix}, \tag{4.4.5}$$

where the entries are ordered from top to bottom as $(i-1, i+k)$ $(i = 1, 2, \ldots, 4-k)$ for $k = 0, 1, 2, 3$ i.e. $(0,1), (1,2), (2,3), (3,4), (0,2), (1,3), (2,4), (0,3), (1,4), (0,4)$. In the maximal chamber, there is a particular point where the potential becomes the monomial one. The TBA equations for this potential are obtained from the diagram in the maximal chamber with identifying the edges under the dihedral symmetry $\mathbb{Z}_{N+1}$. The TBA equations reduce to the $\lceil \frac{N}{2} \rceil$ equations. We assign the label $[k]$ $(k = 1, 2, \ldots, \lceil \frac{N}{2} \rceil)$ to the Y-functions, where the labels become the same if the Y-functions are identified under the symmetry. Then

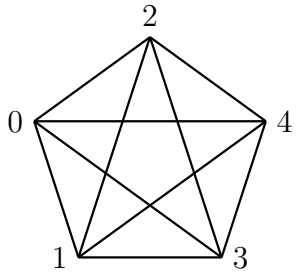

Figure 4.4.3: The complete graph with five vertices which represents the TBA equations in the maximal chamber for the quintic potential.

the TBA equations for the monomial potential are

$$\log \widetilde{Y}_{[k]}(\theta) = \left|\Pi^{(0)}_{[k]}\right| e^{\theta} + \frac{1}{2\pi i} \sum_{l=1}^{\lceil \frac{N}{2} \rceil} \widetilde{K}_{[k],[l]} \star \widetilde{L}_{[l]}(\theta), \qquad k = 1, 2, \ldots, \lceil \frac{N}{2} \rceil, \tag{4.4.6}$$

where the kernel is given by

$$\widetilde{K}_{[k],[l]} \coloneqq \sum_{b \in [l]} \widetilde{K}_{k,b}. \tag{4.4.7}$$

From the explicit form for small N, one can find that these TBA equations (4.4.6) are the (A_N, A_1)-type TBA equations. The classical periods $\left|\Pi^{(0)}_{[k]}\right|$ are calculated for $p(x) = x^{N+1} + u_{N+1}$ as [45]

$$\left|\Pi^{(0)}_{[k]}\right| = \sqrt{-8\pi u_{N+1}} (-u_{N+1})^{\frac{1}{N+1}} \frac{\Gamma(1 + \frac{1}{N+1})}{\Gamma(\frac{3}{2} + \frac{1}{N+1})} \left| \sin\left(\frac{k\pi}{N+1}\right) \right|, \tag{4.4.8}$$

which is proportional to the Perron-Frobenius eigenvector. The TBA equations (4.4.6) together with these driving terms are the same as one in [1], in which the TBA equations are obtained directly from the ODE/IM correspondence for the Schrödinger equation with the monomial potential.

Summary

In this chapter, we reviewed the ODE/IM correspondence for the second order ODE with the polynomial potential in which the WKB periods were connected with the Y-functions.

The classical periods give the driving term of the corresponding TBA equations. Deforming the potential continuously, the driving terms obtain the phases, and then the poles of the kernel functions change the TBA equations, i.e. the wall-crossing phenomenon occurs. Through the wall-crossing, one finds chambers in which the numbers of the equations in the TBA are the minimal and the maximal, respectively. Such chambers are called the minimal and the maximal chamber, respectively. By using the diagrammatic method, one can obtain the TBA equations in each chamber which appear in the continuous deformation from the minimal to the maximal chamber.

Chapter 5

Four dimensional $\mathcal{N} = 2$ theory and the quantum Seiberg-Witten curve

The relation between the ODE/IM correspondence and the 4-dimensional $\mathcal{N} = 2$ supersymmetric field theory is also the subject of this thesis. The 4d $\mathcal{N} = 2$ theory has been studied for decades, and there is known that a class of gauge theories is solvable which means one can obtain the low energy effective actions in the Coulomb branch of them. The effective action is described by a complex one dimensional curve which is called the Seiberg-Witten (SW) curve [47, 48]. There is also another method to calculate the partition function of the theory, which is the Nekrasov partition function [69, 70]. In the calculation of it, one has to introduce the Ω-background which has two deformation parameters ε_1 and ε_2. The partition function is obtained by taking the limit $\varepsilon_1, \varepsilon_2 \to 0$. One can also consider the limit where one of the deformation parameters is left to be finite, which is called the Nekrasov-Shatashvili (NS) limit [71]. In the NS limit, the SW curve, which reproduces the partition function, turns out to be a quantized one [72, 73] which can be regarded as the ODE.

The states contributing to the effective action in supersymmetric theories satisfy the BPS condition, and such states are called the BPS states. Then, the study of the spectra of BPS states is one of the subjects in supersymmetric field theories. The Coulomb branch is parameterized by the expectation values of the scalar fields, and the BPS spectra are dependent on the point in the moduli space of the vacuum. More precisely, the spectra suddenly change at certain values of the moduli parameters, which is called the wall-

crossing phenomenon and governed by the Kontsevich-Soibelman wall-crossing formula [66]. In [67, 68], the BPS spectrum of a certain class of 4d $\mathcal{N} = 2$ theories was studied by using the Hitchin system. Furthermore, in [77], it was pointed out that the conformal limit of the TBA-like equations describing the Hitchen system provides the solutions of the Schrödinger equation with the rational potential, which is also considered as the quantum SW curve of the Argyres-Douglas (AD) theory, which is the 4d $\mathcal{N} = 2$ conformal field theory. The higher rank case is also studied in [78, 79].

In this chapter, we first explain the Seiberg-Witten theory in section 5.1 and then, introduce briefly the BPS spectral problem and the wall-crossing phenomenon of 4d $\mathcal{N} = 2$ theory in section 5.2. The AD theories are reviewed in section 5.3, which emerges at the superconformal point of the moduli space of 4d $\mathcal{N} = 2$ gauge theories. The ODEs, which we used in the previous chapter and will use in the subsequent chapters, are the quantum SW curves of the AD theories, which we discuss in section 5.4.

5.1 Seiberg-Witten theory

In this section, we explain the Seiberg-Witten theory of the $\mathcal{N} = 2$ supersymmetric Yang-Mills theory. We, first, review the case where the gauge group is the simplest i.e. $SU(2)$, and then discuss the case of other gauge groups.

5.1.1 The $\mathcal{N} = 2$ supersymmetric algebra, the BPS bound, and the multiplets

Let us start with the basics of the supersymmetric theory. The $\mathcal{N} = 2$ supersymmetric algebra in four dimensions with supercharges $Q^i_\alpha, \overline{Q}_{\dot{\alpha},j}$ $(\alpha, \dot{\alpha} = 1, 2,\ i, j = 1, 2)$, which are the generators of the algebra, has the following anti-commutators:

$$\begin{aligned} \{Q^i_\alpha, \overline{Q}_{\dot{\alpha},j}\} &= 2\sigma^\mu_{\alpha\dot{\alpha}} P_\mu \delta^i_j, \\ \{Q^i_\alpha, Q^j_\beta\} &= \sqrt{2}\epsilon_{\alpha\beta}\epsilon^{ij} Z, \\ \{\overline{Q}_{\dot{\alpha},i}, \overline{Q}_{\dot{\beta},j}\} &= \sqrt{2}\epsilon_{\dot{\alpha}\dot{\beta}}\epsilon^{ij} Z^\dagger. \end{aligned} \tag{5.1.1}$$

Here α, β $(\dot{\alpha}, \dot{\beta})$ are the (anti-)spinor indices, P_μ generates the translation, and Z is the center of the algebra. The translation generators also satisfy the (four dimensional)

Poincaré algebra with the Lorentz generators. For each representation, the complex eigenvalue of Z takes a constant value which is called the central charge. To consider the representations of the algebra, it is convenient to take the linear combinations of the supercharges:

$$a_\alpha \coloneqq \frac{1}{\sqrt{2}}\left[Q^1_\alpha + \epsilon_{\alpha\beta}(Q^2_\beta)^\dagger\right], \qquad b_\alpha \coloneqq \frac{1}{\sqrt{2}}\left[Q^1_\alpha - \epsilon_{\alpha\beta}(Q^2_\beta)^\dagger\right], \tag{5.1.2}$$

If we consider the massive representation whose mass is M and set the phases of the supercharges so that the central charge becomes real, the non-zero anti-commutation relations of the generators become

$$\{a_\alpha, a^\dagger_\beta\} = \delta_{\alpha\beta}(M + \sqrt{2}Z), \qquad \{b_\alpha, b^\dagger_\beta\} = \delta_{\alpha\beta}(M - \sqrt{2}Z). \tag{5.1.3}$$

One can construct the representations by acting the creation operators $a^\dagger_\alpha$ and $b^\dagger_\alpha$ on the Clifford vacuum $|\Omega\rangle$ which is defined by $a_\alpha|\Omega\rangle = b_\alpha|\Omega\rangle = 0$. The unitarity constraints the mass of the representation as

$$M \geq \sqrt{2}Z, \tag{5.1.4}$$

which is called the BPS bound [64, 65].

The multiplets of the $\mathcal{N} = 2$ supersymmetric algebra, which is relevant in the argument in this section, is the vector multiplet. The $\mathcal{N} = 2$ vector multiplet is composed of the $\mathcal{N} = 1$ vector multiplet V and the chiral multiplet Φ. V is composed of a spin one vector field A_μ and a spin half Weyl fermion Λ, while the chiral multiplet Φ is composed of another Weyl fermion ψ and a complex scalar ϕ. In the following, we consider the $\mathcal{N} = 2$ supersymmetric Yang-Mills theory. The Lagrangian of the theory can be written by these $\mathcal{N} = 1$ multiplets.

5.1.2 The SW analysis of the $\mathcal{N} = 2$ $SU(2)$ Yang-Mills theory

Let us consider the $SU(2)$ $\mathcal{N} = 2$ supersymmetric Yang-Mills theory. One can write the Lagrangian of this theory by the $\mathcal{N} = 1$ multiplets as

$$\mathcal{L} = \frac{1}{4\pi}\,\mathrm{Im}\,\mathrm{Tr}\left[\tau_{\mathrm{cl}}\left(2\int \mathrm{d}^4\theta\ \Phi^\dagger e^{-2V}\Phi + \int \mathrm{d}^2\theta\ W_\alpha W^\alpha\right)\right], \tag{5.1.5}$$

where V is the $\mathcal{N}=1$ vector multiplet, W_α is the field strength defined from V, Φ is the chiral multiplet, $\tau_{\rm cl}$ is the complex coupling constant which is defined by

$$\tau_{\rm cl} \coloneqq \frac{\Theta}{2\pi} + \frac{4\pi i}{g^2}. \tag{5.1.6}$$

Here Θ is the theta angle, and g is the gauge coupling. The Grassmannian variable θ is the coordinate of the $\mathcal{N}=1$ superspace. Each component fields obey the adjoint representation of the gauge group. The scalar potential of this theory is defined from the adjoint scalar field ϕ which is the component of the $\mathcal{N}=1$ chiral multiplet. The potential has the form:

$$\mathcal{V}(\phi) = \frac{1}{2g^2}\,\mathrm{Tr}\left[\phi, \phi^\dagger\right]^2. \tag{5.1.7}$$

In the vacuum $\mathcal{V}=0$, which we call the Coulomb branch vacuum, the scalar potential takes the vacuum expectation value $\langle\phi\rangle = a\sigma_3$, where $\sigma_3 = \mathrm{diag}\ (1,-1)$. Then, the Coulomb branch vacuum has continuous degeneracy and is parameterised by the gauge invariant quantity:

$$u \coloneqq \langle \mathrm{Tr}\,\phi^2\rangle = 2a^2. \tag{5.1.8}$$

For $u \neq 0$, the gauge group breaks to $U(1)$. The low energy effective Lagrangian is obtained by integrating out all massive states. From the constraint of the $\mathcal{N}=2$ supersymmetry, the effective Lagrangian takes the form

$$\mathcal{L}_{\rm eff} = \frac{1}{4\pi}\,\mathrm{Im}\left[\int \mathrm{d}^4\theta\ \Phi_D\overline{\Phi} + \frac{1}{2}\int \mathrm{d}^2\theta\ \tau W_\alpha W^\alpha\right], \tag{5.1.9}$$

where the dual chiral field Φ_D and the effective coupling constant τ are defined by

$$\Phi_D \coloneqq \frac{\partial\mathcal{F}(\Phi)}{\partial\Phi}, \qquad \tau \coloneqq \frac{\partial^2\mathcal{F}(\Phi)}{\partial\Phi^2}. \tag{5.1.10}$$

Here $\mathcal{F}(\Psi)$ is a holomorphic function of Ψ and is called the prepotential. The classical part of the prepotential is given by

$$\mathcal{F}_{\rm cl}(\Phi) = \frac{1}{2}\tau_{\rm cl}\Phi^2. \tag{5.1.11}$$

The mass M of the particle in $\mathcal{N}=2$ theory is bounded by the central charge Z of the $\mathcal{N}=2$ supersymmetric algebra [62, 63]:

$$M \geq \sqrt{2}|Z| = \sqrt{2}|n_e a + m_m a_D|, \tag{5.1.12}$$

where the central charges are written by the vacuum expectation values of the scalar components of the chiral multiplets Φ and Φ_D, which we denoted as a and a_D, and the integers n_e and n_m are the electric and magnetic charge of the particle, respectively. Then, the states contributing to the low energy effective Lagrangian saturate the inequality (5.1.12). Such states are called the BPS states [64, 65]. In [46], it was found that the quantum corrections to the prepotential are composed of the perturbative part, the one-loop effect, and the non-perturbative part which is the effect of the instantons. For the energy scale $\mu > |a|$, the complex coupling τ has the logarithmic behavior, while for $\mu < |a|$, it remains the constant as a result of the Higgs mechanism. Defining the cut-off scale as Λ, the one-loop effect of the coupling constant for the low energy limit is

$$\tau \sim \frac{8i}{\pi} \log \frac{a}{\Lambda}. \tag{5.1.13}$$

The instanton effects are factorized by the $4k$ power of Λ/a for $k \in \mathbb{Z}_{>0}$. The power $4k$ is determined by the broken R-symmetry, which breaks to the $\mathbb{Z}_{4k}$ symmetry by the anomaly. The prepotential containing the quantum effects are given by

$$\mathcal{F}(\Phi) = \frac{1}{2}\tau_{\rm cl}\Phi^2 + \frac{i}{2\pi}\Phi^2 \log\left(\frac{\Phi}{\Lambda}\right)^2 + \frac{1}{4\pi i}\Phi^2 \sum_{k=1}^{\infty} \mathcal{F}_k \left(\frac{\Lambda}{\Phi}\right)^{4k}. \tag{5.1.14}$$

The problem to determine the instanton effects $\mathcal{F}_k$ is solved in [47, 48]. In their analysis, the property of the moduli space of the Coulomb vacuum plays the important role, which is the electric-magnetic duality. Here we mean by the moduli space of vacua the u-plane in which each point represents the vacua of the theory. This electric-magnetic duality is considered by adding the Bianchi identity as the Lagrangian multiplier:

$$\mathcal{L}_{eff} \to \mathcal{L}_{eff} + \frac{1}{4\pi} \mathrm{Im} \int \mathrm{d}^4\theta V_D \mathcal{D} W, \tag{5.1.15}$$

where V_D is a vector multiplet and $\mathcal{D}$ represents the covariant derivative on the $\mathcal{N} = 1$ superspace. Integrating by parts and integrating out the field-strength W, the kinetic term of the vector field becomes

$$\frac{1}{4\pi} \mathrm{Im} \left[\frac{1}{2} \int \mathrm{d}^2\theta \left(-\frac{1}{\tau}\right) W_{D,\alpha} W_D^{\alpha}\right]. \tag{5.1.16}$$

Here W_D is the field-strength of V_D. Note that V_D is the dual gauge field that couples to the magnetic charges. The coupling of the magnetic field is inverse of the original one. Thus the weakly coupled theory expressed by the magnetic fields describes the strongly coupled theory of electric fields. The transformation of the coupling i.e. $\tau \to -1/\tau$ is interpreted as the strong-weak duality. Together with the shift of the coupling i.e. $\tau \to \tau + 1$ which does not affect the Lagrangian, we define the duality transformation of the coupling:

$$\tau \to \frac{a\tau + b}{c\tau + d}, \qquad ad - bc = 1, \quad a, b, c, d \in \mathbb{Z}. \tag{5.1.17}$$

This $SL(2, \mathbb{Z})$ transformation acts on the fields as

$$\begin{pmatrix} \Phi_D, \\ \Phi \end{pmatrix} \to M \begin{pmatrix} \Phi_D, \\ \Phi \end{pmatrix}. \tag{5.1.18}$$

If we set the matrix M as the generator of the T-transformation:

$$M = \begin{pmatrix} 1 & 1 \\ 0 & 1 \end{pmatrix}, \tag{5.1.19}$$

the coupling transforms as $\tau \to \tau + 1$. On the other hand, choosing the matrix to be the generator of the S-transformation:

$$M = \begin{pmatrix} 0 & 1 \\ -1 & 0 \end{pmatrix}, \tag{5.1.20}$$

the coupling transforms as $\tau \to -1/\tau$. Under this transformation, one finds that from (5.1.12), the charge (n_e, n_m) is mapped to the charge $(-n_m, n_e)$. Therefore, by the S-transformation, we again find that this translates the electric description of the theory into the magnetic one. In the weakly coupling region in the moduli space of vacua, the theory is described by the electric field, whereas in the strongly coupled region, the theory is described by the magnetic field. This is the electric-magnetic duality of the $\mathcal{N} = 2$ $SU(2)$ theory. The structure of the moduli space of the Coulomb vacua differs from the classical one, and is studied in the following way. From the prepotential (5.1.14), the vev of the scalar component in the chiral field coupling to the magnetic field is evaluated in the $u \to \infty$ limit as

$$a_D \sim \frac{2ia}{\pi} \log\left(\frac{a}{\Lambda}\right) + \frac{ia}{\pi}. \tag{5.1.21}$$

Let us consider the transformation $u \to e^{2\pi i}u$, under which a and a_D transforms to $-a$ and $-a_D + 2a$, respectively, since $a = \sqrt{u}$ and a_D is approximately (5.1.21). This is the $SL(2,\mathbb{Z})$ transformation whose matrix is

$$M_\infty = \begin{pmatrix} -1 & 2 \\ 0 & -1 \end{pmatrix}, \tag{5.1.22}$$

where we call M_∞ the monodromy matrix at $u = \infty$. The non-trivial monodromy indicates the existence of the singularity at $u = \infty$. Furthermore the existence of the monodromy at $u = \infty$ implies the other singularities on the moduli space. Note that the singular point must not be unique and the origin $u = 0$ because of the positivity of the kinetic energy, which is equal to the constraint that the prepotential is holomorphic. From the $\mathbb{Z}_2$ symmetry $u \to -u$, one can assume the number of the singular points is three and they exist at $u = \pm\Lambda$ and $u\infty$. This is the assumption in [47, 48] and proven in [110]. The singularity arises when some BPS particle becomes massless, hence the assumption indicates at $u = \pm\Lambda$, some non-perturbative become massless and contribute to the effective Lagrangian. The charges of the particles are read off from the monodromies. Let the charge of the particle which becomes massless at $u = u_q$ be (n_e, n_m). By applying the $SL(2,\mathbb{Z})$ transformation, one can move onto the good coordinate $(a_D^{(q)}, a^{(q)})$ where the transformed gauge field couples to the particle in the same way as the usual gauge field couples to the unit electric charge. From the one-loop beta function, the vevs of the scalar in this region are expanded as

$$a^{(q)} \sim c_q(u - u_q), \qquad a_D^{(q)} \sim -\frac{i}{2\pi}a^{(q)} \log\left(\frac{a^{(q)}}{\Lambda}\right) + \frac{i}{\pi}a^{(q)}. \tag{5.1.23}$$

Around the singular point, we consider the transformation $u - u_q \to e^{2\pi i}(u - u_q)$, which leads to the monodromy

$$\begin{pmatrix} a_D^{(q)} \\ a^{(q)} \end{pmatrix} \to \begin{pmatrix} 1 & 2 \\ 1 & 0 \end{pmatrix}\begin{pmatrix} a_D^{(q)} \\ a^{(q)} \end{pmatrix}. \tag{5.1.24}$$

Defining that the transformed coordinate $(a_D^{(q)}, a^{(q)})$ and the original one (a_D, a) is related as

$$\begin{pmatrix} a_D^{(q)} \\ a^{(q)} \end{pmatrix} = \begin{pmatrix} \alpha & \beta \\ \gamma & \delta \end{pmatrix}\begin{pmatrix} a_D \\ a \end{pmatrix}, \tag{5.1.25}$$

where $\alpha\delta - \beta\gamma = 1$, the constraint that the central charge stay unchanged leads the charge transformation rule:

$$\begin{pmatrix} 0 \\ 1 \end{pmatrix} = \begin{pmatrix} \delta & -\gamma \\ -\beta & \alpha \end{pmatrix} \begin{pmatrix} n_m \\ n_e \end{pmatrix}. \tag{5.1.26}$$

Inverting (5.1.25), one obtain $a_D = \delta a_D^{(q)} - \beta a^{(q)}$ and $a = -\gamma a_D^{(q)} + \alpha a^{(q)}$. Then, from the monodromy (5.1.24), one finds the monodromy matrix at $u = u_q$:

$$M_{u_q} = \begin{pmatrix} -\beta + 2\delta & \delta \\ \alpha + 2\gamma & \gamma \end{pmatrix} \begin{pmatrix} -\beta & \delta \\ \alpha & -\gamma \end{pmatrix}^{-1} = \begin{pmatrix} 1 + 2n_e m_m & 2n_e^2 \\ -2n_m^2 & 1 - 2n_e n_m \end{pmatrix}. \tag{5.1.27}$$

If we consider the particle with charge $(n_e, n_m) = (0, 1)$, which becomes massless at $u = \Lambda$, and another one with charge $(-1, 1)$, which becomes massless at $u = -\Lambda$, the monodromy of the moduli space turns out to be consistent:

$$M_\Lambda M_{-\Lambda} = M_\infty, \qquad M_\Lambda = \begin{pmatrix} 1 & 0 \\ -2 & 1 \end{pmatrix}, \qquad M_{-\Lambda} = \begin{pmatrix} -1 & 2 \\ -2 & 3 \end{pmatrix}. \tag{5.1.28}$$

Then one concludes that at the point $u = \Lambda$, a monopole becomes massless and one has $a_D = 0$, while at the point $u = -\Lambda$, a dyon becomes massless and one has $a - a_D = 0$. At this point, we have seen that the moduli space is the complex u-plane with three punctures at $u = \pm\Lambda, \infty$ and has the $\mathbb{Z}_2$-symmetry, and the vev of the scalar fields can be regarded as the section of the $SL(2, \mathbb{Z})$ bundle over the moduli space. Together with the constraint the gauge coupling should be real, the moduli space is the upper half-plane H but with quotient by the monodromy group $\Gamma(2)$ which is the subgroup of $SL(2, \mathbb{Z})$:

$$\Gamma(2) \coloneqq \left\{ \begin{pmatrix} a & b \\ c & d \end{pmatrix} \in SL(2, \mathbb{Z}); \quad a, d = 1 \mod 2, \quad b, c = 0 \mod 2 \right\}. \tag{5.1.29}$$

The moduli space $H/\Gamma(2)$ parameterize the elliptic curve

$$y^2 = (x - \Lambda)(x + \Lambda)(x - u), \tag{5.1.30}$$

which is called the Seiberg-Witten curve. With the appropriate coordinate transformation, the SW curve can also be expressed as

$$y^2 = \frac{1}{4}(x - u)^2 - \Lambda_0^2. \tag{5.1.31}$$

Let us choose the branch cuts to be placed so that one of which starts from $x_3 \coloneqq -\sqrt{u+2\Lambda_0^2}$ and ends on $x_2 \coloneqq -\sqrt{u-2\Lambda_0^2}$, and the other starts from $x_1 \coloneqq \sqrt{u-2\Lambda_0^2}$ and ends on $x_0 \coloneqq \sqrt{u+2\Lambda_0^2}$. The vevs of the scalar potential is identified with the integrals of the holomorphic differential along one-cycles on the SW curve:

$$a = \oint_\alpha \mathrm{d}\lambda, \qquad a_D = \oint_\beta \mathrm{d}\lambda, \qquad \lambda = \frac{1}{2\pi i}\frac{x^2 \mathrm{d}x}{y}. \tag{5.1.32}$$

Here, as shown in figure 5.1.1, the cycle α encircles the branch points x_2 and x_3, while the cycle β encircles x_0 and x_1, respectively. We call the differential $\mathrm{d}\lambda$ the SW differential.

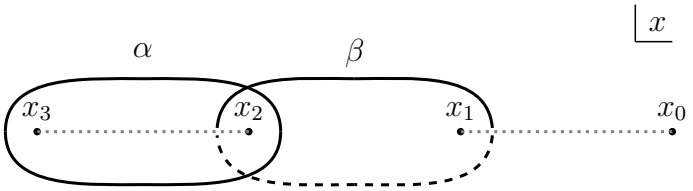

Figure 5.1.1: The cycle α and β on the x-plane.

The coupling constant τ is then

$$\tau = \frac{\partial a_D}{\partial a} = \frac{\partial a_D/\partial u}{\partial a/\partial u}, \tag{5.1.33}$$

and identified with the moduki of the torus defined by the SW curve (5.1.31). Finally, calculating a and a_D from (5.1.32), the prepotential is obtained from $\partial\mathcal{F}/\partial a = a_D$.

5.1.3 Generalization to other gauge groups

Soon after the work of [47, 48], the analysis of the $\mathcal{N} = 2$ suspersymmetric $SU(2)$ Yang-Mills theory was generalized to the $\mathcal{N} = 2$ suspersymmetric gauge theories with other gauge groups [49–52]. In this subsection, we discuss the generalization to the $\mathcal{N} = 2$ gauge theory without matter fields. Let the gauge group G of rank r. In the Coulomb vacuum, the vev of the scalar component of the $\mathcal{N} = 2$ vector multiplet is decomposed as $\langle\phi\rangle = \sum_{i=1}^r a_i H^i$, where H^i $(i = 1, 2, \ldots, r)$ is the Cartan generator of G. It is convenient for the parameterization of the moduli space of vacua to use the vev $\coloneqq \langle\phi^n\rangle$, where n

is the order of the Casimir invariants of G. One can generalize the low energy effective Lagrangian of the $SU(2)$ to this case, which becomes

$$\mathcal{L}_{\text{eff}} = \frac{1}{4\pi}\,\text{Im}\left[\int \mathrm{d}^4\theta\ \Phi_D^i\overline{\Phi_i} + \frac{1}{2}\int \mathrm{d}^2\theta\ \tau^{ij}W_{(i)\alpha}W^{\alpha}_{(j)}\right], \tag{5.1.34}$$

where the dual chiral field Φ_D^i $(i = 1, 2, \ldots, r)$ and the effective coupling constant τ^{ij} is defined by

$$\Phi_D^i \coloneqq \frac{\partial\mathcal{F}}{\partial\Phi_i}, \qquad \tau^{ij} \coloneqq \frac{\partial^2\mathcal{F}}{\partial\Phi_i\partial\Phi_i}. \tag{5.1.35}$$

Here the prepotential $\mathcal{F}$ is again composed of the perturbative one-loop part and the non-perturbative instanton part. The central charge of the BPS particle with electric charge $\vec{n}_e = (n_{e,1}, \ldots, n_{e,r})$ and with magnetic charge $\vec{n}_m = (n_{m,1}, \ldots, n_{m,r})$ is given by the vevs of the scalar components:

$$Z = \vec{n}_e \cdot \vec{a} + \vec{n}_m \cdot \vec{a}_D. \tag{5.1.36}$$

The Seiberg-Witten curve which gives the prepotential of the theory with gauge group G is given by

$$\frac{\overline{\Lambda}}{2}\left(z - \frac{\mu^2}{z}\right) = W_G(x; u_i), \tag{5.1.37}$$

where for $G = A_r$ and $G = D_r$, the $W_G(x, u_i)$ is given by

$$W_{A_r}(x, u_i) = x^{r+1} + u_2x^{r-1} + u_3x^{r-2} + \cdots + u_{r+1}, \tag{5.1.38}$$

$$W_{D_r}(x, u_i) = x^{2r-2} + u_2x^{2r-4} + u_3x^{2r-6} + \cdots u_{r-1}x^2 + u_{r+1} + \frac{u_r}{x^2}. \tag{5.1.39}$$

Here u_i $(i = 2, 3, \ldots, r+1)$ parameterize the moduli space of the Coulomb vacua. The SW differential is given by

$$\lambda = \frac{1}{2\pi i}\ x\ \mathrm{d}\log z. \tag{5.1.40}$$

Changing the coordinate $y \coloneqq z - \frac{W_G(x)}{2}$, one recovers the SW curve of $SU(2)$ introduced in (5.1.31) in the previous section. For other gauge group G, one can compute the SW curve from the spectral curve of the $G^\vee$-type affine Toda field theory, where $G^\vee$ is the Langlands dual of G [53–55].

5.2 BPS spectra and wall-crossings in $\mathcal{N} = 2$ theories

In this section, we review the BPS spectral problem and the wall-crossing phenomenon in the 4d $\mathcal{N} = 2$ supersymmetric field theory following [111]. Let us consider the 4d $\mathcal{N} = 2$ gauge theory with gauge group G of rank r. In the Coulomb branch, the states preserving the $\mathcal{N} = 2$ supersymmetry have the r electric charges $\vec{n}_e = (n_{e,1}, n_{e,2}, \ldots, n_{e,r})$, r magnetic charges $\vec{n}_m = (n_{m,1}, n_{m,2}, \ldots, n_{m,r})$, and f flavor charges $\vec{n}_f = (n_{f,1}, n_{f,2}, \ldots, n_{f,r})$, which are quantized by the Dirac quantization condition. Thus, we can define the charge lattice $\Gamma \simeq \mathbb{Z}^D$, where $D \coloneqq 2r + f$. Each lattice point on Γ denotes the charge $q = (\vec{n}_e, \vec{n}_m, \vec{n}_f)$. The CPT-symmetry ensures that if there is the state with the charge$q \in \Gamma$, so does the state with the charge $-q$. Since the gauge group breaks to $U(1)^r$ in the Coulomb branch, one can define the inner product $\langle \cdot, \cdot \rangle \colon \Gamma \to \mathbb{Z}$, which we call the Dirac paring and define by

$$\langle q, q' \rangle = \langle (\vec{n}_e, \vec{n}_m, \vec{n}_f), (\vec{n}'_e, \vec{n}'_m, \vec{n}'_f) \rangle \coloneqq \vec{n}'_e \cdot \vec{n}_m - \vec{n}_e \cdot \vec{n}'_m. \tag{5.2.1}$$

As mentioned in the previous section, in the four dimensional $\mathcal{N} = 2$ supersymmetric algebra, there exists the center, say the central charge, in the anti-commutation relation of the supercharges [62, 63]. Denoting the mass of the state with charge q as $M(q)$, it is bounded by the central charge $Z(q)$:

$$M(q) \geq \sqrt{2}|Z(q)|, \tag{5.2.2}$$

which is called the BPS bound [64, 65]. The states saturating this inequality is the BPS states, which play the important roles in supersymmetric field theory. The BPS states corresponds to the short multiplets of the $\mathcal{N} = 2$ algebra, which can be expressed as the representation of $SU(2)_{spin} \times SU(2)_R$ by

$$[(\mathbf{2}, \mathbf{1}) \oplus (\mathbf{1}, \mathbf{2})] \otimes \Omega, \tag{5.2.3}$$

where Ω represents the Clifford vacuum. Though Ω is the representation of $SU(2)_{spin} \times SU(2)_R$, it is conjectured that Ω is the singlet of $SU(2)_R$ in the generic point in Coulomb branch [112]. Then, we denote the spin of the representation of $SU(2)_{spin}$ as the spin of the Clifford vacuum Ω.

The BPS spectral problem and Kontsevich-Soibelman wall-crossing formula

Let us consider the charge lattice Γ of the BPS particles. The spectrum of the BPS states in the Coulomb branch is encoded in the charge lattice. If two charges q_1 and q_2 are mutually non-local, these are not in parallel in the charge lattice. The central charge of these charges and that of the charge $q_1 + q_2$ satisfy the triangle inequality:

$$|Z(q_1 + q_2)| \leq |Z(q_1)| + |Z(q_2)|. \tag{5.2.4}$$

Note that the mass of the BPS state is equal to the central charge. At the value of the Coulomb moduli parameters where this inequality saturates i.e. $Z(q_1)$ and $Z(q_2)$ align, the BPS state with the charge $q_1 + q_2$ may be unstable and decays. In general, the decay could occur if any two of the central charges of mutually non-local charges align. The condition that the central charges of mutually non-local states align divide the space of the possible central charges $\mathbb{C}^D$ into several domains $\{\mathcal{D}_a\}$ by real-codimension one loci. This loci is called the marginally stability wall. In each domain $\mathcal{D}_a$, the BPS spectrum differs, and the theory is in different phase. The BPS spectrum $\mathscr{C}_a \in \Gamma$ in the domain $\mathcal{D}_a$ is called the chamber. Mapping the marginal stability walls on the moduli space, they also cut it into several domains which we also call the chamber. If we varying the moduli parameters and crossing the wall, the decays occur and the BPS spectrum changes, which we call the wall-crossing phenomenon. The problem to obtain the chamber in any domain together with the Clifford vacuum is said to the BPS spectral problem. This problem is solved by using the invariant quantity under the wall-crossing, which we define by the quantum torus algebra $\mathbb{T}_\Gamma(p)$ and quantum dilogarithm function $\Psi(x; p)$. For the charge lattice Γ, we define a element X_q, say the spectral coordinate, corresponding to a charge $q \in \Gamma$. The spectral coordinates and the Dirac paring define the quantum torus algebra $\mathbb{T}_\Gamma(p)$. The exchange relation of two coordinates X_q and $X_{q'}$ is

$$X_q X_{q'} = p^{\langle q,q' \rangle} X_{q'} X_q. \tag{5.2.5}$$

The algebra has the commutative and associative product $N : \mathbb{T}_\Gamma(p) \times \mathbb{T}_\Gamma(p) \to \mathbb{T}_\Gamma(p)$ which is defined by

$$X_{q+q'} \coloneqq N[X_q, X_{q'}] \coloneqq p^{-\frac{1}{2}\langle q,q' \rangle} X_q X_{q'}. \tag{5.2.6}$$

One finds a group homomorphism between $(\Gamma, \langle\cdot,\cdot\rangle)$ and $(\mathbb{T}_\Gamma(p), N[\cdot,\cdot])$. The quantum dilogarithm function is characterized by the property and the normalization:

$$\Psi(px;p) = (1 - p^{\frac{1}{2}}x)^{-1}\Psi(x;p), \qquad \Psi(0;p) = 1. \tag{5.2.7}$$

For $|p| < 1$, the quantum dilogarithm function can be expressed by the infinite product:

$$\Psi(x;p) = \prod_{n=0}^{\infty}(1 - p^{n+\frac{1}{2}}x). \tag{5.2.8}$$

The inner automorphism of the algebra $\mathbb{T}_\Gamma(p)$ encodes the solution to the BPS spectral problem, which is described by the adjoint action of co called the Kontsevich-Soibelman (KS) operator $M(p)$ [66]:

$$M(p) = \prod_{q\in\mathscr{C}_a}^{\curvearrowright} \prod_{s=-j_q}^{j_q} \Psi(p^s X_q;p)^{(-1)^{2s}}. \tag{5.2.9}$$

Here j_q denotes the spin of the Clifford vacuum, and the product of the dilogarithm function is taken over the chamber $\mathscr{C}_a$ so that the function corresponding the charge with the smaller argument $0 \leq \arg Z_q < 2\pi$ is arrayed in the left. The remarkable property of the operator, conjectured in [66], is that the conjugacy class of it and all powers does not depend on the chamber $\mathscr{C}_a$. Therefore the KS operator is the wall-crossing invariant. From the KS operators in different chambers, one can obtain the Kontsevich-Soibelman wall-crossing formula (KSWCF) which describe the transition of the BPS spectrum at the marginal stability walls. The KSWCF is classified by the absolute values of the Dirac parings of charges whose central charges align at the wall, and expressed as the identities of the quantum dilogarithm functions. The cases where the absolute value of the paring is one and two are

- Pentagon wall-crossing $|\langle q_1, q_2\rangle| = 1$:

$$\Psi(X_{q_1})\Psi(X_{q_2}) = \Psi(X_{q_2})\Psi(X_{q_1+q_2})\Psi(X_{q_1}), \tag{5.2.10}$$

- Kronecker wall-crossing $|\langle q_1, q_2\rangle| = 2$:

$$\begin{aligned}\Psi(X_{q_1})\Psi(X_{q_2}) = &\overset{\curvearrowright}{\prod_{n\in\mathbb{Z}_{>0}}} \Psi(X_{nq_1+(n+1)q_2})\Big(\Psi(p^{-\frac{1}{2}}X_{q_1+q_2})\Big)^{-1} \\ &\times \Big(\Psi(p^{\frac{1}{2}}X_{q_1+q_2})\Big)^{-1} \overset{\curvearrowright}{\prod_{m\in\mathbb{Z}_{>0}}} \Psi(X_{(m+1)q_1+mq_2}).\end{aligned} \tag{5.2.11}$$

For the case where the absolute value of the paring is greater than two, see [113] for example. Once the BPS spectrum is solved in a certain chamber, one can obtain the spectrum in other chambers through the successive application of KSWCF.

It may helpful to illustrate the simplest wall-crossing i.e. the pentagon wall-crossing. Suppose that in the chamber $\mathscr{C}_1$ there are charges q_1 and q_2 where $\langle q_1, q_2\rangle = 1$ and $\arg Z(q_1) < \arg Z(q_2)$. If we vary the moduli parameters from the chamber $\mathscr{C}_1$ to the chamber $\mathscr{C}_2$ where $\arg Z(q_1) > \arg Z(q_2)$, the pentagon wall-crossing occurs. At the wall, the central charges align $\arg Z(q_1) = \arg Z(q_2)$ and the new BPS particle with charge $q_1 + q_2$ emerges. Then, in the chamber $\mathscr{C}_2$, the BPS spectrum is composed of the states included in the chamber $\mathscr{C}_1$ and the new BPS state with charge $q_1 + q_2$, where the central charges obey $\arg Z(q_2) < \arg Z(q_1 + q_2) < \arg Z(q_1)$. The figure 5.2.1 depicts this process.

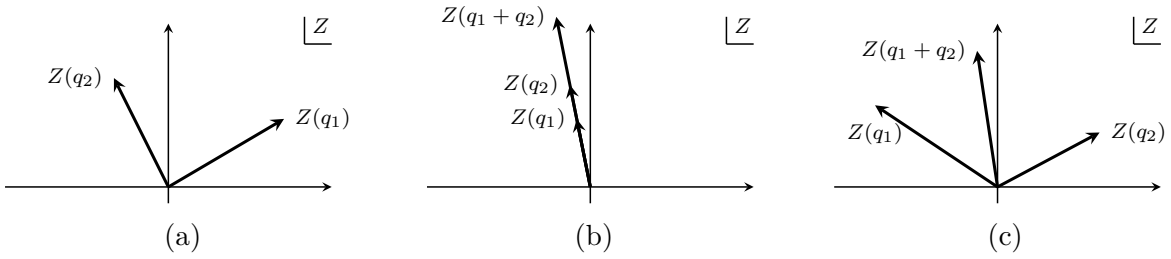

Figure 5.2.1: The central charges $Z(q_1)$ and $Z(q_2)$ in chamber $\mathscr{C}_1$ (a), $Z(q_1), Z(q_2)$ and $Z(q_1 + q_2)$ at the wall (b), and $Z(q_1), Z(q_2)$ and $Z(q_1 + q_2)$ in the chamber $\mathscr{C}_2$ (c).

The BPS quiver and mutations

If the charge lattice Γ has the basis $\{e_i\}_{i=1}^D$ such that any charge $q \in \Gamma$ is in $\Gamma_+ := \oplus_{i=1}^D \mathbb{Z}_{\geq 0} e_i$ or $-q \in \Gamma_+$, the BPS spectrum is said to having the quiver property. Without

loss of generality, we set the argument of the central charges of the basis so that $0 < \arg Z(e_i) < \pi$ $(i = 1, 2, \ldots, D)$. When the BPS spectrum has the quiver property, one can express the spectrum by a diagram which is called the BPS quiver. Generally, the quiver diagram consists of a finite number of nodes and arrows connecting the nodes. In the BPS quiver, nodes represent the basis e_i while the arrows represent the Dirac parings. Concretely, for the Dirac paring $D_{ij} \coloneqq \langle e_i, e_j \rangle$, we assign D_{ij} arrows which start from the node corresponding to the basis e_i to the node of e_j. As an example, we show the BPS quiver for the basis $\{e_1, e_2, e_3, e_4\} = \{q_1, q_2, q_3, q_4\}$ with the non-zero Dirac parings $D_{12} = 1, D_{23} = -2$ and $D_{24} = 1$ in figure 5.2.2. One can recover the BPS spectrum from

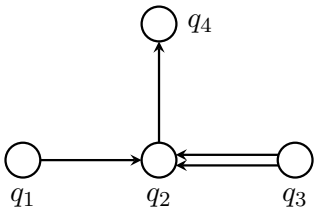

Figure 5.2.2: An example of the BPS quiver

the BPS quiver by the mutation algorithm. There are the left and the right mutations. Let us explain the right mutation first. As we defined, the central charges of the basis are in the upper half plane H. Among the basis e_i $(i = 1, 2, \ldots, D)$, we denote the basis whose argument of the central charge is the largest as e_k. Consider the rotation of the upper half plane with respect to the origin clockwise of angle θ where $\pi - \arg Z(e_k) < \theta < \pi$. The tilting of the plane H_θ contains the central charge of the state with charge $-e_k$ but no longer contain that of the charge e_k. We also set the angle θ such that the central charges of rest of the basis e_i $(i \neq k)$ are contained in H_θ. On the rotated plane, we defined the new basis $\{e_i^\theta\}_{i=1}^D$ which is related to the original basis $\{e_i\}_{i=1}^D$ by

$$e_i^\theta \coloneqq \mu_k(e_i) = \begin{cases} -e_k, & i = k, \\ e_i + [D_{ki}]e_k, & i \neq k. \end{cases} \tag{5.2.12}$$

Here $[x] = \max(x, 0)$. This operation is called the basic quiver right mutation at the node k. The mutated BPS quiver is constructed from the Dirac parings between the new basis,

which are related to that between the original basis as

$$D^{\theta}_{ij} \coloneqq \mu_k(D_{ij}) = \begin{cases} -D_{ij}, & i = k \text{ or } j = k, \\ D_{ij} + \text{sign}(D_{ik})[D_{ik}, D_{kj}], & \text{otherwise.} \end{cases} \tag{5.2.13}$$

Performing the right mutation successively until one reach the plane whose tilting angle is π, the obtained basis with removing redundant ones recover the all charges in Γ_+. In particular, if the BPS spectrum contains a finite number of charges, this operation finishes in finite times of application. Thus, one can obtain the all charges in the spectrum. If we choose the tilting angle to be the minus one i.e. anticlockwise rotation, the operation is called the left mutation. Denoting the left mutation at the node k as $\widetilde{\mu}_k$, the basis after the operation is

$$e^{\theta}_i = \widetilde{\mu}_k(e_i) = \begin{cases} -e_k, & i = k, \\ e_i + [-D_{ki}]e_k, & i \neq k. \end{cases} \tag{5.2.14}$$

The Dirac paring of the mutated quiver is the same one as the right mutation: $\mu_k(D_{ij}) = \widetilde{\mu}_k(D_{ij})$. In the same way as the right mutation, one can obtain the BPS spectrum through the successive application of the left mutation.

5.3 Argyres-Douglas theory

The Argyres-Douglas theory is the simplest $\mathcal{N} = 2$ superconformal field theory (SCFT), which was realized in the particular degeneration point, say AD point, of the SW curve in the Coulomb moduli space of $\mathcal{N} = 2$ $SU(3)$ Yang-Mills theory [56]. In fact, the central charge of the theory saturates the unitarity bound of the $\mathcal{N} = 2$ SCFT. At the AD point, the theory is strongly coupled and particles whose charges are mutually non-local become massless simultaneously. Thus, there have not known the Lorentz invariant Lagrangian of AD theory, but still we can study it by use of the SW curve and SW differential. Searching the AD points of SW curves of other gauge groups with and without matter fields, AD theory was generalized and classified in ADE-types [58]. Moreover, by using the geometric engineering of the type IIB string theory or Hitchen system, the AD theories were generalized and classified as the (G, G')-type, where the labels are

$G, G' = A, D, E$ [59–61]. In this section, we briefly review the SW curves of AD theories of ADE-types in section 5.3.1, and the generalized AD theories in section 5.3.2.

5.3.1 SW curves at the AD points

Let us consider the $\mathcal{N} = 2$ $SU(3)$ Y-ang-Mill theory, whose SW curve is given by

$$y^2 = Q(x) = Q_+(x)Q_-(x), \qquad Q_\pm(x) \coloneqq \frac{1}{2}(x^3 + u_1 x + u_2)^2 \pm \Lambda^3. \tag{5.3.1}$$

If any two the branch points collide, the SW curve becomes singular. Denote the discriminant of $Q(x)$ as $\Delta(Q)$. At the point where the discriminant is zero, a cycle shrinks and the corresponding BPS particle becomes massless. Since the discriminants of $Q_\pm$ are

$$Q_\pm(x) = -4u_1^3 - 27(u_2 \mp \Lambda^3)^2, \tag{5.3.2}$$

at the point $u_1^3 = (3\Lambda^2)^3$ and $u_2 = 0$, where $Q_\pm = 0$, two cycle shrink and two dyon become massless. However, these two dyons are mutually local. Here two charges $q = (\vec{n}_e, \vec{n}_m)$ and $q' = (\vec{n}'_e, \vec{n}'_m)$ are said to be (non-)local if the Dirac paring $\langle q, q' \rangle$ defined in (5.2.1) is (non-)zero. At The AD point, mutually non-local dyons become massless. Such a point is at $u_1 = 0$ and $u_2 = \pm 2\Lambda^3$, at which $\partial\Delta(Q_\pm)/\partial u_1 = \partial\Delta(Q_\pm)/\partial u_2 = 0$ also holds. On the AD point, the theory becomes superconformal, and one can consider the deformation of SW curve around this point. Setting the moduli parameters as $u_1 = \delta u_1$ and $u_2 = 2\Lambda^3 + \delta u_2$ ($\delta u_1, \delta u_2 \ll \Lambda$), three of six branch points are distributed around origin while others are roughly on the circle of radius $(4\Lambda^3)^{1/3}$, which means the curve is composed of two torus connected by a cylinder. Focusing on the branch points around the origin, the SW curve becomes

$$y^2 = x^3 + \delta u_1 x + \delta u_2. \tag{5.3.3}$$

Corresponding SW differential is, up to the total derivative, given by

$$\lambda = \frac{1}{2\pi i}\, y \, \mathrm{d}x. \tag{5.3.4}$$

Since the SW differential has the mass dimension one, the moduli parameters have the fractional dimensions, which is the characteristic property of AD theory.

From the SW curves of other gauge theories, we can obtain that of AD theories of ADE-types. Here we argue the A-type and the D-type curves. For the SW curve (5.1.37), there exist the AD points at [58]

$$u_2 = u_3 = \cdots = u_r = 0, \qquad u_{r+1} = \pm\overline{\Lambda}. \tag{5.3.5}$$

Around this point, we can consider the scaling limits of the curves. For A_r-type, we define the limit by

$$\begin{aligned} &z = e^{\delta\widetilde{\xi}}, \qquad x = \delta^{\frac{2}{r+1}}\overline{\Lambda}^{\frac{1}{r+1}}\widetilde{x}, \qquad u_{r+1} = \overline{\Lambda} + \delta^2\overline{\Lambda}\,\widetilde{u}_{r+1}, \\ &u_i = \delta^{\frac{2i}{r+1}}\overline{\Lambda}^{\frac{i}{r+1}}\widetilde{u}_i, \quad i = 2, 3, \ldots, r. \end{aligned} \tag{5.3.6}$$

The l.h.s. of the curve becomes

$$\frac{\overline{\Lambda}}{2}\left(z + \frac{1}{z}\right) = \overline{\Lambda} + \frac{\overline{\Lambda}}{2}\delta^2\,\overline{\Lambda}\,\widetilde{\xi}^2, \tag{5.3.7}$$

while the r.h.s. of the curve is

$$W_{A_r}(x; u_i) = \overline{\Lambda} + \delta^2\,\overline{\Lambda}\,W_{A_r}(\widetilde{x}; \widetilde{u}_i). \tag{5.3.8}$$

Equating these two and rewriting the variables as $\frac{\widetilde{\xi}}{2} \to \xi$, $\widetilde{x} \to x$ and $\widetilde{u}_i \to u_i$, one obtains the SW curve for A_r-type AD theory:

$$\xi^2 = W_{A_r}(x, u_i) = x^{r+1} + u_2 x^{r-1} + u_3 x^{r-2} + \cdots + u_{r+1}. \tag{5.3.9}$$

The SW differential, up to the total derivative terms, becomes

$$\lambda = \frac{i}{2\pi}\xi \mathrm{d}x. \tag{5.3.10}$$

For D_r-type SW curve, the scaling limit is defined as

$$\begin{aligned} &z = e^{\delta\widetilde{\xi}}, \qquad x = \delta^{\frac{2}{r-2}}\overline{\Lambda}^{\frac{1}{2r-2}}\widetilde{x}, \qquad u_{r+1} = \overline{\Lambda} + \delta^2\overline{\Lambda}\,\widetilde{u}_{r+1}, \\ &u_r = \delta^{\frac{4r}{2r-2}}\overline{\Lambda}^{\frac{2r}{r2-2}}u_r, \qquad u_i = \delta^{\frac{4i-4)}{2r-2}}\overline{\Lambda}^{\frac{2i-2)}{2r-2}}\widetilde{u}_i, \quad i = 2, 3, \ldots, r-1. \end{aligned} \tag{5.3.11}$$

In this limit, the r.h.s. of the curve is the same as that of A_r-type (5.3.7), while the r.h.s. of the curve is

$$W_{D_r}(x; u_i) = \overline{\Lambda} + \delta^2\,\overline{\Lambda}\,W_{D_r}(\widetilde{x}; \widetilde{u}_i). \tag{5.3.12}$$

Again, equating these and rewriting the variables in the same way as the A_r case, we obtain the SW curve of D_r-type AD theory:

$$\xi^2 = W_{D_r}(x, u_i) = x^{2r-2} + u_2 x^{r-4} + u_3 x^{r-6} + \cdots + u_{r-1}x^2 + u_{r+1} + \frac{u_r}{x^2}. \tag{5.3.13}$$

The SW differential takes the same form as in (5.3.10). For the completeness, we mention only that The SW curve of E_r-type AD theories were studied in [114], which we do not write down because of its complexity.

5.3.2 Generalized AD theories

By using the string theoretic constructions, the AD theory has been generalized and classified by the label (G, G'), where G and G' are A_r, D_r or E_r [59–61]. The geometric engineering method provides a large number of 4d $\mathcal{N} = 2$ SCFT, in which one consider the type IIB string theory on hypersurface in $\mathbb{C}^4$ defined by

$$\big\{(x_1, x_2, x_3, x_4) \in \mathbb{C}^4; \quad W(x_1, x_2, x_3, x_4) = 0\big\}. \tag{5.3.14}$$

Here W satisfies the following condition:

- There exist positive numbers $\{q_i\}$ such that $W(\lambda^{q_i} x_i) = \lambda W(x_i)$ $(\lambda \in \mathbb{C}^*)$.
- The numbers $\{q_i\}$ satisfy $\sum_i q_i > 1$.

The deformation around the superconformal point can be realized by adding the miniversal deformation terms as

$$F(x_i, u_i) = W(x_i) + \sum_{i=1}^{n} u_i \phi_i, \tag{5.3.15}$$

where the Milnor number n is associated with the rank of the BPS lattice and ϕ_i is the monomial basis of the algebra

$$\frac{\mathbb{C}[x_1, x_2, x_3, x_4]}{\langle \frac{\partial W}{\partial x_1}, \frac{\partial W}{\partial x_2}, \frac{\partial W}{\partial x_3}, \frac{\partial W}{\partial x_4} \rangle}. \tag{5.3.16}$$

The (G, G')-type AD theory is constructed by considering the type IIB theory on the hypersurface $W(x_1, x_2, x_3, x_4) = 0$ where [59]

$$W(x_1, x_2, x_3, x_4) = f_G(x_1, x_2) + f_{G'}(x_3, x_4). \tag{5.3.17}$$

Here the polynomial $f_G(x,y)$ is given by

$$\begin{aligned} f_{A_r}(x,y) &= x^2 + y^{r+1}, \\ f_{D_r}(x,y) &= x^2 y + y^{r-1}, \\ f_{E_6}(x,y) &= x^3 + y^4, \\ f_{E_7}(x,y) &= x^3 + xy^3, \\ f_{E_8}(x,y) &= x^3 + y^5. \end{aligned} \tag{5.3.18}$$

Note that G-type AD theory is, in this classification, denoted as (A_1, G)-type theory. The remarkable property of these types of theories is the duality. The most obvious one is the level-rank duality which is

$$(G, G') \sim (G', G), \tag{5.3.19}$$

and one can also recognize that there are other dualities, for example

$$(A_2, A_2) \sim (A_1, D_4), \qquad (A_2, A_3) \sim (A_1, E_6), \qquad (A_2, A_4) \sim (A_1, E_8). \tag{5.3.20}$$

The BPS spectrum of these AD theories were studied in [59, 112, 115–118]. It was discovered that there is a chamber in which the BPS quiver of (G, G')-type AD theory becomes the the direct product of the Dynkin diagrams of G and G' algebras. In this thesis, we particularly focus on (A_r, A_N)-type AD theory, whose SW curve at the superconformal point is

$$y^{r+1} + x^{N+1} = 0. \tag{5.3.21}$$

The BPS quiver of (A_r, A_N)-type theory in the minimal chamber is illustrated in figure 5.3.1. The every node is connected by a single arrow, hence we could expect that the wall crossing phenomenon of this theory will be the pentagon type.

5.4 Quantum SW curves and ODE/IM

The SW curves provide the exact solution to 4d $\mathcal{N} = 2$ theories both in the strong coupling and weak coupling region in the moduli space. In the weak coupling region, there is another method to calculate the partition function of the $SU(N)$ theory by using

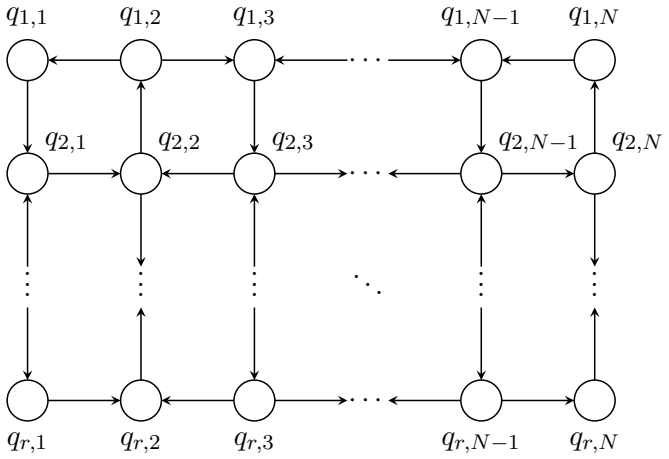

Figure 5.3.1: The BPS quiver of (A_r, A_N)-type AD theory

the localization technique, which is called the Nekrasov partition function [69, 70]. In the calculation of the Nekrasov partition function, one construct the four dimensional theory from the dimensional reduction of the six dimensional theory on the Ω-background. The Ω-background includes the two deformation parameter which we denote ϵ_1 and ϵ_2, so does the obtained partition function. The prepotential $\mathcal{F}(a)$ of the 4d theory is then given from the partition function $Z(a; \epsilon_1, \epsilon_2)$ by

$$\mathcal{F}(a) = \lim_{\epsilon_1, \epsilon_2 \to 0} -\epsilon_1 \epsilon_2 \log Z(a; \epsilon_1, \epsilon_2), \tag{5.4.1}$$

which reproduce the result from the SW curve. Then, the SW prepotential is justified by the result of the field theoretical calculation. One can also consider the limit, where one of the deformation parameters remains finite. This type of the limit is called the Nekrasov-Shatashvili (NS) limit [71]. We denote the prepotential in the NS limit as $\mathcal{F}_{NS}(a; \epsilon)$, where ϵ is the remaining parameter. Even in this limit, one can consider the corresponding SW curve, which is no longer the hyperelliptic curve rather the differential equation called the quantum SW curve [72, 73]. Note that the SW differential $d\lambda = dx \wedge d \log z$ provides the symplectic structure on $(\log z, x)$-space. The quantum SW curve is obtained by applying the canonical quantization scheme to the $(\log z, x)$-space, in which we replace $\log z$ by the

differential operator[1]:

$$\log z \to -i\epsilon\frac{\partial}{\partial x}. \tag{5.4.2}$$

The SW curve (5.1.37) for A_N gauge theory is then quantized as

$$\left[\frac{\overline{\Lambda}}{2}\left(e^{i\epsilon\partial_x}+e^{-i\epsilon\partial_x}\right)-W_{A_N}(x,u_i)\right]\Psi(x,u_i;\epsilon)=0. \tag{5.4.3}$$

As usual WKB analysis for differential equations, we use the ansatz of the solution $\Psi(x) = \exp\left(\frac{i}{\epsilon}\int^x P(x')\mathrm{d}x'\right)$ and define the WKB period $\Pi_\gamma(\epsilon) \coloneqq \oint_\gamma P(x')\mathrm{d}x'$ where γ is the one-cycle on the SW curve. For the canonical α and β-cycle of the curve, the classical period is nothing but the SW period itself. Then we define the quantized SW period as $\hat{a}_i \coloneqq \Pi_{\alpha_i}$ and $\hat{a}_{Di} \coloneqq \Pi_{\beta_i}$. The prepotential in the NS limit is then reproduced by the relations

$$\frac{\partial\mathcal{F}_{NS}}{\partial\hat{a}_i}=\hat{a}_{Di}, \qquad i=1,2,\ldots,N, \tag{5.4.4}$$

which is the analogy of the relations between the SW periods and the prepotential. For the theories with other gauge groups, one can consider the quantum SW curves. However, the Nekrasov partition functions for other gauge groups have not been studied yet.

For AD theory, the quantization of the SW curve is studied in [74–76]. Since the Lagrangians of the AD theories are not known, we cannot calculate the prepotentials in the NS limit from the Nekrasov partition functions. Although, By taking the scaling limit of the SW curve, one can define the quantum SW curves of AD theories. In general, the quantization of the SW curve and the operation of the scaling limit are not mutually commutative. Thus, there is ambiguity in the definition of the quantum SW curve of the AD theory. This has to be taken into account for example in the D-type AD theory, while for A-type AD theory, we can, fortunately, define the quantum curve without ambiguity [75, 76]. Related to the symplectic form of the SW differential $d\lambda = d\xi \wedge dx$, we replace $\xi \to -\epsilon\partial_x$, which leads the quantum SW curve of A-type AD theory[2]

$$\left[-\epsilon^2\partial_x^2+W_{A_r}(x,u_i)\right]\Psi(x,u_i;\epsilon)=0. \tag{5.4.5}$$

[1]We used the quantization scheme in [119], which is different from one in [72, 73].

[2]We use the notation omitting the imaginary unit i.

Adding the term $u_1 x^N$, this ODE is the same as we condier in chapter 4. The WKB curve is nothing but the SW curve and WKB period is the quantum SW curve of AD theory. From the same quantization scheme, one obtains the quantum SW curve of (A_r, A_N)-type AD theory [74]:

$$\left[(-1)^r \epsilon^{r+1} \partial_x^{r+1} + p(x, u_i)\right] \Psi(x, u_i; \epsilon) = 0, \qquad p(x, u_i) = \sum_{i=0}^{N+1} u_i x^{N+1-i}. \tag{5.4.6}$$

Here we added the deformation terms $u_i x^{N+1-i}$ $(i = 1, 2, \ldots, N+1)$ to the curve. This is also the adjoint ODE of $A_r^{(1)}$ algebra if the potential is the monomial one. Related to this fact, for $G = A, D, E$, the quantum curves of the (G, A_1)-type AD theories are conjectured to be the adjoint ODE of $G^{(1)}$ algebras [74].

The quantum SW curve of AD theory has another aspect. The logarithm of the spectral coordinates of 4d $\mathcal{N} = 2$ theory satisfy the TBA like equations [67, 68]. In the conformal limit, the TBA like equations provides the solution of a class of the differential equation [77]. It was also discussed that there is TBA like equations which gives the solution to the quantum SW curve of the (A_1, A_2)-type AD theory. After the work of [77], there was studied for the quantum SW curve of the (A_2, A_2)-type AD theory [78, 79]. Since the spectral coordinates are defined associated with BPS particles and then enjoy the wall-crossing phenomena, the TBA like equations wall-cross at the marginal stability walls. In chapter 4, we discussed the wall-crossing of the TBA equations for the quantum SW curves of the (A_1, A_N)-type AD theories, which are satisfied by the logarithm of the Y-functions. The wall of the TBA equations located at the point where two classical periods, which are now turned out to be the SW periods, align in the complex plane. This condition of the wall is the same as that of the 4d theory. There may be relations between the Y-functions and the spectral coordinates, and then through the wall-crossing of the TBA equations, we could study the higher rank AD theory. This is the one of the motivation in chapter 6 and chapter 7.

Summary

In this chapter, we reviewed the four dimensional $\mathcal{N} = 2$ supersymmetric field theory and discussed the relation to the ODE/IM correspondence. Thanks to the Seiberg-Witten analysis, we can compute the low-energy effective action of the $\mathcal{N} = 2$ supersymmetric gauge theory in which the SW curve and the SW periods were the central elements. Using the SW periods, one can compute the masses/central charges of the BPS particles in the theory. The moduli space of vacua is parameterized by the vevs of the scalar fields, and the changes of the vevs causes the phase transitions of the BPS spectra, which is called the wall-crossing phenomena. In the moduli space of the gauge theory, there exist the superconformal point at which the theory becomes the non-Lagrangian, i.e. the Argyres-Douglas theory appears. If we consider the theory in the Nekrasov-Shatashvili limit of the Ω-background, the SW curve becomes the quantized one which is a differential equation. The ODE we considered in chapter 4 was interpreted as the quantum SW curve of the (A_1, A_N)-type AD theory. The WKB periods correspond to the quantum SW periods. The wall-crossing condition of the TBA equations is associated with that of the four dimensional theory.

Chapter 6

WKB periods and Y-functions for the higher order ODE

We reviewed the ODE/IM correspondence of the WKB periods and Y-functions for the second order ODE with the polynomial potential in chapter 4. The ODE is regarded as the quantum SW curve of the (A_1, A_N)-type AD theory. Furthermore, the wall-crossing of the TBA equations was related to that of the corresponding AD theory. In particular, the marginal stability walls of the TBA were the same as the ones in 4d theory. It is natural to generalize the relation of the WKB periods and Y-functions to the higher order ODE which is the quantum SW curve of more general (A_r, A_N)-type AD theory. This would help us to find a deeper understanding of the connections to the 2d and 4d theories. In this chapter, we investigate and establish the correspondence in the minimal chamber. To deal with the higher order ODE, we will use the Stokes graphs and the so-called abelianization trees, which are useful in the WKB analysis. Using these tools, we establish the relation between the Y-functions and the one cycles on the WKB curves graphically. The argument is based on our works of [85, 86].

6.1 WKB periods for the higher order ODE

Let us start with the discussion of the WKB periods or the quantum SW periods of the ODE. The ODE is the quantum SW curve of the (A_r, A_N)-type AD theory, which is

$$\left[(-1)^r\epsilon^{r+1}\partial_x^{r+1} + p(x,u_i)\right]\psi(x,u_i;\epsilon) = 0, \qquad p(x,u_i) = \sum_{i=0}^{N+1} u_i x^{N+1-i}. \tag{6.1.1}$$

Here the complex parameter ϵ is the plank constant as well as the deformation parameter of the Ω-background, and $u_i \in \mathbb{C}$ is the moduli parameter of the Coulomb vacuum. We consider the ODE in the complex plane, i.e. $x \in \mathbb{C}$, same as in other chapters. We refer the ODE (6.1.1) as the (A_r, A_N)-type ODE. To perform the WKB analysis, we consider the WKB ansatz

$$\psi(x,u_i;\epsilon) = \exp\left(\frac{1}{\epsilon}\int^x P(x',u_i;\epsilon)\mathrm{d}x'\right), \qquad P(x,u_i;\epsilon) = \sum_{n=0}^{\infty}\epsilon^n p_n(x,u_i). \tag{6.1.2}$$

Substituting into the ODE (6.1.1), one obtains the Riccati-equations

$$(-1)^r(\epsilon\partial_x + P(x,u_i;\epsilon))^r P(x,u_i;\epsilon) + p(x,u_i) = 0. \tag{6.1.3}$$

From the recursive calculation, the ϵ-expansion of $P(x,u_i;\epsilon)$ is given. The first few terms up to the total derivative are

$$\begin{aligned}
p_0 &= (-p(x,u_i))^{\frac{1}{h}},\\
p_2 &= \frac{h^2-1}{48}\frac{\partial^2 p_0}{p_0^2},\\
p_4 &= \frac{(h^2-9)(h^2-1)}{768}\frac{(\partial^2 p_0)^2}{p_0^5} - \frac{(h^2-9)(h^2-1)}{5120}\frac{\partial^4 p_0}{p_0^4},\\
p_6 &= a_6\frac{(\partial^2 p_0)^3}{p_0^8} + b_6\frac{(\partial^3 p_0)^2}{p_0^7} + c_6\frac{\partial^2 p_0\partial^4 p_0}{p_0^7} + d_6\frac{\partial^6 p_0}{p_0^6},
\end{aligned} \tag{6.1.4}$$

where $h \coloneqq r+1$ is the Coxeter number of A_r and the coefficients a_6, b_6, c_6 and d_6 are given by

$$\begin{aligned}
a_6 &= \frac{(h^2-5^2)(h^2-1)(401h^2-2081)}{1327104}, \qquad & b_6 &= -\frac{(h^2-5^2)(h^2-1)^2}{387072},\\
c_6 &= -\frac{(h^2-5^2)(h^2-1)(11h^2-59)}{147456}, \qquad & d_6 &= \frac{(h^2-5^2)(h^2-1)(11h^2-59)}{6193152}.
\end{aligned} \tag{6.1.5}$$

Though we have not found the proof, the odd term p_n ($n \in \mathbb{N}_{\rm odd}$) would become the total derivative. We checked this up to $n \leq 20$ for $r \leq 7$. We also found that $S_{2(r+1)k+r+2}$ ($k = 0, 1, \dots$) also becomes the total derivative, which is the feature of higher order ODE. The WKB periods are defined associated with the one-cycle on the WKB curve, which is the quantum SW curve and given by

$$\Sigma : \quad y^{r+1} = (-1)^{r+1} p(x, u_i). \tag{6.1.6}$$

This defines the superelliptic curve on which there are meromorphic differentials of the form [109]

$$\frac{x^{i-1}}{y^a} dx, \qquad i = 1, 2, \dots, N-1, \ a = 1, 2, \dots, r. \tag{6.1.7}$$

In the same way as the Schrödinger case, the WKB periods are defined by

$$\Pi_\gamma(u_i; \epsilon) \coloneqq \oint_\gamma P(x, u_i; \epsilon) \mathrm{d}x, \tag{6.1.8}$$

and its ϵ-expansion are given by

$$\Pi_\gamma(u_i; \epsilon) = \sum_{n=0}^{\infty} \epsilon^n \Pi_\gamma^{(n)}, \qquad \Pi_\gamma^{(n)} \coloneqq \oint_\gamma p_n(x, u_i; \epsilon) \mathrm{d}x. \tag{6.1.9}$$

Here γ is a one-cycle on Σ, and the odd correction terms and $\Pi_\gamma^{(2(r+1)k+r+2)}$ ($k = 0, 1, \dots$) vanish since the related coefficients p_n are total derivative.

6.1.1 The quantum corrections and PF operators

For the Schrödinger case, the quantum corrections were calculated by acting the Picard-Fuchs operators on the classical period. However, for the higher order case, the situation is slightly changed. In general, the differential $p_n dx$ is written as the linear combination of the basis of the one-form:

$$p_n dx = \sum_{a=1}^{r} \sum_{i=1}^{N-1} B_{a,i}^{(n)} \frac{x^{i-1}}{y^a} dx + d(*), \tag{6.1.10}$$

where $d(*)$ stands for the total derivative terms. The WKB periods are then expressed as

$$\Pi_\gamma(\epsilon) = \sum_{a=1}^{r} \sum_{i=1}^{N-1} B_{a,i}(\epsilon) (\Pi_{ai})_\gamma, \qquad B_{a,i}(\epsilon) = \sum_{n=0}^{\infty} B_{a,i}^{(n)} \epsilon^n, \tag{6.1.11}$$

where we defined the integral of the basis $(\Pi_{a,i})_\gamma$ by

$$(\Pi_{a,i})_\gamma = \oint_\gamma \frac{x^{i-1}dx}{y^a}. \tag{6.1.12}$$

We introduce the SW differential $y^a dx$ $(a = 1, 2, \dots, r)$ and the classical SW period $(\hat{\Pi}_a)_\gamma$ by

$$(\hat{\Pi}_a)_\gamma \coloneqq \oint_\gamma y^a dx, \tag{6.1.13}$$

which is the higher order generalization of the classical period. The the cycle integral $(\Pi_{a,i})_\gamma$ is obtained from the classical SW period with the differentiation in terms of u_i:

$$(\Pi_{a,i})_\gamma = (-1)^{r+1}\frac{a}{r+1}\partial_{u_{N+2-i}}(\hat{\Pi}_{r+1-a})_\gamma. \tag{6.1.14}$$

Thus, the quantum corrections are calculated by differentiating the classical SW periods:

$$\Pi_\gamma^{(n)} = \sum_{a=1}^{r} \mathcal{O}_a^{(n)}(\hat{\Pi}_a)_\gamma, \tag{6.1.15}$$

where we defined the Picard-Fuchs operator $\mathcal{O}_a^{(n)}$ by

$$\mathcal{O}_a^{(n)} = (-1)^{r+1}\sum_{i=1}^{N-1} B^{(n)}_{r+1-a,N+2-i}\frac{r+1}{a}\partial_{u_{N+2-i}}. \tag{6.1.16}$$

The PF operators for the higher order ODE with the quadratic potential, which is (A_r, A_1)-type ODE, are in appendix D. In this section, we show the PF operators of (A_2, A_2)-type ODE up to the twelve order. For the third order ODE, the corrections of order $n = 6k + 4$ $(k = 1, 2, \dots)$ vanish. The non-zero corrections are given by

$$\begin{aligned}
\Pi_\gamma^{(6k+2)} &= \mathcal{O}_2^{(6k+2)}(\hat{\Pi}_2)_\gamma = -\sum_{i=1}^{2} B^{(6k+2)}_{2,i}\frac{3}{2}\partial_{u_{4-i}}(\hat{\Pi}_2)_\gamma, \qquad k = 0, 1, \dots. \\
\Pi_\gamma^{(6k+6))} &= \mathcal{O}_1^{(6k+6)}(\hat{\Pi}_1)_\gamma = -B^{(6k+6)}_{1,1}3\partial_{u_3}(\hat{\Pi}_1)_\gamma,
\end{aligned} \tag{6.1.17}$$

The coefficients in the PF operators up to the twelve order are simplified as

$$\begin{aligned}
B^{(2)}_{2,1} &= \frac{1}{6}\frac{D_0}{\Delta}\frac{u_1}{3}, \qquad B^{(2)}_{2,2} = \frac{1}{6}\frac{D_0}{\Delta}u_0, \\
B^{(6)}_{1,1} &= -\frac{1}{349920}\frac{D_0}{\Delta^4}u_1 f^{(6)}(D_0^2, u_0^2\Delta), \\
B^{(8)}_{2,1} &= -\frac{11}{5878656}\frac{D_0}{\Delta^6}\frac{u_1}{3} f^{(8)}(D_0^2, u_0^2\Delta), \\
B^{(8)}_{2,2} &= -\frac{11}{5878656}\frac{D_0}{\Delta^6}u_0 f^{(8)}(D_0^2, u_0^2\Delta), \\
B^{(12)}_{1,1} &= -\frac{19}{53875362816}\frac{D_0}{\Delta^9}u_1 f^{(12)}(D_0^2, u_0^2\Delta),
\end{aligned} \tag{6.1.18}$$

where the function $f^{(n)}(a,b)$ $(n = 6, 8, 12)$ in (6.1.18) are polynomials in a and b, whose explicit forms are

$$\begin{aligned}
f^{(6)}(a,b) &= 21983a^2 - 823446ab + 6633171b^2, \\
f^{(8)}(a,b) &= 2392529a^3 - 124372017a^2b + 1908955755ab^2 - 7756381395b^3, \\
f^{(12)}(a,b) &= 746077731259a^5 - 60630791851665a^4b \\
&\quad + 1819452520503702a^3b^2 - 24379786291304106a^2b^3 \\
&\quad + 137161534405430655ab^4 - 2252144902647848885b^5.
\end{aligned} \tag{6.1.19}$$

The discriminant of the WKB curve Δ is given by

$$\Delta = -u_1^2u_2^2 + 4u_3u_1^3 + 4u_0u_2^3 - 18u_0u_2u_3u_1 + 27u_0^2u_3^2. \tag{6.1.20}$$

We also defined D_0 by

$$\begin{aligned}
D_0 &= 2u_1^3 - 9u_0u_2u_1 + 27u_0^2u_3 \\
&= u_0(x_0 + x_1 - 2x_2)(x_1 + x_2 - 2x_0)(x_2 + x_0 - 2x_1).
\end{aligned} \tag{6.1.21}$$

Here x_0, x_1 and x_2 are the branch points of the WKB curve: $p(x) = 0$. Note that the coefficients in the PF operator has the common numerator D_0. Hence, if one set D_0, which implies the branch points x_0, x_1 and x_2 array on a single line, all corrections vanish and the classical periods becomes the exact results. This situation is similar to the harmonic oscillator for the second order ODE. This phenomenon is also observed from the TBA equations. The quantum corrections for other types of ODEs are calculated in a similar way.

6.1.2 Classical periods

We next discuss the classical SW periods. Let us define the branch points x_k ($k = 0, 1, \ldots, N$): $p(x_k) = 0$, which are all distinct. The WKB curve represents the Riemann surface of $r+1$-fold cover of the complex plane with these branch points. To define the one-cycles on the WKB curve, we set the branch cuts such that they extend from the each branch points to infinity on the lower half plane. Label of the branch points are defined so that $\mathrm{Re}(x_{k-1}) \geq \mathrm{Re}(x_k)$ ($k = 1, 2, \ldots, N$). We introduce the basis of the one-cycle on the WKB curve $\gamma_{l,k}$ ($l = 1, 2, \ldots, r$, $k = 1, 2, \ldots, N$) which encircle x_{k-1} anticlockwise as well as x_k clockwise on the l-th and $l+1$-th sheet. Here we defined the l-th sheet so that on the sheet, $y = y_l := e^{\frac{2\pi i}{r+1}} p(x)^{\frac{1}{r+1}}$. We illustrate the distributions of the branch points and cuts, and the cycle $\gamma_{l,k}$ in figure 6.1.1. The classical SW periods for the one cycle $\gamma_{l,k}$

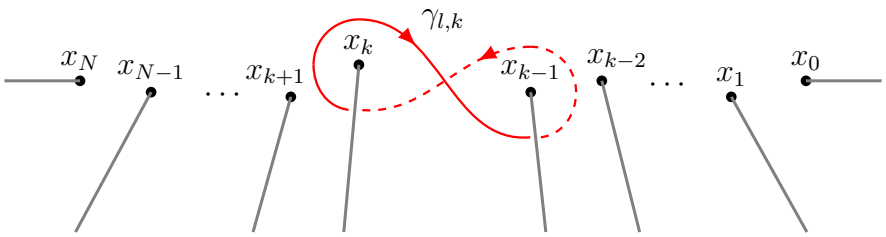

Figure 6.1.1: The distribution of the branch points and cuts as well as the definition of the cycle $\gamma_{l,k}$. The solid lives on the l-th sheet while the dotted line lives on the $l+1$-th sheet of the WKB curve.

is then defined by

$$\begin{aligned}(\hat{\Pi}_a)_{\gamma_{l,k}} &= \left(e^{\frac{2\pi i}{r+1}l} - e^{\frac{2\pi i}{r+1}(l+1)}\right) \oint_{\gamma_{l,k}} p(x)^{\frac{a}{r+1}} \mathrm{d}x \\ &= -2ie^{\frac{\pi i}{r+1}(2l+1)a} u_0^{\frac{a}{r+1}} \sin\frac{\pi a}{r+1} \int_{x_k}^{x_{k-1}} \prod_{i=0}^{N} (x - x_i)^{\frac{a}{r+1}} \mathrm{d}x.\end{aligned} \tag{6.1.22}$$

The equation (6.1.22) is the generalized version of the hypergeometric integral. In this subsection, we show the evaluation of the integral for $N = 2$ and $N = 3$ case. For this purpose, it is convenient to define x_{k+mN} by

$$x_{k+mN} := x_k, \qquad m \in \mathbb{Z}. \tag{6.1.23}$$

First, let us consider the $N = 2$ case. The three branch points are x_0, x_1 and x_2. To perform the integral, we change the integration variable from x to t which is related by $x(t) = \frac{a_k x + b_k}{c_k x + d_k}$ so that

$$\begin{aligned} x_k = x(0) = \frac{b_k}{d_k}, \qquad & x_{k-1} = x(1) = \frac{a_k + b_k}{c_k + d_k}, \\ a_k d_k - b_k c_k = 1, \qquad & d_k = \left(\frac{x_{k+1} - x_{k-1}}{(x_k - x_{k-1})(x_k - x_{k+1})} \right)^{\frac{1}{2}}. \end{aligned} \tag{6.1.24}$$

By this fractional linear transformation, one obtains the closed form of the hypergeometric integral. The classical period is evaluated as

$$\begin{aligned} (\hat{\Pi}_a)_{\gamma_{l,k}} = & -2ie^{\frac{2\pi i}{3}(l+k)a + \delta(k,a)} d_k^{-2-\frac{2}{r+1}a} (x_{k+1} - x_{k-1})^{\frac{a}{r+1}} u_0^{\frac{a}{r+1}} \sin \frac{\pi a}{r+1} \\ & \cdot B\left(1 + \frac{a}{r+1}, 1 + \frac{a}{r+1}\right) {}_2F_1\left(2 + a, 1 + \frac{a}{r+1}; 2 + \frac{2a}{r+1}; z_k^{(1)}\right), \end{aligned} \tag{6.1.25}$$

where we defined $z_k^{(1)}$ $(k = 1, 2)$ by

$$z_k^{(1)} := \frac{x_k - x_{k-1}}{x_{k+1} - x_{k-1}}. \tag{6.1.26}$$

The phase factor $\delta(k, a)$ ensures the hypergeometric integral to be the principal value. The beta function $B(a, b)$ and the Gauss hypergeometric function ${}_2F_1(a, b; c; z)$ is given by

$$\begin{aligned} B(a,b) &= \int_0^1 t^{a-1}(1-t)^{b-1} \mathrm{d}t = \frac{\Gamma(a)\Gamma(b)}{\Gamma(a+b)}, \qquad \mathrm{Re}(a),\ \mathrm{Re}(b) > 0, \\ {}_2F_1(a,b;c;z) &= \frac{1}{B(b, c-b)} \int_0^1 \frac{t^{b-1}(1-t)^{c-b-1}}{(1-zt)^a} \mathrm{d}t, \qquad |z| \leq 1. \end{aligned} \tag{6.1.27}$$

We next consider $N = 3$ case. The basis of the one-cycles is $\gamma_{l,k}$ $(l = 1, 2, \ldots, r,$ $k = 1, 2, 3)$. With the fractional linear transformation same as the one in the $N = 2$ case, we can evaluate the integral. The classical SW periods becomes

$$\begin{aligned} (\hat{\Pi}_a)_{\gamma_{l,k}} = & -2ie^{\frac{2\pi i}{3}(l+k)a + \delta(k,a)} d_k^{-2-\frac{4a}{r+1}} (x_{k+1} - x_{k-1})^{\frac{a}{r+1}} (x_k - x_{k+2})^{\frac{a}{r+1}} \sin \frac{\pi a}{r+1} \\ & \cdot B\left(1 + \frac{a}{r+1}, 1 + \frac{a}{r+1}\right) F_1\left(1 + \frac{a}{r+1}, 2 + \frac{4a}{r+1}, \frac{-a}{r+1}, 2 + \frac{2a}{r+1}; z_k^{(1)}, z_k^{(2)}\right), \end{aligned} \tag{6.1.28}$$

where $z_k^{(2)}$ $(k = 1, 2, 3)$ is defined by

$$z_k^{(2)} := \frac{(x_k - x_{k-1})(x_{k+1} - x_{k+2})}{(x_{k+1} - x_{k-1})(x_k - x_{k+2})}. \tag{6.1.29}$$

$F_1(a, b, b', x, z^{(1)}, z^{(2)})$ represents the Appell hypergeometric function given by

$$F_1(a, b, b', c; z^{(1)}, z^{(2)}) = \frac{1}{B(a, c-a)} \int_0^1 \frac{t^{a-1}(1-t)^{c-a-1}}{(1-z^{(1)}t)^b (1-z^{(2)}t)^{b'}} \mathrm{d}t. \tag{6.1.30}$$

Here again by the phase factor $\delta(k, a)$, the hypergeometric integral is ensured to be the principal value.

The quadratic potential case

Specializing to the quadratic potential, the classical SW periods become simpler. In this case, the branch points are only x_0 and x_1 and the basis of the one-cycles are $\gamma_{l,1}$ $(l = 1, 2, \ldots, r)$. There is no wall in the moduli space and we can fix the phase factor. The classical SW period is evaluated as

$$(\hat{\Pi}_a)_{\gamma_{l,1}} = 2e^{\frac{\pi i a}{r+1}(2l+3)} \sin\left(\frac{\pi a}{r+1}\right) u_2^{\frac{1}{2}+\frac{a}{r+1}} u_0^{-\frac{1}{2}} B\left(\frac{1}{2}, 1 + \frac{a}{r+1}\right), \tag{6.1.31}$$

where $B(a, b)$ is the beta function.

Cycle integrals of the meromorphic differentials for the monomial case

The monomial potential is the most symmetric potential, and the associated TBA would in the maximal chamber like the second order case. For the monomial potential, it is easier to calculate the quantum periods from the direct integration of the basis of the meromorphic differentials. The potential is expressed as

$$p(x) = u_0 x^{N+1} + u_{N+1} = u_0(x^{N+1} - u), \qquad u = -\frac{u_{N+1}}{u_0}. \tag{6.1.32}$$

There are many branch points with the equal values of the real parts. We label them so that

$$\begin{cases} x_{2k-1} = u^{\frac{1}{N+1}} e^{\frac{2\pi i k}{N+1}}, & k = 1, 2, \ldots, \lfloor \frac{N+1}{2} \rfloor, \\ x_{2k} = u^{\frac{1}{N+1}} e^{-\frac{2\pi i k}{N+1}}, & k = 0, 1, 2, \ldots, \lfloor \frac{N}{2} \rfloor. \end{cases} \tag{6.1.33}$$

The cycle integrals of the meromorphic differentials are then takes the form

$$\begin{cases} (\Pi_{a,i})_{\gamma_{l,2k-1}} = \sum_{j=1}^{k-1} \left(I_{l,j}^{a,i} + I_{l,N+2-j}^{a,i} \right) + I_{l,k}^{a,i}, & k = 1, 2, \ldots, \lfloor \frac{N+1}{2} \rfloor, \\ (\Pi_{a,i})_{\gamma_{l,2k}} = -\sum_{j=1}^{k} \left(I_{l,j}^{a,i} + I_{l,N+2-j}^{a,i} \right), & k = 1, 2, \ldots, \lfloor \frac{N}{2} \rfloor, \end{cases} \tag{6.1.34}$$

where $I_{l,j}^{a,i}$ $(j = 1, 2, \ldots, N)$ is the cycle integral of the basis $x^{i-1}/y^{\frac{a}{r+1}}dx$ along the cycle which encircles the branch point $u^{\frac{1}{N+1}}e^{\frac{2\pi i(j-1)}{N+1}}$ anti-clockwise as well as the branch point $u^{\frac{1}{N+1}}e^{\frac{2\pi ij}{N+1}}$ clockwise on the l-th and $l+1$-th sheet. $I_{l,j}^{a,i}$ is given by

$$\begin{aligned} I_{l,j}^{a,i} &= \left(e^{-\frac{2\pi i}{r+1}al} - e^{-\frac{2\pi i}{r+1}(l+1)a} \right) \int_{u^{\frac{1}{N+1}}e^{\frac{2\pi ij}{N+1}}}^{u^{\frac{1}{N+1}}e^{\frac{2\pi i(j-1)}{N+1}}} \frac{x^{i-1}}{(u_0 x^{N+1} - u)^{\frac{a}{r+1}}} dx \\ &= \frac{4}{N+1} e^{2\pi i\left(\frac{j-1}{N+1}i - \frac{1}{r+1}a(l+\frac{1}{2}) + \delta(l,j) \right)} u_{N+1}^{\frac{i}{N+1}-\frac{a}{3}} u_0^{-\frac{i}{N+1}} \sin\frac{\pi a}{r+1} \sin\frac{\pi i}{N+1} B\left(\frac{i}{N+1}, 1 - \frac{a}{r+1} \right), \end{aligned} \tag{6.1.35}$$

where $\delta(l,j)$ represents the phase factor which ensures the integral to be the principal value.

6.2 Identification of Y-functions with WKB periods

Now we discuss the ODE/IM correspondence of the higher ODE (6.1.1). In the second order case, the WKB periods are related to the Y-function satisfying the (A_1, A_N)-type TBA equations. It is straightforward to generalize this relation to the higher ODE, which leads to the (A_r, A_N)-type Y-system. After the relation between the Y-functions and the solutions to the higher ODE is obtained, we will discuss the WKB approximation of the leading term of the logarithm of the Y-functions. From this analysis, we will find the dictionary of the cycle integral on the WKB curve and the Y-functions in the minimal chamber. The extension of the identification to other chambers is the topic of the next chapter.

6.2.1 The ODE/IM correspondence for the higher ODE

First, let us define the Symanzik rotation of the higher ODE (6.1.1). The generalization of the rotation in the second order case describes the invariant property of the higher

case, which is the simultaneous change of the variables

$$x \to \omega^{-1}x, \qquad u_i \to \omega^{-i}u_i, \qquad \omega := e^{\frac{2\pi i}{N+r+2}}. \tag{6.2.1}$$

From the similar argument for the second order case, it is more convenient to regard this transformation as the rotational symmetry of ϵ i.e. $\epsilon \to e^{\frac{2\pi i}{r+1}}\epsilon$. Next, we consider the subdominant solutions. The subdominant solution along the real axis, which we denote ϕ, has the asymptotic behavior

$$\phi(x, u_i; \epsilon) \sim \frac{\epsilon^{\frac{r}{2}} u_0^{-\frac{r}{2r+2}}}{i^{\frac{r}{2}}\sqrt{r+1}} x^{-\frac{r(N+1)}{2r+2}} \exp\left[-\frac{1}{\epsilon}\frac{u_0^{\frac{1}{r+1}}(r+1)}{N+r+2}x^{\frac{N+r+2}{r+1}}\right], \quad |x| \to \infty. \tag{6.2.2}$$

Recall that the rotational symmetry enable us define the subdominant solutions in other regions. We define the k-Symanzik rotated solution ϕ_k by

$$\phi_k(x, u_i; \epsilon) = \phi(x, u_i; e^{\frac{2\pi i k}{r+1}}\epsilon). \tag{6.2.3}$$

One finds ϕ_k is subdominant in the sector $\mathcal{S}_k$ which is defined by

$$\mathcal{S}_k = \left\{ x \in \mathbb{C}; \left| \arg(x) - \frac{2\pi k}{N+r+2} \right| < \frac{\pi}{N+r+2} \right\}. \tag{6.2.4}$$

Since the ODE (6.1.1) has the trivial monodromy around the origin, $\phi_k(e^{2\pi i}x, u_i; \epsilon)$ is proportional to $\phi_k(x, u_i; \epsilon)$. Together with the fact that $\phi_k(e^{2\pi i}x, u_i; \epsilon)$ and $\phi_{k+N+r+2}(x, u_i; \epsilon)$ is subdominant in the same sector, one finds the periodicity $\phi_{k+N+r+2} \propto \phi_k$. Then, the Wronskian of the subdominant solutions ϕ_{k+i} ($k \in \mathbb{Z}$), $i = 0, 1, \ldots, r$) is equal to one:

$$W[\phi_k, \phi_{k+1}, \ldots, \phi_{k+r}] = 1. \tag{6.2.5}$$

Note that the normalization factor in (6.2.2) is set so that this Wronskians becomes one. The Wronskian of the solutions has the property

$$W[\phi_{i_0}, \ldots, \phi_{i_r}]^{[2k]} = W[\phi_{i_0+k}, \ldots, \phi_{i_r+k}], \quad k \in \mathbb{Z}, \tag{6.2.6}$$

where we defined

$$g^{[k]}(u_i; \epsilon) := g(u_i; e^{\frac{\pi i k}{r+1}}\epsilon). \tag{6.2.7}$$

Since the Wronskian is constant, the set $\{\phi_{k+i}\}_{i=0}^{r}$ forms the basis of the solutions. The T-functions were associated with the Stokes multiplier in the second order case. For the higher ODE, we can define the T-functions $T_{a,k}$ $(1 \leq a \leq r,\ k \in \mathbb{Z})$ as the Stokes multiplier:

$$T_{a,k} = \begin{cases} W\left[\phi_{-r+1+\frac{a}{2}}, \phi_{-r+2+\frac{a}{2}}, \ldots, \phi_{1-\frac{a}{2}}, \phi_{l+2-\frac{a}{2}}, \phi_{k+3-\frac{a}{2}}, \ldots, \phi_{k+1+\frac{a}{2}}\right]^{[-k-1]}, & a\text{: even}, \\ W\left[\phi_{-r+1+\frac{a-1}{2}}, \phi_{-r+2+\frac{a-1}{2}}, \ldots, \phi_{-\frac{a-1}{2}}, \phi_{k+1-\frac{a-1}{2}}, \phi_{k+2-\frac{a-1}{2}}, \ldots, \phi_{k+1+\frac{a-1}{2}}\right]^{[-k]}, & a\text{: odd}. \end{cases} \tag{6.2.8}$$

From this definition, it is easy to find $T_{0,k} = T_{r+1,k} = 0$ and the boundary conditions:

$$T_{a,-1} = T_{a,N+2} = 0, \qquad T_{a,0} = T_{a,N+1} = 1, \qquad a = 1, 2, \ldots, r. \tag{6.2.9}$$

Thus, the nontrivial T-functions are only $T_{a,k}$ $(1 \leq k \leq N)$. The functional relation between the T-functions obeys from the Plücker identity of the Wronnskian

$$\begin{aligned} W[f_0, \ldots, f_{r-1}, f_r] W[f_0, \ldots, f_{r-2}, f_{r+1}, f_{r+2}] \\ = W[f_0, \ldots, f_{r-1}, f_{r+1}] W[f_0, \ldots, f_{r-2}, f_r, f_{r+2}] \\ + W[f_0, \ldots, f_{r-1}, f_{r+2}] W[f_0, \ldots, f_{r-2}, f_{r+1}, f_r], \end{aligned} \tag{6.2.10}$$

which, with the boundary condition (6.2.9), leads the (A_r, A_N)-type T-system:

$$T_{a,k}^{[+1]} T_{a,k}^{[-1]} = T_{a,k+1} T_{a,k-1} + T_{a+1,k} T_{a-1,k}. \tag{6.2.11}$$

This T-system can be converted into the (A_r, A_N)-type TBA equations, which we reviewed in chapter 2. The driving term is then computed from the solutions to the higher ODE through the WKB approximation.

6.2.2 Cycle integrals from the abelianization trees

In this subsection, we first discuss the asymptotic behavior of the Y-functions through the WKB approximation. Then, we identify the cycle integrals corresponding to each Y-functions in the minimal chamber. As we saw in the previous subsection, the Y-functions are defined, in the ODE/IM correspondence, as the cross ratios of the Wronskians of

the subdominant solutions. The argument will be similar to that of the second order case in chapter 4, however, we have to refine it by using the Stokes graphs. Here, we consider the third order case as the simplest example of the higher order ODE. The relation between the WKB periods and Y-function for the higher order case is obtained by generalizing the result of the third order. For the third order case, the WKB curve is $\Sigma : q(x,y) \coloneqq y^3 + p(x) = 0$, on which there are three sheets. We label them by $a \in \{1,2,3\}$ on which $y = y_a = e^{\frac{2\pi i}{3}} p(x)^{\frac{1}{3}}$. The definition of the Stokes curve which extends from the turning point x_* is [120]

$$\operatorname{Im} e^{-i\vartheta} \int_{x_*}^{x} (y_a(x) - y_b(x))\,\mathrm{d}x = 0, \qquad a,b = 1,2,3, \quad a \neq b. \tag{6.2.12}$$

Here $\vartheta = \arg\epsilon$. At the turning point x_*, $y_a(x_*) = y_b(x_*)$ holds. The Stokes curve could end on the other turning point or extend to infinity. It is convenient to label the curve (a,b) on which

$$\operatorname{Re} e^{-i\vartheta} \int_{x_*}^{x} (y_a(x) - y_b(x))\,\mathrm{d}x < 0 \tag{6.2.13}$$

holds. The Stokes curve may intersect each other. For the third order case, there are two possible intersection angles which are $\frac{\pi}{3}$ and $\frac{2\pi}{3}$. In the latter case, the intersection point is the so-called virtual turning point [120]. From the virtual turning point, a new Stokes curve stretches [78, 79].

Let us, first, discuss the Stokes curve around the turning points. For general higher order ODE whose WKB curve is $q(y,x) = 0$, the turning point x_* is said to be simple if and only if

$$y_a(x_*) = y_b(x_*), \qquad \left.\frac{\partial q(x,y)}{\partial x}\right|_{x=x_*, y=y_a(x_*)} \neq 0 \tag{6.2.14}$$

are satisfied. From the simple turning point, three Stokes curve stretch [121, 122]. However, the ODE we are considering has no simple turning points. There are eight curves extend from the turning points of our case. Focus on the region around the branch point x_*. Substituting the expansion $x = x_* + re^{i\varphi}$ into y_a, one obtains

$$y_a = e^{\frac{2\pi i}{3}a} p(x_* + re^{i\varphi}) = e^{\frac{2\pi i}{3}a + \frac{i}{3}\arg p'(x_*)} |p'(x_*)|^{\frac{1}{3}} r^{\frac{1}{3}} e^{\frac{1}{3}i\varphi} + \cdots . \tag{6.2.15}$$

Since the turning point x_* satisfies the condition (6.2.12), the argument φ is restricted to the angle

$$\varphi = \frac{3}{4}\left(\frac{(2n+1)\pi}{2} + \vartheta - \frac{(a+b)\pi}{3} - \frac{\arg p'(x_*)}{3}\right), \qquad n \in \mathbb{Z}. \tag{6.2.16}$$

Fixing ϑ, one finds eight directions to which the curve extends. Since we label the curve satisfying (6.2.13) as (a, b), if we suppose $a < b$, the label of the curve is (a, b) for odd n while the label becomes (b, a) for even n. The curves stretching to the to the neighboring angles has the common number in the labels i.e. the set of the labels are (i, j), (k, j), or (j, i), (j, k). Furthermore, one finds the label of the curve extending to the angle $\frac{3}{4}\vartheta - \frac{1}{4}\arg p'(x_*)$ is $(1, 3)$. Thus, going around anticlockwise from the ray labeled by $(1, 3)$, the labels of the successive rays becomes $(1, 3)$, $(1, 2)$, $(3, 2)$, $(3, 1)$, ...

Next, we discuss the Stokes curve in the asymptotic region. Each Stokes curve generated by equation (6.2.12) approaches one of the $2(N + 4)$ directions if the curve does not end on other turning points. For the simplicity, we consider $\vartheta = 0$ case. The Stokes curves extend to the infinity of angle $\frac{\pi i}{2(N+4)}(2k + 1)$ $(k \in \mathbb{Z})$. Let us introduce the asymptotic directions ℓ_k and $\overline{\ell}_k$ by

$$\ell_k \coloneqq e^{\frac{2\pi i k}{N+4}}\mathbb{R}_+, \qquad \overline{\ell}_k \coloneqq e^{\frac{\pi i(2k+3)}{N+4}}\mathbb{R}_+, \qquad k \in \mathbb{Z}. \tag{6.2.17}$$

The direction ℓ_k and $\overline{\ell}_k$ array on the middle of the two asymptotic directions of the Stoke curves. The line ℓ_k is also the mid of the Stokes sector $\mathcal{S}_k$ while $\overline{\ell}_k$ is the mid of $\mathcal{S}_{k+3/2}$. Then, along the line ℓ_k, the subdominant solution ϕ_k decays the fastest among other solutions. One finds that the solution ϕ_k is dominant along the line $\overline{\ell}_k$. Parallel to this, we introduce the solution $\overline{\phi}_k$ which decays the fastest along the line $\overline{\ell}_k$ by

$$\overline{\phi}_k(x, \{u_i\}; \epsilon) \coloneqq \phi_k(x, \{u_i\}; -\epsilon), \qquad k \in \mathbb{Z}, \tag{6.2.18}$$

which is nothing but the solution to the dual (or adjoint) ODE which we introduced in chapter 3. Note that on the real axis, the dual solution $\overline{\phi}_0$ behaves asymptotically as

$$\overline{\phi}_0(x, \{u_i\}; \epsilon) \sim \frac{u_0^{\frac{1}{3}}\epsilon}{i\sqrt{3}} x^{\frac{N+1}{3}} \exp\left(\frac{1}{\epsilon}\frac{3u_0^{\frac{1}{3}}}{N+4} x^{\frac{N+4}{3}}\right), \qquad |x| \to \infty, \tag{6.2.19}$$

which is then dominant solution in the sector $\mathcal{S}_0$. Similarly, the dual solution $\overline{\phi}_k$ is dominant in the sector $\mathcal{S}_k$. The labels of the Stokes curves are read off from the asymptotic behaviors of the subdominant solutions. From the WKB approximation, one finds that the (dual) solutions have the asymptotic behaviors

$$\phi_k \simeq \exp\left[-\frac{\delta_k}{\epsilon}\int_{\infty e^{\frac{2\pi i k}{N+2}}}^{x} y_{a_k}\,\mathrm{d}x'\right], \qquad \overline{\phi}_k \simeq \exp\left[\frac{\overline{\delta}_k}{\epsilon}\int_{\infty e^{\frac{\pi i(2k+3)}{N+2}}}^{x} y_{\overline{a}_k}\,\mathrm{d}x'\right]. \tag{6.2.20}$$

Here $a_k, \overline{a}_k \in \{1,2,3\}$ and the phases $\delta_k, \overline{\delta}_k \in \{1, e^{\pm\frac{2\pi i}{3}}\}$ ensure the subdominant property of the solutions. We set $\delta_k, \overline{\delta}_k = 1$ before we take into account the effects of the branch cuts. We define the label of the sheet the solution ϕ_k ($\overline{\phi}_k$) lives as a_k ($\overline{a}_k$). Consider the situation that there are two solutions ϕ_{k_1} and $\overline{\phi}_{k_2}$ which is subdominant along the neighboring directions ℓ_{k_1} and $\overline{\ell}_{k_2}$. In other words, there are Stokes curves stretching the direction between ℓ_{k_1} and $\overline{\ell}_{k_2}$. These curves divides the asymptotic region into the two areas in which one of the solutions is subdominant. Thus, these curves are characterized by $\mathrm{Im}\, y_{a_{k_1}} = \mathrm{Im}\, y_{\overline{a}_{k_2}}$. Furthermore, since the powers of the exponents of ϕ and $\overline{\phi}$ in (6.2.20) have the opposite sign, subdominance of the solutions implies that $\mathrm{Re}\, y_{a_{k_1}} > \mathrm{Re}\, y_{\overline{a}_{k_2}}$ holds on the curves. As the conclusion, the curves are labeled by $(\overline{a}_{k_2}, a_{k_1})$. As an example, consider $k = 1$ case. Around this curve ϕ_0 and $\overline{\phi}_{-1}$ is subdominant. Since the labels of the sheets these solutions live are 3 and 1, respectively, one finds the label $(1,3)$. Together with the analysis around the turning points, we can define all the labels of the Stokes curves. We call the complex plane, on which all the Stokes curves with the labels are drawn, the Stokes graph.

WKB approximation and identification of the cycles

Now let us apply the WKB approximation to the Y-functions (2.4.21) and associate the one-cycles on the WKB curve. For this purpose, we introduce the notion of the abelianization tree [123]. The abelianization tree is a junction which made up with appropriate numbers of lines. In our case, each lines end on the infinity points of the directions ℓ_k and $\overline{\ell}_k$. The abelianization tree associated with the Wronskian $W[\phi_{k_1}, \phi_{k_2}, \phi_{k_3}]$ is constructed from the three lines which end on ℓ_{k_1}, ℓ_{k_2} and ℓ_{k_3}. The path from the infinity point to the intersection point of the junction along each line is the integration path in the WKB

approximation of each solution. Then, we assign the label to each line, which is the sheet label of the corresponding solution. Since the line represents the integration path, the line with the label a cannot cross the Stokes curve with label $(a, *)$, otherwise, the WKB approximation becomes invalid.

Let us denote the intersection point of the junction as x. At the leading order approximation, the Wronskian $W[\phi_{k_1}, \phi_{k_2}, \phi_{k_3}]$ becomes

$$W[\phi_{k_1}, \phi_{k_2}, \phi_{k_3}] = \exp\left[-\frac{\delta}{\epsilon}\left(\int^x y_{a_{k_1}}\,\mathrm{d}x + \int^x y_{a_{k_2}}\,\mathrm{d}x + \int^x y_{a_{k_3}}\,\mathrm{d}x\right)\right] + \cdots . \quad (6.2.21)$$

Here δ represents some phase and we omit the initial point of the integration. Differentiating the Wronskian with respect to x, one obtains

$$\partial_x W[\phi_{k_1}, \phi_{k_2}, \phi_{k_3}] = -\frac{\delta}{\epsilon}\Big(y_{a_{k_1}}(x) + y_{a_{k_2}}(x) + y_{a_{k_3}}(x)\Big)\exp[\dots] + \cdots . \quad (6.2.22)$$

Since the Wronskian is independent of x, the $1/\epsilon$ term should vanish. This will happen if the set of the labels of the sheets exhaust all the labels i.e. $\{a_{k_1}, a_{k_2}, a_{k_3}\} = \{1, 2, 3\}$. Thus, the abelianization tree is made of the lines with the label $1, 2$ and 3. Let us summarize the definition and the rules of the abelianization tree in the following:

(i) An abelianization tree associate with the Wronskian $W[\phi_{k_1}, \phi_{k_2}, \phi_{k_3}]$ is a junction that has three endpoints at the infinity of l_{k_i} $(i = 1, 2, 3)$.

(ii) A line which end at the infinity point of l_k has the label a_k.

(iii) A line with label a_k cannot cross a the Stokes curve with label $(a_k, *)$.

(iv) The labels of three lines which make up a junction exhaust all the sheet's labels.

By using the Stokes graph and the abelianization tree satisfying above rules, we associate the Y-functions with cycle integrals.

The Y-function is the cross-ratio of the Wronskians, hence we draw the four abelianization trees for each Y-functions. Combining these four trees and regarding the trees as the integration paths, one can construct a closed cycle. To demonstrate this procedure, let us consider the Y-function $Y_{1,1}$ of the (A_2, A_2)-type ODE. We are considering in the

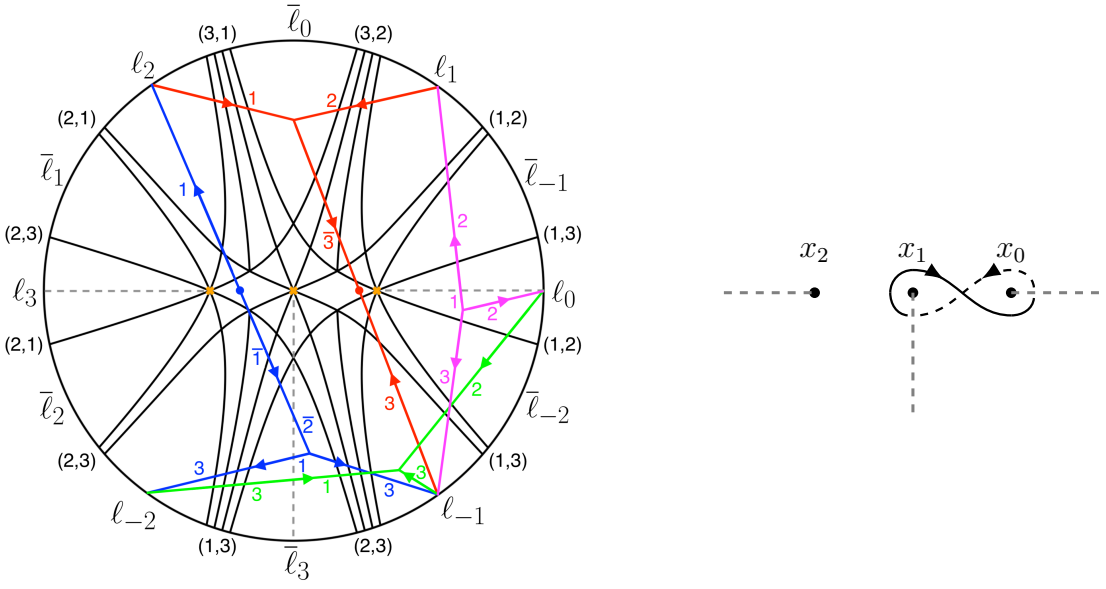

(a) (b)

Figure 6.2.1: The stokes graph and the abelianization tree for $Y_{1,1}$ in the minimal chamber (a) and the corresponding one-cycle $\gamma_{1,1}$ (b). In (b), the solid and the dashed lines are on the sheet 1 and 2, respectively.

minimal chamber, and set all the branch points real. Fixing the argument $\vartheta = 0$, we show the Stokes graph as the black lines in figure 6.2.1. Writing in the form of the cross ratio of the Wronskian, the Y-function is

$$Y_{1,1} = \frac{W[\phi_{-1}, \phi_1, \phi_2] W[\phi_{-2}, \phi_{-1}, \phi_0]}{W[\phi_{-2}, \phi_{-1}, \phi_2] W[\phi_{-1}, \phi_0, \phi_1]}. \tag{6.2.23}$$

The abelianization trees of the Wronskians $W[\phi_{-1}, \phi_1, \phi_2], W[\phi_{-2}, \phi_{-1}, \phi_0], W[\phi_{-2}, \phi_{-1}, \phi_2]$ and $W[\phi_{-1}, \phi_0, \phi_1]$ are represented in figure 6.2.1 as the red, green, blue, and pink junctions, respectively. On each line, we added the arrow corresponding to the direction of the integration path. More precisely, we assigned the arrow pointing to the intersection point to the lines of the tree associated with the Wronskian in the numerator in (6.2.23), while the arrows of the junctions for the denominators are pointing to the infinity points. Let us explain the red and the blue dotted point in the figure. For the line corresponding to the integration path of ϕ_{-1}, which has the label 3, we added the red dotted point. Going from the infinity point of ℓ_{-1}, the solution ϕ_{-1} is subdominant along the line before the

red dotted point. However, in the region after the point, the dual solution $\overline{\phi}_0$, which lives on the sheet 3, becomes subdominant. Then, we regard the exponential of the integration of $y_3(x)$ along the line from the red dotted point to the intersection point as not the solution ϕ_{-1} but the dual solution $\overline{\phi}_0$ with flipping the arrow. Correspondingly, we assign the label $\overline{3}$ to the segment of the line. The line with the label $\overline{3}$ cannot cross the Stokes curve with label $(*, 3)$. In the same way, we added the blue dotted point to the line with the label 1 in the junction associated with the Wronskian $W[\phi_{-2}, \phi_{-1}, \phi_2]$.

As the Wronskians are independent of the arguments of the solutions in them, one can move the intersection points of the trees freely. Moving the intersection points of the red and pink trees, as well as that of the blue and green trees, to the common points, we find that the combined path of these trees coincides with the one-cycle $\gamma_{1,1}$. Thus, the leading order approximation of $1/\epsilon$ term of the Y-function becomes

$$\log Y_{1,1} \sim \epsilon^{-1}\Pi^{(0)}_{\gamma_{1,1}}, \qquad \epsilon \to 0. \tag{6.2.24}$$

Similarly, one can draw the Stokes graph and the abelianization trees for the shifted Y-function $Y^{[+1]}_{1,2}$ rather than $Y_{1,2}$, which is given by

$$Y^{[+1]}_{1,2}(\{u_i\}; \epsilon) = Y_{1,2}(\{u_i\}; e^{-\frac{\pi i}{3}}\epsilon) = \frac{W[\phi_{-1}, \phi_2, \phi_3]W[\phi_{-2}, \phi_{-1}, \phi_0]}{W[\phi_{-1}, \phi_0, \phi_2]W[\phi_{-2}, \phi_{-1}, \phi_3]}. \tag{6.2.25}$$

The phase of the ϵ is $\vartheta = -\frac{\pi}{3}$, hence the asymptotic directions are shifted such that $\ell_k = e^{\frac{\pi i(2k-1)}{N+4}}\mathbb{R}_+$ and $\overline{\ell}_k = e^{\frac{2\pi i(k+1)}{N+4}}\mathbb{R}_+$. However, the Stokes graph without the label is, in fact, the same as the one for $Y_{1,1}$. Figure 6.2.2 shows the Stokes graph and the trees, in which the red, green, blue, and pink junctions are the trees for the Wronskians $W[\phi_{-1}, \phi_2, \phi_3]$,$W[\phi_{-2}, \phi_{-1}, \phi_0]$,$W[\phi_{-1}, \phi_0, \phi_2]$ and $W[\phi_{-2}, \phi_{-1}, \phi_3]$. Combining the trees, one finds the corresponding one-cycle is $\gamma_{3,2}$. Thus, we conclude the the leading term of $Y_{1,2}$ is

$$\log Y_{1,2} \sim e^{-\frac{\pi i}{3}}\epsilon^{-1}\Pi^{(0)}_{\gamma_{3,2}}. \tag{6.2.26}$$

Repeating the same procedure for $Y^{[-1]}_{2,1}$ and $Y_{2,2}$, one obtains $\log Y_{2,1} \sim e^{\frac{\pi i}{3}}\epsilon^{-1}\Pi^{(0)}_{-\gamma_{3,1}}$ and $Y_{2,2} \sim \epsilon^{-1}\Pi^{(0)}_{-\gamma_{2,2}}$. Note that $-\gamma_{3,1} = \gamma_{1,1} + \gamma_{2,1}$ and $-\gamma_{2,2} = \gamma_{3,2} + \gamma_{1,2}$. As we will discuss and test numerically in the next section, the relations of the periods and Y-functions are

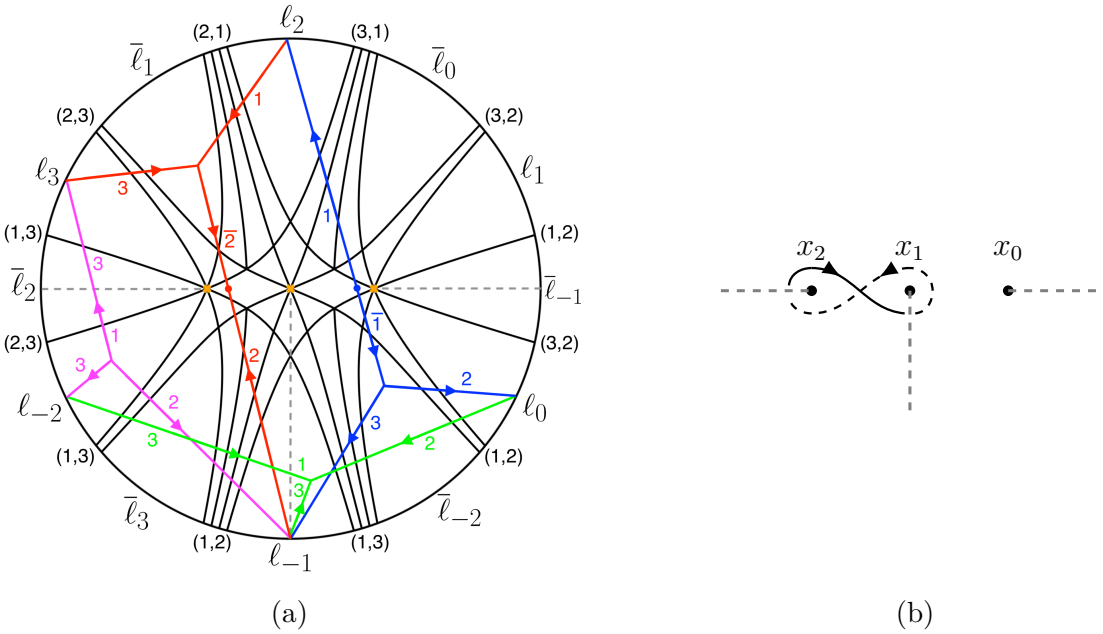

(a) (b)

Figure 6.2.2: The stokes graph and the abelianization tree for $Y_{1,2}^{[+1]}$ in the minimal chamber (a) and the corresponding one-cycle $\gamma_{3,2}$ (b). In (b), the solid and the dashed lines are on the sheet 3 and 1, respectively.

able to extend to the quantum level. For (A_2, A_2)-type ODE, the relation in the minimal chamber then becomes

$$\begin{aligned} \log Y_{1,1} &= \epsilon^{-1}\Pi_{\gamma_{1,1}}, & \log Y_{1,2} &= \left[\epsilon^{-1}\Pi_{\gamma_{3,2}}\right]^{[-1]}, \\ \log Y_{2,1} &= \left[\epsilon^{-1}\Pi_{\gamma_{1,1}+\gamma_{2,1}}\right]^{[+1]}, & \log Y_{2,2} &= \epsilon^{-1}\Pi_{\gamma_{3,2}+\gamma_{1,2}}, \end{aligned} \tag{6.2.27}$$

Analysis of the higher order polynomial potentials leads to the general formula of the relation for the third order ODE. Furthermore, the relation can be extended to the higher (A_r, A_N)-type ODE, which is given by

$$\log Y_{a,k} = \left[\frac{1}{\epsilon}\Pi_{\hat{\gamma}_{a,k}}\right]^{[a-k]}, \quad \hat{\gamma}_{a,k} := \gamma_{2-k,k} + \cdots + \gamma_{a+1-k,k}, \qquad \begin{matrix} a = 1, 2, \ldots, r, \\ k = 1, 2, \ldots, N. \end{matrix} \tag{6.2.28}$$

We will test this formula from the several analyses in the next section, but here we check the consistency for the (A_r, A_1) case. For the quadratic potential, there is only one chamber, and the corresponding TBA equations are the (A_r, A_1)-type. The formula

(6.2.28) shows the relation

$$\log Y_{a,1} = \frac{e^{\frac{\pi i}{r+1}(1-a)}}{\epsilon}\Pi^{(0)}_{\hat{\gamma}_{a,1}} + \cdots, \qquad a = 1, 2, \ldots, r. \tag{6.2.29}$$

Since the classical periods are calculated as

$$\Pi^{(0)}_{\hat{\gamma}_{a,1}} = -2e^{\frac{\pi i}{r+1}(4+a)} \sin\left(\frac{\pi a}{r+1}\right) u_0^{-\frac{1}{2}} u_2^{\frac{1}{r+1}+\frac{1}{2}} B\left(\frac{1}{2}, 1 + \frac{1}{r+1}\right), \tag{6.2.30}$$

one finds the relation between them:

$$2e^{\frac{\pi i}{r+1}(1-a)}\Pi^{(0)}_{\hat{\gamma}_{a,1}} \cos\left(\frac{\pi}{r+1}\right) = \sum_{b=1}^{r} G_{ab} e^{\frac{\pi i}{r+1}(1-b)}\Pi^{(0)}_{\hat{\gamma}_{a,1}}, \tag{6.2.31}$$

which is the Perron-Frobenius relation. Here G_{ab} is the incidence matrix of A_r. Then, from the WKB analysis, one finds that the driving terms of the (A_r, A_1)-type TBA equations are proportional to the PF eigenvector. This is consistent with the result from the asymptotic analysis of the Y-functions from the (A_r, A_1)-type Y-system.

6.3 TBA equations and the tests of the formula

In this section, we discuss the consistency checks of the formula (6.2.28) by using the TBA equations. In the minimal chamber, the TBA equations are obtained from the Y-system and become the (A_r, A_N)-type ones, which we argued in chapter 2. The TBA equations provide not only the numerical results but also the non-perturbative information and exact relations between the quantum corrections, which we call the PNP relation [124, 125]. We first compare the ϵ-expansion of the WKB periods and the Y-functions in section 6.3.1. And then, we derive the relations between the quantum corrections in section 6.3.2. We finally discuss that the discontinuity of the WKB periods is also obtained from the pole structure of the kernel in the TBA equations in section 6.3.3. All of these arguments support the formula (6.2.28).

6.3.1 Numerical tests in the minimal chamber

In this subsection, we compare the ϵ-expansion of the WKB periods and the Y-functions numerically. The logarithm of the Y-function can be expanded in the form:

$$\log Y_{a,k}(\theta) = m_{a,k}e^{\theta} + \sum_{n=1}^{\infty} m_{a,k}^{(n)} e^{-n\theta}, \tag{6.3.1}$$

so we will check the matching

$$m_{a,k}^{(n-1)} = e^{\frac{\pi i}{r+1}(a-k)(n-1)} \Pi_{\hat{\gamma}_{a,k}}^{(n)}, \qquad n = 0, 1, \dots. \tag{6.3.2}$$

Here we set $m_{a,k}^{(-1)} \coloneqq m_{a,k}$ and $m_{a,k}^{(0)} \coloneqq 0$.

The quadratic potential

In the quadratic potential case, the chamber is unique and the corresponding TBA equations are (A_r, A_1)-type, which is given by

$$\log Y_{a,1}(\theta) = m_{a,1}e^{\theta} - \frac{1}{2\pi} \sum_{b=1}^{r} \int_{-\infty}^{\infty} \mathcal{K}_{ab}(\theta - \theta') L_{b,1}(\theta') \, \mathrm{d}\theta' \,. \tag{6.3.3}$$

Here $L_{a,1} = \log\bigl(1 + Y_{a,1}^{-1}\bigr)$ and the kernel is defined by

$$\mathcal{K}_{ab}(\theta) \coloneqq -\int_{-\infty}^{\infty} \left[\sum_{c=1}^{r} \left(2\delta_{ac} \cosh\left(\frac{\pi k}{r+1} \right) - G_{ac} \right)^{-1} G_{cb} \right] e^{ik\theta} \, \mathrm{d}k \,, \tag{6.3.4}$$

where G_{ab} is the incidence matrix of A_r. The definition of the kernel 6.3.4 together with the relations of the classical periods (6.2.31) implies that the the Y-functions have the $\mathbb{Z}_2$-symmetry:

$$Y_{a,1} = Y_{r+1-a,1}, \qquad a = 1, 2, \dots, r. \tag{6.3.5}$$

Using the explicit form of the kernel function, we can write the correction terms in terms of $L_{a,1}$. The corrections $m_{a,1}^{(n)}$ of order $n(r+1)$ ($n \in \mathbb{Z}$) vanish and the non-zero corrections ($n \neq 0 \mod r+1$) are calculated as

$$m_{a,1}^{(n)} = \frac{2}{\pi} \cot\left(\frac{\pi n}{r+1} \right) \sin\left(\frac{\pi n a}{r+1} \right) \sum_{b=1}^{r} \sin\left(\frac{\pi n b}{r+1} \right) \int_{-\infty}^{\infty} L_{b,1}(\theta) e^{n\theta} \, \mathrm{d}\theta \,. \tag{6.3.6}$$

n	$\Pi^{(n)}_{\hat{\gamma}_{1,1}}, e^{\frac{\pi i}{3}(n-1)}\Pi^{(n)}_{\hat{\gamma}_{2,1}}$	$m^{(n-1)}_{1,1}, m^{(n-1)}_{2,1}$
2	$0.1244723667i$	$0.1244723666i$
4	0	0
6	$-0.05721560699i$	$-0.05721561024i$
8	$-0.2089662087i$	$-0.2089662250i$
10	0	0
12	$14.97696460i$	$14.97696419i$
14	$234.1765144i$	$234.1761561i$

Table 6.3.1: The coefficients of the ϵ-expansions of WKB periods and Y-functions for (A_2, A_1)-type ODE with $u_0 = u_2 = 1$ and $u_1 = 0$.

n	$\Pi^{(n)}_{\hat{\gamma}_{1,1}}, e^{\frac{\pi i}{4}(n-1)}\Pi^{(n)}_{\hat{\gamma}_{3,1}}$	$m^{(n-1)}_{1,1}, m^{(n-1)}_{3,1}$	$e^{\frac{\pi i}{4}(n-1)}\Pi^{(n)}_{\hat{\gamma}_{2,1}}$	$m^{(n-1)}_{2,1}$
2	-0.2118032712	-0.2118032752	-0.2995350587	-0.2995350643
4	0.05311151419	0.05311151743	-0.07511102369	-0.07511102827
6	-0.12953645375	-0.1295364668	0.1831922097	0.1831922283
8	0.7882359521	0.7882360637	1.1147339738	1.114734131
10	-7.184548229	-7.184549472	-10.160485545	-10.16048730
12	102.58179442	102.5818017	$-145.0725649+$	-145.0725752
14	-2251.106503	-2251.103294	3183.545348	3183.540809

Table 6.3.2: The coefficients of the ϵ-expansions of WKB periods and Y-functions for (A_2, A_1)-type ODE with $u_0 = u_2 = 1$ and $u_1 = 0$.

In table 6.3.1 and table 6.3.2, we show the ϵ-expansions of the WKB periods and the Y-functions for (A_2, A_1) and (A_3, A_1) case, respectively. We set the potential $p(x) = x^2 + 1$. One can see the coincidences of the numerical results in high precision. In (A_2, A_1) case, one finds that the corrections of order $n = 6k + 4$ ($k \in \mathbb{Z}$) vanishes. This is an A_2 case example of the vanishing of the term $n = 2(r+1)k + r + 2$ for A_r case. We can also check this from (6.3.6). In the same way, we can see the matching of the results from the two computations for the higher ODE.

The cubic and the quartic potentials for the third order

As the simplest examples, here, we discuss the third order case. For the higher order polynomial potential, we have chambers of a number greater than one. In the minimal

chamber, the TBA equations read

$$\log Y_{a,k}(\theta - i\phi_k) = |m_{a,k}|e^{\theta} + K \star \overline{L}_{a,k} - K_{k,k-1} \star \overline{L}_{a,k-1} - K_{k,k+1} \star \overline{L}_{a,k+1}, \tag{6.3.7}$$

where $\phi_{a,k} = \arg m_{a,k}$, $\overline{L}_{a,k}(\theta) = L_{a,k}(\theta - i\phi_k)$, $K_{k_1,k_2}(\theta) = K(\theta - i(\phi_{k_1} - \phi_{k_2}))$ and the kernel function $K(\theta)$ is given by

$$K(\theta) = \frac{1}{2\pi}\frac{4\sqrt{3}\cosh\theta}{1 + 2\cosh 2\theta}. \tag{6.3.8}$$

We also used the $\mathbb{Z}_2$-symmetry $m_{1,k} = m_{2,k}$ which implies $\overline{L}_{1,k} = \overline{L}_{2,k}$. Since $Y_{1,k} = Y_{2,k}$, we only consider the TBA equations for $Y_{1,k}$. The correction term $m^{(n)}_{1,k}$ is obtained as

$$m^{(n)}_{1,k} = k_n \int_{-\infty}^{\infty} (\overline{L}_{1,k}(\theta)e^{n(\theta - i\phi_k)} - \overline{L}_{1,k-1}(\theta)e^{n(\theta - i\phi_{k-1})} - \overline{L}_{1,k+1}(\theta)e^{n(\theta - i\phi_{k+1})})\,\mathrm{d}\theta\,, \tag{6.3.9}$$

where we defined

$$k_n \coloneqq \frac{1}{\pi}\left(\sin\left(\frac{\pi}{3}n\right) + \sin\left(\frac{2\pi}{3}n\right)\right). \tag{6.3.10}$$

The cubic potential Let us consider the cubic potential case. As an example, we set the potential as

$$p(x) = -(x-3)(x+1)(x+2) = -x^3 + 7x + 6, \tag{6.3.11}$$

where all the zeros are real. For this potential, the masses calculated from the classical periods are

$$\begin{aligned} m_{1,1} &= \Pi^{(0)}_{\hat{\gamma}_{1,1}} \simeq 13.14579499i, \\ m_{1,2} &= e^{\frac{\pi i}{3}}\Pi^{(0)}_{\hat{\gamma}_{1,2}} \simeq 1.514970717i. \end{aligned} \tag{6.3.12}$$

Obviously, since $\arg(m_{1,2}/m_{1,1}) = 0$, choosing the potential (6.3.11), we are in the minimal chamber. The TBA equations read

$$\begin{aligned} \log Y_{1,1}(\theta - i\phi_1) &= |m_{1,1}|e^{\theta} + K \star \overline{L}_{1,1} - K_{1,2} \star \overline{L}_{1,2}, \\ \log Y_{1,2}(\theta - i\phi_2) &= |m_{1,2}|e^{\theta} - K_{2,1} \star \overline{L}_{1,1} + K \star \overline{L}_{1,2}. \end{aligned} \tag{6.3.13}$$

Table 6.3.3 shows the quantum corrections of the WKB period for the cycle $\hat{\gamma}_{1,1}$ and $m^{(n)}_{1,1}$ of this case. One can find the agreements of the numerical results. Notice that the corrections for $k = 2$ are same as that of $k = 1$ up to sign i.e. $m^{(n)}_{1,2} = -m^{(n)}_{1,1}$. It is not

n	$\Pi^{(n)}_{\hat{\gamma}_{1,1}}$	$m^{(n-1)}_{1,1}$
2	$0.2172157436i$	$0.2172157436i$
6	$-1.519567945i$	$-1.519567945i$
8	$-20.48661777i$	$-20.48661776i$
12	$20065.20970i$	$20065.20605i$
14	$1160395.676i$	$1160393.422i$

Table 6.3.3: The corrections of WKB periods and Y-functions for the (A_2, A_2)-type ODE with potential $p(x) = -x^3 + 7x + 6$.

hard to see this property from the TBA equations (6.3.13). However, from the viewpoint of the WKB analysis, it is a highly non-trivial result.

There is another interesting property of (A_2, A_2) case. As we discussed in section 6.1, if the three zeros are aligned in a common line and point-symmetric with respect to the middle zero, the Picard-Fuchs operators vanish since they are proportional to D_0. This phenomenon can be seen from the TBA equations, which from $m_{1,1} = m_{1,2}$, become

$$\begin{aligned} \log Y_{1,1}(\theta - i\phi_1) &= |m_{1,1}|e^{\theta} + K \star (\overline{L}_{1,1} - \overline{L}_{1,2}), \\ \log Y_{1,2}(\theta - i\phi_2) &= |m_{1,2}|e^{\theta} + K \star (\overline{L}_{1,2} - \overline{L}_{1,1}). \end{aligned} \tag{6.3.14}$$

The deriving term is equivalent and the TBA equations are symmetric, hence one can conclude $\overline{L}_{1,1} = \overline{L}_{1,2}$. The vanishing of the correction terms in both sides is also non-trivial text of the relations of the periods and Y-functions.

The quartic potential The TBA equations for the third order ODE with quartic potential in the minimal chamber read

$$\begin{aligned} \log Y_{1,1}(\theta - i\phi_1) =& |m_{1,1}|e^{\theta} + K \star \overline{L}_{1,1} - K_{1,2} \star \overline{L}_{1,2}, \\ \log Y_{1,2}(\theta - i\phi_2) =& |m_{1,2}|e^{\theta} - K_{2,1} \star \overline{L}_{1,1} + K \star \overline{L}_{1,2} - K_{2,3} \star \overline{L}_{1,3}, \\ \log Y_{1,3}(\theta - i\phi_3) =& |m_{1,3}|e^{\theta} + K \star \overline{L}_{1,3} - K_{3,2} \star \overline{L}_{1,2} \end{aligned} \tag{6.3.15}$$

Again, we set the zeros of the potential real. One of the choice of the potential is

$$p(x) = -(x-4)(x-1)(x+1)(x+2) = -x^4 + 2x^3 + 9x^2 - 2x - 8. \tag{6.3.16}$$

We show the numerical results of the corrections of the WKB periods and Y-functions in table 6.3.4. One sees the coincidence in high precision.

n	$\Pi^{(n)}_{\hat{\gamma}_{1,1}}$	$e^{\frac{\pi i}{3}(1-n)}\Pi^{(n)}_{\hat{\gamma}_{1,2}}$	$e^{\frac{2\pi i}{3}(1-n)}\Pi^{(n)}_{\hat{\gamma}_{1,3}}$
0	$14.29120679i$	$5.748396528i$	$2.197175863i$
2	$0.06210586398i$	$0.1352435882i$	$-0.09711585835i$
6	$-0.002344098573i$	$-0.2410756322i$	$0.2410502603i$
8	$-0.002115215318i$	$-1.544858396i$	$1.544854731i$
12	$0.009495408700i$	$339.9172291i$	$-339.9172287i$
14	$0.03754344682i$	$9328.147139i$	$-9328.147139i$
n	$m^{(n-1)}_{1,1}$	$m^{(n-1)}_{1,2}$	$m^{(n-1)}_{1,3}$
0	$14.29120679i$	$5.748396528i$	$2.197175863i$
2	$0.06210586398i$	$0.1352435882i$	$-0.09711585835i$
6	$-0.002344098573i$	$-0.2410756322i$	$0.2410502602i$
8	$-0.002115215317i$	$-1.544858396i$	$1.544854731i$
12	$0.009495407453i$	$339.9171779i$	$-339.9171774i$
14	$0.03754338997i$	$9328.131493i$	$-9328.131493i$

Table 6.3.4: The corrections of WKB periods and Y-functions for the (A_2, A_3)-type ODE with potential $p(x) = -x^4 + 2x^3 + 9x^2 - 2x - 8$.

6.3.2 PNP relation

Next, we discuss the relations between the quantum corrections. For the (A_r, A_1)-type TBA equations, the leading correction is computed by

$$m^{(1)}_{a,1} = \frac{2}{\pi}\cot\left(\frac{\pi}{r+1}\right)\sin\left(\frac{\pi a}{r+1}\right)\sum_{b=1}^{r}\sin\left(\frac{\pi b}{r+1}\right)\int_{-\infty}^{\infty} L_{b,1}(\theta)e^{n\theta}\,\mathrm{d}\theta\,. \tag{6.3.17}$$

Multiplying the mass $m_{a,1}$ to both sides and using the relation of masses: $\sin\left(\frac{\pi}{r+1}\right)m_{a,1} = \sin\left(\frac{\pi a}{r+1}\right)m_{1,1}$, one obtains

$$m_{a,1}m^{(1)}_{a,1} = \frac{2}{\pi}\cot\left(\frac{\pi}{r+1}\right)\sin^2\left(\frac{\pi a}{r+1}\right)\sum_{b=1}^{r}\int_{-\infty}^{\infty} m_{b,1}L_{b,1}(\theta)e^{n\theta}\,\mathrm{d}\theta\,. \tag{6.3.18}$$

The right hand side of this equation is proportional to the effective central charge whose definition and the exact value is

$$c_{\text{eff}} \coloneqq \frac{6}{\pi^2}\sum_{a=1}^{r}\int_{-\infty}^{\infty} m_{a,1}L_{a,1}(\theta)e^{\theta}\,\mathrm{d}\theta = \frac{2r}{r+3}. \tag{6.3.19}$$

Using the identification (6.3.2), we reach the relation between the classical period and the second order correction:

$$\Pi^{(0)}_{\hat{\gamma}_{a,1}}\Pi^{(2)}_{\hat{\gamma}_{a,1}} = \frac{\pi}{3}\cot\left(\frac{\pi}{r+1}\right)\sin^2\left(\frac{\pi a}{r+1}\right)c_{\text{eff}} = \frac{2\pi}{3}\frac{r}{r+3}\cot\left(\frac{\pi}{r+1}\right)\sin^2\left(\frac{\pi a}{r+1}\right), \tag{6.3.20}$$

which is regarded as the PNP relation [124, 125]. This relation is also derived from the analytic calculation of the WKB periods. The classical periods and the second order corrections are given by

$$\begin{aligned}\Pi^{(0)}_{\hat{\gamma}_{a,1}} &= -2e^{\frac{\pi i}{r+1}(4+a)}\sin\left(\frac{\pi a}{r+1}\right)u_0^{\frac{1}{r+1}+\frac{1}{2}}u_2^{-\frac{1}{2}}B\left(\frac{1}{2},1+\frac{1}{r+1}\right),\\ \Pi^{(2)}_{\hat{\gamma}_{a,1}} &= -\frac{4r^2-(r+1)^2}{24(r+1)}e^{-\frac{\pi i}{r+1}(4+a)}\sin\left(\frac{\pi a}{r+1}\right)u_0^{\frac{r}{r+1}-\frac{3}{2}}u_2^{\frac{1}{2}}B\left(\frac{1}{2},1+\frac{r}{r+1}\right).\end{aligned} \tag{6.3.21}$$

Multiplying these two, one obtains

$$\begin{aligned}\Pi^{(0)}_{\hat{\gamma}_{a,1}}\Pi^{(2)}_{\hat{\gamma}_{a,1}} &= \frac{r+1}{3}\sin^2\left(\frac{\pi a}{r+1}\right)\frac{\Gamma\left(\frac{1}{2}\right)^2\Gamma\left(1+\frac{1}{r+1}\right)\Gamma\left(1+\frac{r}{r+1}\right)}{\Gamma\left(\frac{3}{2}+\frac{1}{r+1}\right)\Gamma\left(-\frac{1}{2}+\frac{r}{r+1}\right)}\\ &= \frac{r+1}{3}\sin^2\left(\frac{\pi a}{r+1}\right)\frac{\pi\frac{r}{(r+1)^2}\frac{\pi}{\sin\frac{\pi}{r+1}}}{\frac{r+3}{2(r+1)}\frac{\pi}{\cos\frac{\pi}{r+1}}}\\ &= \frac{2\pi}{3}\frac{r}{r+3}\cot\left(\frac{\pi}{h}\right)\sin^2\left(\frac{\pi a}{r+1}\right).\end{aligned} \tag{6.3.22}$$

Here we used the reflection formula $\Gamma(z)\Gamma(1-z) = \pi/\sin(\pi z)$. The PNP relations for higher order corrections have not still obtained, but we expect that one could obtain them in a similar way.

For the higher potential, we only discuss the third order ODE. The leading order correction $m^{(1)}_{1,k}$ for (A_2, A_N)-type TBA equations is obtained by

$$m^{(1)}_{1,k} = \frac{\sqrt{3}}{\pi}\sum_{k'=1}^{N}(\delta_{kk'} - G'_{kk'})\int_{-\infty}^{\infty}\overline{L}_{1,k'}(\theta)e^{\theta-i\phi_{1,k'}}\mathrm{d}\theta, \tag{6.3.23}$$

where G' is the incidence matrix of the algebra A_N, and δ represents the Kronecker delta. For $N \neq 3m+2$, $m \in \mathbb{Z}_{>0}$, we have the inverse matrix of $(\delta - G')_{k,k'}$. Similar to the (A_r, A_1) case, we multiply $m_{1,k}$ to the both sides of (6.3.23). The effective central charge

is

$$c_{\text{eff}} \coloneqq 2 \times \frac{6}{\pi^2} \sum_{k=1}^{N} \int_{-\infty}^{\infty} |m_{1,k}| \overline{L}_{1,k}(\theta) e^{\theta} \, \mathrm{d}\theta = \frac{2N(N+1)}{N+4}, \tag{6.3.24}$$

where the factor 2 is caused by the summation of $a = 1, 2$. Using the identification of the corrections (6.3.2), we reach the PNP relation:

$$\sum_{k,k'=1}^{N} e^{\frac{\pi i}{3}(k-k')} (\delta_{kk'} - G'_{kk'})^{-1} \Pi^{(0)}_{\gamma_{1,k}} \Pi^{(2)}_{\gamma_{1,k'}} = \frac{\pi}{4\sqrt{3}} c_{\text{eff}}. \tag{6.3.25}$$

Unlike the quadratic potential case, it is hard to derive this relation from the analytic form of the WKB periods since they are expressed by the generalized hypergeometric functions.

6.3.3 Discontinuity and the pole structure of the kernel

We have discussed the validity of the identification in ϵ-expansion, which is the perturbative analysis. Although we have defined the WKB periods as the formal power series of ϵ, in the exact WKB analysis, one defines it as the Voros symbol [40] which is the analytic function of ϵ by applying the Borel resummation to the formal sum. On the other hand, the Y-function is also an analytic function on the ϵ-plane. Thus the formula (6.2.28) should be precisely refined as

$$\log Y_{a,k}(\theta) = s\left(\left[\frac{1}{\epsilon} \Pi_{\hat{\gamma}_{a,k}} \right]^{[a-k]} \right), \tag{6.3.26}$$

where the symbol $s(\cdot)$ represents the Borel resummation at real and positive ϵ. The Borel resummation of the WKB period along the the direction φ is defined by

$$s_{\varphi}(\Pi_{\gamma})(\epsilon) \coloneqq \frac{1}{\epsilon} \int_{0}^{\infty e^{i\varphi}} e^{-\xi/\epsilon} \mathcal{B}[\Pi_{\gamma}](\xi) d\xi. \tag{6.3.27}$$

Here $\mathcal{B}[\Pi_{\gamma}](\xi)$ is the Borel transform of the WKB period, which is given by

$$\mathcal{B}[\Pi_{\gamma}](\xi) \coloneqq \sum_{n \geq 0} \frac{1}{n!} \Pi^{(n)}_{\gamma} \xi^n. \tag{6.3.28}$$

For small ϵ, if the Borel resummation $s_{\varphi}(\Pi_{\gamma})(\epsilon)$ converges, the period Π_{γ} is said to be Borrel summable, other wise non- summable. In the non-summable directions, there

are singularities which arises the discontinuity of the Borel resummation of the periods. Denoting the direction of angle $\varphi \pm 0$ as $\varphi_{\pm}$, the discontinuity is written as

$$\begin{aligned} \mathrm{disc}_{\varphi}\Pi_{\gamma}(\epsilon) &= s_{\varphi^+}(\Pi_{\gamma})(\epsilon) - s_{\varphi^-}(\Pi_{\gamma})(\epsilon)\big) \\ &= \lim_{\delta\to 0_+} \big(s(\Pi_{\gamma})(e^{i\varphi+i\delta}\epsilon) - s(\Pi_{\gamma})(e^{i\varphi-i\delta}\epsilon)\big). \end{aligned} \tag{6.3.29}$$

The singularities of $\mathcal{B}[\Pi_{\gamma}](\xi)$ are estimated from the Padé approximation numerically. In figure 6.3.1, we show the singularity structures of $\mathcal{B}[\Pi_{\hat{\gamma}_{1,1}}](\xi)$ and $\mathcal{B}[\Pi_{\hat{\gamma}_{1,2}}](\xi)$ for (A_2, A_2)-type ODE with the potential (6.3.11) in blue and orange dotted points, respectively.

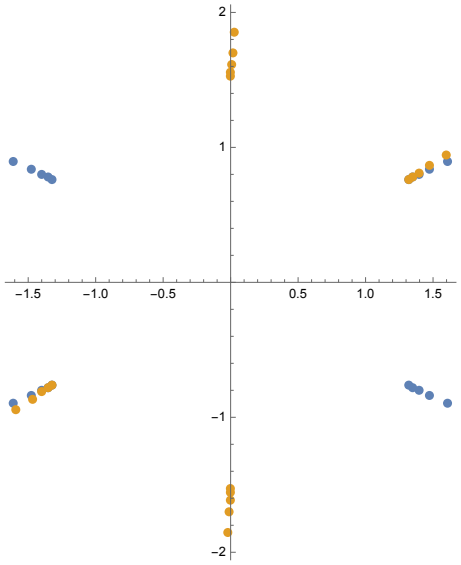

Figure 6.3.1: The singularities of the Borel transforms $\mathcal{B}[\Pi_{\hat{\gamma}_{1,1}}](\xi)$ (blue) and $\mathcal{B}[\Pi_{\hat{\gamma}_{1,2}}](\xi)$ (orange), obtained from the Borel-Padé technique. We calculated up to order ϵ^{160} terms of the ϵ-expansions of the WKB periods and set the potential $p(x) = -x^3 + 7x + 6$.

The discontinuity of the Y-functions is obtained from the pole structures of the kernels in the TBA equations. The (A_2, A_2)-type TBA equations in the minimal chamber are given in (6.3.13). Since the formula says that $\log Y_{1,1}(\theta) = s(\Pi_{\hat{\gamma}_{1,1}})(\theta)$ and $\log Y_{1,2}(\theta) =$

$s(\Pi_{\hat{\gamma}_{1,2}})(\theta+\frac{\pi i}{3})$, we shift the TBA equations as

$$\begin{aligned}\log Y_{1,1}(\theta) &= m_{1,1}e^{\theta} + \int_{-\infty}^{\infty} \mathrm{d}\theta' K(\theta-\theta'+i\phi_1)\overline{L}_{1,1}(\theta') \\ &\quad - \int_{-\infty}^{\infty} \mathrm{d}\theta' K(\theta-\theta'+i\phi_2)\overline{L}_{1,2}(\theta') + \cdots, \\ \log Y_{1,2}^{[+1]}(\theta) &= m_{1,2}e^{\theta-\frac{\pi i}{3}} + \int_{-\infty}^{\infty} \mathrm{d}\theta' K(\theta-\theta'+i\phi_2-\frac{\pi i}{3})\overline{L}_{1,2}(\theta') \\ &\quad - \int_{-\infty}^{\infty} \mathrm{d}\theta' K(\theta-\theta'+i\phi_1-\frac{\pi i}{3})\overline{L}_{1,1}(\theta') + \cdots,\end{aligned} \tag{6.3.30}$$

where $\cdots$ represents the residues which arise from the shift of the argument of the kernels and are not relevant to the discontinuity. The kernel functions in the equation for $Y_{1,1}$ have the poles at

$$\theta = \pm(\frac{\pi}{3}+n\pi) - \phi_i, \qquad i=1,2, \quad n\in\mathbb{Z}, \tag{6.3.31}$$

while that for $Y_{1,2}^{[+1]}$ have the poles at

$$\theta = n\pi-\phi_i, \quad -(\frac{\pi}{3}+n\pi)-\phi_i, \qquad i=1,2, \quad n\in\mathbb{Z}. \tag{6.3.32}$$

Then, these angles provide the Borel non-summable directions. The phases of the masses for the potential (6.3.11) are $\arg m_{1,1} = \arg m_{1,2} = \frac{\pi}{2}$, hence (6.3.31) and (6.3.32) reproduce the angles of the non-summable directions of the Borel transforms of the WKB periods shown in the figure 6.3.1. Therefore, the discontinuity structures of the Y-functions $Y_{1,1}$ and $Y_{1,2}^{[+1]}$ coincide with that of the WKB periods $\Pi_{\hat{\gamma}_{1,1}}$ and $\Pi_{\hat{\gamma}_{1,2}}$.

Summary

In this chapter, we studied the ODE/IM correspondence for the higher order ODE which is interpreted as the quantum SW curve of the (A_r, A_N)-type AD theory. From the WKB analysis, we proposed the formula which relates the WKB periods and the Y-functions in the minimal chamber. We tested the formula by the numerical comparisons of the coefficients in the formal ϵ-expansions, the analytic relation i.e. the PNP relation, and the identification of the discontinuity structure of the WKB periods with the pole distribution of the TBA equations in the minimal chamber.

Chapter 7

Wall-crossing phenomena for the third order ODE

We established the relation between the WKB periods and the Y-functions in the minimal chamber for (A_r, A_N)-type ODE in the previous chapter. For $N \geq 3$, the wall-crossing occurs to the TBA equations. In this chapter, we study the wall-crossing of the TBA equations for the third order ODE with cubic and the quartic potential in detail. As discussed in chapter 4, in the processes of the wall-crossings, we introduce the new Y-functions. For the third and higher ODE, it is straightforward to generalize wall-crossing procedures. Associated with the new Y-functions, we will introduce the corresponding WKB periods. We will also test the relations of the new Y-functions and the periods numerically. The relation to the $\mathcal{N} = 2$ theory implies the duality between the (A_2, A_2)-type and (D_4, A_1)-type quantum curves as well as (A_2, A_3)-type and (E_6, A_1)-type quantum curves, which we argued in chapter 5. We will observe this through the TBA equations for the monomial potential.

7.1 Marginal stability walls and the TBA equations

In this section, we first discuss the wall-crossing of the TBA equations for the third order ODE, which is the higher order generalization of the second order case. The (A_2, A_N)-type

TBA equations for $Y_{1,k}$ $(k = 1, 2, \ldots, N)$ in the minimal chamber takes the form

$$\log Y_{1,k}(\theta - i\phi_k) = |m_{1,k}|e^{\theta} + K \star \overline{L}_{1,k}(\theta) - \sum_{i=k-1,k+1} K_{k,i} \star \overline{L}_{1,i}(\theta). \tag{7.1.1}$$

Here the kernel function K given by

$$K(\theta) = \frac{1}{2\pi}\frac{1}{\cosh\left(\theta + \frac{\pi i}{6}\right)} + \frac{1}{2\pi}\frac{1}{\cosh\left(\theta - \frac{\pi i}{6}\right)}, \tag{7.1.2}$$

and has the poles at

$$\theta = \pm\frac{\pi i}{3} + n\pi i, \qquad n \in \mathbb{Z}. \tag{7.1.3}$$

This TBA equations are valid if $|\phi_k - \phi_{k\pm1}| < \pi/3$, otherwise the residues of the poles contribute and deform them, which is the wall-crossing of the TBA equations. Let us consider the case where $\pi/3 < |\phi_2 - \phi_1| < 2\pi/3$ and $|\phi_k - \phi_{k-1}| < \pi/3$ for $(k \neq 2)$. The residues of the poles deform the equations for $Y_{1,1}$ and $Y_{1,2}$ to

$$\begin{aligned}
\log Y_{1,1}(\theta - i\phi_1) =& |m_{1,1}|e^{\theta} + K \star \overline{L}_{1,1} - K_{1,2} \star \overline{L}_{1,2} - L_{1,2}(\theta - \frac{\pi i}{3} - i\phi_1), \\
\log Y_{1,2}(\theta - i\phi_2) =& |m_{1,2}|e^{\theta} - K_{2,1} \star \overline{L}_{1,1} + K \star \overline{L}_{1,2} - K_{2,3} \star \overline{L}_{1,3} - L_{1,1}(\theta + \frac{\pi i}{3} - i\phi_2).
\end{aligned} \tag{7.1.4}$$

In a similar way to the second order case, we introduce the new Y-functions such that the TBA equations for them do not include the residue terms explicitly. We define them by

$$\begin{aligned}
&Y^{\mathrm{n}}_{1,1}(\theta) = Y_{1,1}(\theta)\left(1 + \frac{1}{Y_{1,2}(\theta - \frac{\pi i}{3})}\right), \quad Y^{\mathrm{n}}_{1,2}(\theta) = Y_{1,2}(\theta)\left(1 + \frac{1}{Y_{1,1}(\theta + \frac{\pi i}{3})}\right), \\
&Y^{\mathrm{n}}_{12}(\theta) = \frac{1 + \frac{1}{Y_{1,2}(\theta - \frac{\pi i}{3})} + \frac{1}{Y_{1,1}(\theta)}}{\frac{1}{Y_{1,1}(\theta)Y_{1,2}(\theta - \frac{\pi i}{3})}}, \quad Y^{\mathrm{n}}_{1,k>2} = Y_{1,k>2}.
\end{aligned} \tag{7.1.5}$$

These new Y-functions and the original ones satisfy the relation

$$\begin{aligned}
&\left(1 + \frac{1}{Y_{1,1}(\theta)}\right) = \left(1 + \frac{1}{Y^{\mathrm{n}}_{1,1}(\theta)}\right)\left(1 + \frac{1}{Y^{\mathrm{n}}_{12}(\theta)}\right), \\
&\left(1 + \frac{1}{Y_{1,2}(\theta)}\right) = \left(1 + \frac{1}{Y^{\mathrm{n}}_{1,2}(\theta)}\right)\left(1 + \frac{1}{Y^{\mathrm{n}}_{12}(\theta + \frac{\pi i}{3})}\right), \\
&Y^{\mathrm{n}}_{1,1}(\theta)Y^{\mathrm{n}}_{1,2}(\theta - \frac{\pi i}{3}) = Y^{\mathrm{n}}_{12}(\theta)\left(1 + \frac{1}{Y^{\mathrm{n}}_{12}(\theta)}\right).
\end{aligned} \tag{7.1.6}$$

We also introduce the mass term for $\log Y^{\mathrm{n}}_{12}$ which is $m_{12} \coloneqq |m_{12}|e^{i\phi_{12}} \coloneqq m_{1,1} + e^{-\frac{\pi i}{3}} m_{1,2}$. The TBA equations (7.1.1) for $k > 2$, deformed ones (7.1.4), and the relations (7.1.6) lead the equations for $Y^{\mathrm{n}}_{1,k}$:

$$\begin{aligned}
\log Y^{\mathrm{n}}_{1,1}(\theta - i\phi_1) =& |m_{1,1}|e^{\theta} + K \star \overline{L}^{\mathrm{n}}_{1,1} - K_{1,2} \star \overline{L}^{\mathrm{n}}_{1,2} + K^{-}_{1,12} \star \overline{L}^{\mathrm{n}}_{12}, \\
\log Y^{\mathrm{n}}_{1,2}(\theta - i\phi_2) =& |m_{1,2}|e^{\theta} + K \star \overline{L}^{\mathrm{n}}_{1,2} - K_{2,1} \star \overline{L}^{\mathrm{n}}_{1,1} - K_{2,3} \star \overline{L}^{\mathrm{n}}_{1,3} - K^{-}_{2,12} \star \overline{L}^{\mathrm{n}}_{12}, \\
\log Y^{\mathrm{n}}_{1,3}(\theta - i\phi_3) =& |m_{1,3}|e^{\theta} + K \star \overline{L}^{\mathrm{n}}_{1,3} - K_{3,2} \star \overline{L}^{\mathrm{n}}_{1,2} - K^{+}_{3,12} \star \overline{L}^{\mathrm{n}}_{12} - K_{3,4} \star \overline{L}^{\mathrm{n}}_{1,4}, \\
\log Y^{\mathrm{n}}_{1,k}(\theta - i\phi_k) =& |m_{1,k}|e^{\theta} + K \star \overline{L}^{\mathrm{n}}_{1,k}(\theta) - \sum_{i=k-1,k+1} K_{k,i} \star \overline{L}^{\mathrm{n}}_{1,i}(\theta), \qquad k > 3.
\end{aligned} \tag{7.1.7}$$

Here we defined the shifted kernel $K^{\pm}(\theta) \coloneqq K^{[\mp 1]}(\theta) = K(\theta \pm \frac{\pi i}{3})$. Note that the phases are $|\phi_{12} - \phi_1|, |\phi_2 - \frac{\pi}{3} - \phi_{12}| < \pi/3$. From the relation for Y^{n}_{12} in (7.1.6) and summing the equations of (7.1.4) evaluated at the appropriate values, one obtains the equation for the new Y-function Y^{n}_{12}:

$$\log Y^{\mathrm{n}}_{12}(\theta - i\phi_{12}) = |m_{12}|e^{\theta} + K \star \tilde{L}^{\mathrm{n}}_{12} - K^{-}_{12,3} \star \overline{L}_{1,3} + K^{+}_{12,1} \star \tilde{L}^{\mathrm{n}}_{1,1} - K^{+}_{12,2} \star \tilde{L}^{\mathrm{n}}_{1,2}. \tag{7.1.8}$$

(7.1.7) and (7.1.8) form the $N+1$ closed system which is the TBA equations in this chamber. The effective central charge is defined from that of the minimal TBA and the relation (7.1.6) by

$$c_{\mathrm{eff}} \coloneqq 2 \times \frac{6}{\pi^2} \int_{-\infty}^{\infty} \Big(\sum_{k=1}^{N} |m_{1,k}| e^{\theta} \overline{L}^{\mathrm{n}}_{1,k} + |m_{12}| e^{\theta} \overline{L}^{\mathrm{n}}_{12} \Big) \mathrm{d}\theta. \tag{7.1.9}$$

The exact value of the effective central charge is calculated from the asymptotic values of the Y-functions, and turn out to be equal to that of the minimal chamber.

Associated with the new Y-function Y^{n}_{12}, we introduce the new WKB period. Note that from the relation (7.1.6), the Y-functions $Y^{\mathrm{n}}_{1,1}$ and $Y^{\mathrm{n}}_{1,2}$ are still related to the cycles $\hat{\gamma}_{1,1} = \gamma_{1,1}$ and $\hat{\gamma}_{1,2} = \gamma_{3,2}$, respectively:

$$\log Y^{\mathrm{n}}_{1,1}(\theta) = e^{\theta} \Pi_{\hat{\gamma}_{1,1}}, \quad \log Y^{\mathrm{n}}_{1,2}(\theta) = e^{\frac{\pi i}{3}} e^{\theta} \Pi_{\hat{\gamma}_{1,2}}(\theta + \frac{\pi i}{3}). \tag{7.1.10}$$

Thus the mass m_{12} is related to the classical period as

$$m_{12} = m_{1,1} + e^{-\frac{\pi i}{3}} m_{1,2} = \Pi^{(0)}_{\hat{\gamma}_{1,1} + \hat{\gamma}_{1,2}}. \tag{7.1.11}$$

Taking into account the quantum corrections, one finds that $Y_{12}^{\rm n}$ is related to the cycle $\hat{\gamma}_{1,1}+\hat{\gamma}_{1,2}$:

$$\log Y_{12}^{\rm n}(\theta) = e^{\theta}\Pi_{\hat{\gamma}_{1,1}}(\theta) + e^{\theta}\Pi_{\hat{\gamma}_{1,2}}(\theta) = e^{\theta}\Pi_{\hat{\gamma}_{1,1}+\hat{\gamma}_{1,2}}. \tag{7.1.12}$$

As we discussed in chapter 5, the WKB periods are regarded as the quantum SW periods in $\mathcal{N}=2$ theories. And the wall crossing of TBA equations is related with that of $\mathcal{N}=2$ theories. At the marginal stability wall, mutually non-local charges of two BPS particles align. In our basis of the charges, there exist the wall when

$$\mathrm{Im}\left(\frac{\Pi^{(0)}_{\hat{\gamma}_{1,k}}}{\Pi^{(0)}_{\hat{\gamma}_{1,k\pm1}}}\right) = \left|\frac{\Pi^{(0)}_{\hat{\gamma}_{1,k}}}{\Pi^{(0)}_{\hat{\gamma}_{1,k\pm1}}}\right| \sin\Big(\phi_k - \phi_{k\pm1} \pm \frac{\pi}{3}\Big) = 0, \tag{7.1.13}$$

which results in the condition $\phi_{k+1}-\phi_k = \frac{\pi i}{3}+n\pi$. Here we used $\Pi^{(0)}_{\hat{\gamma}_{1,k}} = |\Pi^{(0)}_{\hat{\gamma}_{1,k}}|e^{i\phi_k - \frac{\pi i}{3}(k-1)}$. The other half of the condition of the wall is obtained from the condition

$$\mathrm{Im}\left(\frac{\Pi^{(0)}_{\hat{\gamma}_{1,k}}}{\Pi^{(0)}_{\gamma_{2-k,k+1}}}\right) = \left|\frac{\Pi^{(0)}_{\hat{\gamma}_{1,k}}}{\Pi^{(0)}_{\gamma_{2-k,k+1}}}\right| \sin\Big(\phi_k - \phi_{k+1} - \frac{\pi}{3}\Big) = 0, \tag{7.1.14}$$

which leads the condition $\phi_{k+1}-\phi_k = -\frac{\pi i}{3}+n\pi$. Here we used $\Pi^{(0)}_{\gamma_{2-k,k+1}} = e^{\frac{\pi i}{3}}\Pi^{(0)}_{\hat{\gamma}_{2,k+1}} = |\Pi^{(0)}_{\gamma_{2-k,k+1}}|e^{i\phi_{k+1}-\frac{\pi i}{3}(k-2)}$. In the context of the (A_2, A_N)-type AD theory, if the charges of the BPS particles are expressed by the classical periods as in figure 7.1.1, where the central charge of the electric and magnetic charge $q_{\gamma_{a,k}}$ is $\Pi^{(0)}_{\gamma_{a,k}}$, the wall-crossing conditions (in the minimal chamber) becomes the same as that of the (A_2, A_N)-type TBA equations. Crossing the walls, the new charges associated with the BPS particles emerge.

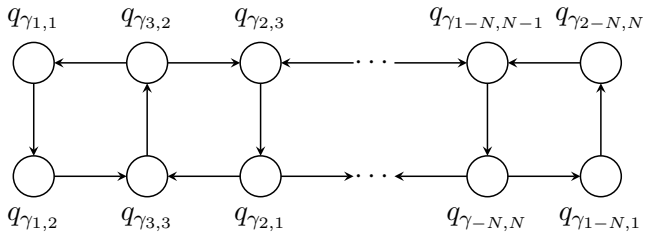

Figure 7.1.1: The charges of the (A_2, A_N)-type AD theory in the minimal chamber.

Since the BPS quiver of the AD theory is simply-laced, the wall-crossing from the minimal to the next chamber would be the pentagon type. For the first wall-crossing where

$\arg(\Pi^{(0)}_{\gamma_{1,1}}/\Pi^{(0)}_{\gamma_{3,2}})$ crosses zero, the new charge $\Pi^{(0)}_{\gamma_{1,1}+\gamma_{3,2}} = \Pi^{(0)}_{\hat{\gamma}_{1,1}+\hat{\gamma}_{1,2}}$ would emerges. This corresponds to the new Y-function Y^{n}_{12} in the wall-crossing of the TBA equations. The wall-crossings of the higher rank $\mathcal{N} = 2$ theories have not been studied well[1]. In the rest of this chapter, we study the wall-crossing of the TBA equations for the third order ODE with the cubic and the quartic potentials, which would correspond to that of the (A_2, A_2)-type and the (A_2, A_3)-type AD theories. We also study the relations between the WKB/quantum SW periods and the Y-functions in other chambers. In the chamber after the i-th wall, we denote the Y-functions as $Y^{(i)}$ which is expanded as

$$\log Y^{(i)} = |m|e^{\theta} + \sum_{n=1}^{\infty} m^{(i),(n)} e^{-n\theta}. \tag{7.1.15}$$

In the following sections, we omit the superscript (i) of $m^{(i),(n)}$ to avoid confusion. Furthermore, at the maximally symmetric point i.e. the monomial potential/AD point, we will see the duality of the AD theories.

7.2 Wall-crossing for the (A_2, A_2)-type ODE

In this section, we study the wall-crossing of the (A_2, A_2) case from the minimal to the maximal chamber, which is the simplest higher order example. We also study the relation of the WKB periods and Y-functions in each chamber numerically.

7.2.1 From the minimal to the maximal chamber

Let us set the potential $p(x) = (x-3)(x+1)(x+2) = x^3 - 7x - 6$ in the minimal chamber and $p(x) = x^3 - 8$ in the maximal chamber, respectively. As in the case of the second order ODE, the moduli parameters of the monomial potential are in the maximal chamber. To study the wall-crossing, we interpolate these two potentials by introducing the auxiliary variable t as

$$x_0(t) = 3 - t, \quad x_1(t) = -1 + \sqrt{3}it, \quad x_2(t) = -2 + t - \sqrt{3}it, \quad 0 \leq t \leq 1, \tag{7.2.1}$$

[1]The relation between the TBA like equations of (A_2, A_2)-type AD theory and the (A_2, A_2)-type ODE was studied in [79].

where the potential at any point in this path is $p(x;t) = (x - x_0(t))(x - x_1(t))(x - x_2(t))$. In the minimal chamber, there are four classical periods/masses of which the independent phases are ϕ_1 and ϕ_2. Thus, when the difference of the phase $\phi_2 - \phi_1$ crosses $\frac{\pi}{3}$ and $\frac{\pi}{3}$, the wall-crossings occur. We plot the phase difference for $0 \leq t \leq 1$ in figure 7.2.1. Then,

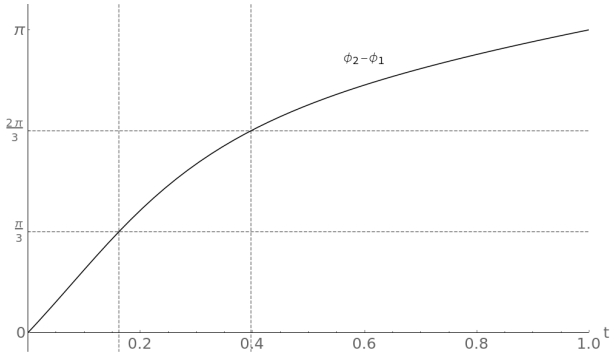

Figure 7.2.1: t-dependence of the phase difference $\phi_2 - \phi_1$ for $0 \leq t \leq 1$.

one finds the walls are located at

$$t = 0.162117..., \qquad \phi_2 - \phi_1 = \frac{\pi}{3}, \qquad \mathrm{Im}\left(\frac{\Pi^{(0)}_{\gamma_{3,2}}}{\Pi^{(0)}_{\gamma_{1,1}}}\right) = 0, \tag{7.2.2}$$

$$t = 0.397459..., \qquad \phi_2 - \phi_1 = \frac{2\pi}{3}, \qquad \mathrm{Im}\left(\frac{\Pi^{(0)}_{\gamma_{1,2}}}{\Pi^{(0)}_{\gamma_{1,1}}}\right) = 0. \tag{7.2.3}$$

The first wall-crossing

The first wall-crossing condition is (7.2.2). After the wall-crossing, we introduce the new Y-functions $Y^{(1)}$ in the same way as we discussed in the previous section:

$$\begin{aligned} &Y^{(1)}_{1,1}(\theta) \coloneqq Y_{1,1}(\theta)\big(1 + \frac{1}{Y_{1,2}(\theta - \frac{\pi i}{3})}\big), \quad Y^{(1)}_{1,2}(\theta) \coloneqq Y_{1,2}(\theta)\big(1 + \frac{1}{Y_{1,1}(\theta + \frac{\pi i}{3})}\big), \\ &Y^{(1)}_{12}(\theta) \coloneqq \frac{1 + \frac{1}{Y_{1,2}(\theta - \frac{\pi i}{3})} + \frac{1}{Y_{1,1}(\theta)}}{\frac{1}{Y_{1,1}(\theta)Y_{1,2}(\theta - \frac{\pi i}{3})}}. \end{aligned} \tag{7.2.4}$$

The TBA equations for these new Y-functions read

$$\begin{aligned} \log Y^{(1)}_{1,1}(\theta - i\phi_1) =& |m_{1,1}|e^{\theta} + K \star \overline{L}^{(1)}_{1,1} - K_{1,2} \star \overline{L}^{(1)}_{1,2} + K^{-}_{1,12} \star \overline{L}^{(1)}_{12}, \\ \log Y^{(1)}_{1,2}(\theta - i\phi_2) =& |m_{1,2}|e^{\theta} + K \star \overline{L}^{(1)}_{1,2} - K_{2,1} \star \overline{L}^{(1)}_{1,1} - K^{-}_{2,12} \star \overline{L}^{(1)}_{12}, \\ \log Y^{(1)}_{12}(\theta - i\phi_{12}) =& |m_{12}|e^{\theta} + K \star \overline{L}^{(1)}_{12} + K^{+}_{12,1} \star \overline{L}^{(1)}_{1,1} - K^{+}_{12,2} \star \overline{L}^{(1)}_{1,2}. \end{aligned} \tag{7.2.5}$$

The new Y-functions are related to the WKB periods as $\log Y^{(1)}_{1,1}(\theta) = e^{\theta}\Pi_{\hat{\gamma}_{1,1}}$, $\log Y^{(1)}_{1,2}(\theta) = e^{\frac{\pi i}{3}}e^{\theta}\Pi_{\hat{\gamma}_{1,2}}(\theta + \frac{\pi i}{3})$ and $\log Y^{(1)}_{12}(\theta) = e^{\theta}\Pi_{\hat{\gamma}_{1,1}+\hat{\gamma}_{1,2}}(\theta)$. To test this relation, one can calculate and compare the ϵ-expansions. As an example, we show the result at the value $t = 1/5 = 0.2$ in table 7.2.1. One can see the agreements in every order in the high digits. The effective central charge is $c_{\text{eff}} = 2$ which is the same value as that in the minimal chamber.

n	$\Pi^{(n)}_{\hat{\gamma}_{1,1}}$	$m^{(n-1)}_{1,1}$
0	$-9.747530080 + 6.701716666i$	$-9.747530080 + 6.701716666i$
2	$0.1568931454 - 0.1561575487i$	$0.1568931454 - 0.1561575487i$
6	$1.037931258 - 0.1841377709i$	$1.037931259 - 0.1841377696i$
8	$-0.7530182822 + 12.31639555i$	$-0.7530183059 + 12.31639556i$
12	$-4657.014593 + 7803.136493i$	$-4657.014191 + 7803.135760i$
n	$e^{\frac{\pi i}{3}(1-n)}\Pi^{(n)}_{\hat{\gamma}_{1,2}}$	$m^{(n-1)}_{1,2}$
0	$-1.280370055 - 1.004961987i$	$-1.280370055 - 1.004961987i$
2	$-0.1568931454 + 0.1561575487i$	$-0.1568931454 + 0.1561575487i$
6	$-1.037931258 + 0.1841377709i$	$-1.037931259 + 0.1841377696i$
8	$0.7530182822 - 12.31639555i$	$0.7530183059 - 12.31639556i$
12	$4657.014593 - 7803.136493i$	$4657.014191 - 7803.135760i$
n	$\Pi^{(n)}_{\hat{\gamma}_{1,1}+\hat{\gamma}_{1,2}}$	$m^{(n-1)}_{12}$
0	$-11.25803772 + 7.308068666i$	$-11.25803772 + 7.308068666i$
2	$-0.05678983152 - 0.2139522239i$	$-0.05678983147 - 0.2139522240i$
6	$0.6784336165 + 0.8068059514i$	$0.6784336157 + 0.8068059527i$
8	$10.28980229 + 6.810330737i$	$10.28980228 + 6.810330760i$
12	$-9086.221728 - 131.5246971i$	$-9086.220893 - 131.5247156i$

Table 7.2.1: The ϵ-expansions of the WKB periods $\Pi_{\hat{\gamma}_{1,1}}, e^{\frac{\pi i}{3}}\Pi^{[-1]}_{\hat{\gamma}_{1,2}}$ and $\Pi_{\hat{\gamma}_{12}}$, and that of the Y-functions $Y^{(1)}_{1,1}, Y^{(1)}_{1,2}$ and $Y^{(1)}_{12}$ for $t = \frac{1}{5} = 0.2$.

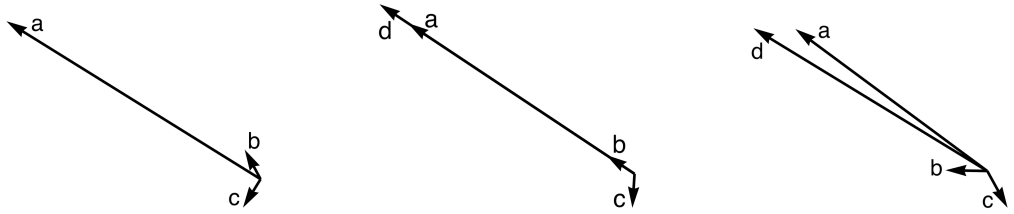

(a) $t = 0.0810585...$ (b) $t = 0.162117...$ (c) $t = 0.279788...$

Figure 7.2.2: The classical periods in the process of the first wall-crossing. The vectors represents the classical periods on the complex plane (a) before, (b) at and (c) after the wall-crossing. The arrows labeled by a, b, c, d and e represent the classical periods $\Pi^{(0)}_{\gamma_{1,1}}, \Pi^{(0)}_{\gamma_{3,2}}, \Pi^{(0)}_{\gamma_{1,2}}$ and $\Pi^{(0)}_{\gamma_{1,1}+\gamma_{3,2}}$, respectively.

To see the relation to the $\mathcal{N} = 2$ theory, we illustrate the classical periods/charges of the BPS particles in the complex plane in figure 7.2.2. Before the wall-crossing, there are three charges[2] $\Pi^{(0)}_{\gamma_{1,1}}, \Pi^{(0)}_{\gamma_{3,2}}$ and $\Pi^{(0)}_{\gamma_{1,2}}$, two of which align at the wall: $\mathrm{Im}(\Pi^{(0)}_{\gamma_{1,1}}/\Pi^{(0)}_{\gamma_{3,2}}) = 0$. After the wall, the new charge $\Pi^{(0)}_{\gamma_{1,1}} + \Pi^{(0)}_{\gamma_{1,2}}$ emerges. This is the wall crossing of the pentagon type.

The second wall-crossing

The condition of the second wall-crossing is (7.2.3). In a similar way to the first wall-crossing, we introduce the new Y-functions $Y^{(2)}$ as

$$\begin{aligned} Y^{(2)}_{1,1}(\theta) &= Y^{(1)}_{1,1}(\theta)\big(1 + \frac{1}{Y^{(1)}_{1,2}(\theta - \frac{2\pi i}{3})}\big), \quad Y^{(2)}_{1,2}(\theta) = Y^{(1)}_{1,2}(\theta)\big(1 + \frac{1}{Y^{(1)}_{1,1}(\theta + \frac{2\pi i}{3})}\big), \\ Y^{(2)}_{\widetilde{12}}(\theta) &= \frac{1 + \frac{1}{Y^{(1)}_{1,2}(\theta - \frac{2\pi i}{3})} + \frac{1}{Y^{(1)}_{1,1}(\theta)}}{\frac{1}{Y^{(1)}_{1,1}(\theta) Y^{(1)}_{1,2}(\theta - \frac{2\pi i}{3})}}, \quad Y^{(2)}_{12}(\theta) = Y^{(1)}_{12}(\theta). \end{aligned} \tag{7.2.6}$$

The TBA equation for these Y-functions are given by

$$\begin{aligned} \log Y^{(2)}_{1,1}(\theta - i\phi_1) =& |m_{1,1}|e^\theta + K \star \overline{L}^{(2)}_{1,1} - K_{1,2} \star \overline{L}^{(2)}_{1,2} + K^-_{1,12} \star \overline{L}^{(2)}_{12} + (K_{1,\widetilde{12}} + K^-_{1,\widetilde{12}}) \star \overline{L}^{(2)}_{\widetilde{12}}, \\ \log Y^{(2)}_{1,2}(\theta - i\phi_2) =& |m_{1,2}|e^\theta - K_{2,1} \star \overline{L}^{(2)}_{1,1} + K \star \overline{L}^{(2)}_{1,2} - K^-_{2,12} \star \overline{L}^{(2)}_{12} - (K^-_{2,\widetilde{12}} + K_{2,\widetilde{12}}) \star \overline{L}^{(2)}_{\widetilde{12}}, \\ \log Y^{(2)}_{12}(\theta - i\phi_{12}) =& |m_{12}|e^\theta + K^+_{12,1} \star \overline{L}^{(2)}_{1,1} - K^+_{12,2} \star \overline{L}^{(2)}_{1,2} + K \star \overline{L}^{(2)}_{12} + (K_{12,\widetilde{12}} + K^+_{12,\widetilde{12}}) \star \overline{L}^{(2)}_{\widetilde{12}}, \\ \log Y^{(2)}_{\widetilde{12}}(\theta - i\phi_{\widetilde{12}}) =& |m_{\widetilde{12}}|e^\theta + (K_{\widetilde{12},1} + K^+_{\widetilde{12},1}) \star \overline{L}^{(2)}_{1,1} - (K^+_{\widetilde{12},2} + K_{\widetilde{12},2}) \star \overline{L}^{(2)}_{1,2} \\ & + (K_{\widetilde{12},12} + K^-_{\widetilde{12},12}) \star \overline{L}^{(2)}_{12} + 3K \star \overline{L}^{(2)}_{\widetilde{12}}, \end{aligned} \tag{7.2.7}$$

[2]We do not plot the charge $\Pi^{(0)}_{\gamma_{3,3}}$ since it's not relevant to the wall-crossing.

where the new mass $m_{\widetilde{12}}$ is defined by $m_{\widetilde{12}} = m_{1,1} + e^{-\frac{2\pi i}{3}} m_{1,2} = \Pi^{(0)}_{\gamma_{1,1}-\gamma_{1,2}}$. Then, the new Y-functions are related to the WKB periods as

$$\begin{aligned} &\log Y^{(2)}_{1,1}(\theta) = e^{\theta}\Pi_{\hat{\gamma}_{1,1}}, \quad \log Y^{(2)}_{1,2}(\theta) = e^{\frac{\pi i}{3}} e^{\theta}\Pi_{\hat{\gamma}_{1,2}}(\theta + \frac{\pi i}{3}), \\ &\log Y^{(2)}_{12}(\theta) = e^{\theta}\Pi_{\hat{\gamma}_{1,1}+\hat{\gamma}_{1,2}}(\theta), \quad \log Y^{(2)}_{\widetilde{12}}(\theta) = e^{\theta}\Pi_{\gamma_{1,1}-\gamma_{1,2}}(\theta), \end{aligned} \tag{7.2.8}$$

which are tested by the numerical comparisons. We perform at the value $t = 3/7 \simeq 0.428571...$ in table 7.2.2 in which we can see the agreements again.

n	$\Pi^{(n)}_{\hat{\gamma}_{1,1}}$	$m^{(n-1)}_{1,1}$
0	$-8.308190190 + 7.043627188i$	$-8.308190190 + 7.043627188i$
2	$-0.009010340904 - 0.1441424592i$	$-0.009010340904 - 0.1441424592i$
6	$-0.01783306296 + 0.03546352561i$	$-0.01783306296 + 0.03546352561i$
8	$-0.07558676701 + 0.1018527964i$	$-0.07558676698 + 0.1018527964i$
12	$5.797603169 - 3.782968514i$	$5.797602298 - 3.782967938i$
n	$e^{\frac{\pi i}{3}(1-n)}\Pi^{(n)}_{\hat{\gamma}_{1,2}}$	$m^{(n-1)}_{1,2}$
0	$-0.2795945545 - 3.111293527i$	$-0.2795945545 - 3.111293527i$
2	$0.009010340904 + 0.1441424592i$	$0.009010340904 + 0.1441424592i$
6	$0.01783306296 - 0.03546352561i$	$0.01783306296 - 0.03546352561i$
8	$0.07558676701 - 0.1018527964i$	$0.07558676698 - 0.1018527964i$
12	$-5.797603169 + 3.782968514i$	$-5.797602298 + 3.782967938i$
n	$\Pi^{(n)}_{\hat{\gamma}_{1,1}+\hat{\gamma}_{1,2}}$	$m^{(n-1)}_{12}$
0	$-11.14244670 + 5.730116412i$	$-11.14244670 + 5.730116412i$
2	$-0.1293362019 - 0.06426804547i$	$-0.1293362019 - 0.06426804547i$
6	$-0.03962884557 + 0.002287877251i$	$-0.03962884557 + 0.002287877251i$
8	$0.05041372566 + 0.1163864586i$	$0.05041372564 + 0.1163864586i$
12	$6.174948420 + 3.129387368i$	$6.174947485 + 3.129386902i$
n	$\Pi^{(n)}_{\gamma_{1,1}-\gamma_{1,2}}$	$m^{(n-1)}_{\widetilde{12}}$
0	$-10.86285215 + 8.841409938i$	$-10.86285215 + 8.841409938i$
2	$-0.1383465428 - 0.2084105046i$	$-0.1383465428 - 0.2084105046i$
6	$-0.05746190853 + 0.03775140286i$	$-0.05746190853 + 0.03775140286i$
8	$-0.02517304135 + 0.2182392551i$	$-0.02517304134 + 0.2182392550i$
12	$11.97255159 - 0.6535811464i$	$11.97254978 - 0.6535810356i$

Table 7.2.2: The coefficients of the ϵ-expansions of the WKB periods $\Pi_{\hat{\gamma}_{1,1}}, e^{\frac{\pi i}{3}}\Pi^{[-1]}_{\hat{\gamma}_{1,2}}, \Pi_{\hat{\gamma}_{12}}$ and $\Pi_{\gamma_{1,1}-\gamma_{1,2}}$, and that of the Y-functions $Y^{(2)}_{1,1}, Y^{(2)}_{1,2}, Y^{(2)}_{12}$ and $Y^{(2)}_{\widetilde{12}}$ for $t = \frac{3}{7} \simeq 0.428571....$

To illustrate this wall-crossing process, we plot the charges in figure 7.2.3. Before the wall, we have the charges $\Pi^{(0)}_{\gamma_{1,1}}, \Pi^{(0)}_{\gamma_{3,2}}, \Pi^{(0)}_{\gamma_{1,2}}, \Pi^{(0)}_{\gamma_{1,1}+\gamma_{3,2}}$. At the wall, two charges align

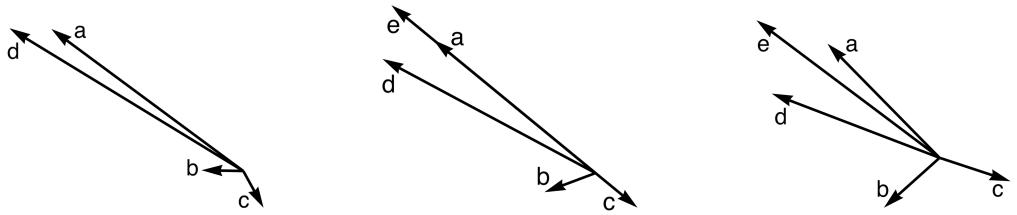

(a) $t = 0.279788...$ (b) $t = 0.397459...$ (c) $t = 0.6$

Figure 7.2.3: The classical periods in the process of the second wall-crossing. The vectors represents the classical periods on the complex plane (a) before, (b) at and (c) after the wall-crossing. The arrows labeled by a, b, c, d and e represent the classical periods $\Pi^{(0)}_{\gamma_{1,1}}, \Pi^{(0)}_{\gamma_{3,2}}, \Pi^{(0)}_{\gamma_{1,2}}, \Pi^{(0)}_{\gamma_{1,1}+\gamma_{3,2}}$ and $\Pi^{(0)}_{\gamma_{1,1}-\gamma_{1,2}}$, respectively.

$\mathrm{Im}(\Pi^{(0)}_{\gamma_{1,1}}/\Pi^{(0)}_{\gamma_{1,2}}) = 0$ and the new BPS particle of charge $\Pi^{(0)}_{\gamma_{1,1}-\gamma_{1,2}}$ emerges.

The TBA equations in this chamber have the kernels whose poles are shifted by the phase differences other than $\phi_2 - \phi_1$. The poles of these kernels could arise the new walls, hence we have to investigate whether the new walls emerge or not. In figure 7.2.4, we plot the phase differences associated with the phases of the new mass terms i.e. ϕ_{12} and $\phi_{\widetilde{12}}$. For the kernel $K^{\pm n}_{k_1,k_2}$, we plot $\phi_{k_1} - \phi_{k_2} \mp n\frac{\pi}{3}(+m\pi)$ $(m \in \mathbb{Z})$. One can see that these

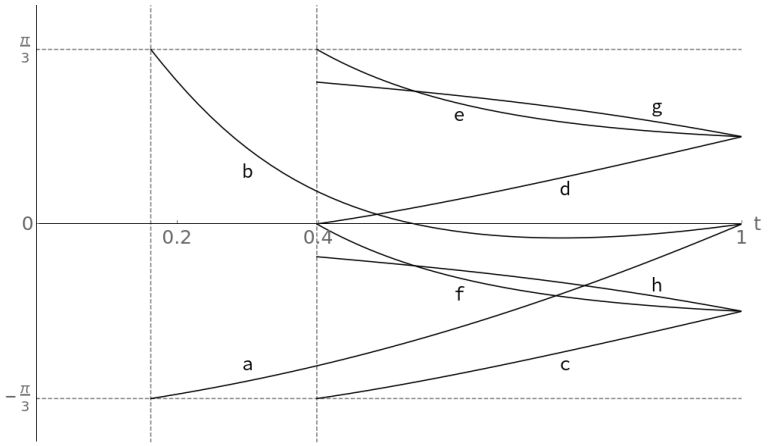

a: $\phi_{12} - \phi_1 - \frac{\pi}{3}$
b: $\phi_{12} - \phi_2 + \frac{2\pi}{3}$
c: $\phi_{\widetilde{12}} - \phi_1 - \frac{\pi}{3}$
d: $\phi_{\widetilde{12}} - \phi_1$
e: $\phi_{\widetilde{12}} - \phi_2 + \frac{\pi}{3}$
f: $\phi_{\widetilde{12}} - \phi_2 + \frac{2\pi}{3}$
g: $\phi_{\widetilde{12}} - \phi_{12} + \frac{\pi}{3}$
h: $\phi_{\widetilde{12}} - \phi_{12}$

Figure 7.2.4: The phase differences associated with ϕ_{12} and $\phi_{\widetilde{12}}$.

phase differences do not cross $\pm\frac{\pi}{3}$, hence conclude that no new walls emerge. The TBA equations (7.2.7) is valid for $0.397459... \leq t \leq 1$, so after the second wall, we are in the maximal chamber.

7.2.2 The monomial potential and the D_4-type TBA

The TBA equations (7.2.7) is valid even at the maximally symmetric/AD point $t = 1$, at which the potential becomes the monomial one:

$$p(x) = x^3 - 8. \tag{7.2.9}$$

At this symmetric point, the mass terms have the following relations

$$|m_{1,1}| = |m_{1,2}| = |m_{12}|, \quad |m_{\widetilde{12}}| = \sqrt{3}|m_{1,1}|, \tag{7.2.10}$$

and

$$\phi_2 - \phi_1 = \pi, \quad \phi_{12} - \phi_1 = \frac{\pi}{3}, \quad \phi_{\widetilde{12}} - \phi_1 = \frac{\pi}{6}. \tag{7.2.11}$$

This leads, together with the TBA equations (7.2.7), the equivalence of the Y-functions:

$$\log Y^{(2)}_{1,1}(\theta - i\phi_1) = \log Y^{(2)}_{1,2}(\theta - i\phi_1 - \pi i) = \log Y^{(2)}_{12}(\theta - i\phi_1 - \frac{\pi i}{3}). \tag{7.2.12}$$

Thus, the TBA equations for the monomial potential become the reduced one

$$\begin{aligned}
\log Y^{(2)}_{1,1}(\theta - i\phi_1) =& |m_{1,1}|e^{\theta} + 3K(\theta - \theta') \star \overline{L}^{(2)}_{1,1} \\
&+ K(\theta - \theta' + \frac{\pi i}{6}) \star \overline{L}^{(2)}_{\widetilde{12}} + K(\theta - \theta' - \frac{\pi i}{6}) \star \overline{L}^{(2)}_{\widetilde{12}}, \\
\log Y^{(2)}_{\widetilde{12}}(\theta - i\phi_1 - \frac{\pi i}{6}) =& \sqrt{3}|m_{1,1}|e^{\theta} + 3K(\theta - \theta') \star \overline{L}^{(2)}_{\widetilde{12}} \\
&+ 3K(\theta - \theta' + \frac{\pi i}{6}) \star \overline{L}^{(2)}_{1,1} + 3K(\theta - \theta' - \frac{\pi i}{6}) \star \overline{L}^{(2)}_{1,1}.
\end{aligned} \tag{7.2.13}$$

This is the D_4-type TBA equations folded by the $\mathbf{Z}_3$-symmetry of the Dynkin diagram of D_4, which we introduced in chapter 2. Then, the (A_2, A_2)-type TBA equation at the monomial point in the maximal chamber is equivalent to the $(D_4/\mathbf{Z}_3, A_1)$-type TBA equations. This is related to the fact that the SW curve of the AD theory of (A_2, A_2)-type at the AD point is $y^3 + x^3 = 0$, and equal to the one for the (D_4, A_1)-type. Therefore, we see the duality of the AD theories through the wall-crossing of the TBA equations.

For completeness, we perform the numerical test of the identification of the WKB periods with the Y-functions for the monomial potential. Table 7.2.3 shows the numerical comparison of the coefficients in the ϵ-expansions, from which one can see the agreements in high precision. The effective central charge is $c_{\text{eff}} = 2$, which is the same value as that in the minimal chamber.

n	$\Pi^{(n)}_{\hat{\gamma}_{1,1}}$	$m^{(n-1)}_{1,1}$
0	$-5.299916251 + 9.179724222i$	$-5.299916251 + 9.179724222i$
2	$-0.04277896287 - 0.07409533719i$	$-0.04277896287 - 0.07409533719i$
6	$0.0001166129817 - 0.0002019796092i$	$0.0001166129817 - 0.0002019796092i$
8	$-0.00003383735446 - 0.00005860801712i$	$-0.00003383735445 - 0.00005860801710i$
12	$0.00001446736332 - 0.00002505820832i$	$0.00001446736106 - 0.00002505820443i$
n	$\Pi^{(n)}_{\gamma_{1,1}-\gamma_{1,2}}$	$m^{(n-1)}_{\widetilde{12}}$
0	$-15.89974875 + 9.179724222i$	$-15.89974875 + 9.179724222i$
2	$-0.1283368886 - 0.07409533719i$	$-0.1283368886 - 0.07409533719i$
6	$0.0003498389452 - 0.0002019796092i$	$0.0003498389452 - 0.0002019796092i$
8	$-0.0001015120634 - 0.00005860801712i$	$-0.0001015120633 - 0.00005860801710i$
12	$0.00004340208996 - 0.00002505820832i$	$0.00004340208323 - 0.00002505820443i$

Table 7.2.3: The coefficients in the ϵ-expansions of the WKB periods $\Pi_{\hat{\gamma}_{1,1}}$ and $\Pi_{\gamma_{1,1}-\gamma_{1,2}}$, and the Y-functions $Y_{1,1}$ and $Y_{\widetilde{12}}$ for $t = 1$.

7.3 Wall-crossing for the (A_2, A_3)-type ODE

Next, let us perform a similar analysis for the (A_2, A_3)-type ODE. We set the zeros in the minimal chamber $\{x_0, x_1, x_2, x_3\} = \{2, 1, -1, -4\}$ and that in the maximal chamber $\{x_0, x_1, x_2, x_3\} = \{3, 3i, -3i, -3\}$. Choosing $u_0 = 1$, the potential in the minimal and the maximal chambers become $p(x) = x^4 + 2x^3 - 9x^2 - 2x + 8$ and $p(x) = x^4 - 81$, respectively. The path interpolating the zeros of these two potentials is given by

$$x_0(t) = 2+t, \quad x_1(t) = 1-t+3it, \quad x_2(t) = -x_1(t), \quad x_3(t) = -4+t, \quad 0 \leq t \leq 1, \tag{7.3.1}$$

where the potential at any point t is $p(x;t) = (x - x_0(t))(x - x_1(t))(x - x_2(t))(x - x_3(t))$. To find the walls, we compute the phase differences of the masses for $0 \leq t \leq 1$. Unlike the cubic potential case, the phase differences associated with the masses of the additionally introduced Y-functions through the wall-crossing processes arise other walls. Then, the procedure of the wall-crossing is as follows. First, we compute all the phase differences of the masses in the minimal chamber and find the first wall. After obtaining the TBA equations in the chamber after the first wall, we compute all the phase differences in the kernels in the TBA equations and find the second wall. Repeating this sequentially, we reach the maximal chamber. In figure 7.3.1, we plot the relevant phase differences to the walls which emerge in the path from the minimal to the maximal chamber (7.3.1).

Here ϕ_i $(i = 1, 2, 3)$ are the phases of the mass terms of $Y_{1,1}, Y_{1,2}, Y_{1,3}$ while $\phi_{12}, \phi_{23}, \phi_{312}$

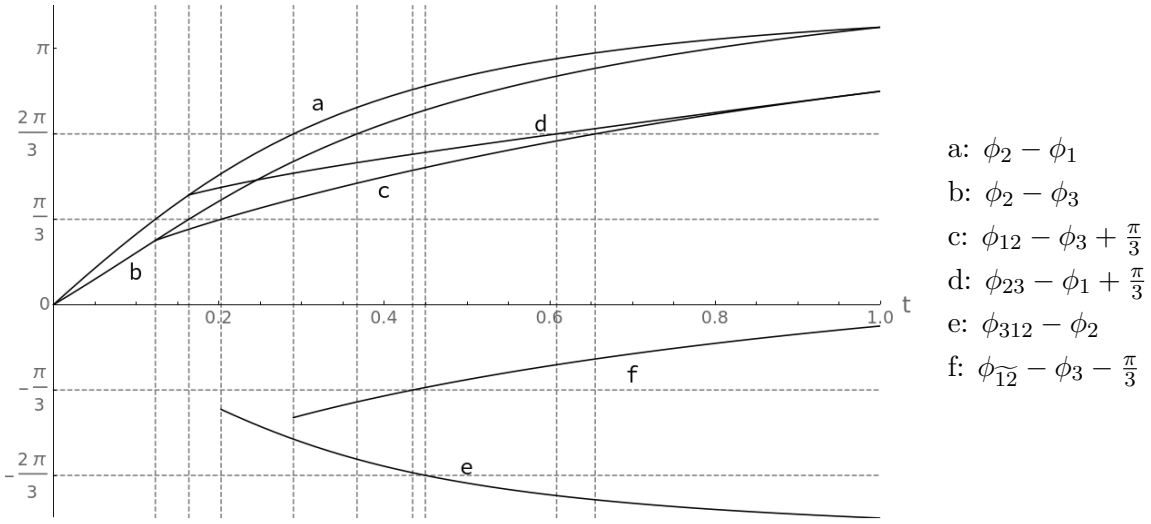

Figure 7.3.1: The phase differences of the masses relevant to the walls in the path.

and $\phi_{\widetilde{12}}$ are that for the Y-functions Y_{12}, Y_{23}, Y_{312} and $Y_{\widetilde{12}}$ which we will introduce after the $1, 2, 3$-th and the 4-th wall-crossing, respectively. For the kernel $K^{\pm n}_{k_1,k_2}$ in the TBA equations, the wall arises when $\phi_{k_1} - \phi_{k_2} \mp n\frac{\pi}{3}$ crosses $\pm\pi/3, \pm 2\pi/3$. From figure 7.3.1,

one finds nine walls located at

$$t = 0.123142..., \qquad \phi_2 - \phi_1 = \frac{\pi}{3}, \qquad \mathrm{Im}\left(\frac{\Pi^{(0)}_{\gamma_{3,2}}}{\Pi^{(0)}_{\gamma_{1,1}}}\right) = 0, \tag{7.3.2}$$

$$t = 0.163685..., \qquad \phi_2 - \phi_3 = \frac{\pi}{3}, \qquad \mathrm{Im}\left(\frac{\Pi^{(0)}_{\gamma_{3,2}}}{\Pi^{(0)}_{\gamma_{3,3}}}\right) = 0, \tag{7.3.3}$$

$$t = 0.202635..., \qquad \phi_{12} - \phi_3 = 0, \qquad \mathrm{Im}\left(\frac{\Pi^{(0)}_{\gamma_{1,1}+\gamma_{3,2}}}{\Pi^{(0)}_{\gamma_{3,3}}}\right) = 0, \tag{7.3.4}$$

$$t = 0.290017..., \qquad \phi_2 - \phi_1 = \frac{2\pi}{3}, \qquad \mathrm{Im}\left(\frac{\Pi^{(0)}_{\gamma_{1,2}}}{\Pi^{(0)}_{\gamma_{1,1}}}\right) = 0, \tag{7.3.5}$$

$$t = 0.366924..., \qquad \phi_2 - \phi_3 = \frac{2\pi}{3}, \qquad \mathrm{Im}\left(\frac{\Pi^{(0)}_{\gamma_{1,2}}}{\Pi^{(0)}_{\gamma_{3,3}}}\right) = 0, \tag{7.3.6}$$

$$t = 0.434148..., \qquad \phi_{\widetilde{12}} - \phi_3 = 0, \qquad \mathrm{Im}\left(\frac{\Pi^{(0)}_{\gamma_{1,1}-\gamma_{1,2}}}{\Pi^{(0)}_{\gamma_{3,3}}}\right) = 0, \tag{7.3.7}$$

$$t = 0.449568..., \qquad \phi_{312} - \phi_2 = -\frac{2\pi}{3}, \qquad \mathrm{Im}\left(\frac{\Pi^{(0)}_{\gamma_{1,1}+\gamma_{3,2}+\gamma_{3,3}}}{\Pi^{(0)}_{\gamma_{1,2}}}\right) = 0, \tag{7.3.8}$$

$$t = 0.608205..., \qquad \phi_{23} - \phi_1 = \frac{\pi}{3}, \qquad \mathrm{Im}\left(\frac{\Pi^{(0)}_{\gamma_{1,2}+\gamma_{1,3}}}{\Pi^{(0)}_{\gamma_{1,1}}}\right) = 0, \tag{7.3.9}$$

$$t = 0.65489..., \qquad \phi_{12} - \phi_3 = \frac{\pi}{3}, \qquad \mathrm{Im}\left(\frac{\Pi^{(0)}_{\gamma_{1,2}+\gamma_{2,1}}}{\Pi^{(0)}_{\gamma_{3,3}}}\right) = 0. \tag{7.3.10}$$

7.3.1 Symmetric potential and numerical test

Since there are many walls throughout the wall-crossing path, in this section, we only show the TBA equations for the symmetric potentials. The TBA equations and the plots of the classical periods in the complex plane are presented in appendix E. The TBA equations in each chamber have a more complicated form compared to the cubic potential case. In the following, we express the TBA equations by using the intersection matrix which we introduced in chapter 4. For the third order case, we need not only the matrix I but also the matrix for the shifted kernels $I^{\pm}$. The TBA equations have the following universal

form:

$$\log Y_k^{(i)}(\theta - i\phi_k) = |m_k|e^{\theta} - \sum_l \left(\widetilde{K}_{k,l} + \widetilde{K}_{k,l}^{+} + \widetilde{K}_{k,l}^{-}\right) \star \overline{L}_l^{(i)}(\theta), \tag{7.3.11}$$

where the kernel matrices $\widetilde{K}_{k,l}, \widetilde{K}_{k,l}^{+}$ and $\widetilde{K}^{-}$ are expressed by the intersection matrices as

$$\begin{aligned} \widetilde{K}_{k,l}(\theta) &= \frac{1}{2\pi} \frac{4\sqrt{3}\cosh(\theta - i(\phi_k - \phi_l))}{1 + 2\cosh(2(\theta - i(\phi_k - \phi_l)))} \, I_{k,l}, \\ \widetilde{K}_{k,l}^{\pm}(\theta) &= \frac{1}{2\pi} \frac{4\sqrt{3}\cosh\left(\theta - i(\phi_k - \phi_l) \pm \frac{\pi}{3}\right)}{1 + 2\cosh\left(2(\theta - i(\phi_k - \phi_l) \pm \frac{\pi}{3})\right)} \, I_{k,l}^{\pm}. \end{aligned} \tag{7.3.12}$$

To avoid confusion, we will denote the Y-functions $Y_{1,i}$ as Y_i $(i = 1, 2, 3)$. Note that since $\widetilde{K} = \widetilde{K}^{+} + \widetilde{K}^{-}$, the intersection matrices $I, I^{\pm}$ are not uniquely determined. In each wall-crossing process, we will show the intersection matrices I, I^{+} and I^{-} instead of the TBA equations. The definitions of the Y-functions are in appendix E.

In the chambers after the third and the sixth wall, there are the points in the moduli space, where the potentials become the symmetric ones. At the points, some Y-functions with the appropriate phase shifts become equal to each other, and then the TBA equations are reduced to the simplified ones. In the following, we show the intersection matrices of the reduced TBA and perform the numerical tests of the relations of the Y-functions and the WKB periods, which provide evidence supporting the identification outside the minimal chamber.

The symmetric case in the fourth chamber

After the third wall, there is the point in the moduli space, where the masses have the symmetry $m_1 = m_3$ and $m_{12} = m_{23}$. The TBA equations reduce to the four equations, whose intersection matrices are given by

$$I = \begin{pmatrix} -1 & 1 & & \\ 2 & -1 & & 1 \\ & & -1 & \\ & 1 & -1 & \end{pmatrix}, \quad I^{+} = \begin{pmatrix} 0 & & 1 & \\ & 0 & & \\ -1 & 1 & 0 & -1 \\ -2 & 1 & & 0 \end{pmatrix}, \quad I^{-} = \begin{pmatrix} 0 & & -1 & -1 \\ & 0 & 2 & 1 \\ 1 & & 0 & \\ & & 2 & 0 \end{pmatrix}. \tag{7.3.13}$$

The entries are ordered as $1, 2, 12, 312$. The corresponding potential is $p(x) = x^4 - 2(8+i)x^2 + 32i$. In table 7.3.1, we show the ϵ-expansions of the WKB periods and the Y-functions, from which one can see the good agreement.

The symmetric case in the seventh chamber

There is also the point in the chamber after the sixth wall, at which the TBA equations reduce. The masses have the relation: $m_1 = m_3, m_{12} = m_{23}$ and $m_{\widetilde{12}} = m_{\widetilde{23}}$. The potential becomes $p(x) = x^4 - 2(11+2)ix^2 + 25(-3+4i)$, whose distribution of the zeros are closer to that of the monomial potential than that in the fourth chamber. The intersection matrices are given by

$$I = \begin{pmatrix} -1 & 1 & & & -1 & -1 \\ 2 & -1 & & 1 & 2 & 2 \\ & & -1 & & -1 & \\ -2 & 1 & & -1 & -4 & -2 \\ -1 & 1 & -1 & -2 & -5 & -3 \\ -2 & 2 & & -2 & -6 & -5 \end{pmatrix}, \qquad I^+ = \begin{pmatrix} 0 & & 1 & & & \\ & 0 & & & & \\ -1 & 1 & 0 & -1 & -2 & -2 \\ & 1 & & 0 & & -1 \\ -2 & 1 & & & 0 & -1 \\ -2 & 1 & & & & 1 \end{pmatrix},$$

$$I^- = \begin{pmatrix} 0 & & -1 & -1 & -2 & -1 \\ & 0 & 2 & 1 & 2 & 2 \\ 1 & & 0 & & & \\ & & -2 & 0 & & \\ & & -2 & & 0 & \\ & & -4 & -1 & -2 & 0 \end{pmatrix}. \tag{7.3.14}$$

Here the entries are ordered as $1, 2, 12, 312, \widetilde{12}, \widehat{312}$. In table 7.3.2, we show the numerical comparisons in the ϵ-expansions of the WKB periods and the Y-functions. Because of the computational difficulty, we only computed the WKB periods $\Pi_{\hat{\gamma}_{1,1}}, \Pi_{\hat{\gamma}_{2,3}}, \Pi_{\gamma_{1,1}+\gamma_{3,2}}$ and $\Pi_{\gamma_{3,2}+\gamma_{3,3}}$. In this case, one can also see the good agreement.

n	$\Pi^{(n)}_{\hat{\gamma}_{1,1}}, e^{\frac{2\pi i}{3}(1-n)}\Pi^{(n)}_{\hat{\gamma}_{1,3}}$	$m^{(n-1)}_{1,1}, m^{(n-1)}_{1,3}$
0	$-11.39881594 + 14.23487415i$	$-11.39881594 + 14.23487415i$
2	$0.01642381444 - 0.03753315426i$	$0.01642381444 - 0.03753315426i$
6	$0.00002288822247 - 0.00002208917405i$	$0.00002288822247 - 0.00002208917405i$
8	$2.625484666 \times 10^{-6} + 4.618462473 \times 10^{-6}i$	$2.625484666 \times 10^{-6} + 4.618462473 \times 10^{-6}i$
12	$5.362388326 \times 10^{-7} + 8.038711226 \times 10^{-7}i$	$5.362387829 \times 10^{-7} + 8.038710559 \times 10^{-7}i$
n	$e^{\frac{\pi i}{3}(1-n)}\Pi^{(n)}_{\hat{\gamma}_{1,2}}$	$m^{(n-1)}_{1,2}$
0	$-9.359933633 - 9.149856867i$	$-9.359933633 - 9.149856867i$
2	$0.004980601291 + 0.05664415536i$	$0.004980601291 + 0.05664415536i$
6	$-0.00002031318068 + 0.00002774220366i$	$-0.00002031318068 + 0.00002774220366i$
8	$-2.074149509 \times 10^{-6} - 4.697564517 \times 10^{-6}i$	$-2.074149509 \times 10^{-6} - 4.697564517 \times 10^{-6}i$
12	$-5.119551461 \times 10^{-7} - 7.947194982 \times 10^{-7}i$	$-5.119550997 \times 10^{-7} - 7.947194331 \times 10^{-7}i$
n	$\Pi^{(n)}_{\gamma_{1,1}+\gamma_{3,2}}, \Pi^{(n)}_{\gamma_{3,2}+\gamma_{3,3}}$	$m^{(n-1)}_{12}, m^{(n-1)}_{23}$
0	$-24.00279124 + 17.76588602i$	$-24.00279124 + 17.76588602i$
2	$-0.03014116243 - 0.004897749341i$	$-0.03014116243 - 0.004897749341i$
6	$0.00003675708525 + 9.373658279 \times 10^{-6}i$	$0.00003675708525 + 9.373658279 \times 10^{-6}i$
8	$5.656620120 \times 10^{-6} + 4.734140485 \times 10^{-7}i$	$5.656620119 \times 10^{-6} + 4.734140483 \times 10^{-7}i$
12	$-4.079860148 \times 10^{-7} + 8.498775356 \times 10^{-7}i$	$-4.079859849 \times 10^{-7} + 8.498774613 \times 10^{-7}i$
n	$\Pi^{(n)}_{\gamma_{1,1}+\gamma_{3,2}+\gamma_{3,3}}$	$m^{(n-1)}_{312}$
0	$-35.40160718 + 32.00076016i$	$-35.40160718 + 32.00076016i$
2	$-0.01371734800 - 0.04243090360i$	$-0.01371734800 - 0.04243090360i$
6	$5.964530772 \times 10^{-5} - 1.271551577 \times 10^{-5}i$	$5.964530772 \times 10^{-5} - 1.271551577 \times 10^{-5}i$
8	$8.282104786 \times 10^{-6} + 5.091876522 \times 10^{-6}i$	$8.282104785 \times 10^{-6} + 5.091876521 \times 10^{-6}i$
12	$1.282528178 \times 10^{-7} + 1.653748658 \times 10^{-6}i$	$1.282527980 \times 10^{-7} + 1.653748517 \times 10^{-6}i$

Table 7.3.1: The coefficients of the ϵ-expansions of the WKB periods and the Y-functions for $p(x) = x^4 - 2(8+i)x^2 + 32i$.

n	$\Pi^{(n)}_{\hat{\gamma}_{1,1}}, e^{\frac{2\pi i}{3}(1-n)}\Pi^{(n)}_{\hat{\gamma}_{1,3}}$	$m^{(n-1)}_{1,1}, m^{(n-1)}_{1,3}$
0	$-19.47567027 + 32.97271875i$	$-19.4756703 + 32.97271875i$
2	$0.002626192340 - 0.02247707343i$	$0.002626192340 - 0.02247707343i$
6	$-2.036305586 \times 10^{-7} - 7.372588250 \times 10^{-8}i$	$-2.036305586 \times 10^{-7} - 7.372588250 \times 10^{-8}i$
8	$-9.420730448 \times 10^{-9} - 4.804141676 \times 10^{-9}i$	$-9.420730444 \times 10^{-9} - 4.804141675 \times 10^{-9}i$
12	$9.580579434 \times 10^{-12} + 2.914660951 \times 10^{-11}i$	$9.580577595 \times 10^{-12} + 2.914660471 \times 10^{-11}i$
n	$\Pi^{(n)}_{\gamma_{1,1}+\gamma_{3,2}}, \Pi^{(n)}_{\gamma_{3,2}+\gamma_{3,3}}$	$m^{(n-1)}_{12}, m^{(n-1)}_{23}$
0	$-51.30966982 + 24.48178658i$	$-51.30966982 + 24.48178658i$
2	$-0.02139033112 + 0.0002004517871i$	$-0.02139033112 + 0.0002004517871i$
6	$4.635097673 \times 10^{-8} - 1.248192815 \times 10^{-7}i$	$4.635097673 \times 10^{-8} - 1.248192815 \times 10^{-7}i$
8	$-9.995973325 \times 10^{-9} + 8.348657318 \times 10^{-9}i$	$-9.995973321 \times 10^{-9} + 8.348657314 \times 10^{-9}i$
12	$-1.583498058 \times 10^{-11} + 2.849646253 \times 10^{-11}i$	$-1.583497796 \times 10^{-11} + 2.849645771 \times 10^{-11}i$

Table 7.3.2: The coefficients of the ϵ-expansions of the WKB periods and the Y-functions for $p(x) = x^4 - 2(11+2)ix^2 + 25(-3+4i)$

7.3.2 The monomial potential and the E_6-type TBA

The tenth chamber is the maximal chamber in which there is the maximally symmetric point where the potential is monomial one. At this point, the mass terms have the relation

$$\begin{aligned}
&|m_1| = |m_3| = |m_{12}| = |m_{23}|, \qquad |m_2| = |m_{312}|, \\
&|m_{\widetilde{12}}| = |m_{\widetilde{23}}| = |m_{231}| = |m_{\overline{123}}|, \qquad |m_{\widehat{312}}| = |m_{3122}|, \\
&\frac{|m_2|}{|m_1|} = \frac{\sin(\pi/4)}{\sin(\pi/6)}, \qquad \frac{|m_{\widetilde{12}}|}{|m_1|} = \frac{\sin(\pi/6)}{\sin(\pi/12)}, \qquad \frac{|m_{\widehat{312}}|}{|m_1|} = \frac{\sin(\pi/4)}{\sin(\pi/12)},
\end{aligned} \tag{7.3.15}$$

and

$$\begin{aligned}
&\phi_1 = \phi_3, \qquad \phi_{12} = \phi_{23}, \qquad \phi_{12} - \phi_1 = \frac{5\pi}{12}, \\
&\phi_{\widetilde{12}} = \phi_{\widetilde{23}}, \qquad \phi_{231} = \phi_{\overline{123}}, \qquad \phi_{\widetilde{12}} - \phi_{231} = \frac{\pi}{6} \\
&\phi_{312} - \phi_2 = \frac{7\pi}{6}, \quad \phi_{3122} - \phi_{\widehat{312}} = \frac{\pi}{6}.
\end{aligned} \tag{7.3.16}$$

Note that the vector $(|m_1|, |m_{\widehat{12}}|, |m_{\widehat{312}}|, , |m_{\widehat{12}}|, , |m_1|, , |m_2|)$ is the Perron-Frobenius eigenvector for the incidence matrix of E_6 algebra. Furthermore, the relations (7.3.15) and (7.3.16) together with the form of the TBA equation give the identifications among the

Y-functions:

$$\begin{aligned}
&\log Y_1(\theta - i\phi_1) = \log Y_3(\theta - i\phi_3) = \log Y_{12}(\theta - i\phi_{12}) = \log Y_{23}(\theta - i\phi_{23}),\\
&\log Y_{\widetilde{12}}(\theta - i\phi_{\widetilde{12}}) = \log Y_{\widetilde{23}}(\theta - i\phi_{\widetilde{23}}) = \log Y_{231}(\theta - i\phi_{231}) = \log Y_{\overline{123}}(\theta - i\phi_{\overline{123}}),\\
&\log Y_2(\theta - i\phi_2) = \log Y_{312}(\theta - i\phi_{312}), \quad \log Y_{\widehat{312}}(\theta - i\phi_{\widehat{312}}) = \log Y_{3122}(\theta - i\phi_{3122}),
\end{aligned} \tag{7.3.17}$$

which leads the reduction of the TBA equations to the four equations. We write down the TBA equations explicitly rather than the incidence matrices, which become

$$\begin{aligned}
\log Y_1^{(9)}(\theta - i\phi_1) =& |m_1|e^\theta + \left(K + K^-_{1,12} - K^+_{1,12}\right) \star \overline{L}^{(9)}_{1,1} + \left(K^-_{1,312} - K_{1,2}\right) \star \overline{L}^{(9)}_{1,2}\\
&+ \left(K_{1,\widetilde{12}} + 2K^-_{1,\widetilde{12}} + 2K_{1,231} + K^-_{1,231}\right) \star \overline{L}^{(9)}_{\widetilde{12}}\\
&+ \left(K_{1,\widehat{312}} + K^-_{1,\widehat{312}} + 2K^-_{1,3122}\right) \star \overline{L}^{(9)}_{\widehat{312}},\\
\log Y_2^{(9)}(\theta - i\phi_2) =& |m_2|e^\theta - \left(2K_{2,1} + 2K^-_{2,12}\right) \star \overline{L}^{(9)}_{1,1} + \left(K - K_{2,312} - K^-_{2,312}\right) \star \overline{L}^{(9)}_{1,2}\\
&- \left(2K_{2,\widetilde{12}} + 2K^-_{2,\widetilde{12}} + 4K_{2,231}\right) \star \overline{L}^{(9)}_{\widetilde{12}}\\
&- \left(2K_{2,\widehat{312}} + K^-_{2,\widehat{312}} + K_{2,3122} + 2K^-_{2,3122}\right) \star \overline{L}^{(9)}_{\widehat{312}},\\
\log Y^{(9)}_{\widetilde{12}}(\theta - i\phi_{\widetilde{12}}) =& |m_{\widetilde{12}}|e^\theta + \left(K_{\widetilde{12},1} + 2K^+_{\widetilde{12},1} + 2K_{\widetilde{12},12} + K^-_{\widetilde{12},12} - K^+_{\widetilde{12},12}\right) \star \overline{L}^{(9)}_{1,1}\\
&- \left(K_{\widetilde{12},2} + K^+_{\widetilde{12},2} - 2K_{\widetilde{12},312}\right) \star \overline{L}^{(9)}_{1,2} + \left(5K + 3K_{\widetilde{12},231} + 3K^+_{\widetilde{12},231}\right) \star L^{(9)}_{\widetilde{12}}\\
&+ \left(K^+_{\widetilde{12},\widehat{312}} + 3K_{\widetilde{12},\widehat{312}} + K^-_{\widetilde{12},3122} + 3K_{\widetilde{12},3122}\right) \star \overline{L}^{(9)}_{\widehat{312}},\\
\log Y^{(9)}_{\widehat{312}}(\theta - i\phi_1) =& |m_{\widehat{312}}|e^\theta + \left(2K_{\widehat{312},1} + 2K^+_{\widehat{312},1} + 4K^-_{\widehat{312},12}\right) \star \overline{L}^{(9)}_{1,1}\\
&+ \left(2K_{\widehat{312},312} + K^-_{\widehat{312},312} - 2K_{\widehat{312},2} - K^+_{\widehat{312},2}\right) \star \overline{L}^{(9)}_{1,2}\\
&+ \left(6K_{\widehat{312},\widetilde{12}} + 2K^-_{\widehat{312},\widetilde{12}} + 6K_{\widehat{312},231} + 2K^+_{\widehat{312},231}\right) \star \overline{L}^{(9)}_{\widetilde{12}}\\
&+ \left(5K + 3K_{\widehat{312},3122} + 3K^-_{\widehat{312},3122}\right) \star \overline{L}^{(9)}_{\widehat{312}}.
\end{aligned} \tag{7.3.18}$$

Simplifying the kernel functions, one finds the TBA equations (7.3.18) is same as that of E_6-type (folded by $\mathbf{Z}_2$) which we introduced in chapter 2 under the identification:

$$\begin{aligned}
&\log Y_1(\theta - i\phi_1) \leftrightarrow \epsilon_1(\theta), \quad \log Y_2(\theta - i\phi_2) \leftrightarrow \epsilon_6(\theta),\\
&\log Y_{\widetilde{12}}(\theta - i\phi_{\widetilde{12}}) \leftrightarrow \epsilon_2(\theta), \quad \log Y_{\widehat{312}}(\theta - i\phi_{\widehat{312}}) \leftrightarrow \epsilon_3(\theta).
\end{aligned} \tag{7.3.19}$$

This can be interpreted as the the realization of duality of the quantum SW curve which would follow from the fact that the (A_2, A_3)-type and the (E_6, A_1)-type AD theories at

the AD point is described by the SW curve $y^3 + x^4 = 0$. Thus we conclude that the (A_2, A_3)-type ODE with monomial potential is the quantum SW curve of (E_6, A_1)-type AD theory. Note that in [22], the relation between the third order ODE with the monomial potential and the NLIE of D_4 and E_6-types have already been studied by comparing the spectrum numerically. In our work of this section, we provided the direct check of this duality by use of the TBA equations. Before closing this section, we show the numerical comparison of the ϵ-expansions of the WKB periods and Y-functions in table 7.3.3, which again present a good agreement and support the validity of the identification even in the maximal chamber.

n	$\Pi^{(n)}_{\hat{\gamma}_{1,1}}, e^{\frac{2\pi i}{3}(1-n)}\Pi^{(n)}_{\hat{\gamma}_{1,3}}$	$m^{(n-1)}_{1,1}, m^{(n-1)}_{1,3}$
0	$-7.469227532 + 27.87553664$	$-7.469227532 + 27.87553664i$
2	$-0.009523311889 - 0.03554148383i$	$-0.009523311889 - 0.03554148383i$
6	$-3.287667860 \times 10^{-7} - 8.809279480 \times 10^{-8}i$	$-3.287667860 \times 10^{-7} - 8.809279480^{-8}i$
8	$-1.483370697 \times 10^{-8} + 3.974679804 \times 10^{-9}i$	$-1.483370697 \times 10^{-8} + 3.974679803 \times 10^{-9}i$
12	$-1.084025230 \times 10^{-10} + 4.045637237 \times 10^{-10}i$	$-1.084025095 \times 10^{-10} + 4.045636732 \times 10^{-10}i$
n	$e^{\frac{\pi i}{3}(1-n)}\Pi^{(n)}_{\hat{\gamma}_{1,2}}$	$m^{(n-1)}_{1,2}$
0	$20.40630911 - 35.34476417i$	$20.40630911 - 35.34476417i$
2	$0.02601817194 + 0.04506479572i$	$0.02601817194 + 0.04506479572i$
6	$-2.406739912 \times 10^{-7} + 4.168595808 \times 10^{-7}i$	$-2.406739912 \times 10^{-7} + 4.168595808 \times 10^{-7}i$
8	$-1.085902717 \times 10^{-8} - 1.880838678 \times 10^{-8}i$	$-1.085902716 \times 10^{-8} - 1.880838677 \times^{-8} i$
12	$2.961612006 \times 10^{-10} - 5.129662467 \times 10^{-10}i$	$2.961611637 \times 10^{-10} - 5.129661827 \times 10^{-10}i$
n	$\Pi^{(n)}_{\gamma_{1,1}-\gamma_{1,2}}, \Pi^{(n)}_{\gamma_{3,3}-\gamma_{1,2}}$	$m^{(n-1)}_{\widetilde{12}}, m^{(n-1)}_{\widetilde{23}}$
0	$-15.89974875 + 9.179724222i$	$-15.89974875 + 9.179724222i$
2	$-0.06155965576 - 0.03554148383i$	$-0.06155965576 - 0.03554148383i$
6	$1.525811964 \times 10^{-7} - 8.809279480 \times 10^{-8}i$	$1.525811964 \times 10^{-7} - 8.809279480 \times 10^{-8}i$
8	$6.884347364 \times 10^{-9} + 3.974679804 \times 10^{-9}i$	$6.884347362 \times 10^{-9} + 3.974679803 \times 10^{-9}i$
12	$-7.007249243 \times 10^{-10} + 4.045637237 \times 10^{-10}i$	$-7.007248369 \times 10^{-10} + 4.045636732 \times 10^{-10}i$
n	$\Pi^{(n)}_{\gamma_{1,1}-\gamma_{1,2}+\gamma_{3,3}}$	$m^{(n-1)}_{\widetilde{312}}$
0	$-23.36897628 + 37.05526087i$	$-23.36897628 + 37.05526087i$
2	$-0.07108296765 - 0.07108296765i$	$-0.07108296765 - 0.07108296765i$
6	$-1.761855896 \times 10^{-7} - 1.761855896 \times 10^{-7}i$	$-1.761855896 \times 10^{-7} - 1.761855896 \times 10^{-7}i$
8	$-7.949359608 \times 10^{-9} + 7.949359608 \times 10^{-9}i$	$-7.949359605 \times 10^{-9} + 7.949359605 \times 10^{-9}i$
12	$-8.091274473 \times 10^{-10} + 8.091274473 \times 10^{-10}i$	$-8.091273464 \times 10^{-10} + 8.091273464 \times 10^{-10}i$

Table 7.3.3: The coefficients of the ϵ-expansions of the WKB periods and the Y-functions for the monomial potential $p(x) = x^4 - 81$.

Summary

In this section, we studied the wall-crossing of the TBA equations for the third order ODE with the cubic and the quartic potentials in detail. The formula that relates the WKB periods and the Y-functions was extended to the one in other chambers, which was supported by the numerical tests. The structures of the walls were different from the second order case. The wall-crossing conditions were related to that of the AD theory. In the minimal chamber, the TBA equations were the (A_2, A_N)-type $(N = 2, 3)$ while at the monomial point in the maximal chamber, that became the (D_4, A_1)-type and the (E_6, A_1)-type, respectively. The monomial point is the superconformal point in the context of the four dimensional theory, so this can be understood as the associated phenomenon with the duality of the AD theories.

Chapter 8

Conclusion and discussions

In this thesis, we studied the ODE/IM correspondence for the higher order ODE with the polynomial potential, especially focusing on the relation between the WKB periods and the Y-functions as well as the wall-crossing phenomena of the TBA equations. First, we summarize what we did in each chapter.

In chapter 3, we first discussed the ODE/IM correspondence for the conformal limit of the modified affine Toda field theory. The correspondence was derived from the relation between the Bethe ansatz equations and the functional relations of the solutions to the linear problem, which were the analogy of the relations the fundamental representations. For BAE of type $\mathfrak{g}$, the ODE associated with the Langlands dual algebra $\mathfrak{g}^\vee$ corresponds. We also discussed the numerical test of this correspondence based on our work [39]. We established the method to calculate the zeros of the Q-functions from the spectral problem of the linear problems for any affine Lie algebras. Using this method, we observed the good agreements of the zeros and the Bethe roots calculated from the NLIE.

In chapter 4, we reviewed the relations between the WKB periods and Y-functions for the second order case i.e. the Schrödinger equations. The notion of the wall-crossing of the TBA equations was also introduced, and we argued both the algebraic and diagrammatic way of its calculations based on [42, 44, 45].

In chapter 5, the relation between the ODE/IM correspondence discussed in chapter 4 and the four dimensional $\mathcal{N} = 2$ theory was discussed. This relation was one of our motivations for the studies in chapters 6 and 7. We introduced the Seiberg-Witten analysis

of the low energy physics of the $\mathcal{N} = 2$ gauge theory [47,48]. In the analysis, the Riemann surface called the SW curve, and the cycle integrals of the meromorphic differentials on it, the SW periods, played the essential roles. It was also introduced the Argyres-Douglas theory which was first discovered in [56,57] and generalized to (G, G')-type where $G, G' = A, D, E$ in [59, 60]. In the NS limit of the Ω-background, the SW curves are quantized and become the ODE. The second order ODE with the polynomial potential is regarded as the quantum SW curve of the (A_1, A_N)-type AD theory. The WKB periods were interpreted as the quantum SW periods. We also argued about the BPS spectral problem and the wall-crossing phenomenon in the 4d $\mathcal{N} = 2$ theory. The wall-crossing of the TBA equations in chapter 4 was related to that of the (A_1, A_N)-type AD theory.

Motivated by the works of the second order case, we generalized the identification of the WKB periods with the Y-functions for the higher order ODE which is, in the context of the $\mathcal{N} = 2$ theory, the quantum SW curve of the (A_r, A_N)-type AD theory. In chapter 6, we proposed the formula in the minimal chamber, which was derived by the WKB analysis of the asymptotic behaviors of the Y-functions. In the analysis, we used the Stokes graphs and abelianization trees. The formula was tested by the numerical calculations of the formal expansions, the analytic relation which is the PNP relation, and the discontinuity structures.

The extension of the relation between the WKB periods and the Y-functions outside the minimal chambers and the wall-crossing phenomena were studied in chapter 7 for the third order case in detail. We performed the wall-crossing from the minimal chamber to the maximal chamber both in the cubic and the quartic potentials. As expected, the moduli spaces included richer wall structures than the second order case. At the AD points where the potential becomes the monomial one, we have observed that the TBA equations of (A_2, A_2)-type became the D_4-type while that of the (A_2, A_3)-type became the E_6-type one. These are associated with the dualities of the AD theories.

Remaining problems toward the unified understanding

Next, let us discuss the role of the study in this thesis and the remaining problems for the unified understanding of the (exact) WKB analysis of ODE, 2d integrable models,

and BPS spectra of 4d $\mathcal{N} = 2$ theories, which we mentioned in the introduction as the ultimate goal of our study.

In this thesis, we studied the relation between the higher order ODE with the polynomial potential, the (A_r, A_N)-type of TBA equations and their wall-crossings, and the (A_r, A_N)-type AD theory. The ODE is the simple generalization of the second order ODE with the polynomial potential, but whose exact WKB analysis is not well formulated. The AD theories are the kind of simplest strongly interacting 4d $\mathcal{N} = 2$ theories. Furthermore, their wall-crossings of the BPS spectra are also the simplest one i.e. the pentagon type wall-crossing. In these senses, we have studied the relation for the simplest class of examples. So far, we have not achieved the establishment of the exact WKB analysis for the higher order ODE yet, but at least, we obtained the evidence that it is connected to the theory of wall-crossings in 4d theory for some examples. As for the classification of integrable models, our result suggests that the duality of the 4d theory is helpful. In the following, we discuss the remaining problem concretely.

We computed the wall-crossing of the TBA equations algebraically. However, it would be hard to calculate for the higher rank ODE with higher order polynomial potential, so the diagrammatic way of the wall-crossing like the second order case in [44, 45] would be needed to establish. We are expecting that the (A_2, A_4)-type TBA equations will become the E_8-type one at the AD point, and it may be possible to study by using the diagrammatic way of the wall-crossing for the higher order case. In relation to the 4d theory, the Y-functions may be connected to the spectral coordinates which are defined for each BPS particles. The Kontsevich-Soibelman wall-crossing formula (KSWCF) provides a uniform expression of the wall-crossing for the spectral coordinates. So once we could establish the systematic way of the wall-crossing for the higher order ODE with polynomial potential, the connection to the formula of Kontsevich-Soibelman may become clearer. In the study of the wall-crossings, it may be helpful to consider the relation to the cluster algebras, which appear both in the context of the wall-crossing of 4d theory and exact WKB analysis [126, 127]. If one could relate the wall-crossing of the TBA equations to that of the four dimensional theories in a more refined way, the cluster algebras might provide a hint to the systematic study of the discontinuity formula for higher order ODE.

It would also be worthwhile to study the discontinuity formula of the WKB periods for the higher order case and how the TBA equations, which we derived in each chamber, will be obtained.

The ODE we studied in this thesis is relatively simple to study the ODE/IM correspondence. It would be interesting to consider more general ODE, including other derivative terms, so that one could study the level-rank duality of the ODE or AD theories through the wall-crossings. This may support the relation between the 4d theory and the 2d theory. As discussed in chapter 5, there were the TBA-like equations that were satisfied by the spectral coordinates of $\mathcal{N} = 2$ theories [68]. They also wall-cross at the marginal stability wall of the four dimensional theory. Indeed, some spectral coordinates are exactly the same as the Y-functions. Especially for the third order ODE with lower derivative terms, the spectral coordinates were constructed in [128], but still, the relation to the Y-functions is not clear. The study of the relations between the TBA equations we dealt with in this thesis and the TBA-like equations is necessary to the uniform understanding of these two. There are other generalizations of study of the ODE/IM correspondence for the quantum AD theory. In this thesis, we only deal with the AD theory of the A_r-type, but quantum curves of other types of AD theories have already been conjectured to be obtained from the conformal limit of the modified affine Toda equations [74]. Thus, studying the application of the WKB analysis to the linear problem is worthwhile to investigate the ODE/IM correspondence for other types. We expect that one can obtain the D_r-type and E_r-type TBA equations directly from the (D_r, A_1)-type and the (E_r, A_1)-type linear problems, respectively. Furthermore, the wall-crossing of the AD theory is the pentagon type which is the simplest one. If we want to study a deeper connection to the KSWCF, we should investigate the wall-crossings of TBA corresponding to the quantum SW curve of 4d theory, which enjoys more complicated wall-crossing phenomena, for example, the $SU(2)$ supersymmetric gauge theory.

Lastly, let us mention the relation to the 4d/2d correspondence. As mentioned, the ODE with the polynomial potential corresponds to many integrable models, but we only studied the form of the TBA equations in each chamber. Identifying the integrable models and understanding the connection between them may help us in the study of the 4d/2d

correspondence. In the study of the ODE/IM correspondence for the second order ODE with the monomial potential, there have been pointed out the relation to the 4d/2d correspondence. The two dimensional theory in the context of the 4d/2d correspondence by Beem *et. al.* [80] appears in the maximal chamber [74]. It may be worthwhile to study the relation to the higher order or more general ODE which is interpreted as the quantum SW curve of more complicated 4d theory than the AD theory.

Appendix A

The notation and the data of Lie algebras

In this appendix, we summarise the notations and data of the Lie algebras, which we used in the main text. For a rank r semi-simple Lie algebra $\mathfrak{g}$, we denote the root as α and the set of roots as Δ. The linear combinations of the simple roots $\alpha_a \in \Delta$ $(a = 1, 2, \ldots, r)$ with positive integer coefficients generate the all the positive roots. The Cartan matrix C_{ab} is defined by $C_{ab} \coloneqq \alpha_a \cdot \alpha_b^\vee$ where the co-root $\alpha^\vee$ is given by $\alpha \coloneqq 2\alpha/\alpha^2$. Setting the length of long roots $\alpha^2_{\text{long}} = 2$, the Cartan matrices are

$$A_{r\geq 1}: \begin{pmatrix} 2 & -1 & & & \\ -1 & 2 & \ddots & & \\ & \ddots & \ddots & -1 & \\ & & -1 & 2 & -1 \\ & & & -1 & 2 \end{pmatrix}, \qquad B_{r\geq 2}: \begin{pmatrix} 2 & -1 & & & \\ -1 & 2 & \ddots & & \\ & \ddots & \ddots & -1 & \\ & & -1 & 2 & -2 \\ & & & -1 & 2 \end{pmatrix},$$

$$C_{r\geq 2}: \begin{pmatrix} 2 & -1 & & & \\ -1 & 2 & \ddots & & \\ & \ddots & \ddots & -1 & \\ & & -1 & 2 & -1 \\ & & & -2 & 2 \end{pmatrix}, \qquad D_{r\geq 3}: \begin{pmatrix} 2 & -1 & & & & \\ -1 & 2 & \ddots & & & \\ & \ddots & \ddots & -1 & & \\ & & -1 & 2 & -1 & -1 \\ & & & -1 & 2 & \\ & & & -1 & & 2 \end{pmatrix},$$

$$
E_6: \begin{pmatrix} 2 & -1 & & & & \\ -1 & 2 & -1 & & & \\ & -1 & 2 & -1 & & -1 \\ & & -1 & 2 & -1 & \\ & & & -1 & 2 & \\ & & -1 & & & 2 \end{pmatrix}, \qquad
E_7: \begin{pmatrix} 2 & -1 & & & & & \\ -1 & 2 & -1 & & & & \\ & -1 & 2 & -1 & & & \\ & & -1 & 2 & -1 & & -1 \\ & & & -1 & 2 & -1 & \\ & & & & -1 & 2 & \\ & & & -1 & & & 2 \end{pmatrix},
$$

$$
E_8: \begin{pmatrix} 2 & -1 & & & & & & \\ -1 & 2 & -1 & & & & & \\ & -1 & 2 & -1 & & & & \\ & & -1 & 2 & -1 & & & \\ & & & -1 & 2 & -1 & & -1 \\ & & & & -1 & 2 & -1 & \\ & & & & & -1 & 2 & \\ & & & & -1 & & & 2 \end{pmatrix}, \qquad
F_4: \begin{pmatrix} 2 & -1 & & \\ -1 & 2 & -1 & \\ & -2 & 2 & -1 \\ & & -1 & 2 \end{pmatrix},
$$

$$
G_2: \begin{pmatrix} 2 & -1 \\ -3 & 2 \end{pmatrix}. \tag{A.0.1}
$$

Instead of using the Cartan matrices, the connections of the simple roots are also expressed by the Dynkin diagrams listed in figure A.0.1. Expanding the (co-)highest weight θ ($\theta^\vee$) as $\theta = \sum_{a=1}^r n_a \alpha_a$ ($\theta^\vee = \sum_{a=1}^r n_a^\vee \alpha_a^\vee$), the (dual) Coxeter number h ($h^\vee$) is defined by $h \coloneqq \sum_{a=0}^r n_a$ ($h^\vee \coloneqq \sum_{a=0}^r n_a^\vee$), where we set $n_0 \coloneqq 1$ ($n_0^\vee \coloneqq 1$) and call the coefficient n_a ($n_a^\vee$) the (co-)label. The fundamental weight ω_a ($a = 1, 2, \ldots, r$) is defined as the dual basis to the simple roots i.e. $\omega_a \cdot \alpha_b = \delta_{a,b}$. The co-fundamental weight is also defined by $\omega_a^\vee \coloneqq 2\omega_a/\alpha_a^2$. We also define the (co-)Wyle vector ρ ($\rho^\vee$) as the sum of the (co-)fundamental weights: $\rho \coloneqq \sum_{a=1}^r \omega_a$ ($\rho^\vee \coloneqq \sum_{a=1}^r \omega_a^\vee$). Denoting the generator associated with the root α as E_α, the generators E_α ($\alpha \in \Delta$) and the Cartan generators H^a ($a = 1, 2, \ldots, r$) satisfy the $\mathfrak{g}$-type Lie algebra:

$$
\begin{aligned}
&[H^a, E_\alpha] = \alpha^a E_\alpha, \qquad [H^a, H^b] = 0, \\
&[E_\alpha, E_\beta] = \begin{cases} N_{\alpha,\beta} E_{\alpha+\beta}, & \alpha + \beta \in \Delta, \\ \alpha^\vee \cdot H, & \alpha + \beta = 0, \\ 0, & \text{otherwise.} \end{cases}
\end{aligned} \tag{A.0.2}
$$

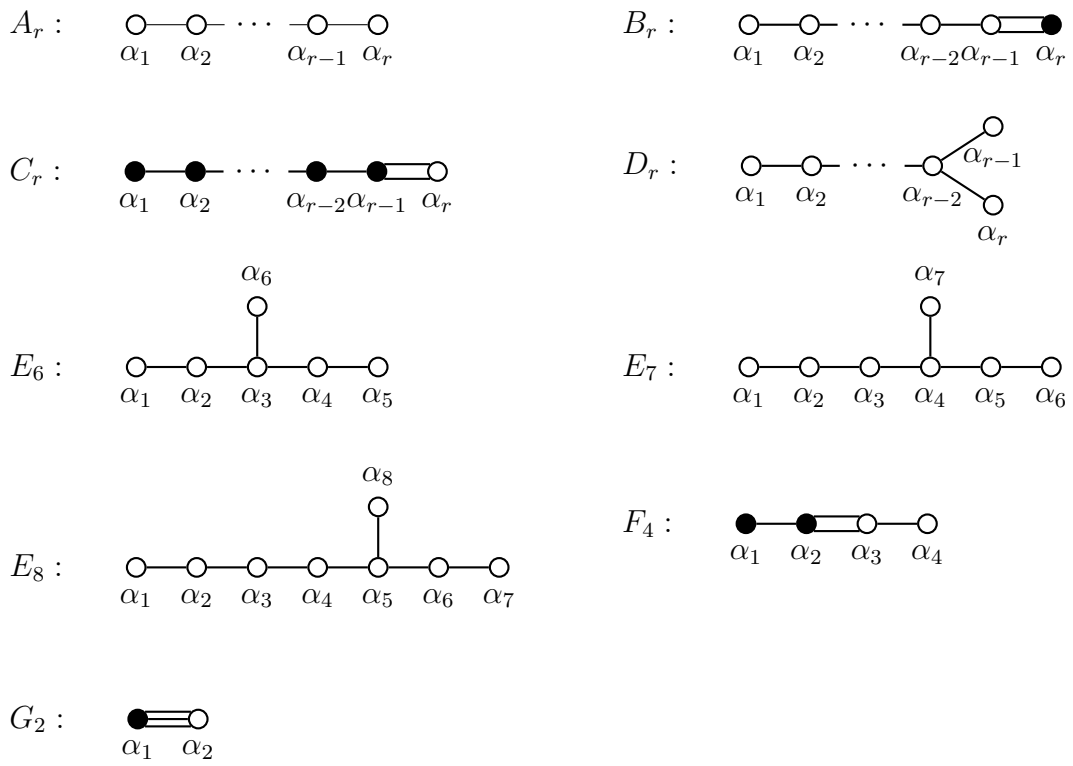

Figure A.0.1: The Dynkin diagrams of semi-simple Lie algebras

Here $N_{\alpha,\beta}$ is the structure constant[1] and we used the notation $\alpha^\vee \cdot H \coloneqq \sum_{a=1}^{r} \alpha^{\vee a} H^a$. The untwisted affine Lie algebra $\mathfrak{g}$ is obtained by the $\mathfrak{g}$-type Dynkin diagram with adding the root $\alpha_0 \coloneqq -\theta$ [132]. Then it can be generated by the generators E_{α_a} $(a = 1, 2, \ldots, r)$ and ζE_{α_0} $(\zeta \in \mathbb{C})$.

A.1 The folding procedures

The non-simply-lace algebras are obtained from simply-laced algebras by folding procedures. Associated with the symmetry of the Dynkin diagram of the simply-laced algebra, which induces the automorphism of the Lie algebra, we relate the roots and the generators of the algebra to that of the non-simply-lace one.

First, let us explain this folding procedure which relates A_{2r-1} and C_r. The roots of

[1]For the structure constants of the exceptional groups, see [129], and the algorithm to obtain them is in [130, 131].

A_{2r-1} are $\alpha_1, \alpha_2, \ldots, \alpha_{2r-1}$. The symmetry of the Dynkin diagram induces automorphism which interchanges the simple roots as $\alpha_a \leftrightarrow \alpha_{2r-a}$. Associated with this symmetry, we relate the simple roots α_a of A_{2r-1} to that of C_r, which we denote β_a, as

$$\beta_a = \frac{1}{2}(\alpha_a + \alpha_{2r-a}), \quad a = 1, \ldots, r-1, \quad \beta_r = \alpha_r. \tag{A.1.1}$$

We denote the generator associated with the simple roots of A_{2r-1} and C_r as $E^{A_{2r-1}}_{\alpha_a}$ and $E^{C_r}_{\beta_a}$, respectively. They are related as

$$E^{C_r}_{\beta_a} = E^{A_{2r-1}}_{\alpha_a} + E^{A_{2r-1}}_{\alpha_{2r-a}}, \quad a = 1, \ldots, r-1, \quad E^{C_r}_{\beta_r} = E^{A_{2r-1}}_{\alpha_r}. \tag{A.1.2}$$

This procedure is illustrated in figure A.1.1.

Figure A.1.1: The folding of A_{2r-1} to C_r

Next, we discuss the relation between D_{r+1} and B_r. The simple roots of D_{r+1} are $\alpha_1, \alpha_\nu, \ldots, \alpha_{r+1}$. The $\mathbf{Z}_2$-symmetry of the Dynkin diagram of D_{r+1} induces the automorphism interchanging the simple roots as $\alpha_r \leftrightarrow \alpha_{r+1}$. Thus, the simple roots β_a of B_r are related by α_a as

$$\beta_a = \alpha_a, \quad a = 1, \ldots, r-1, \quad \beta_r = \frac{1}{2}(\alpha_r + \alpha_{r+1}). \tag{A.1.3}$$

The generators of D_{r+1} and B_r are identified as

$$E^{B_r}_{\beta_a} = E^{D_{r+1}}_{\alpha_a}, \quad a = 1, \ldots, r-1, \quad E^{B_r}_{\beta_r} = E^{D_{r+1}}_{\alpha_r} + E^{D_{r+1}}_{\alpha_{r+1}}. \tag{A.1.4}$$

This folding is depicted in figure A.1.2.

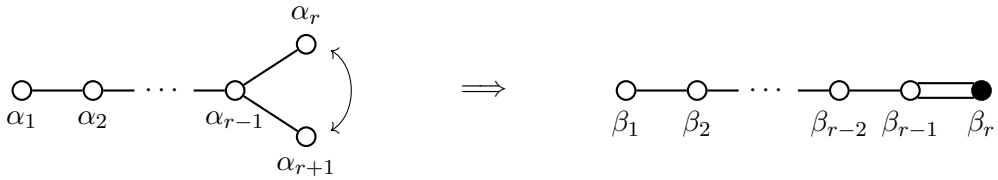

Figure A.1.2: The folding of D_{r+1} to B_r

The F_4 algebra is obtained by folding E_6. Denoting the simple roots of E_6 as $\alpha_1, \ldots, \alpha_6$, since the $\mathbf{Z}_2$-symmetry of the Dynkin diagram of E_6 induces the automorphism exchanging them as $\alpha_a \leftrightarrow \alpha_{6-a}$ $(a = 1, 2)$, the root β_a of F_4 and the generators are related as

$$\beta_4 = \frac{1}{2}(\alpha_1 + \alpha_5), \quad \beta_3 = \frac{1}{2}(\alpha_2 + \alpha_4), \quad \beta_2 = \alpha_3, \quad \beta_1 = \alpha_6, \tag{A.1.5}$$

and

$$E^{F_4}_{\beta_1} = E^{E_6}_{\alpha_1} + E^{E_6}_{\alpha_5}, \quad E^{F_4}_{\beta_2} = E^{E_6}_{\alpha_2} + E^{E_6}_{\alpha_4}, \quad E^{F_4}_{\beta_3} = E^{E_6}_{\alpha_3}, \quad E^{F_4}_{\beta_4} = E^{E_6}_{\alpha_6}, \tag{A.1.6}$$

which is visualized in figure A.1.3.

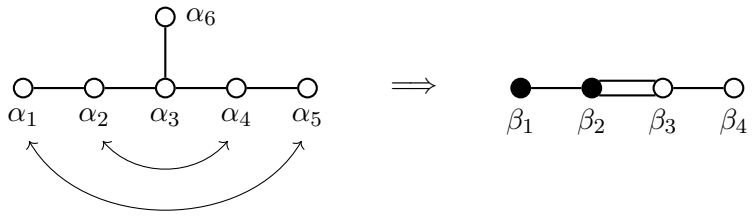

Figure A.1.3: The folding of E_6 to F_4

The algebra D_4 is folded to G_2 by the $\mathbf{Z}_3$-symmetry of the Dynkin diagram of D_4. Let the simple roots of D_4 be $\alpha_1, \ldots, \alpha_4$. The automorphism associated the the symmetry interchanges the roots α_1, α_3 and α_4, which leads the relation to the roots β_a of G_2 as

$$\beta_1 = \frac{1}{3}(\alpha_1 + \alpha_2 + \alpha_3), \quad \beta_2 = \alpha_2. \tag{A.1.7}$$

The identification of the generators is given by

$$E^{G_2}_{\beta_1} = E^{D_4}_{\alpha_1} + E^{D_4}_{\alpha_2} + E^{D_4}_{\alpha_3}, \quad E^{G_2}_{\beta_2} = E^{D_4}_{\alpha_2}. \tag{A.1.8}$$

Figure A.1.4 illustrate this folding procedure.

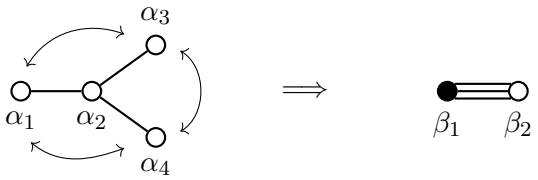

Figure A.1.4: The folding of D_4 to G_2

A.2 The representations

For each weight, we can define the representation of the algebras. Let us denote the fundamental representation on the vector space $V^{(a)}$), whose highest weight is the fundamental weight ω_a, as $\rho^{(a)}$. The vector space $V^{(a)}$ has the basis $\mathbf{e}_i$ $(i = 1, 2, \ldots, \dim V^{(a)})$ which has the weight h_i: $H^b\mathbf{e}_i = (h_i)^b\mathbf{e}_i$. In this section, we summarize the generators of the representations of the simply-laced Lie algebras. The representations of the non-simply-laced algebras are constructed from that of the simply-laced ones by the folding procedures. We show the generators associated with the simple roots α_a and the lowest root α_0. The generators of the negative roots are obtained by transposing that of the positive ones except for the adjoint representation. The Cartan generators are defined from (A.0.2). In the following, we use the matrix $e_{a,b}$ whose (i, j) element is $\delta_{a,i}\delta_{b,j}$.

The representations of A_r The first fundamental representation $(\rho^{(1)}, V^{(1)})$ of A_r is $r + 1$ dimensional. The generators are given by

$$\rho^{(1)}(E_{\alpha_0}) = e_{r+1,1}, \quad \rho^{(1)}(E_{\alpha_a}) = e_{a,a+1}, \quad a = 1, \ldots, r. \tag{A.2.1}$$

The other fundamental representations are constructed from the anti symmetric product of the first fundamental representations i.e. $V^{(a)} = \wedge^a V^{(1)}$. The r-th representation $(\rho^{(r)}, V^{(r)})$ is dual to the first fundamental one. Then, the generators are

$$\rho^{(r)}(E_{\alpha_0}) = e_{r+1,1}, \quad \rho^{(r)}(E_{\alpha_a}) = e_{r+1-a,r+2-a}, \quad a = 1, \ldots, r. \tag{A.2.2}$$

The representations of D_r The first fundamental representation of D_r is $2r$ dimensional, whose generators are given by

$$\begin{aligned} &\rho^{(1)}(E_{\alpha_0}) = e_{2r-1,1} + e_{2r,2}, \quad \rho^{(1)}(E_{\alpha_r}) = e_{r-1,r+1} + e_{r,r+2}, \\ &\rho^{(1)}(E_{\alpha_a}) = e_{a,a+1} + e_{2r-a,2r+1-a}, \quad a = 1, \ldots, r-1. \end{aligned} \tag{A.2.3}$$

The representation $V^{(a)}$ $(a = 1, 2, \ldots, r-2)$ is the anti symmetric product of $V^{(1)}$ in the same way as the A_r case. The representation $V^{(r-1)}$ and $V^{(r)}$ are 2^{r-1} dimensional, which are the spinor and the anti spinor representation, respectively. The generator of the representation $V^{(r-1)}$ is the same as that of $V^{(r)}$ with the swap $E_{\alpha_{r-1}} \leftrightarrow E_{\alpha_r}$.

The representations of E_6 The first fundamental representation is 27 dimensional. The generators are

$$\begin{aligned}
\rho^{(1)}(E_{\alpha_1}) &= e_{1,2} + e_{12,15} + e_{14,17} + e_{16,19} + e_{18,21} + e_{20,22},\\
\rho^{(1)}(E_{\alpha_2}) &= e_{2,3} + e_{10,12} + e_{11,14} + e_{13,16} + e_{21,23} + e_{22,24},\\
\rho^{(1)}(E_{\alpha_3}) &= e_{3,4} + e_{8,10} + e_{9,11} + e_{16,18} + e_{19,21} + e_{24,25},\\
\rho^{(1)}(E_{\alpha_4}) &= e_{4,5} + e_{6,8} + e_{11,13} + e_{14,16} + e_{17,19} + e_{25,26},\\
\rho^{(1)}(E_{\alpha_5}) &= e_{5,7} + e_{8,9} + e_{10,11} + e_{12,14} + e_{15,17} + e_{26,27},\\
\rho^{(1)}(E_{\alpha_6}) &= e_{4,6} + e_{5,8} + e_{7,9} + e_{18,20} + e_{21,22} + e_{23,24},\\
\rho^{(1)}(E_{\alpha_0}) &= e_{20,1} + e_{22,2} + e_{24,3} + e_{25,4} + e_{26,5} + e_{27,7}.
\end{aligned} \tag{A.2.4}$$

The fifth fundamental representation $V^{(5)}$ is given by swapping $E_{\alpha_1} \leftrightarrow E_{\alpha_5}$ and $E_{\alpha_2} \leftrightarrow E_{\alpha_4}$ of the first fundamental representation. The sixth fundamental representation $V^{(6)}$ is the adjoint one, whose dimension is 78. The generators are given by

$$\begin{aligned}
\rho^{(6)}(E_{\alpha_1}) =& e_{4,7} + e_{6,9} + e_{10,12} + e_{11,13} + e_{14,17} + e_{15,19} + e_{18,22} + e_{20,24}\\
&+ e_{25,29} + e_{30,35} - e_{36,37} + 2e_{37,43} - e_{38,43} - e_{44,49} - e_{50,54} - e_{55,59}\\
&- e_{57,61} - e_{60,64} - e_{62,65} - e_{66,68} - e_{67,69} - e_{70,73} - e_{72,75},\\
\rho^{(6)}(E_{\alpha_2}) =& e_{3,4} + e_{5,6} + e_{8,11} + e_{12,16} + e_{17,21} + e_{19,23} + e_{22,26} + e_{24,28}\\
&+ e_{29,34} - e_{30,36} - e_{35,38} - e_{37,44} + 2e_{38,44} - e_{39,44} + e_{43,49} - e_{45,50}\\
&- e_{51,55} - e_{53,57} - e_{56,60} - e_{58,62} - e_{63,67} - e_{68,71} - e_{73,74} - e_{75,76},\\
\rho^{(6)}(E_{\alpha_3}) =& e_{2,3} + e_{6,10} + e_{9,12} + e_{11,14} + e_{13,17} + e_{23,27} - e_{25,30} + e_{26,31} + e_{28,33}\\
&- e_{29,35} - e_{34,39} - e_{38,45} + 2e_{39,45} - e_{40,45} - e_{42,45} + e_{44,50} - e_{46,51}\\
&- e_{48,53} + e_{49,54} - e_{52,56} - e_{62,66} - e_{65,68} - e_{67,70} - e_{69,73} - e_{76,77},\\
\rho^{(6)}(E_{\alpha_4}) =& e_{3,5} + e_{4,6} + e_{7,9} + e_{14,18} + e_{17,22} - e_{20,25} + e_{21,26} - e_{24,29}\\
&+ e_{27,32} - e_{28,34} - e_{33,40} - e_{39,46} + 2e_{40,46} - e_{41,46} + e_{45,51} - e_{47,52}\\
&+ e_{50,55} - e_{53,58} + e_{54,59} - e_{57,62} - e_{61,65} - e_{70,72} - e_{73,75} - e_{74,76},\\
\rho^{(6)}(E_{\alpha_5}) =& e_{5,8} + e_{6,11} + e_{9,13} + e_{10,14} + e_{12,17} - e_{15,20} + e_{16,21} - e_{19,24}\\
&- e_{23,28} - e_{27,33} - e_{32,41} - e_{40,47} + 2e_{41,47} + e_{46,52} + e_{51,56} + e_{55,60}
\end{aligned} \tag{A.2.5}$$

$$
\begin{aligned}
&- e_{58,63} + e_{59,64} - e_{62,67} - e_{65,69} - e_{66,70} - e_{68,73} - e_{71,74},\\
\rho^{(6)}(E_{\alpha_6}) =& e_{1,2} - e_{10,15} - e_{12,19} + e_{14,20} - e_{16,23} + e_{17,24} - e_{18,25} + e_{21,28}\\
&- e_{22,29} - e_{26,34} - e_{31,42} - e_{39,48} + 2e_{42,48} + e_{45,53} + e_{50,57} - e_{51,58}\\
&+ e_{54,61} - e_{55,62} + e_{56,63} - e_{59,65} + e_{60,67} + e_{64,69} - e_{77,78},\\
\rho^{(6)}(E_{\alpha_0}) =& + e_{42,1} + e_{48,2} - e_{59,3} + e_{60,4} + e_{62,5} - e_{63,6} - e_{61,7} + e_{64,8} + e_{65,9}\\
&- e_{66,10} + e_{67,11} - e_{68,12} + e_{69,13} - e_{70,14} - e_{71,15} + e_{73,16} + e_{65,9} - e_{66,10}\\
&+ e_{67,11} - e_{68,12} + e_{69,13} - e_{70,14} - e_{71,15} + e_{73,16} - e_{74,17} + e_{72,18} - e_{75,19}\\
&+ e_{76,20} - e_{77,31} - e_{78,37} - 2e_{78,38} - 3e_{78,39} - 2e_{78,40} - e_{78,41} - 2e_{78,42}.
\end{aligned}
$$

The generators associated with the negative roots are given by

$$\rho^{(6)}(E_{-\alpha_a}) = S\ {}^t\rho^{(6)}(E_{\alpha_a})\ S^{-1}, \tag{A.2.6}$$

where the matrix S is defined by

$$S = \mathbf{1}_{36} \oplus C_{E_6} \oplus \mathbf{1}_{36}. \tag{A.2.7}$$

Appendix B

The TBA equations from the relativistic many-body system

In this appendix, we derive the TBA equations following [133, 134]. The TBA equation is useful to compute the free energy by which we calculated the effective central charge in the main text. Before deriving the TBA, let us explain the relation of the free energy and the effective central charge.

Consider a quantum system on a two dimensional Euclidean space with periodic lengths L and R. If we regard the direction with periodic length L as the space direction, the partition function Z is expressed by the Hamiltonian along the L direction H_L as $Z = \mathrm{tr}\, e^{-RH_L}$. Here the trace is taken over the Hilbert space of the quantum one dimensional system along the L direction. In the same sense, the partition function is also written as $Z = \mathrm{tr}\, e^{-LH_R}$ where H_R is the Hamiltonian along the R direction. If we take the limit $L \to \infty$, the ground state energy $E_0(R)$ of H_R becomes dominant: $Z \simeq e^{-LE_0(R)}$. On the other hand, the limit $L \to \infty$ corresponds to the thermodynamic limit when we think of the L direction as the space direction, and the theory becomes a one dimensional model with the inverse temperature $1/R$. Denoting $f(R)$ as the free energy per unit length, the partition function becomes $Z \simeq e^{-LRf(R)}$. Thus, the ground state energy of a finite volume system $E_0(R)$ and the free energy of a system with inverse temperature $1/R$ are related as

$$E_0(R) = Rf(R). \tag{B.1}$$

In the limit $R \to \infty$, the ground state energy becomes

$$\lim_{R\to\infty} E_0(R) = -\frac{\pi}{6R} c_{eff}, \tag{B.2}$$

where c_{eff} is the effective central charge of the conformal theory which emerges in the UV limit. To see this, consider a conformal field theory with central charge c on the complex plane with coordinate $(z, \overline{z})$. Under the conformal transformation $w = g(z)$ from the complex plane to the torus with circumferences R and L:

$$g(z) = \frac{R}{2\pi} \log z, \tag{B.3}$$

the holomorphic and the anti-holomorphic parts of the stress-energy tensor $T(z)$ and $\overline{T}(\overline{z})$ transform to $T'(w)$ and $\overline{T}(\overline{w})$, respectively as

$$T'(w) = \left(\frac{2\pi}{R}\right)^2 \Big(z^2 T(z) - \frac{c}{24}\Big), \qquad \overline{T}'(\overline{w}) = \left(\frac{2\pi}{R}\right)^2 \Big(\overline{z}^2 T(\overline{z}) - \frac{c}{24}\Big). \tag{B.4}$$

The stress-energy tensor has the mode expansion $T(z) = \sum_n L_n e^{-\frac{2\pi n}{R} z}$ ($\overline{T}(\overline{z}) = \sum_n \overline{L}_n e^{-\frac{2\pi n}{R}\overline{z}}$) where L_n ($\overline{L}_n$) generates the Virasoro algebra with central charge c. Regarding the R direction as the space and integrating $\frac{1}{2\pi}(T(w) + \overline{T}(\overline{w}))$ over the R direction, one obtains the Hamiltonian H:

$$H = \frac{2\pi}{R}(L_0 + \overline{L}_0) - \frac{\pi}{6R} c. \tag{B.5}$$

The partition function of this theory is written as

$$Z = \mathrm{tr} \exp\left[-\frac{2\pi L}{R}\Big(L_0 + \overline{L}_0 - \frac{c}{12}\Big)\right]. \tag{B.6}$$

Thus, the ground state energy $E_0(R)$ in the UV limit is related to the energy of this conformal theory as

$$\lim_{R\to\infty} E_0(R) = \frac{2\pi}{R}(\Delta_{min} + \overline{\Delta}_{min} - \frac{c}{12}) = -\frac{\pi}{6R}(c - 24\Delta_{min}). \tag{B.7}$$

Here Δ_{min} and $\overline{\Delta}_{min}$ represent the minimum conformal dimensions of the operators in this theory. In the last equation, we identified the holomorphic part and the anti-holomorphic part. $c - 24\Delta_{min}$ is nothing but the effective central charge c_{eff}. For the unitary theory, $\Delta_{min} = 0$ and then c_{eff} becomes the central charge.

Now let us derive the TBA equations which compute the free energy $f(R)$ in the above argument. Thus we consider a one dimensional quantum system on a circle with length L. The system is composed of r types of particles, and the number of each type of particle is N_a $(a = 1, 2, \ldots, r)$ with the total number $N = \sum_a N_a$. We set the masses of the particles m_a $(a = 1, 2, \ldots, r)$, so the correlation length is about $\xi \sim 1/m_{min}$ where m_{min} is the smallest mass. Suppose the coordinates of the particles x_i $(i = 1, 2, \ldots, N)$ are sufficiently separated, i.e. $|x_i - x_j| \gg \xi$, and ordered as $x_i < x_j$ $(i < j)$. This ensures that we can ignore the off-shell effects. The wave function of this system is then

$$\Psi(x_1, x_2, \ldots, x_N) = \prod_{i=1}^{N} e^{ip_i x_i}, \tag{B.8}$$

where we denote the momentum of the particle at x_i by p_i. In the following, we impose the integrability of this system. Concretely, we assume that the numbers of the particles conserve and the scattering is purely elastic. Introducing the rapidity θ_i, the relativistic energy and the momentum of the particle at x_i are written as

$$E_i = m_i \cosh\theta_i \qquad p_i = m_i \sinh\theta_i. \tag{B.9}$$

Here $m_i \in \{m_a\}_a$. Consider the scattering which exchanges the ordering of x_i and x_{i+1}. This changes the wave function and we denote the effect of the scattering by S-matrix $S(\theta_i - \theta_j)$. If we move the particle at x_i along the circle with scattering all the other particles once, the wave function becomes

$$e^{ip_i L} \prod_{j \neq i} S(\theta_i - \theta_j) \Psi(x_1, x_2, \ldots, x_N). \tag{B.10}$$

Imposing the periodic boundary condition, we obtain

$$e^{ip_i L} \prod_{j \neq i} S(\theta_i - \theta_j) = 1, \qquad i = 1, 2, \ldots, N, \tag{B.11}$$

which is the Bethe ansatz equation. Taking the suitable amplitude, one recovers the BAE in chapter 2. From here, we consider the system in the thermodynamic limit. In the thermodynamic limit $L \to \infty$, the numbers of the particles also go to infinity

$N_a \to \infty$. Thus it is convenient to introduce the occupied density of the particles $\rho'_a(\theta)$ $(a = 1, 2, \ldots, r)$. The total energy per unit is then calculated by

$$E = \sum_{a=1}^{r} \int_{-\infty}^{\infty} \mathrm{d}\theta \; m_a \cosh\theta \rho'_a(\theta). \tag{B.12}$$

Denoting the S-matrix associated with the scattering of a and b particles with rapidity θ and θ' by $S_{ab}(\theta - \theta')$, the logarithm of the condition (B.11) is written as

$$m_a \sinh\theta + i \sum_{b=1}^{r} \rho'_b \star \log S_{ab}(\theta) = \frac{2\pi n^{(a)}(\theta)}{L}. \tag{B.13}$$

Here $n^{(a)}(\theta)$ is an integer, and $\star$ represents the convolution. Differentiating this equation with respect to the rapidity θ, we obtain

$$m_a \cosh\theta + \sum_{b=1}^{r} \rho'_b \star K_{ab}(\theta) = 2\pi\rho_a(\theta). \tag{B.14}$$

$\rho_a(\theta)$ is the allowed density in the rapidity space, and $K_{ab} \coloneqq -i\frac{\mathrm{d}}{\mathrm{d}\theta}\log S_{ab}(\theta)$, which we called the kernel in the main text. To construct the free energy, let us consider the entropy S. If the particles are fermions, introducing the hole density $\overline{\rho} \coloneqq \rho - \rho'$ and using Stirling's formula, the entropy is

$$S = S_f = \sum_{a=1}^{r} \int \mathrm{d}\theta \; [\rho_a \log\rho_a - \rho'_a \log\rho'_a - \overline{\rho}_a \log\overline{\rho}_a]. \tag{B.15}$$

For the bosonic case, the entropy becomes

$$S = S_b = \sum_{a=1}^{r} \int \mathrm{d}\theta \; [(\rho_a + \rho'_a)\log(\rho_a + \rho'_a) - \rho_a \log\rho_a - \rho'_a \log\rho'_a]. \tag{B.16}$$

Since the temperature is R, The free energy is $f = E - RS$. In the thermodynamic equilibrium, we have to minimize this function. Varying the free energy with respect to the density ρ but with the constraint (B.14), one obtains the conditions for the densities. To write down these, it is convenient to introduce the pseudo-energy $\epsilon_a(\theta)$ which is defined from the densities by

$$e^{-\epsilon_a} \coloneqq \begin{cases} \dfrac{\rho'_a}{\overline{\rho}_a} & \text{for fermionic case,} \\ \dfrac{\rho'_a}{\rho_a + \rho'_a} & \text{for bosonic case.} \end{cases} \tag{B.17}$$

Note that these are equivalently written as

$$\frac{\rho_a'}{\rho_a} = \begin{cases} \dfrac{e^{-\epsilon_a}}{1+e^{-\epsilon_a}} & \text{for fermionic case,} \\ \dfrac{e^{-\epsilon_a}}{1-e^{-\epsilon_a}} & \text{for bosonic case,} \end{cases} \tag{B.18}$$

which are nothing but the distribution functions. In this sense, we call ϵ_a the pseudo-energy. The minimum conditions show the pseudo-energies satisfy the TBA equations

$$\epsilon_a(\theta) = m_a R\cosh\theta \mp \frac{1}{2\pi}\sum_{a=1}^{r} K_{ab} \star \log\bigl(1 \pm e^{-\epsilon_b}\bigr)(\theta). \tag{B.19}$$

Here we take the upper or lower sign depending on the fermions or bosons, respectively. The free energy (multiplied by R) is then

$$Rf(R) = E_0(R) = \mp\frac{1}{2\pi}\sum_{a=1}^{r}\int_{-\infty}^{\infty} \mathrm{d}\theta\; m_a \cosh\theta \log\bigl(1 \pm e^{-\epsilon_a}\bigr). \tag{B.20}$$

In the main text, we used the TBA equations in the kink limit in which the driving term $m_a R\cosh\theta$ becomes $m_a R e^{\theta}$. The TBA equations can be converted into Y-systems from which we derived TBA in the main text. From the asymptotic Y-system, one obtains the condition for the mass of the particles m_a which is the proportionality to the Perron-Frobenius vector. Furthermore, from the asymptotic behaviors of the Y-functions in the UV limit, one can calculate the effective central charge of the underlying conformal theory.

Appendix C

The Cheng's algorithm for the linear problems

In this appendix, we discuss the numerical method to obtain the solutions to the linear problems which we argued in chapter 3 as the formal series expansion around the origin. For the Schrödinger equation, the solution around the origin is obtained by an iterative method which we call the Cheng's algorithm [135]. This method is generalized and used to solve the adjoint ODE in [29], and then we applied it to the (dual) linear problems in [39]. The linear problem we consider in chapter 3 of dimension n has the form

$$\mathcal{L}\Psi(x) = 0, \quad \mathcal{L} = \mathcal{D}[\boldsymbol{q}] + \mathcal{P}, \tag{C.1}$$

where the differential operator $\mathcal{D}[\boldsymbol{q}]$ is defined by

$$\mathcal{D}[\boldsymbol{q}] \coloneqq \mathbf{I}_n \frac{\mathrm{d}}{\mathrm{d}x} - \frac{\boldsymbol{q}}{x}, \quad \boldsymbol{q} = \mathrm{diag}(q_1, \ldots, q_n). \tag{C.2}$$

Here $\sum_{i=1}^{n} q_i = 0$ and $\mathcal{P}$ is the off-diagonal matrix where the elements are the polynomials in x. To obtain the solutions to the linear problem as the formal power series, we introduce the inverse differential operator $\mathbf{L}[\boldsymbol{q}]$ in terms of the action on the vector with monomial elements. Denoting the vector as $\boldsymbol{v} \coloneqq {}^t(x^{p_1}, \ldots, x^{p_n})$, the action of $\mathbf{L}[\boldsymbol{q}]$ on $\boldsymbol{v}$ is given by

$$\mathbf{L}[\boldsymbol{q}]\ \boldsymbol{v} = {}^t\left(\frac{x^{p_1+1}}{p_1+1-q_1}, \ldots, \frac{x^{p_n+1}}{p_1+1-q_n}\right). \tag{C.3}$$

One can easily show that $\mathbf{L}[\boldsymbol{q}]$ is the inverse operator of $\mathcal{D}[\boldsymbol{q}]$:

$$\mathbf{L}[\boldsymbol{q}]\ \mathcal{D}[\boldsymbol{q}]\ \boldsymbol{v} = \mathcal{D}[\boldsymbol{q}]\ \mathbf{L}[\boldsymbol{q}]\ \boldsymbol{v} = \boldsymbol{v}. \tag{C.4}$$

Using the inverse operator, we define the function $\mathcal{X}_i^m$ $(m = 0, 1, \dots)$ iteratively:

$$\mathcal{X}_i^{m+1}(x) = \mathcal{X}_i^0(x) - \mathbf{L}[\boldsymbol{q}]\left(\mathcal{P}\mathcal{X}_i^m(x)\right), \qquad m = 0, 1, 2, \dots, \tag{C.5}$$

where the initial condition is defined by

$$\mathcal{X}_i^0(x) \coloneqq {}^t(0, \dots, \underbrace{x^{q_i}}_{\text{i-th component}}, \dots, 0). \tag{C.6}$$

Taking the limit $m \to \infty$, the function $\mathcal{X}_i(x) \coloneqq \lim_{m\to\infty} \mathcal{X}_i^m(x)$ become the solution $\mathcal{X}_i$ to the linear problem. This can be proven as follows:

$$\begin{aligned} \mathcal{L}\ \mathcal{X}_i(x) &= (\mathcal{D}[\boldsymbol{q}] + \mathcal{P})(\mathcal{X}_i^0(x) - \mathbf{L}[\boldsymbol{q}](\mathcal{P}\mathcal{X}_i(x))) \\ &= \mathcal{P}\big(\mathcal{X}_i^0(x) - \mathcal{X}_i(x) - \mathbf{L}[\boldsymbol{q}](\mathcal{P}\mathcal{X}_i(x))\big) = 0. \end{aligned} \tag{C.7}$$

Here we used $\mathcal{D}[\boldsymbol{q}]\mathcal{X}_i^0(x) = 0$. One can also easily show that $\{\mathcal{X}_1(x), \dots, \mathcal{X}_n(x)\}$ are linearly independent from the asymptotic behavior around the origin.

As an example, let us explain the $E_6^{(1)}$ case. The linear problem for $V^{(1)}$ of $E_6^{(1)}$ is

$$\mathcal{D}[\boldsymbol{q}] = \mathbf{1}_{27}\frac{\mathrm{d}}{\mathrm{d}x} - \frac{\boldsymbol{q}}{x}, \qquad \boldsymbol{q} = \sum_{a=1}^{6} l_a\, \rho^{(1)}(\alpha_a \cdot H), \tag{C.8}$$

$$\begin{aligned} \mathcal{P} = {} & \rho^{(1)}(E_{\alpha_1}) + \sqrt{2}\rho^{(1)}(E_{\alpha_2}) + \sqrt{3}\rho^{(1)}(E_{\alpha_3}) + \sqrt{2}\rho^{(1)}(E_{\alpha_4}) \\ & + \rho^{(1)}(E_{\alpha_5}) + \sqrt{2}\rho^{(1)}(E_{\alpha_6}) + p(x, E)\ \rho^{(1)}(E_{\alpha_0}). \end{aligned} \tag{C.9}$$

For the case in chapter 3, where the potential is $p(x) = x^2 - E$ with the monodromy parameter $l = (5/12, 1/3, 0, -1/3, -5/12, 1/10)$, the highest component of $\mathcal{X}_1$ is

$$\begin{aligned} \chi_{1,1} = {} & x^{5/12} - \frac{160451840000E}{137931559732275309\sqrt{3}}x^{149/12} + \frac{437678816000}{306222694971001484 13\sqrt{3}}x^{173/12} \\ & + \frac{54927641304141824000000000E^2}{123250530950611521206117920934009534567691 03}x^{293/12} + \cdots. \end{aligned} \tag{C.10}$$

The dual linear problem is obtained by replacing $E_{\alpha_a} \to -E_{-\alpha_a}$ in (C.9). The lowest component of $\overline{\mathcal{X}}_1$ becomes

$$\begin{aligned} \bar{\chi}_{1,27} = {} & x^{187/12} - \frac{9697109248000E}{576643307246746695263025 9\sqrt{3}}x^{331/12} \\ & + \frac{5142734920000000}{120930362299627795428928243 83\sqrt{3}}x^{355/12} + \cdots. \end{aligned} \tag{C.11}$$

Evaluating this at the appropriate x_{fixed} and equating to zero, one obtains the zeros of the Q-function $Q^{(1)}(E)$.

Appendix D

Picard-Fuchs operators and quantum corrections for the higher order ODE

In this appendix, we summarize the Picard-Fuchs operators and the quantum corrections for the (A_r, A_1)-type ODE with the quadratic potential $p(x) = u_0x^2 + u_2$ for $r \leq 6$ up to ϵ^{16} order. Since the absence of u_1 i.e. $u_1 = 0$, we use the other expression rather than that we explained in the main text. The corrections are written as

$$\Pi_\gamma^{(n)} = \mathcal{O}^{(n)}(u_0, u_2, \partial_{u_2})(\hat{\Pi}_{a_n})_\gamma, \qquad (\hat{\Pi}_{a_n})_\gamma = \oint_\gamma y^{a_n} \mathrm{d}x, \tag{D.1}$$

where $a_n = 0, 1, \ldots, r$ and the WKB curve is defined by $\Sigma : y^{r+1} = p(x)$. For the odd $r = 2k + 1$ $(k = 0, 1, \ldots)$, a_n is given by

$$\{l_{2n}\}_{n=1,2,\ldots} = \{2k + 1, 2k - 1, \ldots, 1, 2k + 1, \ldots\}. \tag{D.2}$$

For the even $r = 2k$ $(k = 0, 1, \ldots)$, a_n is

$$\{l_{2n}\}_{n=1,2,\ldots} = \{2k, 2k - 2, \ldots, 0, 2k - 1, 2k - 3, \ldots, 1, 2k, \ldots\}. \tag{D.3}$$

The third order: (A_2, A_1) The PF operators $\mathcal{O}^{(n)}(u_0, u_2, \partial_{u_2})$ for the third order ODE are given by

$$\begin{aligned} &\mathcal{O}_2^{\mathrm{PF}} = \frac{u_0}{4}\partial_{u_2}^2, && \mathcal{O}_6^{\mathrm{PF}} = \frac{89u_0^3}{5040}\partial_{u_2}^5, && \mathcal{O}_8^{\mathrm{PF}} = -\frac{211u_0^4}{40320}\partial_{u_2}^7, \\ &\mathcal{O}_{12}^{\mathrm{PF}} = -\frac{2160997u_0^6}{3632428800}\partial_{u_2}^{10}, && \mathcal{O}_{14}^{\mathrm{PF}} = \frac{897629u_0^7}{4151347200}\partial_{u_2}^{12}. \end{aligned} \tag{D.4}$$

The quantum corrections divided by the classical SW periods are given by

$$\begin{aligned}
&\frac{\Pi_\gamma^{(2)}}{(\hat{\Pi}_2)_\gamma} = \frac{7u_0}{144u_2^2}, && \frac{\Pi_\gamma^{(6)}}{(\hat{\Pi}_1)_\gamma} = \frac{21983u_0^3}{1119744u_2^5},\\
&\frac{\Pi_\gamma^{(8)}}{(\hat{\Pi}_2)_\gamma} = \frac{26317819u_0^4}{322486272u_2^7}, && \frac{\Pi_\gamma^{(12)}}{(\hat{\Pi}_1)_\gamma} = \frac{70877384469605u_0^6}{13792092880896u_2^{10}},\\
&\frac{\Pi_\gamma^{(14)}}{(\hat{\Pi}_2)_\gamma} = \frac{429318166799748793u_0^7}{4694326886006784u_2^{12}}.
\end{aligned} \tag{D.5}$$

The fourth order: (A_3, A_1) The PF operators for the fourth order ODE are given by

$$\begin{aligned}
&\mathcal{O}_2^{\mathrm{PF}} = \frac{u_0}{3}\partial_{u_2}^2, && \mathcal{O}_4^{\mathrm{PF}} = -\frac{11u_0^2}{120}\partial_{u_2}^3, && \mathcal{O}_6^{\mathrm{PF}} = \frac{61u_0^3}{1080}\partial_{u_2}^5,\\
&\mathcal{O}_8^{\mathrm{PF}} = -\frac{353u_0^4}{8064}\partial_{u_2}^6, && \mathcal{O}_{10}^{\mathrm{PF}} = \frac{11099u_0^5}{362880}\partial_{u_2}^8, && \mathcal{O}_{12}^{\mathrm{PF}} = -\frac{49707277u_0^6}{2075673600}\partial_{u_2}^9,\\
&\mathcal{O}_{14}^{\mathrm{PF}} = \frac{4828591u_0^7}{230630400}\partial_{u_2}^{11}, && \mathcal{O}_{16}^{\mathrm{PF}} = -\frac{4477909193u_0^8}{219967488000}\partial_{u_2}^{12}.
\end{aligned} \tag{D.6}$$

The quantum corrections divided by the classical SW periods are

$$\begin{aligned}
&\frac{\Pi_\gamma^{(2)}}{(\hat{\Pi}_3)_\gamma} = \frac{5u_0}{48u_2^2}, && \frac{\Pi_\gamma^{(4)}}{(\hat{\Pi}_1)_\gamma} = -\frac{11u_0^2}{512u_2^3},\\
&\frac{\Pi_\gamma^{(6)}}{(\hat{\Pi}_3)_\gamma} = -\frac{4697u_0^3}{73728u_2^5}, && \frac{\Pi_\gamma^{(8)}}{(\hat{\Pi}_1)_\gamma} = \frac{1170195u_0^4}{3670016u_2^6},\\
&\frac{\Pi_\gamma^{(10)}}{(\hat{\Pi}_3)_\gamma} = \frac{266764465u_0^5}{75497472u_2^8}, && \frac{\Pi_\gamma^{(12)}}{(\hat{\Pi}_1)_\gamma} = -\frac{122528437805u_0^6}{2952790016u_2^9},\\
&\frac{\Pi_\gamma^{(14)}}{(\hat{\Pi}_3)_\gamma} = -\frac{61815211551765u_0^7}{55834574848u_2^{11}}, && \frac{\Pi_\gamma^{(16)}}{(\hat{\Pi}_1)_\gamma} = \frac{15168742752828973u_0^8}{549755813888u_2^{12}}.
\end{aligned} \tag{D.7}$$

The fifth order: (A_4, A_1) The PF operators for the fifth order ODE are given by

$$\begin{aligned}
&\mathcal{O}_2^{\mathrm{PF}} = \frac{5u_0}{12}\partial_{u_2}^2, && \mathcal{O}_4^{\mathrm{PF}} = -\frac{13u_0^2}{72}\partial_{u_2}^3, && \mathcal{O}_8^{\mathrm{PF}} = -\frac{3889u_0^4}{18144}\partial_{u_2}^6,\\
&\mathcal{O}_{10}^{\mathrm{PF}} = \frac{8177u_0^5}{28512}\partial_{u_2}^7, && \mathcal{O}_{12}^{\mathrm{PF}} = -\frac{5801857u_0^6}{13837824}\partial_{u_2}^9, && \mathcal{O}_{14}^{\mathrm{PF}} = \frac{6172661u_0^7}{8491392}\partial_{u_2}^{10}.
\end{aligned} \tag{D.8}$$

The quantum corrections divided by the classical SW periods are

$$\begin{aligned}
&\frac{\Pi_\gamma^{(2)}}{(\hat{\Pi}_4)_\gamma} = \frac{13u_0}{80u_2^2}, && \frac{\Pi_\gamma^{(4)}}{(\hat{\Pi}_2)_\gamma} = -\frac{143u_0^2}{8000u_2^3},\\
&\frac{\Pi_\gamma^{(8)}}{(\hat{\Pi}_3)_\gamma} = -\frac{306425977u_0^4}{672000000u_2^6}, && \frac{\Pi_\gamma^{(10)}}{(\hat{\Pi}_1)_\gamma} = \frac{39003856619u_0^5}{2880000000u_2^7},\\
&\frac{\Pi_\gamma^{(12)}}{(\hat{\Pi}_4)_\gamma} = \frac{1965108059811387u_0^6}{5632000000000u_2^9}, && \frac{\Pi_\gamma^{(14)}}{(\hat{\Pi}_2)_\gamma} = -\frac{57186073300864563u_0^7}{16640000000000u_2^{10}}.
\end{aligned} \tag{D.9}$$

The sixth order: (A_5, A_1) The PF operators for the sixth order ODE are given by

$$\begin{aligned}
&\mathcal{O}_2^{\mathrm{PF}} = \frac{u_0}{2}\partial_{u_2}^2, && \mathcal{O}_6^{\mathrm{PF}} = \frac{5135u_0^3}{12096}\partial_{u_2}^4, && \mathcal{O}_8^{\mathrm{PF}} = -\frac{75709u_0^4}{96768}\partial_{u_2}^6,\\
&\mathcal{O}_{12}^{\mathrm{PF}} = -\frac{50444678155u_0^6}{11955879936}\partial_{u_2}^8, && \mathcal{O}_{14}^{\mathrm{PF}} = \frac{271675168801u_0^7}{23911759872}\partial_{u_2}^{10}.
\end{aligned} \tag{D.10}$$

The quantum corrections divided by the classical SW periods are

$$\begin{aligned}
&\frac{\Pi_\gamma^{(2)}}{(\hat{\Pi}_5)_\gamma} = \frac{2u_0}{9u_2^2}, && \frac{\Pi_\gamma^{(6)}}{(\hat{\Pi}_1)_\gamma} = -\frac{5135u_0^3}{17496u_2^4},\\
&\frac{\Pi_\gamma^{(8)}}{(\hat{\Pi}_5)_\gamma} = -\frac{4163995u_0^4}{1102248u_2^6}, && \frac{\Pi_\gamma^{(12)}}{(\hat{\Pi}_1)_\gamma} = \frac{4792244424725u_0^6}{3367210176u_2^8},\\
&\frac{\Pi_\gamma^{(14)}}{(\hat{\Pi}_5)_\gamma} = \frac{2655624775029775u_0^7}{35814871872u_2^{10}}.
\end{aligned} \tag{D.11}$$

Note that for the quadratic potential, the quantum corrections of order $n = 6k + 4$ $(k = 0, 1, \dots)$ vanish while they do not vanish for the general potential.

The seventh order: (A_6, A_1) The PF operators for the seventh order ODE are given by

$$\begin{aligned}
&\mathcal{O}_2^{\mathrm{PF}} = \frac{7u_0}{12}\partial_{u_2}^2, && \mathcal{O}_4^{\mathrm{PF}} = -\frac{119u_0^2}{240}\partial_{u_2}^3,\\
&\mathcal{O}_6^{\mathrm{PF}} = \frac{29u_0^3}{30}\partial_{u_2}^4, && \mathcal{O}_{10}^{\mathrm{PF}} = \frac{765289u_0^5}{95040}\partial_{u_2}^7,\\
&\mathcal{O}_{12}^{\mathrm{PF}} = -\frac{171906011u_0^6}{5702400}\partial_{u_2}^8, && \mathcal{O}_{14}^{\mathrm{PF}} = \frac{434398427u_0^7}{3706560}\partial_{u_2}^9,\\
&\mathcal{O}_{16}^{\mathrm{PF}} = -\frac{3131950604279u_0^8}{5930496000}\partial_{u_2}^{11}.
\end{aligned} \tag{D.12}$$

The quantum corrections divided by the classical SW periods are

$$\begin{aligned}
\frac{\Pi_\gamma^{(2)}}{(\hat{\Pi}_6)_\gamma} &= \frac{95u_0}{336u_2^2}, & \frac{\Pi_\gamma^{(4)}}{(\hat{\Pi}_4)_\gamma} &= \frac{221u_0^2}{6272u_2^3}, \\
\frac{\Pi_\gamma^{(6)}}{(\hat{\Pi}_2)_\gamma} &= -\frac{168113u_0^3}{384160u_2^4}, & \frac{\Pi_\gamma^{(10)}}{(\hat{\Pi}_5)_\gamma} &= -\frac{428983295585u_0^5}{2891341824u_2^7}, \\
\frac{\Pi_\gamma^{(12)}}{(\hat{\Pi}_3)_\gamma} &= \frac{63908958440313493u_0^6}{37402397835264u_2^8}, & \frac{\Pi_\gamma^{(14)}}{(\hat{\Pi}_1)_\gamma} &= \frac{5422964705164303925u_0^7}{17189990924288u_2^9}, \\
\frac{\Pi_\gamma^{(16)}}{(\hat{\Pi}_6)_\gamma} &= \frac{506426186528223207627 59u_0^8}{1692552952545280u_2^{11}}.
\end{aligned} \tag{D.13}$$

Appendix E

Wall-crossings for (A_2, A_3) from the minimal to the maximal chamber

In this appendix, we write down the TBA equations in each chamber from the minimal to the maximal for the (A_2, A_3)-type ODE. The path and the walls of the wall-crossing are in chapter 7. Same as in chapter 7, we express the TBA equations by the intersection matrices together with the definitions of the Y-functions. Since $I^- = {}^tI^+$, we only show the matrices I and I^+. We also illustrate the charges on the complex plane, which may be helpful to see the relation to the wall-crossing of the $\mathcal{N} = 2$ theory.

The first wall-crossing

After the first wall whose condition is (7.3.2), the new Y-functions are defined by

$$\begin{aligned} &Y_1^{(1)}(\theta) = Y_1(\theta)\big(1 + \frac{1}{Y_2(\theta - \frac{\pi i}{3})}\big), \quad Y_2^{(1)}(\theta) = Y_2(\theta)\big(1 + \frac{1}{Y_1(\theta + \frac{\pi i}{3})}\big), \\ &Y_{12}^{(1)}(\theta) = \frac{1 + \frac{1}{Y_2(\theta - \frac{\pi i}{3})} + \frac{1}{Y_1(\theta)}}{\frac{1}{Y_1(\theta)Y_2(\theta - \frac{\pi i}{3})}}, \quad Y_3^{(1)}(\theta) = Y_3(\theta), \end{aligned} \tag{E.1}$$

which satisfy the relation (7.1.6). The intersection matrices of the TBA equation in this chamber read

$$I = \begin{pmatrix} -1 & 1 & & \\ 1 & -1 & 1 & \\ & 1 & -1 & \\ & & & -1 \end{pmatrix}, \qquad I^+ = \begin{pmatrix} 0 & & & \\ & 0 & & \\ & & 0 & 1 \\ -1 & 1 & & 0 \end{pmatrix}. \tag{E.2}$$

Here the entries are ordered from the top to the bottom as $1, 2, 3, 12$. The new mass is given by $m_{12} \coloneqq |m_{12}|e^{i\phi_{12}} \coloneqq m_1 + e^{-\frac{\pi}{3}} m_2$. The Y-functions and the WKB periods are related by

$$\begin{aligned} \log Y_1^{(1)}(\theta) &= e^{\theta}\Pi_{\gamma_{1,1}}(\theta), & \log Y_2^{(1)}(\theta) &= e^{\frac{\pi i}{3}} e^{\theta}\Pi^{[-1]}_{\gamma_{3,2}}(\theta), \\ \log Y_3^{(1)}(\theta) &= e^{\frac{2\pi i}{3}} e^{\theta}\Pi^{[-2]}_{\gamma_{2,3}}(\theta), & \log Y_{12}^{(1)}(\theta) &= e^{\theta}\Pi_{\gamma_{1,1}+\gamma_{3,2}}(\theta). \end{aligned} \tag{E.3}$$

We depict the charges $\Pi^{(0)}_{\gamma_{1,1}}, \Pi^{(0)}_{\gamma_{3,2}}, \Pi^{(0)}_{\gamma_{3,3}}, \Pi^{(0)}_{\gamma_{1,2}}$ and $\Pi^{(0)}_{\gamma_{1,1}+\gamma_{3,2}}$ in figure D.1. At the wall, the classical periods $\Pi^{(0)}_{\gamma_{1,1}}$ and $\Pi^{(0)}_{\gamma_{3,2}}$ align and the new BPS particle with charge $\Pi^{(0)}_{\gamma_{1,1}+\gamma_{3,2}}$ emerges, which is illustrated by the arrow label by e in the figure. We also show the vector of $\Pi^{(0)}_{\gamma_{2,1}+\gamma_{1,2}} = e^{\frac{2\pi}{3}}\Pi^{(0)}_{\gamma_{1,1}+\gamma_{3,2}}$, which is labeled by f for the illustration of the later wall-crossings.

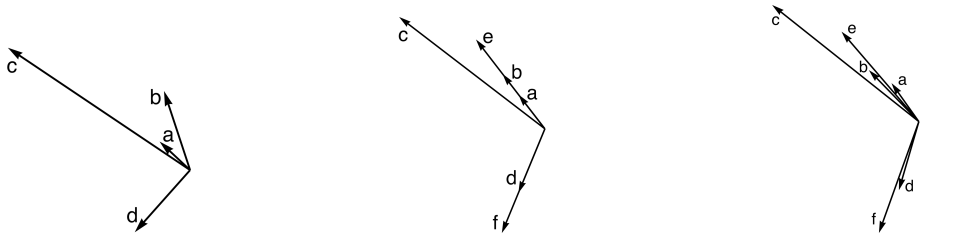

(a) $t = 0.061571...$ (b) $t = 0.123142...$ (c) $t = 0.143414...$

Figure D.1: The classical periods in the process of the first wall-crossing. The vectors represents the classical periods on the complex plane (a) before, (b) at and (c) after the wall-crossing. The arrows labeled by a, b, c, d, e and f represent the classical periods $\Pi^{(0)}_{\gamma_{1,1}}, \Pi^{(0)}_{\gamma_{3,2}}, \Pi^{(0)}_{\gamma_{3,3}}, \Pi^{(0)}_{\gamma_{1,2}}, \Pi^{(0)}_{\gamma_{1,1}+\gamma_{3,2}}$ and $\Pi^{(0)}_{\gamma_{2,1}+\gamma_{1,2}}$, respectively.

The second wall-crossing

For the second wall-crossing, we define the new Y-functions by

$$\begin{aligned} Y_3^{(2)}(\theta) &= Y_3^{(1)}(\theta)\big(1 + \frac{1}{Y_2^{(1)}(\theta - \frac{\pi i}{3})}\big), & Y_2^{(2)}(\theta) &= Y_2^{(1)}(\theta)\big(1 + \frac{1}{Y_3^{(1)}(\theta + \frac{\pi i}{3})}\big), \\ Y_{23}^{(2)}(\theta) &= \frac{1 + \frac{1}{Y_2^{(1)}(\theta - \frac{\pi i}{3})} + \frac{1}{Y_3^{(1)}(\theta)}}{\frac{1}{Y_3^{(1)}(\theta)Y_2^{(1)}(\theta - \frac{\pi i}{3})}}, & Y_{\text{others}}^{(2)}(\theta) &= Y_{\text{others}}^{(1)}(\theta), \end{aligned} \tag{E.4}$$

which satisfy the relation

$$\begin{aligned} 1+\frac{1}{Y_3^{(1)}(\theta)} &= \big(1+\frac{1}{Y_3^{(2)}(\theta)}\big)\big(1+\frac{1}{Y_{23}^{(2)}(\theta)}\big), \\ 1+\frac{1}{Y_2^{(1)}(\theta)} &= \big(1+\frac{1}{Y_2^{(2)}(\theta)}\big)\big(1+\frac{1}{Y_{23}^{(2)}(\theta+\frac{\pi i}{3})}\big) \\ Y_3^{(2)}(\theta)Y_2^{(2)}(\theta-\frac{\pi i}{3}) &= Y_{23}^{(2)}(\theta)\big(1+\frac{1}{Y_{23}^{(2)}(\theta)}\big). \end{aligned} \tag{E.5}$$

From this relation, one obtain the TBA equations in this chamber, whose intersection matrices are

$$I=\begin{pmatrix} -1 & 1 & & & & \\ 1 & -1 & 1 & & & \\ & 1 & -1 & & & \\ & & & -1 & & \\ & & & & -1 & \end{pmatrix}, \qquad I^+=\begin{pmatrix} 0 & & & & & 1 \\ & 0 & & & & \\ & & & 0 & 1 & \\ -1 & 1 & & & 0 & \\ & 1 & -1 & & & 0 \end{pmatrix}. \tag{E.6}$$

Here the entries are ordered as $1, 2, 3, 12, 23$. The new mass is $m_{23} \coloneqq |m_{23}|e^{i\phi_{23}} \coloneqq m_3 + e^{-\frac{\pi i}{3}} m_2$. The identification between the WKB periods and the Y-functions are the same one in (E.3) with replacing $Y^{(1)} \to Y^{(2)}$ and that for $Y_{23}^{(2)}$:

$$\log Y_{23}^{(2)}(\theta) = e^{\theta}\Pi_{\gamma_{3,2}+\gamma_{3,3}}(\theta). \tag{E.7}$$

The charge vector in this wall-crossing process is illustrated in figure D.2. At the wall, $\Pi^{(0)}_{\gamma_{3,2}}$ (b) and $\Pi^{(0)}_{\gamma_{3,3}}$ (c) align and the new charge $\Pi^{(0)}_{\gamma_{3,2}+\gamma_{3,3}}$ (g) emerges. In the figure, we also draw the charge $\Pi^{(0)}_{\gamma_{1,2}+\gamma_{1,3}} = e^{\frac{2\pi i}{3}}\Pi^{(0)}_{\gamma_{3,2}+\gamma_{3,3}}$ (h) for the later wall-crossing.

The third wall-crossing

The new Y-functions for this chamber is given by

$$\begin{aligned} Y_{1,3}^{(3)}(\theta) &= Y_{1,3}^{(2)}(\theta)\big(1+\frac{1}{Y_{12}^{(2)}(\theta)}\big) \quad Y_{12}^{(3)}(\theta) = Y_{12}^{(2)}(\theta)\big(1+\frac{1}{Y_{1,3}^{(2)}(\theta)}\big) \\ Y_{312}^{(3)}(\theta) &= \frac{1+\frac{1}{Y_{1,3}^{(2)}(\theta)}+\frac{1}{Y_{12}^{(2)}(\theta)}}{\frac{1}{Y_{1,3}^{(2)}(\theta)Y_{12}^{(2)}(\theta)}}, \qquad Y_{\text{other}}^{(3)} = Y_{\text{other}}^{(2)}, \end{aligned} \tag{E.8}$$

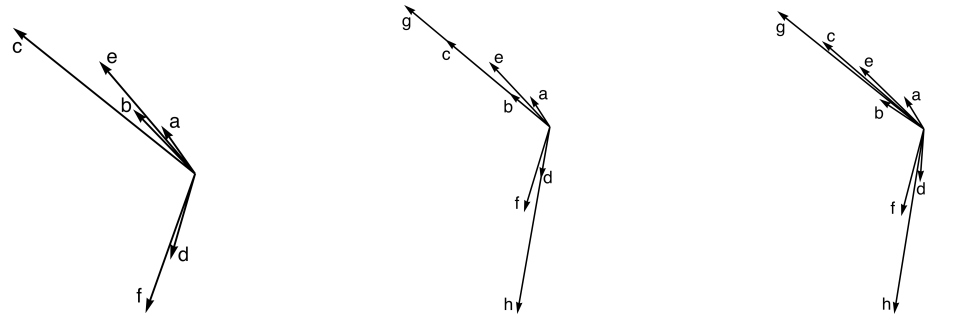

(a) $t = 0.143414...$ (b) $t = 0.163685...$ (c) $t = 0.18316...$

Figure D.2: The classical periods in the process of the second wall-crossing. The vectors represents the classical periods on the complex plane (a) before, (b) at and (c) after the wall-crossing. The arrows labeled by a, b, c, d, e, f, g and h represent the classical periods $\Pi^{(0)}_{\gamma_{1,1}}, \Pi^{(0)}_{\gamma_{3,2}}, \Pi^{(0)}_{\gamma_{3,3}}, \Pi^{(0)}_{\gamma_{1,2}}, \Pi^{(0)}_{\gamma_{1,1}+\gamma_{3,2}}, \Pi^{(0)}_{\gamma_{2,1}+\gamma_{1,2}}, \Pi^{(0)}_{\gamma_{3,2}+\gamma_{3,3}}$ and $\Pi^{(0)}_{\gamma_{1,2}+\gamma_{1,3}}$, respectively.

which satisfy the relation

$$1+\frac{1}{Y_3^{(2)}(\theta)}=\big(1+\frac{1}{Y_3^{(3)}(\theta)}\big)\big(1+\frac{1}{Y_{312}^{(3)}(\theta)}\big),\quad 1+\frac{1}{Y_{12}^{(2)}(\theta)}=\big(1+\frac{1}{Y_{12}^{(3)}(\theta)}\big)\big(1+\frac{1}{Y_{312}^{(3)}(\theta)}\big)$$
$$Y_3^{(3)}(\theta)Y_{12}^{(3)}(\theta)=Y_{312}^{(3)}\big(1+\frac{1}{Y_{312}^{(3)}(\theta)}\big). \tag{E.9}$$

The intersection matrices of the TBA equations are obtained as

$$I=\begin{pmatrix} -1 & 1 & & & & & \\ 1 & -1 & 1 & & & & 1 \\ & 1 & -1 & & & & \\ & & & -1 & & & \\ & & & & -1 & & \\ & 1 & & & & & -1 \end{pmatrix},\qquad I^+=\begin{pmatrix} 0 & & & & & 1 & \\ & 0 & & & & & \\ & & 0 & 1 & & & \\ -1 & 1 & & 0 & & -1 & \\ & 1 & -1 & & 0 & -1 & \\ -1 & 1 & -1 & & & 0 & \end{pmatrix}. \tag{E.10}$$

Here the entries are ordered as $1, 2, 3, 12, 23, 312$. The new mass is defined by $m_{312} \coloneqq |m_{312}|e^{i\phi_{312}} \coloneqq m_3 + m_{12}$. The identification with the new Y-function with the WKB period is

$$\log Y_{312}^{(3)} = e^{\theta}\Pi_{\gamma_{1,1}+\gamma_{3,2}+\gamma_{3,3}}(\theta). \tag{E.11}$$

The process of this wall-crossing is visualized in figure D.3, in which at the wall, $\Pi^{(0)}_{\gamma_{3,3}}$ (c) and $\Pi^{(0)}_{\gamma_{1,1}+\gamma_{3,2}}$ (e) align, then the new charge $\Pi^{(0)}_{\gamma_{1,1}+\gamma_{3,2}+\gamma_{3,3}}$ (i) emerges.

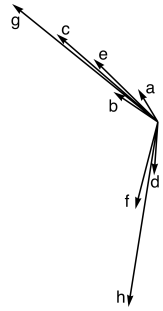

(a) $t = 0.18316...$

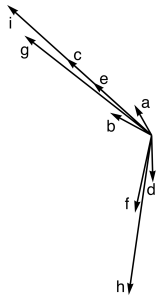

(b) $t = 0.202635...$

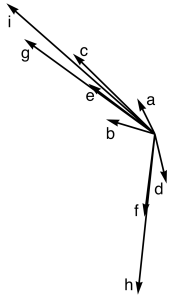

(c) $t = 0.246326...$

Figure D.3: The classical periods in the process of the third wall-crossing. The vectors represents the classical periods on the complex plane (a) before, (b) at and (c) after the wall-crossing. The arrows labeled by a, b, c, d, e, f, g, h and i represent the classical periods $\Pi^{(0)}_{\gamma_{1,1}}, \Pi^{(0)}_{\gamma_{3,2}}, \Pi^{(0)}_{\gamma_{3,3}}, \Pi^{(0)}_{\gamma_{1,2}}, \Pi^{(0)}_{\gamma_{1,1}+\gamma_{3,2}}, \Pi^{(0)}_{\gamma_{2,1}+\gamma_{1,2}}, \Pi^{(0)}_{\gamma_{3,2}+\gamma_{3,3}}, \Pi^{(0)}_{\gamma_{1,2}+\gamma_{1,3}}$ and $\Pi^{(0)}_{\gamma_{1,1}+\gamma_{3,2}+\gamma_{3,3}}$, respectively.

The fourth wall-crossing

The new Y-functions are

$$\begin{aligned} Y_1^{(4)}(\theta) &= Y_1^{(3)}(\theta)\big(1+\frac{1}{Y_2^{(3)}(\theta-\frac{2\pi i}{3})}\big), \quad Y_2^{(4)}(\theta) = Y_2^{(3)}(\theta)\big(1+\frac{1}{Y_1^{(3)}(\theta+\frac{2\pi i}{3})}\big) \\ Y^{(4)}_{\widetilde{12}}(\theta) &= \frac{1+\frac{1}{Y_2^{(3)}(\theta-\frac{2\pi i}{3})}+\frac{1}{Y_1^{(3)}(\theta)}}{\frac{1}{Y_1^{(3)}(\theta)Y_2^{(3)}(\theta-\frac{2\pi i}{3})}}, \qquad Y^{(4)}_{\text{other}}(\theta) = Y^{(3)}_{\text{other}}(\theta), \end{aligned} \tag{E.12}$$

which satisfy

$$1+\frac{1}{Y^{(3)}_{1,1}(\theta)} = \big(1+\frac{1}{Y^{(4)}_{1,1}(\theta)}\big)\big(1+\frac{1}{Y^{(4)}_{\widetilde{12}}(\theta)}\big), \; 1+\frac{1}{Y^{(3)}_{1,2}(\theta)} = 1+\frac{1}{Y^{(4)}_{1,2}(\theta)}\big)\big(1+\frac{1}{Y^{(4)}_{\widetilde{12}}(\theta+\frac{2\pi i}{3})}\big),$$
$$Y^{(4)}_{1,1}(\theta)Y^{(4)}_{1,2}(\theta-\frac{2\pi i}{3}) = Y^{(4)}_{\widetilde{12}}(\theta)\big(1+\frac{1}{Y^{(4)}_{\widetilde{12}}(\theta)}\big). \tag{E.13}$$

The intersection matrices read

$$I = \begin{pmatrix} -1 & 1 & & & & & -1 \\ 1 & -1 & 1 & & & 1 & 1 \\ & 1 & -1 & & & & \\ & & & -1 & & & -1 \\ & & & & -1 & & \\ & 1 & & & & -1 & 2 \\ -1 & 1 & & -1 & & 2 & -3 \end{pmatrix}, \quad I^+ = \begin{pmatrix} 0 & & & & 1 & & \\ & 0 & & & & & \\ & & 0 & 1 & & & \\ -1 & 1 & & 0 & & -1 & -1 \\ & 1 & -1 & & 0 & -1 & -1 \\ -1 & 1 & -1 & & & 0 & \\ -1 & 1 & -1 & & & & 0 \end{pmatrix}. \tag{E.14}$$

Here the entries are arrayed in the order $1, 2, 3, 12, 23, 312, \widetilde{12}$. The new mass is $m_{\widetilde{12}} := |m_{\widetilde{12}}|e^{i\phi_{\widetilde{12}}} := m_1 + e^{-\frac{2\pi i}{3}} m_2$, and the identification of $Y^{(4)}_{\widetilde{12}}$ with the periods becomes

$$\log Y^{(4)}_{\widetilde{12}} = e^{\theta} \Pi_{\gamma_{1,1}-\gamma_{1,2}}(\theta). \tag{E.15}$$

Figure D.4 shows the plots of the charge in this wall-crossing process. At the wall, the two charges $\Pi^{(0)}_{\gamma_{1,1}}$ (a) and $\Pi^{(0)}_{\gamma_{1,2}}$ (d) align, and the new charge $\Pi^{(0)}_{\gamma_{1,1}-\gamma_{1,2}}$ (j) emerges.

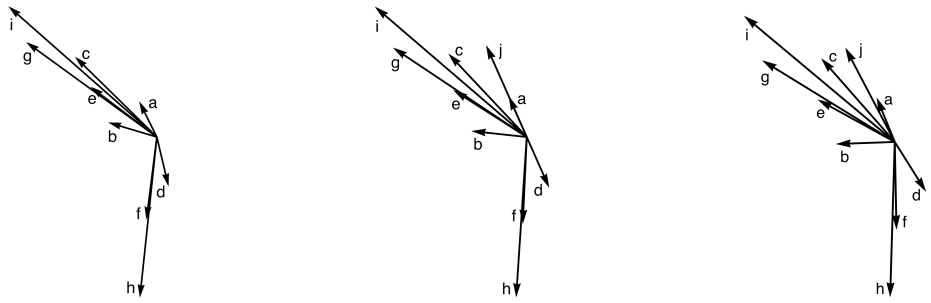

(a) $t = 0.246326...$ (b) $t = 0.290017...$ (c) $t = 0.328471...$

Figure D.4: The classical periods in the process of the fourth wall-crossing. The vectors represents the classical periods on the complex plane (a) before, (b) at and (c) after the wall-crossing. The arrows labeled by $a, b, c, d, e, f, g, h, i$ and j represent the classical periods $\Pi^{(0)}_{\gamma_{1,1}}, \Pi^{(0)}_{\gamma_{3,2}}, \Pi^{(0)}_{\gamma_{3,3}}, \Pi^{(0)}_{\gamma_{1,2}}, \Pi^{(0)}_{\gamma_{1,1}+\gamma_{3,2}}, \Pi^{(0)}_{\gamma_{2,1}+\gamma_{1,2}}, \Pi^{(0)}_{\gamma_{3,2}+\gamma_{3,3}}, \Pi^{(0)}_{\gamma_{1,2}+\gamma_{1,3}}, \Pi^{(0)}_{\gamma_{1,1}+\gamma_{3,2}+\gamma_{3,3}}$ and $\Pi^{(0)}_{\gamma_{1,1}-\gamma_{1,2}}$, respectively.

The fifth wall-crossing

The Y-function in this chamber is defined by

$$\begin{aligned} Y^{(5)}_3(\theta) &= Y^{(4)}_3(\theta)\big(1 + \frac{1}{Y^{(4)}_2(\theta - \frac{2\pi i}{3})}\big), \quad Y^{(5)}_2(\theta) = Y^{(4)}_2(\theta)\big(1 + \frac{1}{Y^{(4)}_3(\theta + \frac{2\pi i}{3})}\big) \\ Y^{(5)}_{\widetilde{23}}(\theta) &= \frac{1 + \frac{1}{Y^{(4)}_2(\theta - \frac{2\pi i}{3})} + \frac{1}{Y^{(4)}_{1,3}(\theta)}}{\frac{1}{Y^{(4)}_3(\theta) Y^{(4)}_2(\theta - \frac{2\pi i}{3})}}, \qquad Y^{(5)}_{\text{other}}(\theta) = Y^{(4)}_{\text{other}}(\theta), \end{aligned} \tag{E.16}$$

The intersection matrices are given by

$$I = \begin{pmatrix} -1 & 1 & & & & & -1 & \\ 1 & -1 & 1 & & & 1 & 1 & 1 \\ & 1 & -1 & & & & & -1 \\ & & & -1 & & & -1 & \\ & & & & -1 & & & -1 \\ & 1 & & & & -1 & 2 & -2 \\ -1 & 1 & & -1 & & 2 & -3 & -2 \\ & 1 & -1 & & -1 & -2 & -2 & -3 \end{pmatrix}, \quad I^+ = \begin{pmatrix} 0 & & & & 1 & & & \\ & 0 & & & & & & \\ & & 0 & 1 & & & & \\ -1 & 1 & & 0 & & -1 & -1 & -1 \\ & 1 & -1 & & 0 & -1 & -1 & -1 \\ -1 & 1 & -1 & & & 0 & & \\ -1 & 1 & -1 & & & & 0 & \\ -1 & 1 & -1 & & & & & 0 \end{pmatrix}, \tag{E.17}$$

whose entries are ordered as $1, 2, 3, 12, 23, 312, \widetilde{12}, \widetilde{23}$. The new mass is defined by $m_{\widetilde{23}} := |m_{\widetilde{23}}|e^{i\phi_{\widetilde{23}}} := m_3 + e^{-\frac{2\pi i}{3}} m_2$. The identification of $Y_{\widetilde{23}}$ with periods is

$$\log Y^{(5)}_{\widetilde{23}} = e^{\theta} \Pi_{\gamma_{3,3}-\gamma_{1,2}}(\theta). \tag{E.18}$$

The charges are plotted in figure D.5. In the process, the classical periods $\Pi^{(0)}_{\gamma_{3,3}}$ (c) and $\Pi^{(0)}_{\gamma_{1,2}}$ (d) align, and then the new period $\Pi^{(0)}_{\gamma_{3,3}-\gamma_{1,2}}$ (k) emerges.

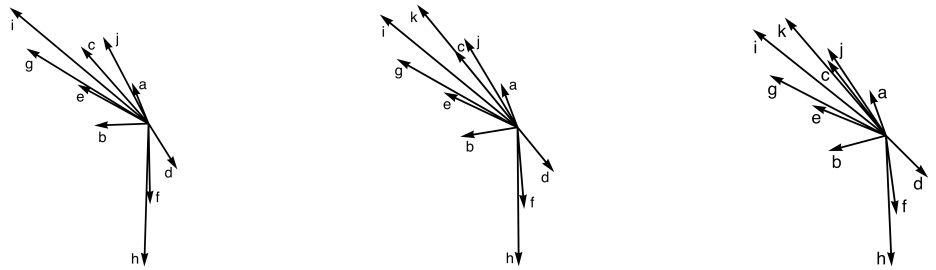

(a) $t = 0.328471...$ (b) $t = 0.366924...$ (c) $t = 0.400536...$

Figure D.5: The classical periods in the process of the fifth wall-crossing. The vectors represents the classical periods on the complex plane (a) before, (b) at and (c) after the wall-crossing. The arrows labeled by $a, b, c, d, e, f, g, h, i, j$ and k represent the classical periods $\Pi^{(0)}_{\gamma_{1,1}}, \Pi^{(0)}_{\gamma_{3,2}}, \Pi^{(0)}_{\gamma_{3,3}}, \Pi^{(0)}_{\gamma_{1,2}}, \Pi^{(0)}_{\gamma_{1,1}+\gamma_{3,2}}, \Pi^{(0)}_{\gamma_{2,1}+\gamma_{1,2}}, \Pi^{(0)}_{\gamma_{3,2}+\gamma_{3,3}}, \Pi^{(0)}_{\gamma_{1,2}+\gamma_{1,3}}, \Pi^{(0)}_{\gamma_{1,1}+\gamma_{3,2}+\gamma_{3,3}}, \Pi^{(0)}_{\gamma_{1,1}-\gamma_{1,2}}$ and $\Pi^{(0)}_{\gamma_{3,3}-\gamma_{1,2}}$, respectively.

The sixth wall-crossing

In this chamber, we introduce the Y-functions by

$$\begin{aligned} Y_3^{(6)}(\theta) =& Y_3^{(5)}(\theta)\big(1+\frac{1}{Y_{\widetilde{12}}^{(5)}(\theta)}\big), \quad Y_{\widetilde{12}}^{(6)}(\theta) = Y_{\widetilde{12}}^{(5)}(\theta)\big(1+\frac{1}{Y_3^{(5)}(\theta)}\big) \\ Y_{\widehat{312}}^{(6)}(\theta) =& \frac{1+\frac{1}{Y_3^{(5)}(\theta)}+\frac{1}{Y_{\widetilde{12}}^{(5)}(\theta)}}{\frac{1}{Y_3^{(5)}(\theta)}\frac{1}{Y_{\widetilde{12}}^{(5)}(\theta)}} \qquad Y_{\text{other}}^{(6)} = Y_{\text{other}}^{(5)}. \end{aligned} \tag{E.19}$$

The intersection matrices of the TBA equations in this chamber are

$$I = \begin{pmatrix} -1 & 1 & & & & & -1 & & -1 \\ 1 & -1 & 1 & & & 1 & 1 & 1 & 2 \\ & 1 & -1 & & & & & -1 & -1 \\ & & & -1 & & & -1 & & \\ & & & & -1 & & & -1 & \\ & 1 & & & & -1 & 2 & -2 & -2 \\ -1 & 1 & & -1 & & 2 & -3 & -2 & -3 \\ & 1 & -1 & & -1 & -2 & -2 & -3 & -3 \\ -1 & 2 & -1 & & & -2 & -3 & -3 & -5 \end{pmatrix}, \; I^+ = \begin{pmatrix} 0 & & & & 1 & & & & \\ & 0 & & & & & & & \\ & & 0 & 1 & & & & & \\ -1 & 1 & & 0 & & -1 & -1 & -1 & -2 \\ & 1 & -1 & & 0 & -1 & -1 & -1 & -2 \\ -1 & 1 & -1 & & & 0 & & & -1 \\ -1 & 1 & -1 & & & & 0 & & -1 \\ -1 & 1 & -1 & & & & & 0 & -1 \\ -1 & 1 & -1 & & & & & & 0 \end{pmatrix}, \tag{E.20}$$

whose entries are arrayed as $1, 2, 3, 12, 23, 312, \widetilde{12}, \widetilde{23}, \widehat{312}$. The new mass is $m_{\widehat{312}} := |m_{\widehat{312}}|e^{i\phi_{\widehat{312}}} := m_3 + m_{\widetilde{12}}$. The identification for the new Y-function $Y_{\widehat{312}}^{(6)}$ is given by

$$\log Y_{\widehat{312}}^{(6)} = e^{\theta}\Pi_{\gamma_{1,1}-\gamma_{1,2}+\gamma_{3,3}}(\theta). \tag{E.21}$$

We plot the charges in this process in figure D.6. At the wall, $\Pi_{\gamma_{3,3}}^{(0)}$ (c) and $\Pi_{\gamma_{1,1}-\gamma_{1,2}}^{(0)}$ (j) align and new charge $\Pi_{\gamma_{1,1}-\gamma_{1,2}+\gamma_{3,3}}^{(0)}$ (l) emerges.

The seventh wall-crossing

We define the Y-functions in this chamber by

$$\begin{aligned} Y_2^{(7)}(\theta) =& Y_2^{(6)}(\theta)\big(1+\frac{1}{Y_{312}^{(6)}(\theta+\frac{2\pi i}{3})}\big), \quad Y_{312}^{(7)}(\theta) = Y_{312}^{(6)}(\theta)\big(1+\frac{1}{Y_2^{(6)}(\theta-\frac{2\pi i}{3})}\big) \\ Y_{3122}^{(7)}(\theta) =& \frac{1+\frac{1}{Y_2^{(6)}(\theta-\frac{2\pi i}{3})}+\frac{1}{Y_{312}^{(6)}(\theta)}}{\frac{1}{Y_2^{(6)}(\theta-\frac{2\pi i}{3})}\frac{1}{Y_{312}^{(6)}(\theta)}}, \qquad Y_{\text{other}}^{(7)}(\theta) = Y_{\text{other}}^{(6)}(\theta). \end{aligned} \tag{E.22}$$

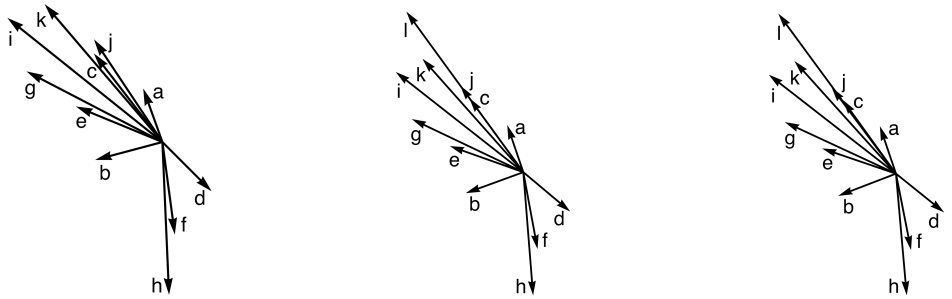

(a) $t = 0.400536...$ (b) $t = 0.434148...$ (c) $t = 0.441858...$

Figure D.6: The classical periods in the process of the sixth wall-crossing. The vectors represents the classical periods on the complex plane (a) before, (b) at and (c) after the wall-crossing. The arrows labeled by $a, b, c, d, e, f, g, h, i, j, k$ and l represent the classical periods $\Pi^{(0)}_{\gamma_{1,1}}$, $\Pi^{(0)}_{\gamma_{3,2}}$, $\Pi^{(0)}_{\gamma_{3,3}}$, $\Pi^{(0)}_{\gamma_{1,2}}$, $\Pi^{(0)}_{\gamma_{1,1}+\gamma_{3,2}}$, $\Pi^{(0)}_{\gamma_{2,1}+\gamma_{1,2}}$, $\Pi^{(0)}_{\gamma_{3,2}+\gamma_{3,3}}$, $\Pi^{(0)}_{\gamma_{1,2}+\gamma_{1,3}}$, $\Pi^{(0)}_{\gamma_{1,1}+\gamma_{3,2}+\gamma_{3,3}}$, $\Pi^{(0)}_{\gamma_{1,1}-\gamma_{1,2}}$, $\Pi^{(0)}_{\gamma_{3,3}-\gamma_{1,2}}$ and $\Pi^{(0)}_{\gamma_{1,1}-\gamma_{1,2}+\gamma_{3,3}}$, respectively.

The intersection matrices are

$$I = \begin{pmatrix} -1 & 1 & & & & & -1 & & -1 & \\ 1 & -1 & 1 & & & 1 & 1 & 1 & 2 & 1 \\ & 1 & -1 & & & & & -1 & -1 & \\ & & & -1 & & & -1 & & & -1 \\ & & & & -1 & & & -1 & -1 & \\ & 1 & & & & -1 & 2 & -2 & -2 & -3 \\ -1 & 1 & & -1 & & 2 & -3 & -2 & -3 & -4 \\ & 1 & -1 & & -1 & -2 & -2 & -3 & -3 & -4 \\ -1 & 2 & -1 & & & -2 & -3 & -3 & -5 & -6 \\ & 1 & & -1 & -1 & -3 & -4 & -4 & -6 & -5 \end{pmatrix},$$

$$I^+ = \begin{pmatrix} 0 & & & & 1 & & & & & \\ & 0 & & & & & & & & \\ & & 0 & 1 & & & & & & \\ -1 & 1 & & 0 & & -1 & -1 & -1 & -2 & -1 \\ & 1 & -1 & & 0 & -1 & -1 & -1 & -2 & -1 \\ -1 & 1 & -1 & & & 0 & & & -1 & 1 \\ -1 & 1 & -1 & & & & 0 & & -1 & 1 \\ -1 & 1 & -1 & & & & & 0 & -1 & 1 \\ -1 & 1 & -1 & & & & & & 0 & 3 \\ -2 & 2 & -2 & & & & & & & 0 \end{pmatrix}, \tag{E.23}$$

Here the entries are arrayed in the order as $1, 2, 3, 12, 23, 312, \widetilde{12}, \widetilde{23}, \widehat{312}, 3122$. The new mass is defined by $m_{3122} \coloneqq |m_{3122}|e^{i\phi_{3122}} \coloneqq m_{312} + e^{-\frac{2\pi i}{3}} m_2$. The new Y-function $Y^{(7)}_{3122}$ is identified with the WKB period by

$$\log Y^{(7)}_{\widehat{3122}} = e^{\theta} \Pi_{\gamma_{1,1}-\gamma_{1,2}+\gamma_{3,2}+\gamma_{3,3}}(\theta). \tag{E.24}$$

The plot of the charges in this wall-crossing process is illustrated in figure D.7. The two charges $\Pi^{(0)}_{\gamma_{1,2}}$ (d) and $\Pi^{(0)}_{\gamma_{1,1}+\gamma_{3,2}+\gamma_{3,3}}$ (i) align at the wall, and then the new charge $\Pi^{(0)}_{\gamma_{1,1}-\gamma_{1,2}+\gamma_{3,2}+\gamma_{3,3}}$ (m) emerges.

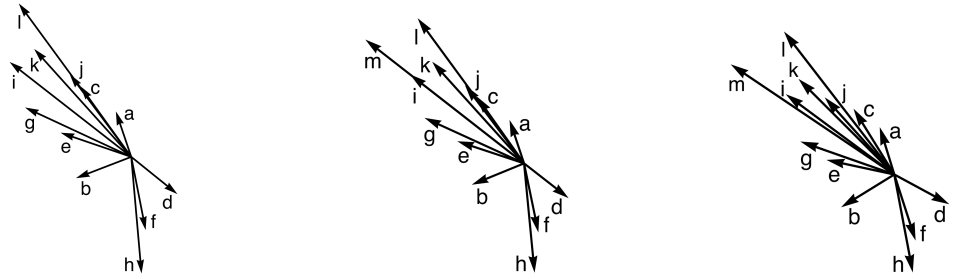

(a) $t = 0.441858...$ (b) $t = 0.449568...$ (c) $t = 0.528887...$

Figure D.7: The classical periods in the process of the seventh wall-crossing. The vectors represents the classical periods on the complex plane (a) before, (b) at and (c) after the wall-crossing. The arrows labeled by $a, b, c, d, e, f, g, h, i, j, k, l$ and m represent the classical periods $\Pi^{(0)}_{\gamma_{1,1}}$, $\Pi^{(0)}_{\gamma_{3,2}}$, $\Pi^{(0)}_{\gamma_{3,3}}$, $\Pi^{(0)}_{\gamma_{1,2}}$, $\Pi^{(0)}_{\gamma_{1,1}+\gamma_{3,2}}$, $\Pi^{(0)}_{\gamma_{2,1}+\gamma_{1,2}}$, $\Pi^{(0)}_{\gamma_{3,2}+\gamma_{3,3}}$, $\Pi^{(0)}_{\gamma_{1,2}+\gamma_{1,3}}$, $\Pi^{(0)}_{\gamma_{1,1}+\gamma_{3,2}+\gamma_{3,3}}$, $\Pi^{(0)}_{\gamma_{1,1}-\gamma_{1,2}}$, $\Pi^{(0)}_{\gamma_{3,3}-\gamma_{1,2}}$, $\Pi^{(0)}_{\gamma_{1,1}-\gamma_{1,2}+\gamma_{3,3}}$, and $\Pi^{(0)}_{\gamma_{1,1}-\gamma_{1,2}+\gamma_{3,2}+\gamma_{3,3}}$, respectively.

The eighth wall-crossing

Th Y-functions in this chamber is defined by

$$\begin{aligned} Y^{(8)}_{1}(\theta) &= Y^{(7)}_{1}(\theta)\big(1 + \frac{1}{Y^{(7)}_{23}(\theta - \frac{\pi i}{3})}\big), \quad Y^{(8)}_{23}(\theta) = Y^{(7)}_{23}(\theta)\big(1 + \frac{1}{Y^{(7)}_{1}(\theta + \frac{\pi i}{3})}\big) \\ Y^{(8)}_{231}(\theta) &= \frac{1 + \frac{1}{Y^{(7)}_{23}(\theta - \frac{\pi i}{3})} + \frac{1}{Y^{(7)}_{1}(\theta)}}{\frac{1}{Y^{(7)}_{1}(\theta) Y^{(7)}_{23}(\theta - \frac{\pi i}{3})}}, \qquad Y^{(8)}_{\text{other}} = Y^{(7)}_{\text{other}}, \end{aligned} \tag{E.25}$$

where the intersection matrices of the TBA equations for them are

$$
I = \begin{pmatrix}
-1 & 1 & & & & & -1 & & -1 & -1 & \\
1 & -1 & 1 & & & 1 & 1 & 1 & 2 & 1 & 2 \\
 & 1 & -1 & & & & & -1 & -1 & & -1 \\
 & & & -1 & & & -1 & & & -1 & \\
 & & & & -1 & & & -1 & -1 & 1 & \\
 & 1 & & & & -1 & 2 & -2 & -2 & -3 & -1 \\
-1 & 1 & & -1 & & 2 & -3 & -2 & -3 & -4 & -2 \\
 & 1 & -1 & & -1 & -2 & -2 & -3 & -3 & -4 & -1 \\
-1 & 2 & -1 & & & -2 & -3 & -3 & -5 & -6 & -3 \\
 & 1 & & -1 & -1 & -3 & -4 & -4 & -6 & -5 & -1 \\
-1 & 2 & -1 & & 1 & -1 & -2 & -1 & -3 & -1 & -3
\end{pmatrix},
$$

$$
I^+ = \begin{pmatrix}
0 & & & & 1 & & & & & & \\
 & 0 & & & & & & & & & \\
 & & 0 & 1 & & & & & & & \\
-1 & 1 & & 0 & & -1 & -1 & -1 & -2 & -1 & -1 \\
 & 1 & -1 & & 0 & -1 & -1 & -1 & -2 & -1 & -2 \\
-1 & 1 & -1 & & & 0 & & & -1 & 1 & -1 \\
-1 & 1 & -1 & & & & 0 & & -1 & 1 & -1 \\
-1 & 1 & -1 & & & & & 0 & -1 & 1 & -2 \\
-1 & 1 & -1 & & & & & & 0 & 3 & -1 \\
-2 & 2 & -2 & & & & & & & 0 & -3 \\
-1 & & & & & & & & & & 0
\end{pmatrix}.
$$

(E.26)

Here the entries are aligned in the order of $1, 2, 3, 12, 23, 312, \widetilde{12}, \widetilde{23}, \widehat{312}, 3122, 231$. The new mass term is $m_{231} \coloneqq |m_{231}|e^{i\phi_{231}} \coloneqq m_1 + e^{-\frac{\pi i}{3}} m_{23}$. We identify the Y-function $Y^{(8)}_{231}$ with the WKB period as

$$
\log Y^{(8)}_{231} = e^{\theta} \Pi_{\gamma_{1,1}-\gamma_{3,2}-\gamma_{3,3}}(\theta). \tag{E.27}
$$

The charges in this wall-crossing process is depicted in figure D.8. The two periods $\Pi^{(0)}_{\gamma_{1,1}}$ (a) and $\Pi^{(0)}_{\gamma_{3,2}+\gamma_{3,3}}$ (h) align and the new period $\Pi^{(0)}_{\gamma_{1,1}-\gamma_{3,2}-\gamma_{3,3}}$ (n) emerges.

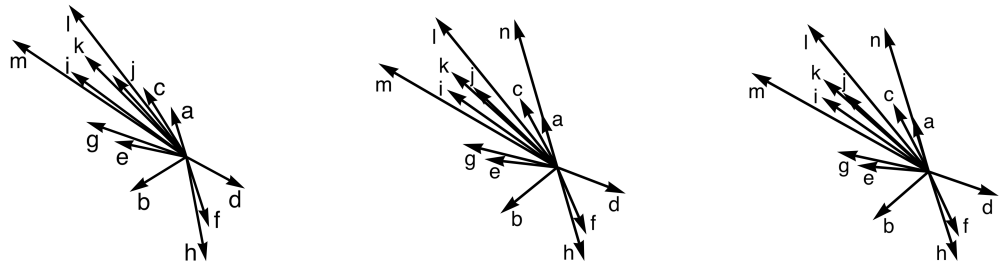

(a) $t = 0.528887...$ (b) $t = 0.608205...$ (c) $t = 0.631547...$

Figure D.8: The classical periods in the process of the eighth wall-crossing. The vectors represents the classical periods on the complex plane (a) before, (b) at and (c) after the wall-crossing. The arrows labeled by $a, b, c, d, e, f, g, h, i, j, k, l, m$ and n represent the classical periods $\Pi^{(0)}_{\gamma_{1,1}}$, $\Pi^{(0)}_{\gamma_{3,2}}$, $\Pi^{(0)}_{\gamma_{3,3}}$, $\Pi^{(0)}_{\gamma_{1,2}}$, $\Pi^{(0)}_{\gamma_{1,1}+\gamma_{3,2}}$, $\Pi^{(0)}_{\gamma_{2,1}+\gamma_{1,2}}$, $\Pi^{(0)}_{\gamma_{3,2}+\gamma_{3,3}}$, $\Pi^{(0)}_{\gamma_{1,2}+\gamma_{1,3}}$, $\Pi^{(0)}_{\gamma_{1,1}+\gamma_{3,2}+\gamma_{3,3}}$, $\Pi^{(0)}_{\gamma_{1,1}-\gamma_{1,2}}$, $\Pi^{(0)}_{\gamma_{3,3}-\gamma_{1,2}}$, $\Pi^{(0)}_{\gamma_{1,1}-\gamma_{1,2}+\gamma_{3,3}}$, $\Pi^{(0)}_{\gamma_{1,1}-\gamma_{1,2}+\gamma_{3,2}+\gamma_{3,3}}$, and $\Pi^{(0)}_{\gamma_{1,1}-\gamma_{3,2}-\gamma_{3,3}}$, respectively.

The ninth wall-crossing

After the ninth wall-crossing, we reach the maximal chamber, in which we defined the Y-function by

$$\begin{aligned} Y_3^{(9)}(\theta) &= Y_3^{(8)}(\theta)\big(1+\frac{1}{Y_{12}^{(8)}(\theta-\frac{\pi i}{3})}\big), \quad Y_{12}^{(9)}(\theta) = Y_{12}^{(8)}(\theta)\big(1+\frac{1}{Y_3^{(8)}(\theta+\frac{\pi i}{3})}\big) \\ Y_{\overline{123}}^{(9)}(\theta) &= \frac{1+\frac{1}{Y_{12}^{(8)}(\theta-\frac{\pi i}{3})}+\frac{1}{Y_3^{(8)}(\theta)}}{\frac{1}{Y_3^{(8)}(\theta)Y_{12}^{(8)}(\theta-\frac{\pi i}{3})}}, \qquad Y_{\text{other}}^{(9)} = Y_{\text{other}}^{(8)}. \end{aligned} \tag{E.28}$$

The intersection matrices of the TBA equations in the maximal chamber read

$$I = \begin{pmatrix} -1 & 1 & & & & & -1 & & -1 & -1 & -1 & & \\ 1 & -1 & 1 & & & 1 & 1 & 1 & 2 & 1 & 2 & 2 \\ & 1 & -1 & & & & & -1 & -1 & & -1 & -1 \\ & & & -1 & & & -1 & & & -1 & & 1 \\ & & & & -1 & & & -1 & -1 & 1 & & \\ & 1 & & & & -1 & 2 & -2 & -2 & -3 & -1 & -1 \\ -1 & 1 & & -1 & & 2 & -3 & -2 & -3 & -4 & -2 & -1 \\ & 1 & -1 & & -1 & -2 & -2 & -3 & -3 & -4 & -1 & -2 \\ -1 & 2 & -1 & & & -2 & -3 & -3 & -5 & -6 & -3 & -3 \\ & 1 & & -1 & -1 & -3 & -4 & -4 & -6 & -5 & -1 & -1 \\ -1 & 2 & -1 & & 1 & -1 & -2 & -1 & -3 & -1 & -3 & -2 \\ -1 & 2 & -1 & 1 & & -1 & -1 & -2 & -3 & -1 & -2 & -3 \end{pmatrix},$$

$$I^+ = \begin{pmatrix}
0 & & & & 1 & & & & & & & \\
 & 0 & & & & & & & & & & \\
 & & 0 & 1 & & & & & & & & \\
-1 & 1 & & 0 & & -1 & -1 & -1 & -2 & -1 & -1 & -2 \\
 & 1 & -1 & & 0 & -1 & -1 & -1 & -2 & -1 & -2 & -1 \\
-1 & 1 & -1 & & & 0 & & & -1 & 1 & -1 & -1 \\
-1 & 1 & -1 & & & & 0 & & -1 & 1 & -1 & -2 \\
-1 & 1 & -1 & & & & & 0 & -1 & 1 & -2 & -1 \\
-1 & 1 & -1 & & & & & & 0 & 3 & -1 & -1 \\
-2 & 2 & -2 & & & & & & & 0 & -3 & -3 \\
-1 & & & & & & & & & & 0 & \\
 & & -1 & & & & & & & & & 0
\end{pmatrix}, \tag{E.29}$$

where the entries are arrayed in the order as $1, 2, 3, 12, 23, 312, \widetilde{12}, \widetilde{23}, \widehat{312}, 3122, 231, \overline{123}$. The new mass is defined by $m_{\overline{123}} \coloneqq |m_{\overline{123}}|e^{i\phi_{\overline{123}}} \coloneqq m_3 + e^{-i\frac{\pi i}{3}}m_{12}$. The relation between the Y-function $Y^{(9)}_{\overline{123}}$ and the WKB period is

$$\log Y^{(9)}_{\overline{123}} = e^{\theta}\Pi_{\gamma_{3,3}-\gamma_{1,2}-\gamma_{2,1}}(\theta). \tag{E.30}$$

We visualize this process inn figure D.9. At the wall, the two charges $\Pi^{(0)}_{\gamma_{3,3}}$ (c) and $\Pi^{(0)}_{\gamma_{1,2}+\gamma_{2,1}}$ (f) align and the new charge $\Pi^{(0)}_{\gamma_{3,3}-\gamma_{1,2}-\gamma_{2,1}}$ (o) emerges.

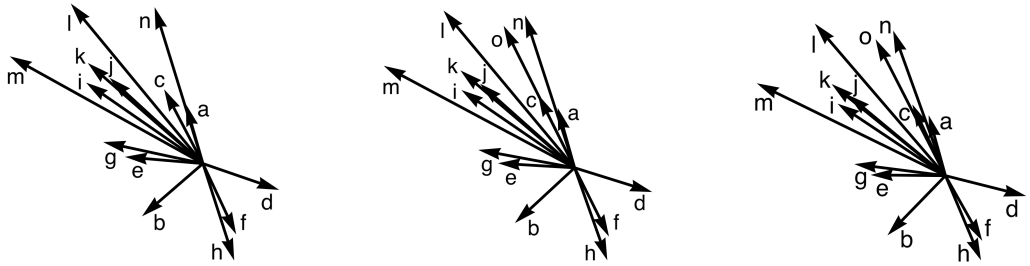

(a) $t = 0.631547...$ (b) $t = 0.65489...$ (c) $t = 0.7$

Figure D.9: The classical periods in the process of the ninth wall-crossing. The vectors represents the classical periods on the complex plane (a) before, (b) at and (c) after the wall-crossing. The arrows labeled by $a, b, c, d, e, f, g, h, i, j, k, l, m, n$ and o represent the classical periods $\Pi^{(0)}_{\gamma_{1,1}}$, $\Pi^{(0)}_{\gamma_{3,2}}$, $\Pi^{(0)}_{\gamma_{3,3}}$, $\Pi^{(0)}_{\gamma_{1,2}}$, $\Pi^{(0)}_{\gamma_{1,1}+\gamma_{3,2}}$, $\Pi^{(0)}_{\gamma_{2,1}+\gamma_{1,2}}$, $\Pi^{(0)}_{\gamma_{3,2}+\gamma_{3,3}}$, $\Pi^{(0)}_{\gamma_{1,2}+\gamma_{1,3}}$, $\Pi^{(0)}_{\gamma_{1,1}+\gamma_{3,2}+\gamma_{3,3}}$, $\Pi^{(0)}_{\gamma_{1,1}-\gamma_{1,2}}$, $\Pi^{(0)}_{\gamma_{3,3}-\gamma_{1,2}}$, $\Pi^{(0)}_{\gamma_{1,1}-\gamma_{1,2}+\gamma_{3,3}}$, $\Pi^{(0)}_{\gamma_{1,1}-\gamma_{1,2}+\gamma_{3,2}+\gamma_{3,3}}$, $\Pi^{(0)}_{\gamma_{1,1}-\gamma_{3,2}-\gamma_{3,3}}$, and $\Pi^{(0)}_{\gamma_{3,3}-\gamma_{1,2}-\gamma_{2,1}}$, respectively.

Bibliography

[1] P. Dorey and R. Tateo, "Anharmonic oscillators, the thermodynamic Bethe ansatz, and nonlinear integral equations," J. Phys. A **32**, L419-L425 (1999) [arXiv:hep-th/9812211 [hep-th]].

[2] C. S. Gardner, J. M. Greene, M. D. Kruskal and R. M. Miura, "Method for solving the Korteweg-deVries equation," Phys. Rev. Lett. **19**, 1095-1097 (1967)

[3] H. Bethe, "On the theory of metals. 1. Eigenvalues and eigenfunctions for the linear atomic chain," Z. Phys. **71**, 205-226 (1931).

[4] E. H. Lieb, "Exact Solution of the Problem of the Entropy of Two-Dimensional Ice," Phys. Rev. Lett.**18**, 692–694 (1967).

[5] B. Sutherland, "Exact Solution of a Two-Dimensional Model for Hydrogen-Bonded Crystals," Phys. Rev. Lett.**19**(3), 103–104 (1967).

[6] R. J. Baxter, "Eight-Vertex Model in Lattice Statistics," Phys. Rev. Lett. **26**, 832-833 (1971).

[7] R. J. Baxter, "One-Dimensional Anisotropic Heisenberg Chain," Phys. Rev. Lett. **26**, 834-834 (1971).

[8] R. J. Baxter, "Eight vertex model in lattice statistics and one-dimensional anisotropic Heisenberg chain. 1. Eigenvectors of the transfer matrix and Hamiltonian," Annals Phys. **76**, 48-71 (1973)

[9] V. G. Drinfeld, "Quantum groups," Zap. Nauchn. Semin. **155**, 18-49 (1986).

[10] O. Babelon, H. J. de Vega and C. M. Viallet, "Exact Excitation Spectrum of the $Z(n^+1)$ X $Z(n^+1)$ Generalized Heisenberg Model," Nucl. Phys. B **220**, 283-301 (1983).

[11] N. Y. Reshetikhin, "Integrable Models of Quantum One-dimensional Magnets With O(N) and Sp(2k) Symmetry," Theor. Math. Phys. **63**, 555-569 (1985).

[12] N. Y. Reshetikhin, "The spectrum of the transfer matrices connected with Kac-Moody algebras," Letters in Mathematical Physics **14**(3), 235-246 (1987).

[13] N. Y. Reshetikhin and P. B. Wiegmann, "Towards the Classification of Completely Integrable Quantum Field Theories," Phys. Lett. B **189**, 125-131 (1987)

[14] C. N. Yang and C. P. Yang, "Thermodynamics of one-dimensional system of bosons with repulsive delta function interaction," J. Math. Phys. **10**, 1115-1122 (1969)

[15] A. B. Zamolodchikov, "Thermodynamic Bethe Ansatz in Relativistic Models. Scaling Three State Potts and Lee-yang Models," Nucl. Phys. B **342**, 695-720 (1990)

[16] A. B. Zamolodchikov, "On the thermodynamic Bethe ansatz equations for reflectionless ADE scattering theories," Phys. Lett. B **253**, 391-394 (1991)

[17] F. Ravanini, R. Tateo and A. Valleriani, "Dynkin TBAs," Int. J. Mod. Phys. A **8**, 1707-1728 (1993) [arXiv:hep-th/9207040 [hep-th]].

[18] F. Ravanini, "Thermodynamic Bethe ansatz for G(k) x G(l) / G(k+l) coset models perturbed by their phi(1,1,Adj) operator," Phys. Lett. B **282**, 73-79 (1992) [arXiv:hep-th/9202020 [hep-th]].

[19] Y. Sibuya "Global theory of a second order linear ordinary differential equation with a polynomial coefficient," North-Holland, 1975.

[20] V. V. Bazhanov, S. L. Lukyanov and A. B. Zamolodchikov, "Spectral determinants for Schrodinger equation and Q operators of conformal field theory," J. Statist. Phys. **102**, 567-576 (2001) [arXiv:hep-th/9812247 [hep-th]].

[21] P. Dorey and R. Tateo, "On the relation between Stokes multipliers and the T-Q systems of conformal field theory," Nucl. Phys. B **563**, 573-602 (1999) [arXiv:hep-th/9906219 [hep-th]].

[22] P. Dorey and R. Tateo, "Differential equations and integrable models: The SU(3) case," Nucl. Phys. B **571**, 583-606 (2000) [arXiv:hep-th/9910102 [hep-th]].

[23] J. Suzuki, "Functional relations in Stokes multipliers and solvable models related to $U_q(A_n^{(1)})$," J. Phys. A **33**, 3507-3522 (2000) [arXiv:hep-th/9910215 [hep-th]].

[24] P. Dorey, C. Dunning and R. Tateo, "Differential equations for general SU(n) Bethe ansatz systems," J. Phys. A **33**, 8427-8442 (2000) [arXiv:hep-th/0008039 [hep-th]].

[25] P. Dorey, C. Dunning and R. Tateo, "Spectral equivalences, Bethe Ansatz equations, and reality properties in PT-symmetric quantum mechanics," J. Phys. A **34**, 5679-5704 (2001) [arXiv:hep-th/0103051 [hep-th]].

[26] C. Destri and H. J. de Vega, "New thermodynamic Bethe ansatz equations without strings," Phys. Rev. Lett. **69**, 2313-2317 (1992)

[27] P. Zinn-Justin, "Nonlinear integral equations for complex affine Toda models associated to simply laced Lie algebras," J. Phys. A **31**, 6747-6770 (1998) [arXiv:hep-th/9712222 [hep-th]].

[28] C. Dunning, "Massless flows between minimal W models," Phys. Lett. B **537**, 297-305 (2002) [arXiv:hep-th/0204090 [hep-th]].

[29] P. Dorey, C. Dunning, D. Masoero, J. Suzuki and R. Tateo, "Pseudo-differential equations, and the Bethe ansatz for the classical Lie algebras," Nucl. Phys. B **772**, 249-289 (2007) [arXiv:hep-th/0612298 [hep-th]].

[30] P. Dorey, C. Dunning and R. Tateo, "The ODE/IM Correspondence," J. Phys. A **40**, R205 (2007) [arXiv:hep-th/0703066 [hep-th]].

[31] J. Sun, "Polynomial relations for q-characters via the ODE/IM correspondence," SIGMA **8**, 028 (2012) [arXiv:1201.1614 [math.QA]].

[32] S. L. Lukyanov and A. B. Zamolodchikov, "Quantum Sine(h)-Gordon Model and Classical Integrable Equations," JHEP **07**, 008 (2010) [arXiv:1003.5333 [math-ph]].

[33] P. Dorey, S. Faldella, S. Negro and R. Tateo, "The Bethe Ansatz and the Tzitzeica-Bullough-Dodd equation," Phil. Trans. Roy. Soc. Lond. A **371**, 20120052 (2013) [arXiv:1209.5517 [math-ph]].

[34] K. Ito and C. Locke, "ODE/IM correspondence and modified affine Toda field equations," Nucl. Phys. B **885**, 600-619 (2014) [arXiv:1312.6759 [hep-th]].

[35] K. Ito and C. Locke, "ODE/IM correspondence and Bethe ansatz for affine Toda field equations," Nucl. Phys. B **896**, 763-778 (2015) [arXiv:1502.00906 [hep-th]].

[36] V. V. Bazhanov, S. L. Lukyanov and A. B. Zamolodchikov, "Higher level eigenvalues of Q operators and Schroedinger equation," Adv. Theor. Math. Phys. **7**, no.4, 711-725 (2003) [arXiv:hep-th/0307108 [hep-th]].

[37] B. Feigin and E. Frenkel, "Quantization of soliton systems and Langlands duality," [arXiv:0705.2486 [math.QA]].

[38] D. Masoero and A. Raimondo, "Opers for higher states of quantum KdV models," Commun. Math. Phys. **378**, no.1, 1-74 (2020) [arXiv:1812.00228 [math-ph]].

[39] K. Ito, T. Kondo, K. Kuroda and H. Shu, "ODE/IM correspondence for affine Lie algebras: A numerical approach," J. Phys. A **54**, no.4, 044001 (2021) [arXiv:2004.09856 [hep-th]].

[40] A. Voros, "The return of the quartic oscillator. The complex WKB method," Annales de l'I.H.P. Physique théorique **39** (1983) 211.

[41] E. Delabaere and F. Pham, "Resurgent methods in semi-classical asymptotics," Annales de l'I.H.P. Physique théorique **71** (1999) 1.

[42] K. Ito, M. Mariño and H. Shu, "TBA equations and resurgent Quantum Mechanics," JHEP **01**, 228 (2019) [arXiv:1811.04812 [hep-th]].

[43] P. Dorey and R. Tateo, "Excited states by analytic continuation of TBA equations," Nucl. Phys. B **482**, 639-659 (1996) [arXiv:hep-th/9607167 [hep-th]].

[44] J. Toledo, "Exact results in QFT: Minimal Areas and Maximal Couplings," PhD thesis, University of Waterloo, https://uwspace.uwaterloo.ca/handle/10012/10841, 2016.

[45] Y. Emery, "TBA equations and quantization conditions," JHEP **07**, 171 (2021) [arXiv:2008.13680 [hep-th]].

[46] N. Seiberg, "Supersymmetry and Nonperturbative beta Functions," Phys. Lett. B **206**, 75-80 (1988)

[47] N. Seiberg and E. Witten, "Monopoles, duality and chiral symmetry breaking in N=2 supersymmetric QCD," Nucl. Phys. B **431**, 484-550 (1994) [arXiv:hep-th/9408099 [hep-th]].

[48] N. Seiberg and E. Witten, "Electric - magnetic duality, monopole condensation, and confinement in N=2 supersymmetric Yang-Mills theory," Nucl. Phys. B **426**, 19-52 (1994) [arXiv:hep-th/9407087 [hep-th]].

[49] A. Klemm, W. Lerche, S. Yankielowicz and S. Theisen, "Simple singularities and N=2 supersymmetric Yang-Mills theory," Phys. Lett. B **344**, 169-175 (1995) [arXiv:hep-th/9411048 [hep-th]].

[50] P. C. Argyres and A. E. Faraggi, "The vacuum structure and spectrum of N=2 supersymmetric SU(n) gauge theory," Phys. Rev. Lett. **74**, 3931-3934 (1995) [arXiv:hep-th/9411057 [hep-th]].

[51] U. H. Danielsson and B. Sundborg, "The Moduli space and monodromies of N=2 supersymmetric SO(2r+1) Yang-Mills theory," Phys. Lett. B **358**, 273-280 (1995) [arXiv:hep-th/9504102 [hep-th]].

[52] A. Brandhuber and K. Landsteiner, "On the monodromies of N=2 supersymmetric Yang-Mills theory with gauge group SO(2n)," Phys. Lett. B **358**, 73-80 (1995) [arXiv:hep-th/9507008 [hep-th]].

[53] E. J. Martinec and N. P. Warner, "Integrable systems and supersymmetric gauge theory," Nucl. Phys. B **459**, 97-112 (1996) [arXiv:hep-th/9509161 [hep-th]].

[54] K. Ito and S. K. Yang, "A-D-E singularity and prepotentials in N=2 supersymmetric Yang-Mills theory," Int. J. Mod. Phys. A **13**, 5373-5390 (1998) [arXiv:hep-th/9712018 [hep-th]].

[55] K. Ito, "A-D-E singularity and the Seiberg-Witten theory," Prog. Theor. Phys. Suppl. **135** (1999), 94-108 [arXiv:hep-th/9906023 [hep-th]].

[56] P. C. Argyres and M. R. Douglas, "New phenomena in SU(3) supersymmetric gauge theory," Nucl. Phys. B **448**, 93-126 (1995) [arXiv:hep-th/9505062 [hep-th]].

[57] P. C. Argyres, M. R. Plesser, N. Seiberg and E. Witten, "New N=2 superconformal field theories in four-dimensions," Nucl. Phys. B **461**, 71-84 (1996) [arXiv:hep-th/9511154 [hep-th]].

[58] T. Eguchi, K. Hori, K. Ito and S. K. Yang, "Study of N=2 superconformal field theories in four-dimensions," Nucl. Phys. B **471**, 430-444 (1996) [arXiv:hep-th/9603002 [hep-th]].

[59] S. Cecotti, A. Neitzke and C. Vafa, "R-Twisting and 4d/2d Correspondences," [arXiv:1006.3435 [hep-th]].

[60] D. Xie, "General Argyres-Douglas Theory," JHEP **01**, 100 (2013) [arXiv:1204.2270 [hep-th]].

[61] Y. Wang and D. Xie, "Classification of Argyres-Douglas theories from M5 branes," Phys. Rev. D **94**, no.6, 065012 (2016) [arXiv:1509.00847 [hep-th]].

[62] C. Montonen and D. I. Olive, "Magnetic Monopoles as Gauge Particles?," Phys. Lett. B **72**, 117-120 (1977)

[63] E. Witten and D. I. Olive, "Supersymmetry Algebras That Include Topological Charges," Phys. Lett. B **78**, 97-101 (1978)

[64] E. B. Bogomolny, "Stability of Classical Solutions," Sov. J. Nucl. Phys. **24**, 449 (1976) PRINT-76-0543 (LANDAU-INST.).

[65] M. K. Prasad and C. M. Sommerfield, "An Exact Classical Solution for the 't Hooft Monopole and the Julia-Zee Dyon," Phys. Rev. Lett. **35**, 760-762 (1975)

[66] M. Kontsevich and Y. Soibelman, "Stability structures, motivic Donaldson-Thomas invariants and cluster transformations," arXiv:0811.2435 [math.AG].

[67] D. Gaiotto, G. W. Moore and A. Neitzke, "Wall-crossing, Hitchin Systems, and the WKB Approximation," arXiv:0907.3987 [hep-th].

[68] D. Gaiotto, G. W. Moore and A. Neitzke, "Four-dimensional wall-crossing via three-dimensional field theory," Commun. Math. Phys. **299**, 163-224 (2010) [arXiv:0807.4723 [hep-th]].

[69] N. A. Nekrasov, "Seiberg-Witten prepotential from instanton counting," Adv. Theor. Math. Phys. **7**, no.5, 831-864 (2003) [arXiv:hep-th/0206161 [hep-th]].

[70] N. Nekrasov and A. Okounkov, "Seiberg-Witten theory and random partitions," Prog. Math. **244**, 525-596 (2006) [arXiv:hep-th/0306238 [hep-th]].

[71] N. A. Nekrasov and S. L. Shatashvili, "Quantization of Integrable Systems and Four Dimensional Gauge Theories," arXiv:0908.4052 [hep-th].

[72] A. Mironov and A. Morozov, "Nekrasov Functions and Exact Bohr-Zommerfeld Integrals," JHEP **04**, 040 (2010) [arXiv:0910.5670 [hep-th]].

[73] A. Mironov and A. Morozov, "Nekrasov Functions from Exact BS Periods: The Case of SU(N)," J. Phys. A **43**, 195401 (2010) [arXiv:0911.2396 [hep-th]].

[74] K. Ito and H. Shu, "ODE/IM correspondence and the Argyres-Douglas theory," JHEP **08**, 071 (2017) [arXiv:1707.03596 [hep-th]].

[75] K. Ito, S. Koizumi and T. Okubo, "Quantum Seiberg-Witten curve and Universality in Argyres-Douglas theories," Phys. Lett. B **792**, 29-34 (2019) [arXiv:1903.00168 [hep-th]].

[76] K. Ito, S. Koizumi and T. Okubo, "Quantum Seiberg-Witten periods for $\mathcal{N} = 2$ $SU(N_c)$ SQCD around the superconformal point," Nucl. Phys. B **954**, 115004 (2020) [arXiv:2001.08891 [hep-th]].

[77] D. Gaiotto, "Opers and TBA," arXiv:1403.6137 [hep-th].

[78] A. Neitzke, "Integral iterations for harmonic maps," arXiv:1704.01522 [math.DG].

[79] D. Dumas and A. Neitzke, "Opers and nonabelian Hodge: numerical studies," arXiv:2007.00503 [math.DG].

[80] C. Beem, M. Lemos, P. Liendo, W. Peelaers, L. Rastelli and B. C. van Rees, "Infinite Chiral Symmetry in Four Dimensions," Commun. Math. Phys. **336**, no.3, 1359-1433 (2015) [arXiv:1312.5344 [hep-th]].

[81] C. Cordova and S. H. Shao, "Schur Indices, BPS Particles, and Argyres-Douglas Theories," JHEP **01**, 040 (2016) [arXiv:1506.00265 [hep-th]].

[82] M. Buican and T. Nishinaka, "On the superconformal index of Argyres–Douglas theories," J. Phys. A **49**, no.1, 015401 (2016) [arXiv:1505.05884 [hep-th]].

[83] D. Xie, W. Yan and S. T. Yau, "Chiral algebra of the Argyres-Douglas theory from M5 branes," Phys. Rev. D **103**, no.6, 065003 (2021) [arXiv:1604.02155 [hep-th]].

[84] S. Cecotti, J. Song, C. Vafa and W. Yan, "Superconformal Index, BPS Monodromy and Chiral Algebras," JHEP **11**, 013 (2017) [arXiv:1511.01516 [hep-th]].

[85] K. Ito, T. Kondo, K. Kuroda and H. Shu, "WKB periods for higher order ODE and TBA equations," JHEP **10**, 167 (2021) [arXiv:2104.13680 [hep-th]].

[86] K. Ito, T. Kondo and H. Shu, "Wall-crossing of TBA equations and WKB periods for the third order ODE," arXiv:2111.11047 [hep-th].

[87] A. Torrielli, "Lectures on Classical Integrability," J. Phys. A **49**, no.32, 323001 (2016) [arXiv:1606.02946 [hep-th]].

[88] A. A. Belavin and V. G. Drinfel'd, "Solutions of the classical Yang - Baxter equation for simple Lie algebras," Funct. Anal. Appl.**16**:3, (1982) 159–180.

[89] V. V. Bazhanov, S. L. Lukyanov and A. B. Zamolodchikov, "Integrable structure of conformal field theory. 2. Q operator and DDV equation," Commun. Math. Phys. **190**, 247-278 (1997) [arXiv:hep-th/9604044 [hep-th]].

[90] P. P. Kulish and E. K. Sklyanin, "QUANTUM SPECTRAL TRANSFORM METHOD. RECENT DEVELOPMENTS," Lect. Notes Phys. **151**, 61-119 (1982)

[91] A. N. Kirillov and N. Y. Reshetikhin, "Exact solution of the integrable XXZ Heisenberg model with arbitrary spin. I. The ground state and the excitation spectrum," J. Phys. A **20**, 1565-1585 (1987)

[92] A. Klumper and P. A. Pearce, "Conformal weights of RSOS lattice models and their fusion hierarchies," Physica A **183**, 304 (1992)

[93] A. Kuniba, T. Nakanishi and J. Suzuki, "Functional relations in solvable lattice models. 1: Functional relations and representation theory," Int. J. Mod. Phys. A **9**, 5215-5266 (1994) [arXiv:hep-th/9309137 [hep-th]].

[94] G. P. Pronko and Y. G. Stroganov, "Bethe equations 'on the wrong side of equator'," J. Phys. A **32**, 2333-2340 (1999) [arXiv:hep-th/9808153 [hep-th]].

[95] C. Korff, "Auxiliary matrices on both sides of the equator," J. Phys. A **38**, 47-66 (2005) [arXiv:math-ph/0408023 [math-ph]].

[96] C. Korff, "A Q-operator identity for the correlation functions of the infinite XXZ spin-chain," J. Phys. A **38**, 6641-6658 (2005) [arXiv:hep-th/0503130 [hep-th]].

[97] V. V. Bazhanov, S. L. Lukyanov and A. B. Zamolodchikov, "Integrable structure of conformal field theory, quantum KdV theory and thermodynamic Bethe ansatz," Commun. Math. Phys. **177**, 381-398 (1996) [arXiv:hep-th/9412229 [hep-th]].

[98] C. J. Hamer, G. R. W. Quispel and M. T. Batchelor, "Conformal Anomaly and Surface Energy for Potts and Ashkin-teller Quantum Chains," J. Phys. A **20**, 5677 (1987)

[99] C. Destri and H. J. De Vega, "Twisted Boundary Conditions in Conformally Invariant Theories," Phys. Lett. B **223**, 365-370 (1989)

[100] H. J. De Vega, "Yang-Baxter Algebras, Integrable Theories and Quantum Groups," Int. J. Mod. Phys. A **4**, 2371-2463 (1989)

[101] A. Klumper, M. T. Batchelor and P. A. Pearce, "Central charges of the 6- and 19-vertex models with twisted boundary conditions," J. Phys. A **24**, 3111 (1991)

[102] H. W. Braden, E. Corrigan, P. E. Dorey and R. Sasaki, "Affine Toda Field Theory and Exact S Matrices," Nucl. Phys. B **338**, 689-746 (1990)

[103] V. Bazhanov and N. Reshetikhin, "Restricted Solid on Solid Models Connected With Simply Based Algebras and Conformal Field Theory," J. Phys. A **23**, 1477 (1990)

[104] P. F. Hsieh and Y. Sibuya, "On the asymptotic integration of second order linear ordinary differential equations with polynomial coefficients," Journal of Mathematical Analysis and Applications **16**(1), 84-103 (1966)

[105] J. Suzuki, "Functional relations in Stokes multipliers: Fun with $x^6 + alphax^2$ potential," J. Statist. Phys. **102**, 1029-1047 (2001) [arXiv:quant-ph/0003066 [quant-ph]].

[106] S. L. Lukyanov and A. B. Zamolodchikov, "Integrable circular brane model and Coulomb charging at large conduction," J. Stat. Mech. **0405**, P05003 (2004) [arXiv:hep-th/0306188 [hep-th]].

[107] S. L. Lukyanov, E. S. Vitchev and A. B. Zamolodchikov, "Integrable model of boundary interaction: The Paperclip," Nucl. Phys. B **683**, 423-454 (2004) [arXiv:hep-th/0312168 [hep-th]].

[108] D. Masoero, A. Raimondo and D. Valeri, "Bethe Ansatz and the Spectral Theory of Affine Lie Algebra-Valued Connections I. The simply-laced Case," Commun. Math. Phys. **344**, no.3, 719-750 (2016) [arXiv:1501.07421 [math-ph]].

[109] H. M. Farkas and I. Kra, "Riemann Surfaces," Graduate Texts in Mathematics, Springer New York (1992).

[110] R. Flume, M. Magro, L. O'Raifeartaigh, I. Sachs and O. Schnetz, "Uniqueness of the Seiberg-Witten effective Lagrangian," Nucl. Phys. B **494** (1997), 331-345 [arXiv:hep-th/9611123 [hep-th]].

[111] M. Del Zotto, "Four-dimensional $\mathcal{N} = 2$ superconformal quantum field theories and BPS-quivers," PhD thesis, International School for Advanced Studies, https://www.sissa.it/tpp/phdsection/AlumniThesis, 2013.

[112] D. Gaiotto, G. W. Moore and A. Neitzke, "Framed BPS States," Adv. Theor. Math. Phys. **17** (2013) no.2, 241-397 [arXiv:1006.0146 [hep-th]].

[113] D. Galakhov, P. Longhi, T. Mainiero, G. W. Moore and A. Neitzke, "Wild Wall Crossing and BPS Giants," JHEP **11** (2013), 046 [arXiv:1305.5454 [hep-th]].

[114] T. Eguchi and K. Hori, "N=2 superconformal field theories in four-dimensions and A-D-E classification," arXiv:hep-th/9607125 [hep-th].

[115] A. D. Shapere and C. Vafa, "BPS structure of Argyres-Douglas superconformal theories," arXiv:hep-th/9910182 [hep-th].

[116] S. Cecotti and C. Vafa, "Classification of complete N=2 supersymmetric theories in 4 dimensions," arXiv:1103.5832 [hep-th].

[117] M. Alim, S. Cecotti, C. Cordova, S. Espahbodi, A. Rastogi and C. Vafa, "BPS Quivers and Spectra of Complete N=2 Quantum Field Theories," Commun. Math. Phys. **323** (2013), 1185-1227 [arXiv:1109.4941 [hep-th]].

[118] M. Alim, S. Cecotti, C. Cordova, S. Espahbodi, A. Rastogi and C. Vafa, "$\mathcal{N} = 2$ quantum field theories and their BPS quivers," Adv. Theor. Math. Phys. **18** (2014) no.1, 27-127 [arXiv:1112.3984 [hep-th]].

[119] A. Grassi and M. Mariño, "A Solvable Deformation of Quantum Mechanics," SIGMA **15** (2019), 025 [arXiv:1806.01407 [hep-th]].

[120] N. Honda, T. Kawai, and Y. Takei, "Virtual Turning Points," Springer Japan, 2015.

[121] T. Aoki, T. Kawai and Y. Takei, "New Turning Points in the Exact WKB Analysis for Higher-order Ordinary Differential Equations," Kyoto U. Research Institute for Mathematical Sciences, (1991).

[122] T. Aoki, T. Kawai and Y. Takei, "On The Exact Wkb Analysis For The Third Order Ordinary Differential Equations With A Large Parameter," Asian J. Math. **2** (1998).

[123] D. Gaiotto, G. W. Moore and A. Neitzke, "Spectral networks," Annales Henri Poincare **14** (2013), 1643-1731 [arXiv:1204.4824 [hep-th]].

[124] G. V. Dunne and M. Unsal, "Uniform WKB, Multi-instantons, and Resurgent Trans-Series," Phys. Rev. D **89** (2014) no.10, 105009 [arXiv:1401.5202 [hep-th]].

[125] S. Codesido and M. Marino, "Holomorphic Anomaly and Quantum Mechanics," J. Phys. A **51** (2018) no.5, 055402 [arXiv:1612.07687 [hep-th]].

[126] K. Iwaki and T. Nakanishi, "Exact WKB analysis and cluster algebras," J. Phys. A: Math. Theor. **47** (2014), 474009 [arXiv:1401.7094 [math.CA]].

[127] S. Cecotti and M. Del Zotto, "Y systems, Q systems, and 4D $\mathcal{N} = 2$ supersymmetric QFT," J. Phys. A **47** (2014) no.47, 474001 [arXiv:1403.7613 [hep-th]].

[128] F. Yan, "Exact WKB and the quantum Seiberg-Witten curve for 4d $N = 2$ pure $SU(3)$ Yang-Mills, Part I: Abelianization," [arXiv:2012.15658 [hep-th]].

[129] P. B. Gilkey and G. M. Seitz, "Some representations of exceptional Lie algebras," Geometriae Dedicata **25**, 407-416 (1988).

[130] N. A. Vavilov, "Do It Yourself: the Structure Constants for Lie Algebras of Types E_l," Journal of Mathematical Sciences **120**, 1513-1548 (2004).

[131] N. A. Vavilov, "Structure of Chevalley groups: The proof from the book," Journal of Mathematical Sciences **140**, 626-645 (2007).

[132] V. G. Kac, "Infinite Dimensional Lie Algebras," Birkhäuser Boston, 1983.

[133] G. Mussardo, "Statistical field theory: An introduction to exactly solved models in statistical physics," Oxford Univ. Press, 2010.

[134] S. J. van Tongeren, "Introduction to the thermodynamic Bethe ansatz," J. Phys. A **49**, no.32, 323005 (2016) [arXiv:1606.02951 [hep-th]].

[135] H. Cheng, "Meromorphic Property of the S Matrix in the Complex Plane of Angular Momentum," Phys. Rev. **127**(2), 647-648 (1962).